

# CONTEMPORARY PROBLEMS OF POWER ENGINEERING AND ENVIRONMENTAL PROTECTION



## EPAE 2023

ENVIRONMENTAL PROTECTION & ENERGY CONFERENCE



Silesian University  
of Technology



# CONTEMPORARY PROBLEMS OF POWER ENGINEERING AND ENVIRONMENTAL PROTECTION 2023

Gliwice, July 2024

**Scientific Editors:** Magdalena Bogacka

**Technical Editors:** Natalia Patoń, Niola Dąbek, Natalia Nowak, Mateusz Halladin, Remigiusz Matusik, Julia Rytczak, Alesander Skiba

**Cover design:** Elżbieta Łysoń

**List of Reviewers:**

dr Edo Begna Tinu

dr hab. inż. Anna Grosser, prof. PCz

dr inż. Michal Jurczyk

dr inż. Kishore Kumar Kadimpati

dr hab. inż. Adam Klimanek, prof. PolSI

dr inż. Piotr Koper

dr hab. inż. Marcin Lemanowicz, prof PolSI

dr Enkeleba Mera

dr inż. Arsalan Muhammad Soomar

dr Hari Prasadarao Pydi

dr hab. inż. Grzegorz S. Jodłowski

dr Małgorzata Worwąg

dr hab. inż. Magdalena Zaborowska

ISBN 978-83-964116-5-5

Published by Department of Technologies and Installations for Waste Management, Silesian University of Technology

Copyright © Department of Technologies and Installations for Waste Management, Silesian University of Technology

**Copyright Notice**

No parts of this book may be reproduced in any written, electronic, recording, or photocopying without written permission of the publisher or author. The exception would be in the case of brief quotations embodied in the critical articles or reviews and pages where permission is specifically granted by the publisher or author.

Although every precaution has been taken to verify the accuracy of the information contained herein, the authors assume no responsibility for any errors or omissions. No liability is assumed for damages that may result from the use of information contained within.

## List of content

A short Communication on the Advanced Surface Engineering: The Advancement in Materials Engineering	6
Agrivoltaics- execution and analysis of an Energy Project for an Animal Farm in Ogun State Nigeria.	25
Application of LSTM Networks and Selected AutoML Techniques for Short-Term Forecasting of Sewage Inflow to a Municipal Wastewater Treatment Plant	36
Application of walnut shells as a fuel and alternative reducer of slags from non-ferrous metallurgy industry	48
Biodegradability and Kinetics of anaerobic co-digestion of coffee husk with food waste: Effect of mixing ratio and initial pH value	53
Characterization of the properties of essential oils obtained by various distillation methods	68
Critical assessment of slagging and fouling indicators for animal derived biomass with the use of aluminosilicate additives.	80
Determining the current-voltage characteristics of colored BIPV modules based on experimental research.	90
Energy transition and climate change in the opinion of Poles over the past few years.	96
Estimation of soil pollution from hydrocarbons in Vlora region	102
Experimental study on low-temperature combustion engine mode operations (RCCI)	108
Impacts of Site Ambient Temperature and Wind Speed on Photovoltaic Performance with Varying Tilt Angles.	121
Integrated emergency response and telehealth systems for enhanced crisis management- A cross-sectorial approach	133
Numerical Model of Solar Pond in Simulink Environment to Use Pond as Energy Storage	139
On MILD: The Future of Hydrogen Combustion	146
Polymeric approaches to the removal of endocrine disrupting compounds from water: a comprehensive review	160
Production of bioethanol from apple pomace and its suitability as a fuel	168
Prospects for the application of mycorrhizal fungi in phytoremediation techniques	176
Scientific analysis of the negative effect of the war in Ukraine on environment	183
Selectively collected biowaste as an organic-rich feedstock for composting	188
The application of numerical modal analysis in simulation of dynamics of HDPE fuel tank	195
The coffee industry and environmental protection: New trends in wastewater treatment	202
Water quality assessment of Vjosa river near an oil extraction area	210



# A short Communication on the Advanced Surface Engineering: The Advancement in Materials Engineering

Amjad Iqbal<sup>1</sup>

<sup>1</sup>Department of Materials Technology, Faculty of Materials Engineering, Silesian university of Technology, Krasińskiego 9, 40-018, Katowice, Poland, e-mail: amjad.iqbal@polsl.pl

---

## Abstract

This article delves into the intricacies of Advanced Surface Engineering, a multidisciplinary field that intricately combines principles from materials science, chemistry, physics, and engineering to modify and enhance the surface properties of materials. The comprehensive overview explores a myriad of techniques including physical and chemical vapor deposition, thermal spray coatings, surface etching, and surface modification treatments. By meticulously manipulating surface characteristics such as chemical composition, roughness, hardness, adhesion, and lubricity, the field aims to achieve specific objectives, including but not limited to, improving wear resistance, corrosion protection, thermal stability, biocompatibility, and tribological properties.

The versatility of the techniques employed underscores the adaptability of Advanced Surface Engineering to diverse challenges across industries. The interdisciplinary nature of the field is emphasized, highlighting the collaborative efforts of experts from different scientific and engineering backgrounds. As technology continues to advance, the role of advanced surface engineering becomes increasingly vital in developing innovative solutions, pushing the boundaries of material performance, and addressing the evolving needs of various industries. This article provides a holistic understanding of the field's current state and its potential for future advancements.

---

## 1. Introduction

### 1.1 Overview of Advanced Surface Engineering

Advanced Surface Engineering is a multidisciplinary field that focuses on modifying and enhancing the surface properties of materials to improve their performance and functionality. It encompasses a wide range of techniques and processes, including physical and chemical vapor deposition, thermal spray coatings, surface etching, and surface modification treatments. These techniques allow for precise control over surface characteristics such as chemical composition, roughness, hardness, adhesion, and lubricity. By manipulating the surface properties of materials, advanced surface engineering aims to achieve specific objectives such as improving wear resistance, corrosion protection, thermal stability, biocompatibility, and tribological properties. The field draws upon principles from materials science, chemistry, physics, and engineering to develop innovative solutions for various industries [1].

### 1.2 Importance and applications of Advanced Surface Engineering

Advanced Surface Engineering plays a crucial role in numerous industries due to its wide-ranging applications and the benefits it offers. In the aerospace industry, for example, surface coatings are applied to aircraft components to enhance their resistance to wear, corrosion, and high temperatures. These coatings improve the durability, efficiency, and safety of critical parts, resulting in extended service life and reduced maintenance costs. In the automotive industry, surface engineering techniques are employed to enhance the performance and durability of engine components. Coatings with low friction properties are applied to piston rings and cylinder liners to reduce frictional losses and improve fuel efficiency. Additionally, surface treatments can protect against wear, leading to longer engine life and improved reliability.

Advanced Surface Engineering also finds applications in the biomedical field, particularly in the development of medical implants. Surface modifications can improve the biocompatibility of implant materials, allowing for better integration with the surrounding tissues and reducing the risk of rejection or complications. Coatings with antibacterial properties can help prevent infections, while enhanced wear resistance can prolong the lifespan of implants, such as hip or knee replacements.

Furthermore, the electronics industry benefits from advanced surface engineering techniques to improve the performance and reliability of microelectronic devices. Surface coatings are applied to enhance adhesion, protect against moisture and environmental factors, and optimize electrical conductivity. The figure 1 can elaborate more application in a productive way.

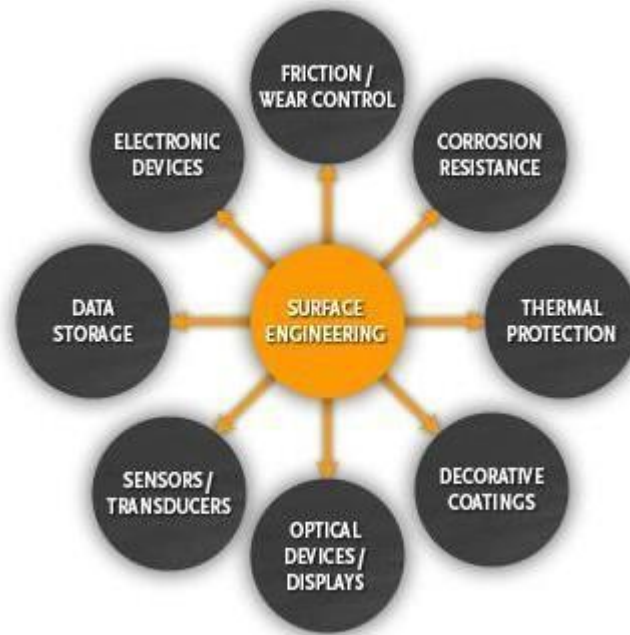


Fig. 1. Application of surface Engineering in various industry [2]

### 1.3 Objectives of the reports

Providing a comprehensive understanding of the different surface modification techniques employed in advanced surface engineering: This objective involves explaining the principles, processes, and specific applications of techniques such as physical vapor deposition (PVD), chemical vapor deposition (CVD), and thermal spray coatings. The reports aim to provide detailed insights into how these techniques are utilized to achieve desired surface properties.

Exploring various surface characterization techniques and their significance in evaluating and analyzing engineered surfaces: This objective involves discussing techniques such as scanning electron microscopy (SEM), X-ray diffraction (XRD), and atomic force microscopy (AFM). The reports aim to highlight the role of these characterization methods in examining surface topography, crystallographic structure, and other surface properties critical for understanding and optimizing advanced surface engineering processes.

Discussing different surface coating materials, their properties, and their applications in different industries: This objective involves providing an overview of various coating materials, including ceramics, polymers, and metals. The reports aim to explore the unique properties, advantages, and limitations of each material type, as well as their specific applications in industries such as aerospace, automotive, and biomedical sectors.

Examining the diverse applications of advanced surface engineering in key industries like aerospace, automotive, and biomedical sectors: This objective involves delving into specific examples of how advanced surface engineering techniques are applied in these industries. The reports aim to highlight the challenges faced, the solutions implemented, and the resulting improvements in performance, efficiency, and reliability.

Discussing future trends and challenges in advanced surface engineering, including emerging technologies and integration with other fields: This objective involves exploring the evolving modeling techniques and applications as shows in Figure 2.

CURRENT RESEARCH ACTIVITIES

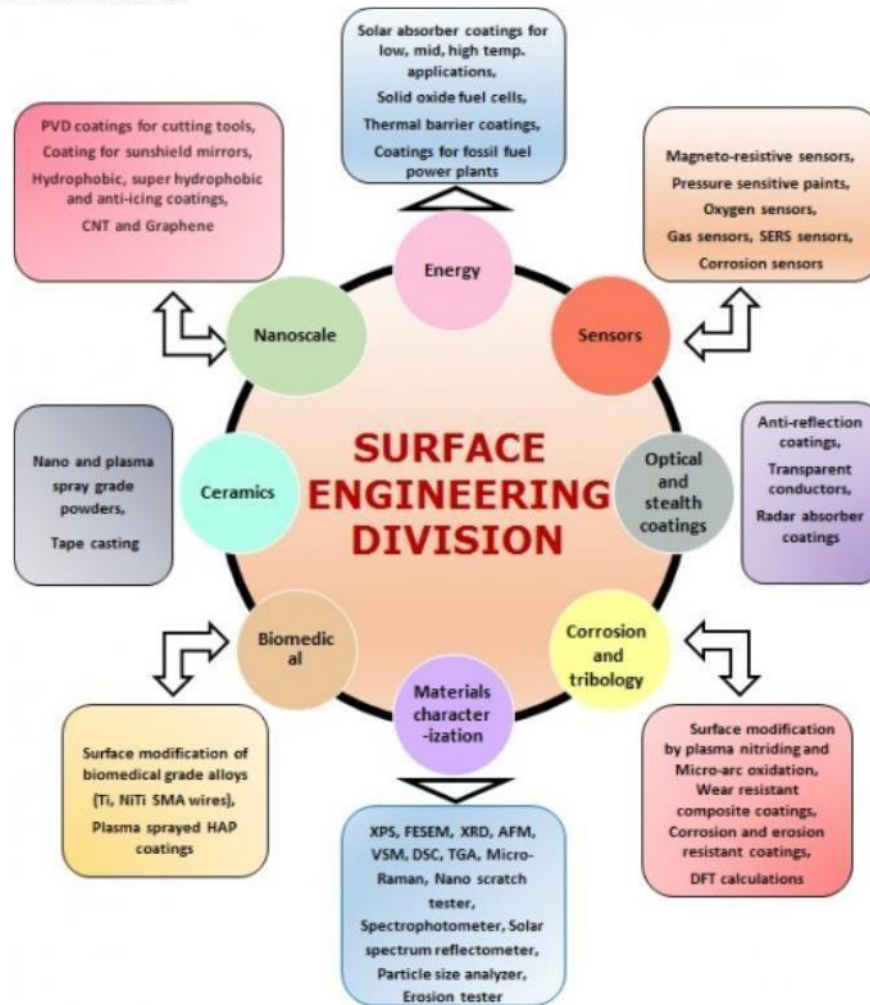


Fig. 2. The Successful technologies in the surface engineering

## 2. Surface Modification Techniques

### 2.1 Physical Vapor Deposition (PVD)

#### 2.2 Principles and process

Physical Vapor Deposition (PVD) is a surface modification technique that involves the deposition of thin films or coatings onto a substrate through physical processes. The principle behind PVD is the conversion of solid or liquid materials into a vapor phase, which is then condensed onto the substrate surface to form a thin film. The process generally consists of three main steps: vaporization, transport, and deposition.

During vaporization, the material to be deposited is heated in a vacuum chamber, causing it to undergo sublimation or evaporation. The resulting vapor or gaseous atoms then travel through the vacuum chamber, colliding with gas molecules and the chamber walls. Eventually, the vapor reaches the substrate surface, where it condenses and forms a thin film.



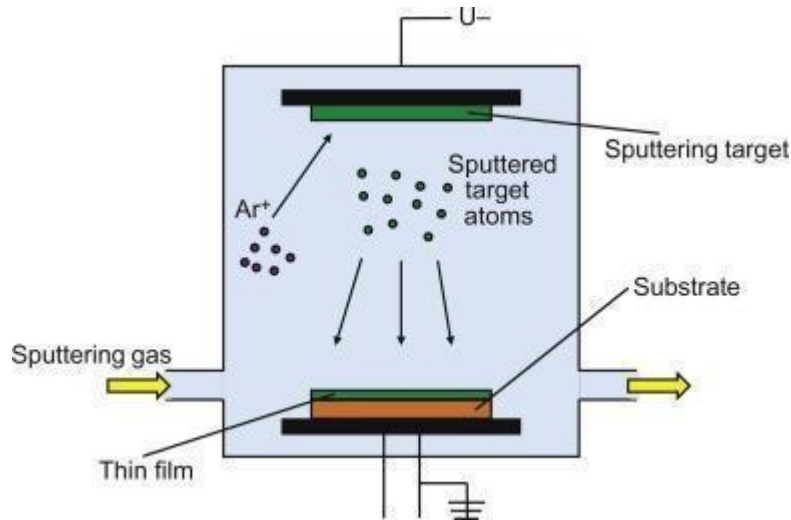


Fig. 3. Schematic illustration of the physical vapor deposition process

### 2.3 Types of PVD techniques (e.g., sputtering, evaporation)

PVD encompasses various techniques, each with its specific advantages and applications. Some commonly used PVD techniques include:

**Sputtering:** In sputtering, a high-energy ion beam bombards a target material, causing atoms or molecules to be ejected from the target surface. These ejected particles then deposit onto the substrate to form a coating. Sputtering can be further categorized into magnetron sputtering, reactive sputtering, and ion beam sputtering, depending on the method used to generate the ion beam and control the deposition process.

**Evaporation:** Evaporation involves the heating of a solid material, typically in a resistive or electron beam evaporator, to produce a vapor. The vaporized material then condenses onto the substrate, forming a thin film. Evaporation can be performed under high vacuum conditions or in the presence of a reactive gas, known as reactive evaporation.

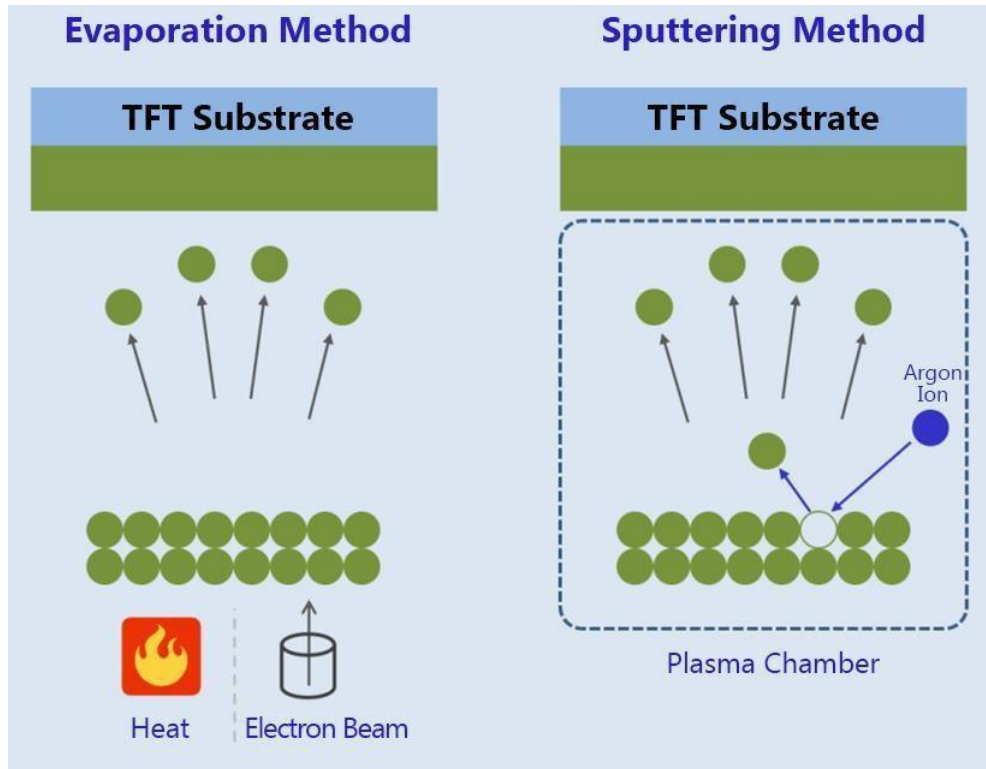


Fig. 4. Method and type of PVD techniques [4]

## 2.4 Advantages and limitations

PVD techniques offer several advantages for surface modification:

- **Precise control:** PVD allows for precise control over film thickness, composition, and microstructure. This control enables the tailoring of specific surface properties to meet desired requirements.
- **Versatility:** PVD can be used to deposit a wide range of materials, including metals, alloys, ceramics, and even organic compounds. This versatility makes it suitable for various applications.
- **Adhesion and uniformity:** PVD coatings exhibit excellent adhesion to the substrate, ensuring long-term durability. Additionally, PVD processes often result in uniform coatings with good thickness uniformity over large areas.

However, PVD techniques also have limitations:

- **High vacuum requirements:** PVD processes require high vacuum conditions, which can be technically challenging and costly to maintain.
- **Limited deposition rate:** PVD processes generally have relatively low deposition rates compared to other techniques, which may limit their suitability for high-volume production.
- **Restricted substrate compatibility:** Some PVD processes, such as sputtering, require the use of conductive substrates. This limitation can restrict the range of substrates that can be coated using certain PVD techniques.
- **Line-of-sight deposition:** PVD processes typically rely on line-of-sight deposition, which means that complex-shaped or non-planar surfaces may experience limited coating uniformity.

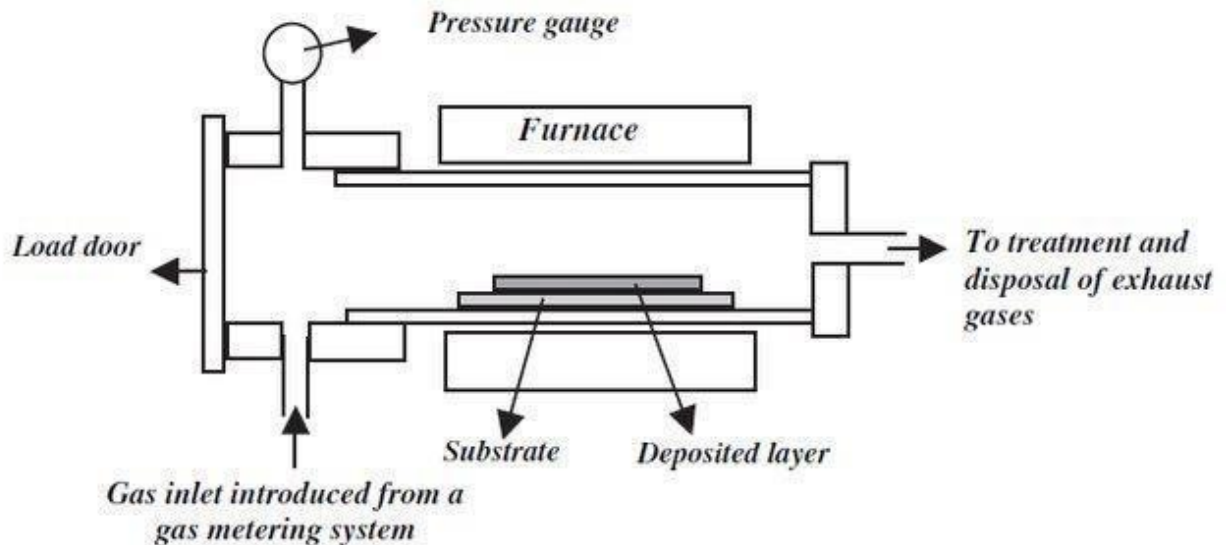
## 2.5 Chemical Vapor Deposition (CVD)

### 2.6 Principles and process

Chemical Vapor Deposition (CVD) is a surface modification technique that involves the deposition of thin films or coatings onto a substrate through chemical reactions in a vapor phase. Unlike PVD, CVD relies on the reaction of precursor gases or vapors to form a solid film on the substrate surface. The process generally consists of four main steps: precursor delivery, reaction, film growth, and byproduct removal.

During precursor delivery, the precursor gases are introduced into a reaction chamber along with a carrier gas. The gases flow over the heated substrate, where the precursor molecules undergo chemical reactions, leading to the deposition of a solid film. The reaction may involve decomposition, reduction, oxidation, or a combination of these processes.

The film growth occurs as the reaction byproducts settle onto the substrate surface, forming a thin film layer. Simultaneously, the byproducts are removed from the reaction chamber to maintain a controlled environment and prevent unwanted deposition.



- Uniform coating layer
- Thickness: 2–100  $\mu\text{m}$

Fig. 5. Chemical vapor deposition (CVD) method [5]

### 2.7 Types of CVD techniques (e.g., plasma-enhanced, low-pressure)

CVD encompasses various techniques, each with its specific advantages and applications. Some commonly used CVD techniques include:

- **Plasma-Enhanced CVD (PECVD):** In PECVD, the precursor gases are energized by a plasma source, such as radio frequency (RF) or microwave energy. The plasma enhances the reactivity of the precursors, enabling lower deposition temperatures and faster growth rates. PECVD is commonly used for depositing thin films of silicon-based materials, such as silicon dioxide ( $\text{SiO}_2$ ) or silicon nitride ( $\text{Si}_3\text{N}_4$ ), for applications in microelectronics and optoelectronics [6-7].
- **Low-Pressure CVD (LPCVD):** LPCVD involves operating the CVD process at reduced pressure, typically below atmospheric pressure. The lower pressure helps control the growth rate, film composition, and crystallinity. LPCVD is widely used for depositing materials like polysilicon, silicon carbide, and silicon germanium. It finds applications in the fabrication of microelectronic devices, sensors, and photovoltaic cells.
- **Atmospheric Pressure CVD (APCVD):** APCVD operates at atmospheric pressure, eliminating the need for vacuum equipment. This technique is relatively simpler and cost-effective compared to low-pressure alternatives. APCVD is commonly used for depositing metal oxide films, such as tin oxide or zinc oxide, for applications in transparent conductive coatings and gas sensors.

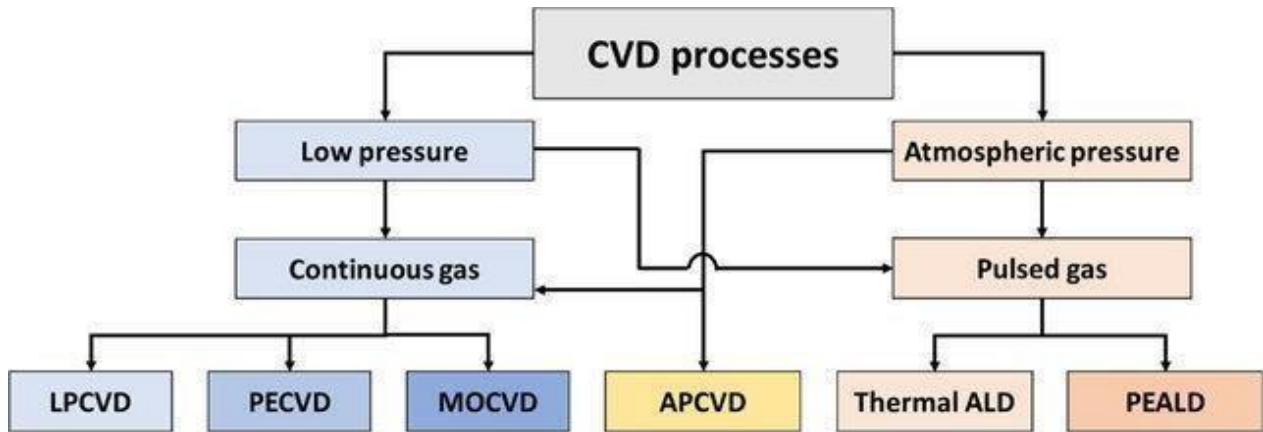


Fig. 6. Main types of chemical vapor deposition (CVD) reactors and processes [7]

## 2.8 Advantages and limitations

CVD techniques offer several advantages for surface modification:

- Conformal coating: CVD processes enable the deposition of conformal coatings, meaning the films conform to the contours of complex or irregularly shaped substrates. This property is beneficial for applications that require uniform coverage on intricate geometries.
- Control over composition and stoichiometry: CVD allows precise control over the composition and stoichiometry of the deposited films. By adjusting the precursor gases and process parameters, the film properties can be tailored to meet specific requirements.
- Large-area deposition: CVD techniques can be scaled up for large-area deposition, making them suitable for industrial-scale production.

However, CVD techniques also have limitations:

- High equipment and maintenance costs: CVD equipment can be expensive to purchase, operate, and maintain. The requirement for precise control of precursor delivery, reaction conditions, and byproduct removal adds to the complexity and cost of the process.
- Limited growth rates: CVD processes often have lower growth rates compared to some PVD techniques, which may be a constraint for high-throughput production.
- Precursor compatibility: CVD techniques rely on the availability of suitable precursor materials that can be vaporized and react under the desired process conditions. This limitation may restrict the choice of materials that can be deposited.

## 3. Thermal Spray Coatings

### 3.1 Principles and process

Thermal spray coatings are a surface modification technique that involves the deposition of molten or partially molten particles onto a substrate. The process utilizes the heat energy generated by various thermal spray devices to melt or soften the coating material, which is then propelled onto the substrate surface.

The principles of thermal spray coatings as show in figure 7 revolve around the conversion of solid materials into a fine powder or wire form, which is then accelerated towards the substrate through a high-velocity gas stream. The particles impact and bond with the substrate, forming a cohesive coating layer.

The process typically consists of four main steps: powder or wire feeding, particle heating and acceleration, particle impact and deformation, and coating buildup. The choice of thermal spray technique determines the specific mechanisms involved in each step.

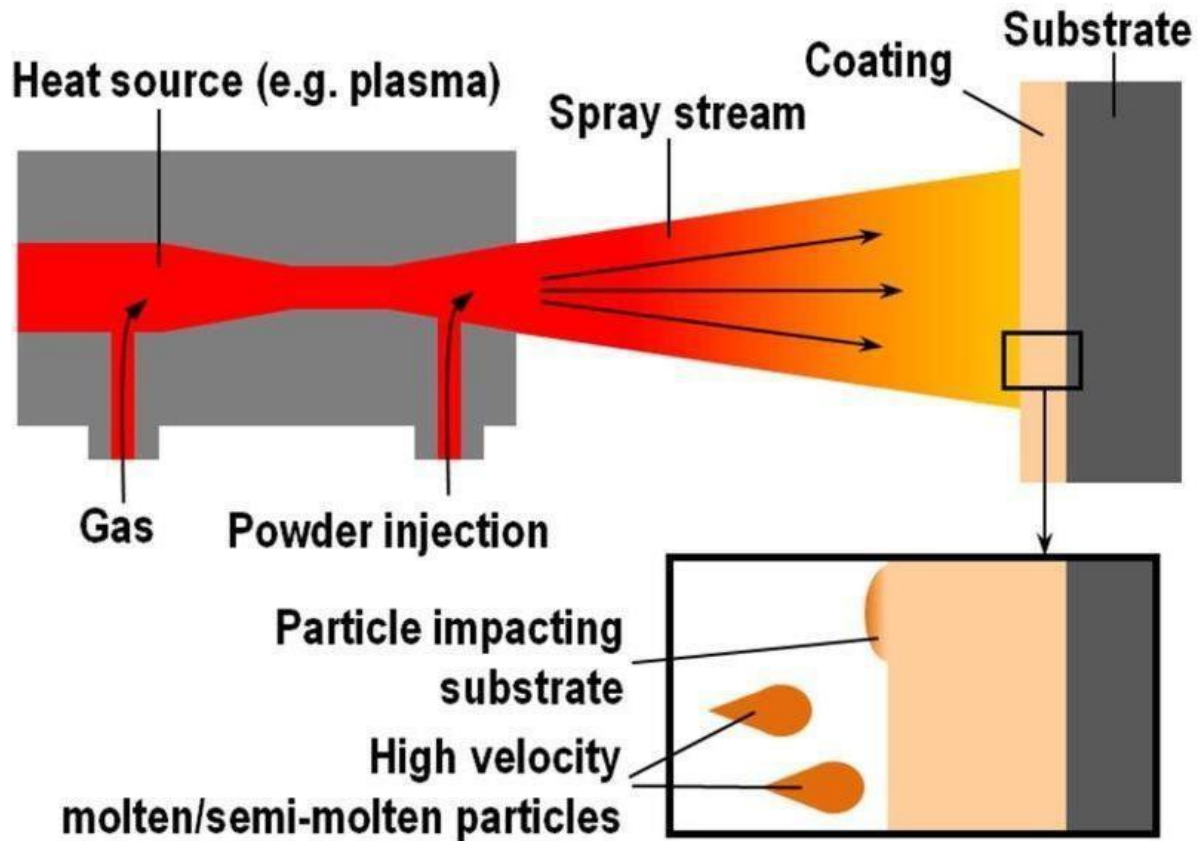


Fig. 7. Schematic illustration of thermal spray process [8]

### 3.2 Types of thermal spray techniques (e.g., flame spraying, plasma spraying)

There are several types of thermal spray techniques as can be seen in figure 8, but I am writing only three, each offering unique advantages and suitability for specific applications. Some commonly used thermal spray techniques include:

- **Flame Spraying:** Flame spraying is one of the oldest and simplest thermal spray methods. It involves the combustion of a fuel gas, such as acetylene or propane, mixed with oxygen to generate a high-temperature flame. The coating material, in the form of powder or wire, is introduced into the flame, where it melts and is propelled onto the substrate surface. Flame spraying is versatile and can accommodate a wide range of coating materials, including metals, ceramics, and polymers.
- **Plasma Spraying:** Plasma spraying utilizes a plasma torch to generate a high-temperature plasma jet. The coating material, in the form of powder, is injected into the plasma jet, where it melts or partially melts. The molten particles are accelerated and propelled towards the substrate, forming a dense and adherent coating upon impact. Plasma spraying offers precise control over the coating parameters and is suitable for a variety of materials, including metals, ceramics, and composite powders.
- **HVOF (High-Velocity Oxygen Fuel) Spraying:** HVOF spraying is a high-velocity thermal spray technique that uses a combination of high-pressure fuel gas and oxygen to generate a supersonic combustion flame. The flame accelerates the coating particles to high velocities before impact. HVOF coatings exhibit high bond strength, low porosity, and excellent wear resistance. This technique is commonly used for applying dense, high-performance coatings, such as carbides and metallic alloys, for applications requiring exceptional wear and corrosion resistance.

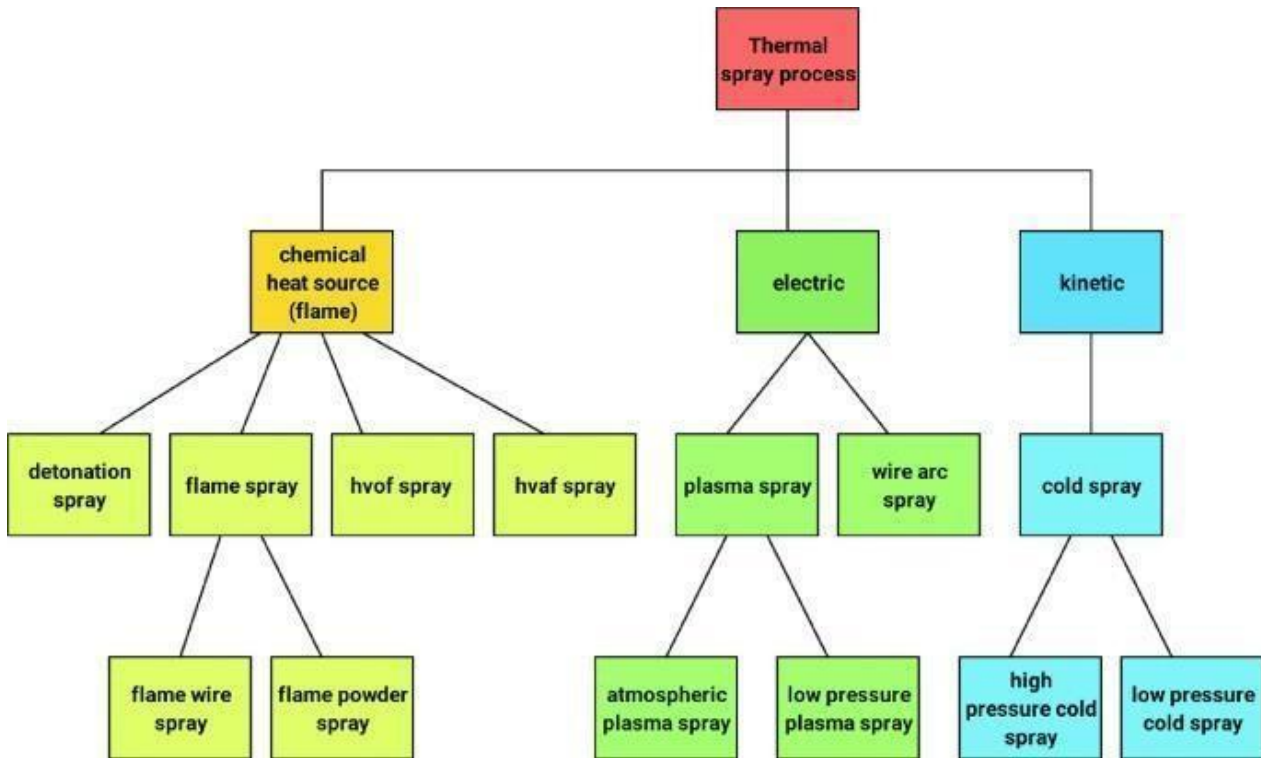


Fig. 8. Various Thermal Spray Process [9]

### 3.3 Advantages and limitations

Thermal spray coatings offer several advantages for surface modification:

**Versatility:** Thermal spray techniques can be used to deposit a wide range of materials, including metals, alloys, ceramics, polymers, and composites. This versatility allows for tailored coatings with specific properties suitable for various applications.

- **Thickness and coverage control:** Thermal spray coatings can be applied to achieve a wide range of thicknesses, from a few micrometers to several millimeters. The process allows for efficient coating buildup on complex shapes and large surface areas.
- **Improved substrate properties:** Thermal spray coatings can significantly enhance substrate properties such as wear resistance, corrosion resistance, thermal insulation, thermal conductivity, electrical conductivity, and biocompatibility.

However, thermal spray coatings also have limitations:

- **Porosity and roughness:** Thermal spray coatings can exhibit higher porosity and roughness compared to some other coating techniques. This porosity may require additional sealing or post-treatment processes to achieve desired properties.
- **Limited precision:** Thermal spray coatings may have less precise control over coating thickness and composition compared to other techniques such as PVD or CVD.
- **Substrate heat sensitivity:** Some substrates may be sensitive to the heat generated during thermal spraying, limiting the range of materials that can be coated without causing substrate damage.
- **Limited substrate compatibility:** Thermal spray coatings may be limited in their compatibility with certain substrate materials. Some substrates may not withstand the high temperatures involved in the thermal spray process or may experience thermal stresses that can lead to coating delamination or substrate deformation.
- **Coating adhesion:** While thermal spray coatings generally exhibit good adhesion, the bonding between the coating and substrate may not be as strong as with other techniques. The adhesion can be influenced by factors such as surface preparation, coating material properties, and substrate composition.
- **Post-processing requirements:** Depending on the application and desired properties, thermal spray coatings may require additional post-processing steps such as machining, grinding, or polishing to achieve the

desired surface finish, dimensional accuracy, or specific coating properties.

- Despite these limitations, thermal spray coatings remain a widely used and effective surface engineering technique, offering excellent versatility, high deposition rates, and the ability to coat large and complex geometries. They find applications in industries such as aerospace, automotive, energy, and manufacturing, where enhanced surface properties are critical for improved performance and durability.

## 4. Surface Characterization Techniques

There are several surface characterization techniques available [10], it depend what material you are going to characterize and what type of application do you need. In this section I will shortly discuss the main techniques, which I found useful for surface engineering.

### 4.1 Scanning Electron Microscopy (SEM)

#### 4.2 Principles and applications

Scanning Electron Microscopy (SEM) is a powerful surface characterization technique that utilizes a focused beam of electrons to examine the surface morphology and composition of materials. The basic principle involves scanning a fine electron beam across the sample surface and collecting signals emitted or scattered by the interactions between the beam and the sample.

SEM is widely used in various fields for surface analysis. Its applications include:

- Surface morphology analysis: SEM provides high-resolution images that reveal detailed surface features, such as roughness, texture, and grain structure. It is particularly useful for studying surface defects, cracks, and contaminants.
- Elemental composition analysis: SEM can be coupled with energy-dispersive X-ray spectroscopy (EDS) to analyze the elemental composition of the sample. By detecting characteristic X-rays emitted when the sample is bombarded with electrons, EDS provides qualitative and quantitative information about the distribution of elements within the sample.

#### 4.3 Image analysis and interpretation

SEM images require careful analysis and interpretation to extract meaningful information. Image analysis techniques include:

- Measurement of surface roughness: SEM images can be used to measure parameters such as surface roughness, grain size, and particle size distribution. These measurements aid in understanding the surface characteristics and evaluating the effectiveness of surface engineering processes.
- Identification of surface defects: SEM images help identify various surface defects, such as cracks, voids, and inclusions. By quantifying the size, shape, and distribution of these defects, their impact on the material's performance can be assessed.

### 4.4 X-ray Diffraction (XRD)

#### 4.5 Principles and applications

X-ray Diffraction (XRD) is a widely used technique for determining the crystallographic structure and phase composition of materials. It works based on the principle of Bragg's law, which describes the diffraction of X-rays by a crystal lattice.

XRD is used for various surface characterization purposes, including:

Phase identification: XRD can identify the crystalline phases present in a material. By comparing the measured diffraction pattern with known patterns from a database, the phases can be identified, even in complex mixtures.

#### 4.5 Crystallographic analysis

XRD provides information about the crystal structure, lattice parameters, and orientation of the crystal planes. This

data is crucial for understanding material properties such as mechanical behavior, chemical reactivity, and electrical conductivity.

Crystallographic Analysis: XRD data is analyzed using crystallographic techniques, including:

Peak identification: XRD patterns exhibit distinctive peaks corresponding to specific crystal planes. These peaks are identified and matched with known crystallographic data to determine the crystal structure and phase composition.

Quantitative phase analysis: XRD intensity measurements can be used to determine the relative abundance of different phases in a sample, enabling quantitative phase analysis.

### **4.6 Atomic Force Microscopy (AFM)**

#### **4.7 Principles and applications**

Atomic Force Microscopy (AFM) is a high-resolution surface characterization technique that utilizes a sharp tip mounted on a cantilever to scan the sample surface. The interaction between the tip and the surface generates a force that is measured, allowing the topography and surface properties to be mapped with nanoscale resolution.

AFM has numerous applications, including:

Surface topography analysis: AFM provides three-dimensional surface topographic maps, revealing details such as surface roughness, height variations, and surface defects at the nanoscale level. It is particularly useful for studying nanomaterials, thin films, and biological surfaces.

Mechanical and electrical characterization: AFM can probe mechanical properties, such as surface hardness, elasticity, and adhesion, by measuring the forces between the tip and the surface. It can also be used for electrical characterization, such as mapping electrical conductivity or surface charge distribution on the sample surface. AFM has numerous applications, including: Surface topography analysis: AFM provides three-dimensional surface topographic maps, revealing details such as surface roughness, height variations, and surface defects at the nanoscale level. It is particularly useful for studying nanomaterials, thin films, and biological surfaces. Mechanical and electrical characterization: AFM can probe mechanical properties, such as surface hardness, elasticity, and adhesion, by measuring the forces between the tip and the surface.

#### **4.8 Surface topography analysis**

AFM operates by scanning a sharp tip across the sample surface while maintaining a constant force between the tip and the surface. The deflection of the cantilever, resulting from the forces between the tip and the surface, is measured and used to generate a topographic map of the surface. This allows for high-resolution imaging of surface features, including atomic-scale details.

AFM provides valuable information for surface characterization, such as:

- Surface roughness: AFM can quantify surface roughness by measuring height variations across the sample surface. This information is crucial for assessing the quality of surface modifications and coatings.
- Surface defects and morphology: AFM enables the detection and characterization of surface defects, such as scratches, cracks, and contaminants. It also provides insights into the morphology and shape of nanostructures, thin films, and surface patterns.
- Surface properties mapping: AFM can map local surface properties, such as hardness, elasticity, adhesion, and friction. This information helps understand the mechanical behavior and surface interactions of materials.
- AFM is widely used in various fields, including materials science, nanotechnology, biology, and semiconductor industry.

## **5 Surface Coating Materials**

### **5.1 Ceramic Coatings**



## 5.2 Types of ceramic coatings (e.g., oxides, nitrides)

Ceramic coatings encompass a wide range of materials, including oxides, nitrides, carbides, and silicides. Some common types of ceramic coatings include [11]:

**Oxide coatings:** Examples include alumina ( $\text{Al}_2\text{O}_3$ ), zirconia ( $\text{ZrO}_2$ ), and titania ( $\text{TiO}_2$ ) coatings. These coatings offer excellent thermal and chemical stability, high hardness, and resistance to wear and corrosion.

**Nitride coatings:** Silicon nitride ( $\text{Si}_3\text{N}_4$ ) and titanium nitride ( $\text{TiN}$ ) are common examples of nitride coatings. They provide high hardness, thermal resistance, and low friction properties.

**Carbide coatings:** Tungsten carbide ( $\text{WC}$ ) and titanium carbide ( $\text{TiC}$ ) coatings are used for their exceptional hardness, wear resistance, and high temperature performance.

## 5.3. Properties and applications

Ceramic coatings offer several desirable properties and find applications in various industries, including:

**High temperature resistance:** Ceramic coatings exhibit excellent thermal stability, allowing them to withstand extreme temperatures. They are used in aerospace, power generation, and automotive industries for components exposed to high temperatures, such as turbine blades, exhaust systems, and heat shields.

**Wear and corrosion resistance:** Ceramic coatings provide superior wear resistance, reducing friction and extending the lifespan of components. They are applied to cutting tools, bearings, and engine components. Additionally, their corrosion resistance makes them suitable for protecting surfaces in chemical and marine environments.

**Insulation properties:** Some ceramic coatings possess excellent electrical and thermal insulation properties. They are used in electrical components, semiconductor devices, and thermal barrier coatings for turbine blades.

## 5.4 Polymer Coatings

### 5.4.1 Types of polymer coatings (e.g., polyurethane, epoxy)

Polymer coatings encompass a broad range of materials, including polyurethane, epoxy, acrylics, and silicone. Some common types of polymer coatings include [12]:

**Polyurethane coatings:** Polyurethane coatings offer excellent durability, flexibility, and chemical resistance. They are used in automotive coatings, furniture finishes, and protective coatings.

**Epoxy coatings:** Epoxy coatings are known for their high adhesion, chemical resistance, and mechanical strength. They are widely used in industrial and commercial applications, such as floor coatings, corrosion protection, and electronic encapsulation.

**Acrylic coatings:** Acrylic coatings provide good weatherability, UV resistance, and color retention. They are commonly used in architectural coatings, automotive finishes, and decorative coatings.

### 5.4.2 Properties and applications

Polymer coatings offer diverse properties and applications, including:

**Protective coatings:** Polymer coatings serve as barriers, protecting substrates from environmental factors such as moisture, chemicals, and abrasion. They are used for corrosion protection, waterproofing, and surface enhancement.

**Aesthetics and decoration:** Polymer coatings provide color, gloss, and texture to surfaces, enhancing their appearance. They are used in architectural coatings, automotive finishes, and consumer goods.

**Adhesion promotion:** Polymer coatings can improve the adhesion between the substrate and subsequent layers, such as adhesives or paints. They are used as primers or adhesion promoters in various industries.

## 5.5 Metallic Coatings

### 5.5.1 Types of Metallic Coatings:

Metallic coatings involve the deposition of metal layers onto a substrate. Some common types of metallic coatings include [13]:

**Electroplating:** Electroplating is a widely used technique that involves the deposition of a metal coating on a substrate through an electrochemical process. The substrate is placed in an electrolyte bath containing metal ions, and an electric current is passed through the system to facilitate the deposition of metal atoms onto the surface. Common metals used in electroplating include gold, silver, nickel, chromium, and copper. Electroplated coatings offer enhanced corrosion resistance, improved appearance, increased conductivity, and can provide wear resistance or act as a diffusion barrier.

**Electroless plating:** Electroless plating, also known as autocatalytic plating, is a process in which a metal coating is deposited on a substrate without the use of an electric current. Instead, the deposition occurs through a chemical reaction between a reducing agent and metal ions in a solution. Electroless plating is particularly suitable for coating complex shapes and non-conductive materials. It offers advantages such as uniform coating thickness, good adhesion, and the ability to coat materials with irregular or intricate geometries.

### 5.5.2 Properties and applications

**Corrosion protection:** Metallic coatings act as a barrier between the substrate and the corrosive environment, protecting the underlying material from degradation. They can enhance the corrosion resistance of the substrate and extend its lifespan. For example, electroplated or electroless nickel

coatings are commonly used for corrosion protection of components in the aerospace, automotive, and electronics industries.

**Wear resistance:** Metallic coatings can provide improved wear resistance to the substrate surface. They can enhance the hardness, lubricity, and durability of the substrate, reducing friction and wear. For instance, electroplated or electroless chrome coatings are used for wear-resistant applications, such as automotive components, tools, and molds.

**Decorative finishes:** Metallic coatings are often applied for aesthetic purposes, providing decorative finishes with desirable appearances such as brightness, color, and reflectivity. Electroplated gold or silver coatings are commonly used for decorative applications in jewelry, consumer electronics, and luxury items.

**Conductivity and solderability:** Metallic coatings can enhance the electrical conductivity of the substrate surface, making them valuable for electrical and electronic applications. They can also improve the solderability of surfaces, ensuring reliable solder joints in electronic assemblies.

**Heat resistance:** Certain metallic coatings, such as thermal barrier coatings applied through techniques like electron beam physical vapor deposition (EB-PVD) or plasma spraying, provide thermal insulation and resistance to high temperatures. They are used in gas turbines, aerospace engines, and other high-temperature applications.

**Adhesion promotion:** Metallic coatings can serve as adhesion promoters for subsequent layers, such as adhesives or paints. They enhance the bonding between the substrate and the coating, improving overall adhesion and performance.

## 6. Advanced Surface Engineering Applications

### 6.1 Aerospace Industry

#### 6.1.1 Surface Coatings for Aircraft Components:

Advanced surface engineering finds extensive applications in the aerospace industry, where the performance and durability of aircraft components are critical. Surface coatings are used to enhance the properties of various aircraft

parts, including [13]:

**Engine components:** Coatings are applied to turbine blades, combustion chambers, and engine casings to improve their performance, durability, and efficiency. These coatings can provide thermal barrier protection, reduce friction, enhance erosion resistance, and increase the lifespan of critical engine parts.

**Airframe components:** Surface coatings are applied to airframe components such as wings, fuselage, and landing gear to improve their resistance to wear, corrosion, and environmental degradation. These coatings help to prolong the service life of the aircraft and reduce maintenance requirements.

### 6.1.2 Enhanced Wear Resistance and Corrosion Protection:

Advanced surface engineering techniques offer enhanced wear resistance and corrosion protection to aerospace components, addressing the challenges of harsh operating conditions and environmental exposure. Some specific applications include:

**Hard coatings:** Hard coatings, such as diamond-like carbon (DLC) coatings, are applied to critical components to improve wear resistance and reduce friction. These coatings increase the lifespan of moving parts, such as bearings, gears, and shafts, while minimizing energy losses due to friction.

**Corrosion-resistant coatings:** Aerospace components are exposed to corrosive environments, including moisture, saltwater, and atmospheric contaminants. Advanced surface coatings, such as metallic or ceramic coatings, are applied to provide corrosion protection and extend the lifespan of components. These coatings act as a barrier between the substrate and the corrosive medium, preventing degradation and maintaining the structural integrity of the aircraft.

**Thermal barrier coatings:** Gas turbine engines operate at high temperatures, and thermal barrier coatings are applied to critical components such as turbine blades and combustors. These coatings provide thermal insulation, protecting the underlying components from excessive heat and thermal fatigue. Ceramic-based coatings, such as yttria-stabilized zirconia (YSZ), are commonly used for thermal barrier applications.

**Erosion and impact-resistant coatings:** Aircraft components, particularly those exposed to high-velocity airflow or abrasive particles, require protection against erosion and impact damage. Advanced coatings with high hardness, such as HVOF (High-Velocity Oxygen Fuel) coatings or composite coatings, are applied to critical surfaces to resist erosion and impact, improving the component's lifespan and performance.

The aerospace industry demands high-performance materials and coatings that can withstand extreme conditions, reduce maintenance costs, and improve aircraft efficiency and safety. Advanced surface engineering plays a crucial role in achieving these goals by providing enhanced wear resistance, corrosion protection, thermal insulation, and improved performance for aerospace components.

## 6.2 Automotive Industry

### 6.2.1 Coatings for Engine Components:

Advanced surface engineering plays a significant role in the automotive industry, particularly in enhancing the performance and durability of engine components. Surface coatings are applied to various parts within the engine to address specific challenges and improve overall efficiency. Some examples include [14]:

**Cylinder liners and piston rings:** Coatings such as thermal spray coatings or diamond-like carbon (DLC) coatings are applied to cylinder liners and piston rings to reduce friction, improve wear resistance, and enhance the overall efficiency of the engine. These coatings minimize energy losses due to friction, resulting in improved fuel economy and reduced emissions.

**Valves and valve seats:** Surface coatings are used on valves and valve seats to improve wear resistance and reduce friction. Coatings such as hard chrome or DLC coatings provide increased durability and extend the service life of these critical engine components.

**Bearings and gears:** Advanced coatings are applied to bearings and gears to reduce friction, improve load-

carrying capacity, and enhance wear resistance. These coatings, such as diamond-

like carbon (DLC) or molybdenum disulfide (MoS<sub>2</sub>) coatings, minimize friction losses, increase component lifespan, and contribute to improved fuel efficiency.

### 6.2.2 Improved Fuel Efficiency and Durability:

Advanced surface engineering techniques in the automotive industry aim to improve fuel efficiency, reduce emissions, and enhance the overall durability of vehicles. Some key applications include:

**Friction-reducing coatings:** Surface coatings with low friction coefficients are applied to various engine components, such as pistons, rings, and bearings, to minimize energy losses due to friction. These coatings reduce the frictional forces within the engine, leading to improved fuel efficiency and reduced wear on moving parts.

**Corrosion protection:** Automotive components, especially those exposed to harsh environments or road conditions, require effective corrosion protection. Surface coatings, such as electroplated or electroless coatings, are applied to protect components from corrosion, extending their lifespan and maintaining their functionality.

**Thermal barrier coatings:** In high-performance and high-efficiency engines, thermal barrier coatings are employed to minimize heat transfer to surrounding components and improve combustion efficiency. These coatings reduce thermal stresses, enhance heat management, and contribute to improved engine performance and durability.

**Surface hardness and wear resistance:** Advanced coatings with high hardness, such as ceramic or composite coatings, are used to improve the wear resistance of engine components. By reducing wear and minimizing material loss, these coatings contribute to increased durability and extended service life.

The automotive industry continuously seeks advanced surface engineering solutions to enhance fuel efficiency, reduce emissions, and improve overall vehicle performance and durability. Surface coatings applied to engine components play a crucial role in achieving these goals by reducing friction, improving wear resistance, providing corrosion protection, and enhancing the efficiency of automotive engines.

## 6.3 Biomedical Applications

### 6.3.1 Surface Modifications for Medical Implants

Advanced surface engineering techniques have revolutionized the field of biomedical applications, particularly in improving the performance and integration of medical implants. Surface modifications are applied to medical implants to enhance their functionality, biocompatibility, and interaction with the surrounding biological tissues. Some key examples include [15]:

**Surface coatings:** Biocompatible coatings are applied to implant surfaces to improve their interaction with the surrounding biological environment. These coatings may include materials such as hydroxyapatite, bioactive glasses, or polymers that mimic the natural composition of bone or other tissues. These coatings promote osseointegration, the process of direct bone bonding to the implant surface, leading to improved implant stability and long-term success.

**Surface roughening:** Controlled surface roughening techniques, such as sandblasting or etching, are utilized to create micro- or nano-scale surface features on implant materials. This roughening enhances the implant's surface area, promotes cell adhesion, and facilitates tissue integration. It allows for better attachment and proliferation of cells, promoting faster healing and improved integration between the implant and surrounding tissues.

**Surface functionalization:** Surface functionalization involves modifying the implant surface to incorporate specific biomolecules or chemical groups that promote desired biological responses. For instance, the attachment of bioactive peptides or growth factors onto the implant surface can stimulate specific cellular behaviors, such as enhanced cell adhesion, proliferation, and tissue regeneration.

### 6.3.2 Enhanced Biocompatibility and Tissue Integration:

Advanced surface engineering techniques in biomedical applications aim to improve the biocompatibility and tissue integration of medical implants. The following benefits are achieved through surface modifications:

**Biocompatibility:** Surface modifications optimize the interactions between the implant and the surrounding biological environment, minimizing adverse reactions and immune responses. By promoting biocompatibility, the risk of implant rejection or complications is reduced.

**Tissue integration:** Surface modifications facilitate the integration of implants with host tissues. They enhance the interactions between cells and the implant surface, promoting cellular adhesion, proliferation, and differentiation. This integration improves the stability and long-term performance of the implants.

**Reduced infection risk:** Surface modifications can incorporate antimicrobial agents or coatings with antibacterial properties. These modifications inhibit bacterial colonization on the implant surface, reducing the risk of infection and improving patient outcomes.

**Controlled drug delivery:** Surface modifications can enable the controlled release of therapeutic agents from the implant surface. This localized drug delivery helps in promoting tissue regenera

## 7. Future Trends and Challenges

As advanced surface engineering continues to evolve and expand its applications across various industries, several trends and challenges are shaping the field's future. Understanding these trends and addressing the associated challenges will drive innovation and ensure the continued progress of advanced surface engineering. Here are some notable future trends and challenges:

**Nanotechnology and Nanomaterials:** The integration of nanotechnology and nanomaterials in surface engineering is a growing trend. Nanoscale surface modifications and the development of novel nanomaterials offer enhanced properties, such as improved mechanical strength, increased corrosion resistance, and advanced functionalities. However, challenges related to large-scale manufacturing, cost-effectiveness, and potential environmental impacts need to be addressed to realize the full potential of nanotechnology in surface engineering [16].

**Bio-inspired Surface Engineering:** Inspired by natural structures and processes, bio-inspired surface engineering is gaining momentum. Mimicking biological surfaces, such as lotus leaves or shark skin, can lead to advancements in self-cleaning, anti-fouling, and drag reduction coatings. Challenges in replicating complex biological structures and scaling up bio-inspired surface engineering techniques remain areas of active research.

**Sustainable and Environmentally Friendly Solutions:** The demand for sustainable and environmentally friendly surface engineering solutions is increasing. The development of eco-friendly coatings, reduced energy consumption in surface engineering processes, and the use of green materials are important considerations. Addressing the challenges of waste management, toxic byproducts, and resource consumption is crucial to achieving sustainable practices in advanced surface engineering.

**Multi-Functional and Smart Coatings:** Future surface engineering is likely to focus on developing multi-functional and smart coatings that offer a combination of properties and functionalities. These coatings may possess self-healing capabilities, adaptability to changing environmental conditions, and the ability to sense and respond to external stimuli. Challenges in material design, integration of functional components, and long-term performance need to be overcome to realize the potential of multi-functional and smart coatings.

**Integration with Additive Manufacturing:** The integration of advanced surface engineering with additive manufacturing, such as 3D printing, opens up new possibilities for customized surface modifications and coatings. Combining the design freedom of additive manufacturing with tailored surface functionalities can result in highly optimized components for specific applications. Overcoming challenges related to material compatibility, process control, and achieving desired surface properties in additive manufacturing will be critical for successful integration.

**Characterization and Quality Control:** Accurate and efficient characterization techniques are essential for surface engineering to ensure quality control and performance assessment. The development of advanced surface

characterization methods, such as in situ imaging and real-time monitoring, will enable better understanding and control of surface modifications. Addressing challenges related to cost, accessibility, and the interpretation of complex surface data will be crucial for advancing surface characterization techniques.

**Regulatory Compliance and Standardization:** As advanced surface engineering finds applications in critical industries such as healthcare and aerospace, regulatory compliance and standardization become increasingly important. Establishing industry-wide standards, guidelines, and certification processes will ensure the safety, reliability, and performance of surface-engineered products. Collaboration between industry, academia, and regulatory bodies is crucial to address the challenges associated with standardization.

### 7.1 Emerging Surface Engineering Technologies:

**Graphene-based Coatings:** Graphene, a two-dimensional material with exceptional properties, holds promise for surface engineering applications. Graphene-based coatings offer excellent mechanical strength, thermal conductivity, and barrier properties. Ongoing research aims to

harness the potential of graphene and develop scalable manufacturing methods for its incorporation into coatings.

**Biomimetic Coatings:** Inspired by nature, biomimetic coatings mimic the properties and functionalities found in biological systems. These coatings can exhibit self-healing capabilities, anti-fouling properties, or enhanced adhesion, among others. Advancements in biomimetic materials and fabrication techniques will drive the development of innovative surface engineering technologies.

**Advanced Hybrid Coatings:** Hybrid coatings combining different materials, such as polymers, ceramics, and metals, offer a broad range of properties and functionalities. These coatings can exhibit superior wear resistance, corrosion protection, thermal stability, and tailored surface interactions. Further research in the design and synthesis of advanced hybrid coatings will expand their applications across industries [17].

### 7.2 Integration of Surface Engineering with Other Fields (e.g., Nanotechnology):

**Nanoscale Surface Modification:** The integration of nanotechnology with surface engineering allows precise control over surface properties at the nanoscale. Nanoparticles, nanocomposites, and nanocoatings can be engineered to achieve desired surface functionalities, such as enhanced catalytic activity, improved electrical conductivity, or selective surface interactions. The integration of surface engineering with nanotechnology opens up new possibilities for advanced materials and applications.

**Surface-Enhanced Spectroscopy and Sensing:** Nanotechnology-based surface enhancements enable highly sensitive spectroscopic and sensing techniques. Surface-enhanced Raman spectroscopy (SERS), plasmonic sensing, and surface-enhanced fluorescence offer improved detection limits and specificity. Integrating these techniques with surface engineering allows for enhanced analytical capabilities in various fields, including biomedical diagnostics, environmental monitoring, and chemical analysis.

### 7.3 Challenges and Opportunities in Scaling up Advanced Surface Engineering Processes: Manufacturing Scalability:

One of the key challenges is scaling up advanced surface engineering processes from laboratory-scale to industrial production. Ensuring consistent coating quality, high throughput, and cost-effectiveness requires optimization of material synthesis, deposition techniques, and process control parameters. Developing scalable manufacturing methods without compromising performance or increasing production costs is a major focus of research and development.

**Process Integration and Compatibility:** Integrating advanced surface engineering processes into existing manufacturing workflows and materials systems can be challenging. Compatibility with different substrate materials, process conditions, and compatibility with other manufacturing steps (e.g., joining, machining) need to be addressed. Developing surface engineering processes that seamlessly integrate with existing manufacturing practices will facilitate adoption across industries.

**Durability and Long-term Performance:** Advanced surface engineering solutions should demonstrate long-term

durability and performance under real-world conditions. Understanding the degradation mechanisms, optimizing coating adhesion, and improving the stability of surface modifications are ongoing challenges. Enhancing the long-term reliability and performance of surface-engineered products is crucial for their successful commercialization.

**Cost-effectiveness and Economic Viability:** Advanced surface engineering technologies should be economically viable to be adopted on a large scale. Reducing material and process costs, optimizing energy consumption, and improving process efficiency are essential. Cost-effective solutions will drive widespread adoption and market competitiveness of advanced surface engineering technologies.

**Environmental Impact and Sustainability:** As surface engineering processes expand, minimizing their environmental footprint is essential. Addressing challenges related to waste management, energy consumption, and the use of hazardous materials will contribute to sustainable practices. Developing environmentally friendly coatings, recycling or reusing process by products, and implementing green manufacturing processes will mitigate environmental impacts.

By addressing these challenges, advanced surface engineering technologies can unlock new opportunities for industries, enable novel functionalities, and improve the performance and durability of materials and products.

## References

- [1] Matthews, A., & Rickerby, D. S. (Eds.), *Advanced surface coatings: a handbook of surface engineering*, Glasgow: Blackie, 1991.
- [2] Bell, T, Surface engineering: past, present, and future. *Surface Engineering*, 6(1), 31-40, 1990.
- [3] Surface engineering division. CSIR-National aerospace laboratories, retrieved from <https://www.nal.res.in/en/articledivision/surface-engineering-division.>, last Access 21-06- 2023.
- [4] Samsung Display news room, retrieved from <https://global.samsungdisplay.com/29363/> last Access 21-06-2023.
- [5] Amin, S. K., Abdallah, H. A. M., Roushdy, M. H., & El-Sherbiny, S. A, *An overview of production and development of ceramic membranes*, 11(12), Int. J. Appl. Eng. Res, 7708-7721, 2016.
- [6] Sherman, A, *Chemical vapor deposition for microelectronics: principles, technology, and applications*, 1987.
- [7] Fraga, M., & Pessoa, R., *Progresses in Synthesis and Application of SiC Films: From CVD to ALD and from MEMS to NEMS*, 11(9), Micromachines, 799, 2020.
- [8] Yao, K., Chen, S., Guo, K., Tan, C. K. I., Mirshekarloo, M. S., & Tay, F. E. H. *Lead-free piezoelectric ceramic coatings fabricated by thermal spray process. IEEE Transactions on Ultrasonics, Ferroelectrics, and Frequency Control*, 64(11), 1758-1765, 2017.
- [9] Gupta, G., Tyagi, R. K., Rajput, S. K., Maan, R., Jacob, S., & Verma, S., *Review on Thermal Spray Coating Methods and Property of Different Types of Metal-Based Coatings. In Advances in Engineering Materials: Select Proceedings of FLAME 2020 Springer Singapore*, (pp. 427-439), 2021.
- [10] Stewart, S., & Ahmed, R. *Rolling contact fatigue of surface coatings—a review. Wear*, 253(11-12), 1132-1144, 2002.
- [11] Almusallam, A. A., Khan, F. M., Dulaijan, S. U., & Al-Amoudi, O. S. B. *Effectiveness of surface coatings in improving concrete durability*, 25(4-5), Cement and concrete composites, 473- 481, 2003.
- [12] Wen, C. (Ed.). *Surface coating and modification of metallic biomaterials*, Woodhead Publishing, 2015.
- [13] Gray, J., & Luan, B., *Protective coatings on magnesium and its alloys—a critical review*, Journal of alloys and compounds, 336(1-2), 88-113, 2002.

- [14] Louda, P. *Applications of thin coatings in automotive industry*, 24(1), Journal of achievements in materials and manufacturing engineering, 50-56, 2007.
- [15] Gao, A., Hang, R., Bai, L., Tang, B., & Chu, P. K., *Electrochemical surface engineering of titanium-based alloys for biomedical application*, Electrochimica Acta, 271, 699-718, 2018.
- [16] Gupta, A. K., Naregalkar, R. R., Vaidya, V. D., & Gupta, M. *Recent advances on surface engineering of magnetic iron oxide nanoparticles and their biomedical applications*, 2007.
- [17] Bell, T. *Surface engineering: a rapidly developing discipline*, 12(1), European Journal of Engineering Education, 27-32, 1987.
- [18] Iqbal, A., Siddique, S., Maqsood, M., Atiq Ur Rehman, M., & Yasir, M. Comparative analysis on the structure and properties of iron-based amorphous coating sprayed with the thermal spraying techniques. *Coatings*, 10(10), 1006. <https://doi.org/10.3390/coatings10101006>, 2020.
- [19] Iqbal, A., Iqbal, A., Moskal, G., Yasir, M., Al-Mansour, A. I., Khan, M. A., ... & Ejaz, A. Long-Term Potentiodynamic Testing and Tribometric Properties of Amorphous Alloy Coatings under Saline Environment. *Molecules*, 27(4), 1421. <https://doi.org/10.3390/molecules27041421>, 2022.
- [20] Iqbal, A., Moskal, G., Głowacka, H. M., Pawlik, T., & Cavalerio, A. Phase decompositions of Gd<sub>2</sub>Zr<sub>2</sub>O<sub>7</sub>+8YSZ TBC systems under the condition of long-term high-temperature oxidation. *Surface and Coatings Technology*, 462, 129471. <https://doi.org/10.1016/j.surfcoat.2023.129471>, 2023.
- [21] Iqbal, A., Khan, M. J., & Moskal, G. A review on the Degradation of Coatings Under Hot Corrosion Process. *CONTEMPORARY PROBLEMS OF POWER ENGINEERING AND ENVIRONMENTAL PROTECTION 2022*, 27.
- [22] Iqbal, A., & Moskal, G. Recent development in advance ceramic materials and understanding the mechanisms of thermal barrier coatings degradation. *Archives of Computational Methods in Engineering*, 30(8), 4855-4896, 2023.
- [23] Iqbal, A., Khan, M. J., & Moskal, G. A review on the degradation of coatings under hot corrosion process. In K. Pikoń & M. Bogacka (Eds.), *Contemporary problems of power engineering and environmental protection 2022* (pp. 27–34), 2023.
- [24] Iqbal, A. An overview of the current status and emerging trends in thermally sprayed barrier coatings. In B. Balon (Ed.), *Interdyscyplinarne badania młodych naukowców* (No. 987; pp. 165–177), 2023.
- [25] Iqbal, A., & Khan, M. J. An overview of the current status and emerging trends in thermally sprayed barrier coatings. In T. Maciąg (Ed.), *Materiały i technologie XXI wieku : XXIV Międzynarodowa studencka sesja konferencja naukowa, Katowice, 24 maj 2023. Książka abstraktów* (p. 9), 2023.



# Agrivoltaics- execution and analysis of an Energy Project for an Animal Farm in Ogun State Nigeria.

*Olushola Tomilayo Olapade<sup>1</sup>, Szymon Wieteska<sup>1</sup>, Marek Jaszczur<sup>1</sup>*

<sup>1</sup>*Affiliation: Faculty of Energy and Fuels, AGH University of Science and Technology, 30-059 Krakow, Poland*

---

## Abstract

At present, our society is at a crucial crossroads where the incorporation of sustainable energy alternatives is imperative to combat the impact of climate change and fulfill the world's energy requirements. Simultaneously, agricultural output must rise considerably by the middle of the century to nourish an estimated 10 billion individuals globally. Nevertheless, these forthcoming food and energy necessities result in a conflict of land use between crops and energy production, particularly with solar photovoltaics (PV). A promising resolution to this predicament is the integration of agriculture and solar PV, commonly referred to as agrivoltaics.

The aim of this paper is to explore the potential of using free, under-utilized solar energy to power a hybrid system for a poultry farm owned by the TGI group in Owode, Ogun state, Nigeria. The study utilizes the PV-sol Valentine software to analyze the techno-economic viability and environmental performance of the system under three different scenarios using three PV slope angles: 11 degrees, 30 degrees, and 37 degrees. The total investment cost of the infrastructure and equipment was constant at \$195500. The study found that the lowest levelized cost of electricity of \$0.0923/kWh was achieved when the PV slope was set to 11 degrees. Additionally, the scenario with the 11-degree PV slope resulted in a reduction of fuel costs of over \$6000 per year when compared to the scenario with the 37-degree PV slope. The success of this test case scenario could lead to the deployment of similar solutions to other farms across Nigeria.

**Keywords:** Agrivoltaics, PV sol valentine, PV, Solar energy

---

## 1. Introduction

Over the years, the availability of electricity in Nigeria has deteriorated. The country has been unable to satisfy demand due to its policies, regulations, and operations management. Its deficiency of sufficient and dependable energy is well documented, specifically its economic impact. Nigeria, being a tropical country, has an abundance of Sun around the year, but there has yet to be a solar farm in Nigeria (Newman, 2019). Nevertheless, several studies have been on utilizing solar energy, amongst other renewable energy sources in Nigeria (Sambo, 2009), (Cloutier, 2011), (Adaramola, 2014).

Nigeria's shortage of reliable power constrains the country's economic growth, and Poultry farmers are not left out of this plight. The country must diversify its economy outside oil and gas revenues because that market is volatile. An expansion in self-generation would increase greenhouse gas emissions. However, if the energy-hungry private sector funded more in self-generation to make this possible, pollution would rise, which is why turning to abundant free solar irradiation is promoted to be used, as much support is gotten from the government policies. (Hercher-Pasteur et al. 2020), (Bahramara, 2016).

The current situation is that many farms spend a lot of money to run their operations due to the epileptic power supply in the country; a lot is spent on diesel generator operation, from the buying and transportation of the fuel and on the servicing of the generator sets since the grid has collapsed a lot of time and is not there now.



Fig. 1. Pen Houses at the Selected location in Owode, Ogun State

### 1.1 Site Location

The proposed site for the trial of the hybrid solution is one of Chi Farms located in Owode with a latitude of 6.7° and longitude of 2.99°, and an average temperature of 26.3°C as seen in Fig.2, with March having the highest monthly average. Also, the annual sum of global irradiation is 1824 kWh/m<sup>2</sup>.

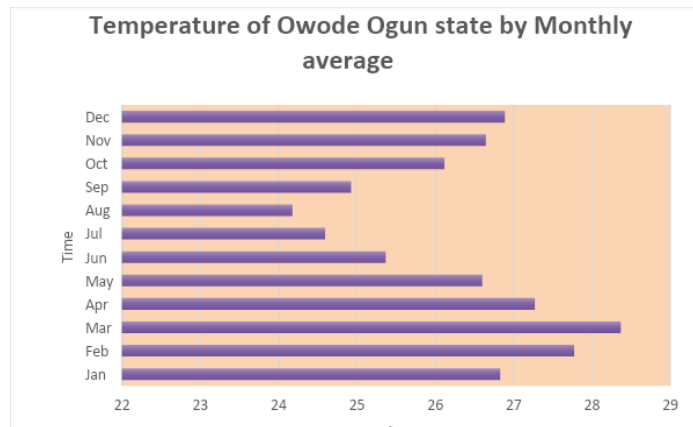


Fig. 2. Monthly average temperature of Owode, Ogun state from PVGIS

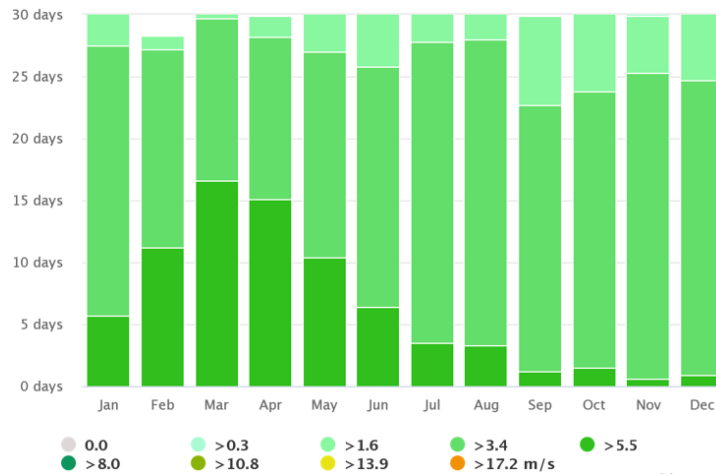


Fig. 3. Wind Profile of Owode, Ogun state (meteoblue, 2023)

The diagram for Owoode Ogun State indicates the monthly days when the wind gets to a specific speed. A fascinating illustration is the Tibetan Plateau, where the monsoon makes constant, potent winds from December to April and calm winds from June to October. (meteoblue, 2023)

### 1.2 Load Profile

The animal farm contains 10 pen houses with other equipment listed below in Table 1.

Table. 1. Equipment in the Farm

Type of Equipment	# of Units per House	kW/unit	KW
Fan	10	1,2	12
Lighting	120	0,02	2,4
Cooling Pump	2	3	6
Feeding line	6	0,6	3,6
Heater	2	15	30
CCTV camera	6	0,060	0,36
32 inches television	2	0,070	0,14

The Load profile was not readily available, so a scenario was created after speaking with the production engineer to understand how the Farm operates; for the Load profile creation, the Cooling pump was used daily for 8 hours between 8 am to 3 pm; also, the pump is used water for the daily farm usage at the same time.

The daily load Requirement to run the 10 pen houses is 196.8 kW/day for a typical dry day and around 236,16 kW/day for the wet season because the heating requirement would be more. Feeding is done 2 times daily at 7 am, where 80% of Feeds are dispersed, and at 2 pm, where the other 20% of feeding is done.

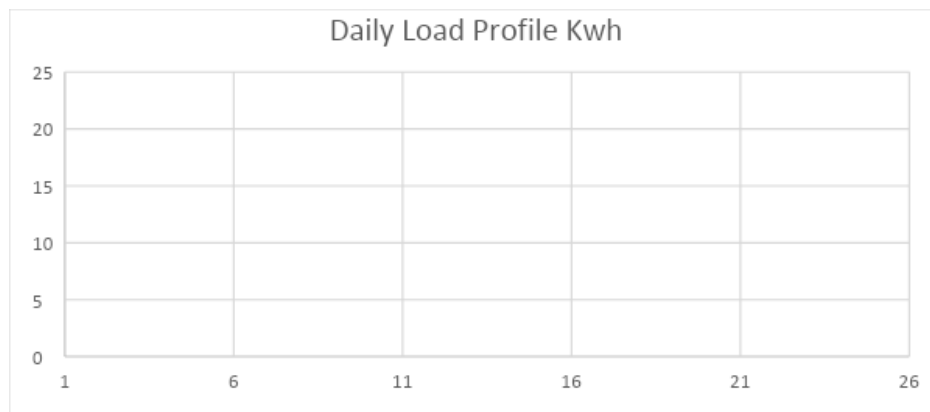


Fig. 4. Daily Load Profile

In Ogun State, Nigeria, the wet season typically lasts about seven months, from April to October as seen in Figure 5 below. But the very Cold period for the Chicken is between November and February when extra heating would be necessary for the 4 (236.16 kw/h). Nevertheless, the wet season's exact start and end dates may vary from year to year and can also differ within distinct regions of the state.

## Contemporary Problems of Power Engineering and Environmental Protection

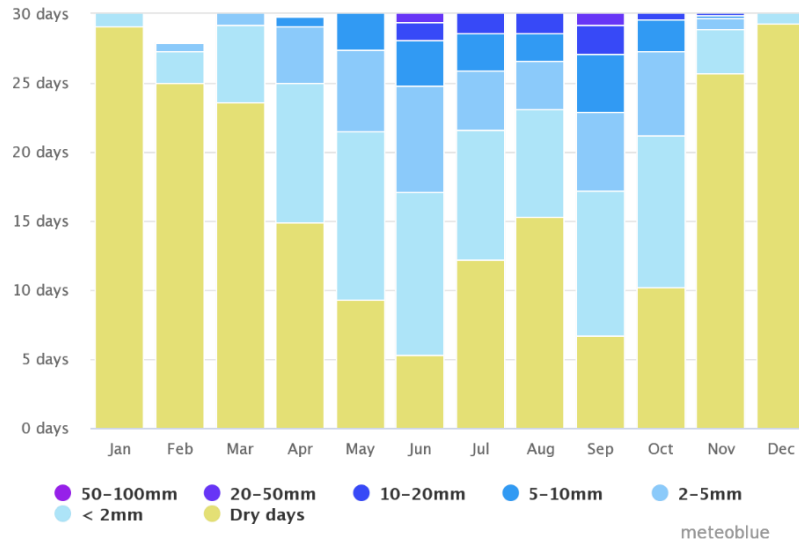


Fig. 5. Precipitation amounts during the year in Owode (meteoblue, 2023)

It is important to note that rainfall amounts can vary from light showers to heavy downpours during the wet season, and flooding can occur in some areas.

Rainfall amounts can vary from light showers to heavy downpours during the wet season rainfall amounts can vary from light showers to heavy downpours during the wet season rainfall amounts can vary from light showers to heavy downpours during the wet season rainfall amounts can vary from light showers to heavy downpours during the wet season.

The Total energy requirement would be 243 days of 196.8 kW/day in the dry season and 122 days of 236.16 kW/day in the wet season) which comes to a total of 77,664 kWh for the whole year as represented in below in Figure 6.

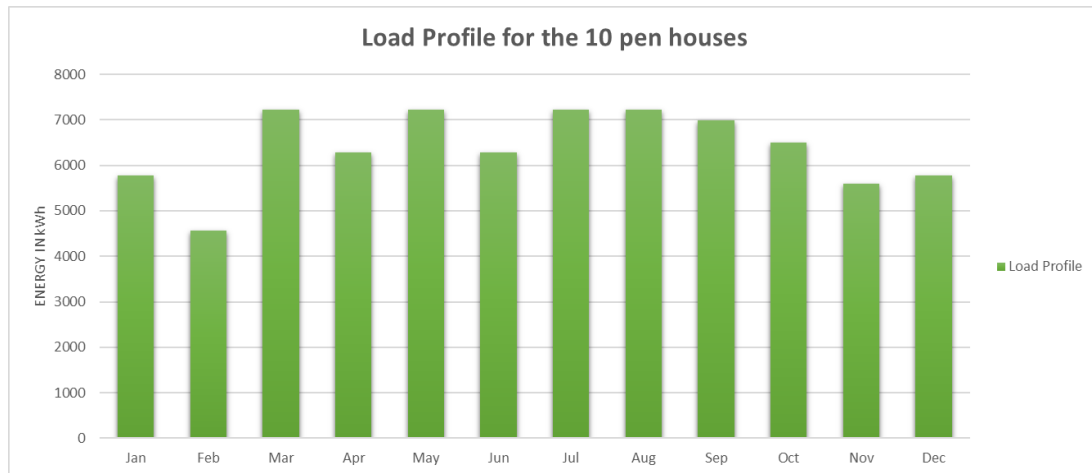


Figure 6: Energy Demand for the year by Months totaling 76664 kWh

## 2. Methodology

In the calculation of output power for PV arrays, the model used the Equations 1 listed below:

$$P_{pv} = Y_{pv} f_{pv} [1 + p(T_c - T_T, STC)] \quad 1$$

on the PV page of the software, we decided to neglect the Temperature effect; the software assumes that the temperature coefficient of power is zero, so the equation above is simplified:

$$P_{pv} = Y_{pv} f_{pv} \quad 2$$

where:

$Y_{PV}$ [kW]	the rated capacity of the PV array, meaning its power output under standard test conditions
$f_{PV}$	the PV derating factor [%]
$\overline{G}_T$	the solar radiation incident on the PV array in the current time step [kW/m <sup>2</sup> ]
$\overline{G}_{T,STC}$	the incident radiation at standard test conditions [1 kW/m <sup>2</sup> ]
$\alpha_p$	the temperature coefficient of power [%/°C]
$T_c$	the PV cell temperature in the current time step [°C]
$T_{c,STC}$	the PV cell temperature under standard test conditions [25°C]

## 2. Effect of slope on the pv with hay and dives kucher and reindl hdkr

The depiction of the orientation of the PV array using two parameters, the slope and azimuth. The slope is the angle between the panel's surface and the horizontal, so a zero slope indicates a horizontal orientation, whereas a 90° slope indicates a vertical orientation. The azimuth is the direction towards which the surface faces. (J.K. Copper et al. 2020)

The relationship between the slope angle of a photovoltaic (PV) panel and its power production is complex. It depends on several factors, including the location's latitude, the time of year, and the specific PV panel technology used. However, the relationship between slope angle and power production is not linear. For example, if the slope angle is too low, the panel may receive too much sunlight during summer, leading to overheating and decreased power production. If the slope angle is too high, the panel may not receive enough sunlight during the winter months, also to a decrease in power production. (Salih, Salih. 2014)

Declination is the angle made between the plane of the equator and the line joining the two centers of the earth and the sun, and to calculate the solar declination, equation 2 below is compelling.

$$\delta = 23.45^\circ \sin\left(360^\circ \frac{284+n}{365}\right) \quad 3$$

where:

$n$  the day of the year [a number 1 through 365]

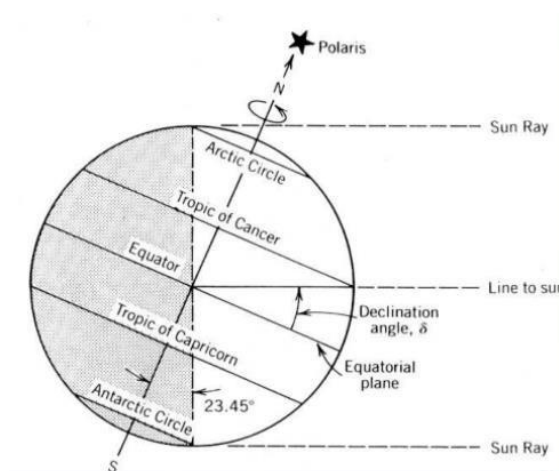


Fig. 5. Diagram showing the declination angel.

The Declination varies between  $-23.45^\circ \leq \delta \leq 23.45^\circ$  and is positive during summer and negative during winter. The time of day affects the location of the sun in the sky, which we can describe by an hour angle. PV sol Valentine uses the convention whereby the hour angle is zero at solar noon (the time of day at which the sun is at its highest point in

the sky), which is negative before solar noon, and positive after solar noon. Furthermore, the software uses the following equation to calculate the hour angle:

$$\omega = (t_s - 12\text{hr}) \cdot 15^\circ/\text{hr} \quad 4$$

where:

$T_s$  the solar time [hr]

The value of  $t_s$  is 12 hr at solar noon and 13.5 hr ninety minutes later. The equation above is that the sun moves across the sky at 15 degrees per hour. The ratio of surface radiation to extraterrestrial radiation is called the clearness index. The following equation defines the clearness index:

$$k_T = \frac{\bar{G}}{\bar{G}_o} \quad 5$$

where:

$\bar{G}$  the global horizontal radiation on the earth's surface averaged over the time step [kW/m<sup>2</sup>]

$\bar{G}_o$  the horizontal extraterrestrial radiation averaged over the time step [kW/m<sup>2</sup>]

Figure 6. below shows the solar radiation on the earth's surface; some of the radiation is beam radiation, which travels from the sun to the earth's surface without any scattering by the atmosphere. Beam radiation (sometimes called direct radiation) casts a shadow.

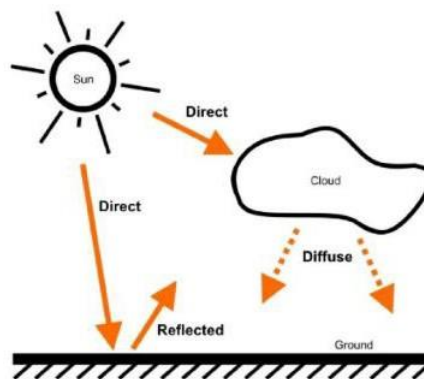


Fig. 6. Solar irradiation components (Francois, 2017)

The rest of the radiation is diffuse radiation, defined as solar radiation whose direction has been changed by the earth's atmosphere. Diffuse radiation comes from all parts of the sky and does not cast a shadow. The sum of the beam and diffuse radiation is called global solar radiation, a relation expressed by the following equation:

$$\bar{G} = \bar{G}_b + \bar{G}_d \quad 6$$

where:

$\bar{G}_b$  the beam radiation [kW/m<sup>2</sup>]

$\overline{G}_d$  the diffuse radiation [kW/m<sup>2</sup>]

The distinction between beam and diffuse radiation is essential when calculating the amount of radiation incident on an inclined surface. The orientation of the surface has a more substantial effect on the beam radiation, which comes from only one part of the sky than it does on the diffuse radiation, which comes from all parts of the sky. Finally, the Pvsol Valentine software uses the correlation of Erbs et al. (1982), as one of the Models which gives the diffuse fraction as a function of the clearness index as follows:

$$\frac{\overline{G}_d}{\overline{G}} = \begin{cases} 1.0 - 0.09 \cdot k_T & \text{for } k_T \leq 0.22 \\ 0.9511 - 0.1604 \cdot k_T + 4.388 \cdot k_T^2 - 16.638 \cdot k_T^3 + 12.336 \cdot k_T^4 & \text{for } 0.22 < k_T \leq 0.80 \\ 0.165 & \text{for } k_T > 0.80 \end{cases} \quad 7$$

For each time step, the software uses the average global horizontal radiation to calculate the clearness index, then the diffuse radiation. It then calculates the beam radiation by subtracting the diffuse radiation from the global horizontal radiation.

To calculate the global radiation striking the tilted surface of the PV array, the software used the Hay and Davies, Klucher and Reindl HDKR model, which assumes that there are three components to the diffuse solar radiation: an isotropic component that comes from all parts of the sky equally, a circumsolar component that emanates from the direction of the sun, and a horizon brightening component that emanates from the horizon. Before applying this model, three more factors are to be defined, which includes the  $R_b$ , the ratio of beam radiation on the tilted surface to beam radiation on the horizontal surface:

$$R_b = \frac{\cos \theta}{\cos \theta_z} \quad 8$$

The anisotropy index, with the symbol  $A_i$ , measures the atmospheric transmittance of beam radiation. This factor estimates the amount of circumsolar diffuse radiation, also called forward scattered radiation. The following equation gives the anisotropy index:

$$A_i = \frac{\overline{G}_b}{\overline{G}_o} \quad 9$$

Finally, the factor used to account for horizon brightening or the fact that more diffuse radiation comes from the horizon than from the rest of the sky. This term is related to cloudiness and is given by the following equation:

$$f = \sqrt{\frac{\overline{G}_b}{\overline{G}}} \quad 10$$

The Hay and Davies, Klucher and Reindl (HDKR) Isotropic Sky Model model calculates the global radiation incident on the PV array according to the following equation:

$$\overline{G}_T = (\overline{G}_b + \overline{G}_d A_i) R_b + \overline{G}_d (1 - A_i) \left( \frac{1 + \cos \beta}{2} \right) \left[ 1 + f \sin^3 \left( \frac{\beta}{2} \right) \right] + \overline{G} \rho_g \left( \frac{1 - \cos \beta}{2} \right) \quad 11$$

where:

- B the slope of the surface [°]
- $\rho_g$  the ground reflectance, which is also called the albedo [%]

### 3. Experimental part

The current situation on the farm's ground is that the total energy demand of 76664 kWh of energy is met with a 30-kw generator set to meet the peak load of around 26 kW noticed in the energy demand. However, the experimental

scenario includes the integration of solar PV, inverters, and batteries to make a Hybrid energy system as seen in Figure 7 below, also the Climate data used, and the unit Price used in the Software are highlighted in Table 1 and Table 4 below respectively.

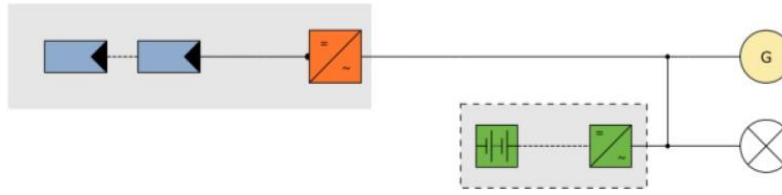


Fig. 7. Proposed system of Type of System 3D, Stand-alone PV System with Backup Generator

Table. 1. Simulation inputs used in Pv-sol Valentine for Climate data

Location	Owode, NGA (2005 - 2020)
Values source	PVGIS-SARAH2/ERA-Interim
Resolution of the data	1 h
Simulation models used:	
- Diffuse Irradiation onto Horizontal Plane	Hofmann
- Irradiance onto tilted surface	Hay & Davies

The Poultry farm currently relies 100 per cent on the use of 30 kW generator sets to cater to its energy demands; the use of Solar panels to meet most, or if not all, its energy demands will help the farm to utilize the already abundant solar radiation and escape the costly diesel price, and in all save the environment of Pollution.

System components

PV Modules

The PV module used is a 0.72 m<sup>2</sup> First Solar Fs-267 thin film solar panel with an efficiency of 9.42%. The schematic indicated a PV system with a rated capacity of 66.7 W with a lifespan of 30 years, also the slope angle of 11°, 30°, and 37° were used to see the difference in Power Output with some other details in Table 2.

Table. 2. PV Generator, 1. Module Area - Open Area 02-Area South

Name	Open Area 02-Area South	
PV Modules	680 x FS-267 (v1)	
Manufacturer	First Solar	
Inclination	11	°, 30°, 37°
Orientation	South 180	°
Installation Type	Mounted - Open Space	
PV Generator Surface	489,6	m <sup>2</sup>

Inverter

The converter is a device that converts DC supply to AC, called inversion or AC to DC, called rectification. It has 97.3% efficiency at 100 % utilization as the inverter, however for this simulation the model selected was the Vitocharge VX3, Typ 8.0A with other details in Table 3 below.

Table. 3. Inverter Properties

Module Area	Open Area 02-Area South
Inverter 1	
Model	Vitocharge VX3, Typ 8.0A (PV+BAT) (v1)
Manufacturer	Viessmann Climate Solutions SE
Quantity	5
Sizing Factor	114,8 %
Configuration	MPP 1: 7 x 10



	MPP 2: 11 x 6
--	---------------

**Battery Inverter and Batteries**

Included in the system configuration is the use of batteries and batteries inverters as seen in the schematics of the system in figure 6, the battery storage was added to increase the stability of the microgrid and to store excess energy not needed when generated which can then be injected into the grid later. The battery inverter used in this case was the GIV-AC-3.0 (v1) manufactured by GivEnergy Ltd in conjunction with a lithium Iron phosphate battery of model Alpha ESS M4856-S 2.9 kWh / 51.2V / LiFePo (v2) manufactured by Alpha ESS Co., Ltd.

**Backup Generator**

A 30 kW - 230/400 V - 3p (v2) of constant power which uses diesel fuel is used to provide the base load to run the poultry farm at Owode.

Table. 4. Unit Price of the Components

Components	Type	Unit Price (\$)
Modules	FS-267	\$ 100.00
Inverters	Vitocharge VX3, Typ 8.0A	\$ 500.00
Battery Inverters	GIV-HY-3.0	\$ 1,000.00
Battery Inverters	GIV-HY-5.0	\$ 500.00
Batteries	Alpha ESS M4856-S 2.9	\$ 500.00
Backup Generators	Alpha ESS M	\$ 10,000.00

**4. Simulation Result**

The Techno-economic analysis for the project involves setting the prices of the components, where the Diesel fuel price for powering the generator was set as \$3/L to reflect the realities on ground in Nigeria, and even the government is set to remove the subsidy on fuels, which means the price could skyrocket by 50% increase yearly as a new government is set to be installed after the just concluded elections, also other costs include the cable cost of \$10000.00, works cost of \$5000,00 and Miscellaneous costs of \$1000.00, the other components prices are all listed in Table 5 below.

Also, for the simulation, it was assumed that the service life of the equipment would be 30 years, and the interest rate on capital would be 8%.

Table 5: Component Price Used in the Simulation

Components	Type	Installed elements	Unit Price (\$)	Installation Costs (\$)	Service Life (years)
Modules	FS-267	680	\$ 100.00	\$ 68,000.00	30
Inverters	Vitocharge VX3, Typ	5	\$ 500.00	\$ 2,500.00	30
Battery Inverters	GIV-HY-3.0	6	\$ 1,000.00	\$ 6,000.00	30
Battery Inverters	GIV-HY-5.0	3	\$ 500.00	\$ 1,500.00	30
Batteries	Alpha ESS M4856-S 2.	183	\$ 500.00	\$ 91,500.00	30

Backup Generators	Alpha ESS M	1	\$ 10,000.00	\$ 10,000.00	30
-------------------	-------------	---	--------------	--------------	----

For the simulated results three different slope angle of the PV installation was used keeping the azimuth constant, all of other component costs selected were also constant, according to PVgis database (PVGIS, 2023) the Optimal PV slope angel for the location of the Poultry farm , Owode in Ogun state Nigeria is 11° and this is consistent with the result obtained from the PV-sol valentine simulation as confirmed in both Figure 8 , with the PV generator Energy and other parameter shows the best slope angle is that of 11°.

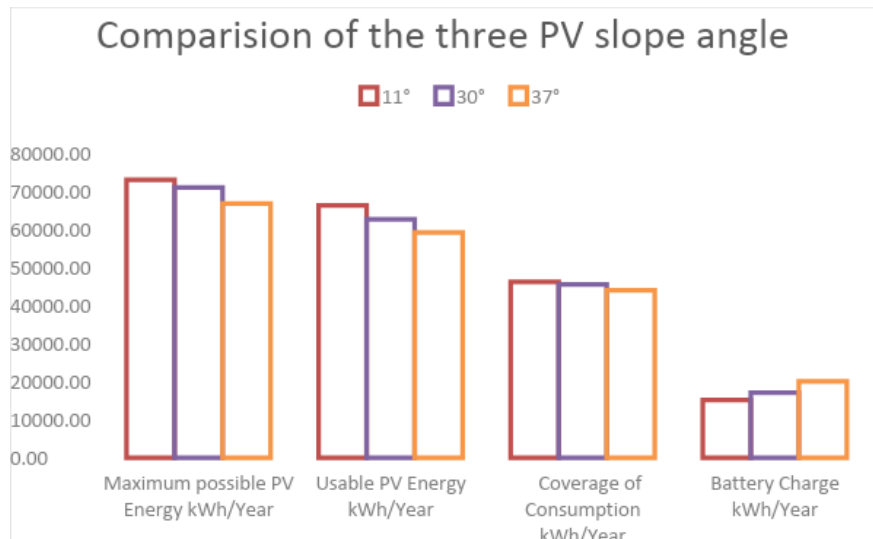


Fig. 8. The Comparison of the three scenarios with constant azimuth but different slope

Table. 6. Results of the PV System for the 11° Slope angle


PV Generator Output	45,90	kWp	
Spec. Annual Yield	1 578,68	kWh/kWp	
Performance Ratio (PR)	86,21	%	
Yield Reduction due to Shading	0,1	%	
Maximum possible PV Energy	72 775	kWh/Year	
Usable PV Energy	66 083	kWh/Year	
Coverage of Consumption	46 079	kWh/Year	
Battery Charge	20 004	kWh/Year	
Fuel Costs	15039.72	\$/Year	
Total investment costs	195500	\$	
Internal Rate of Return (IRR)	11,92	%	
Amortization Period	1,1	Years	
Electricity Production Costs	0,0923	\$/kWh	
Specific Costs	2454.32	\$/kWh	

Table 6 above gives a snapshot of the optimal simulation results showing the breakdown of the Consumption coverage by the PV system when the Slope angle is set to 11 degrees with a performance ratio of 86,21%, and useable PV energy of 66,083 kWh/year, with the amortization period being 1.1 years, and 11.92% Internal rate of return.

## 5. Conclusion

Agrivoltaics represents a harmonious integration of agriculture and solar power, offering a promising solution to optimize land use in the face of growing global demands for food and clean energy. Solar PV is Nigeria's preferred renewable energy technology because of its abundant sunshine. Currently Diesel and petrol generators are used on the average for around 18 hours of the day to meet energy demand and in our case 24 hours of supply all year round, but with the use of Solar PV which is modular and scalable and puts energy security in the hands of households and businesses, the cost of running businesses will reduce, also the possibility to monitor energy costs will be feasible, thereby guaranteeing savings, and better environmental quality.

The business proposal of substituting 78.8% of the 76,664kWh of the annual energy demand using a Solar PV system is a good win for both Chi Farms Ltd and the surrounding community as the air and noise pollution would reduce drastically.

The best-case scenario is placing the PV modules at a tilt angle of 11 degrees, this is from the angle of economics and the angle of technical superiority comparing with the simulations results from both when the angle is 30 degrees and 37 degrees.

## References

- [1] Adaramola, M. S., Assessment of decentralized hybrid PV solar-diesel power system for applications in Northern part of Nigeria. *Energy for Sustainable Development*, 19, 2014.
- [2] Bahramara, S. M., *Optimal planning of hybrid renewable energy systems using HOMER: A review*. . *Renewable and Sustainable Energy Reviews*, 62, 609-620, 2016.
- [3] Cloutier, M., *The feasibility of renewable energy sources for pumping clean water in sub-Saharan Africa: A case study for Central Nigeria*. *Renewable Energy*, 8, 2011.
- [4] Erbs, D. G. Estimation of the diffuse radiation fraction for hourly, daily and monthly-average global radiation. *Solar Energy*, 28(4), 293–302. [https://doi.org/10.1016/0038-092X\(82\)90302-4](https://doi.org/10.1016/0038-092X(82)90302-4), 1982.
- [5] Francois, S. *Energy and Sustainability in Chile: simulation Modeling of Low-carbon Technologies and Energy Efficiency in Buildings*, 2017.
- [6] meteoblue. (2023). Simulated historical climate & weather data for Ogun State. Retrieved from [https://www.meteoblue.com/en/weather/historyclimate/climatemodelled/ogun-state\\_nigeria\\_2327546](https://www.meteoblue.com/en/weather/historyclimate/climatemodelled/ogun-state_nigeria_2327546)
- [7] Newman, N. ( 2019, February 20). Retrieved from Off-the-grid thinking to end Nigeria's blackouts. Retrieved from Engineering and Technology: : <https://eandt.theiet.org/content/articles/2019/02/off-the-grid-thinking-to-end-nigeria-s-blackouts/>
- [8] PVGIS. (2023). Retrieved from [https://re.jrc.ec.europa.eu/pvg\\_tools/en/](https://re.jrc.ec.europa.eu/pvg_tools/en/)
- [9] Sambo, A. S. (2009). Strategic developments in renewable energy in Nigeria. *International Association for Energy Economics* , 15-19.
- [10] Hercher-Pasteur, J., Loiseau, E., Sinfort, C. et al. (2020) Energetic assessment of the agricultural production system. A review. *Agron. Sustain. Dev.* 40, 29. <https://doi.org/10.1007/s13593-020-00627-2>
- [11] J.K. Copper, A.B. Sproul, A.G. Bruce, A method to calculate array spacing and potential system size of photovoltaic arrays in the urban environment using vector analysis, (2020) *Applied Energy*, Volume 161, Pages 11-23, ISSN 0306-2619, <https://doi.org/10.1016/j.apenergy.2015.09.074>.
- [12] Salih, Salih. (2014). Effect of Tilt Angle Orientation on Photovoltaic Module Performance. *ISESCO Centre for Promotion of Scientific Research (ICPSR)*. 10.
- [13] A. Osamede, S. James, P. Christo, (2012) Optimum tilt angles for photovoltaic panels during winter months in the Vaal triangle, South Africa, *Smart Grid and Renewable Energy*, vol. 3, pp. 119-125.

# Application of LSTM Networks and Selected AutoML Techniques for Short-Term Forecasting of Sewage Inflow to a Municipal Wastewater Treatment Plant

Lesław Plonka<sup>1</sup>

<sup>1</sup>Department of Environmental Biotechnology, The Silesian University of Technology, e-mail: leslaw.plonka@polsl.pl

---

## Abstract

The article discusses the application of LSTM neural networks to forecast the hydraulic load of wastewater treatment plants. The paper uses data from a Polish wastewater treatment plant, processed into hourly averages. The process of data preparation, model construction and model training using Keras Tuner are described. Experimental results on 30 models showed the effectiveness of the LSTM network in forecasting, especially during stable weather conditions, with a relative error of less than 10%. The work highlights the potential of neural models in optimizing the operation of wastewater treatment plants, despite the difficulties in modeling flows during rainfall.

---

## 1. Introduction

The wastewater volume load is one of the most important factors affecting the operation of a wastewater treatment plant [1]. Depending on the season and the weather, the amount of wastewater flowing into a wastewater treatment plant can vary significantly. In Poland, where combined sewers dominate, municipal wastewater is mixed with rainwater, so that during the rainy season the amount of wastewater increases sharply. In contrast, during the dry season, the amount of wastewater is more regular and cyclical, depending on the rhythm of people's lives [4]. Under such conditions, it is easier to predict the amount of wastewater that will flow into the treatment plant in the coming hours, which can be useful for controlling the plant's equipment [4]. However, this is not a simple task, since each treatment plant has its own catchment characteristics that affect the flow of wastewater [4]. Therefore, simple theoretical rules cannot be applied, but a specific model must be developed for each treatment plant. Such a model should consider not only the amount of wastewater that will hit the treatment plant in a day, but also the degree of irregularity of inflow and flow for a specific hour with sufficient accuracy for control purposes.

Calculating the amount of wastewater expected to flow into the treatment plant in the near future is a task within the realm of time series analysis and forecasting. Time series are sequences of data points ordered in time, reflecting changes in specific phenomena. Time series analysis involves examining the statistical properties and structure of time series data, while time series forecasting entails predicting future values of time series based on historical data [8]. There are numerous methods for analyzing and forecasting time series, which can be broadly categorized into two main groups: classical methods and modern methods [12][15][2].

Examples of classical methods include trend analysis, moving averages, exponential smoothing, autoregression, AutoRegressive Integrated Moving Average (ARIMA), and regression modeling. "Modern" methods encompass machine learning techniques such as random forests, support vector machines (SVM), neural networks, as well as hybrid methods.

One of the more effective methods for time series analysis and forecasting involves the use of artificial neural networks [7]. Artificial neural networks, while not new, have been increasingly and boldly employed in engineering as an efficient way to identify complex relationships between effects and multiple concurrent causes [11][4][12]. Over the past few months, interest in artificial intelligence techniques has been particularly high, especially in the context of the latest advancements in neural networks (such as GPT). Artificial neural networks are inspired by the functioning of the human brain and consist of multiple interconnected elements called neurons. Neurons process input

signals and generate output signals, which are passed to subsequent layers of the network. During a process called network training, they learn from data and adjust their parameters to minimize the error between real values contained in the training data and predicted values calculated by the network. In other words, the network is trained based on training sets comprising "input" information and correct "responses." During training, the network's internal structure is fine-tuned so that after each training step – after one presentation of input data – the network provides a slightly better "response" to the given "question." This process, involving the presentation of input data, computation of the network's response, and modification of the network's structure to improve performance, is repeated for each input-output example from the training set, and when the entire set has been used, learning continues with the re-presentation of all sets. This is done many times (sometimes 10, other times 10,000 or more times) until the network's structure is adjusted to provide the best possible response. A single pass of presenting all training examples is called an epoch. Batch training is often used, where structural modification doesn't occur after each presentation of a training example but after the presentation of multiple examples. Batch training can speed up the training process and increase efficiency but may require more computational resources.

Modification of a network's structure usually involves adjusting the "weights" of connections between neurons, which are numerical values that determine the extent to which one neuron's influence affects another. In feedforward networks, which are the most commonly used, neurons in a deeper layer receive "signals" from neurons in the previous layer. Each neuron receives signals from multiple previous neurons simultaneously, but it assigns different strengths or "weights" to signals from different neurons. For example, a neuron from the previous layer might send a signal of "5," but it could be weighted by "0.1," resulting in an effective value of "0.5." All incoming signals to a neuron are summed and form the argument of the neuron's internal function, known as the activation function. This is a mathematical formula that determines how the sum of excitations should translate into the neuron's output signal, which is then passed through connections to subsequent neurons. In practice, various activation functions are used, such as the sigmoid function, ReLU (Rectified Linear Unit), etc., which dictate how the input signal is transformed into the output signal of the neuron. The choice of activation function depends on various factors, including the nature of the problem, model complexity, and issues like vanishing gradients during training.

In most cases, neural networks are organized into layers. However, there are also types of neural networks that do not have clearly defined layers.

Another important concept is distinguishing between supervised and unsupervised learning networks. The former, as described above, are trained using labeled data containing "inputs" and corresponding "outputs" or "responses." Unsupervised neural networks, on the other hand, do not require labeled training data. Unlike supervised networks, which need training data with "inputs" and corresponding "outputs," unsupervised networks learn from unlabeled data where correct responses are not provided. There are various techniques and types of unsupervised neural networks, but they generally work on principles of data clustering or dimensionality reduction.

Contemporary language models, such as transformers, are advanced artificial neural networks designed for natural language processing. Thanks to a special "attention mechanism," they can analyze long sequences of text, focusing on important elements. They are trained on vast datasets of textual data for various language tasks, such as automatic translation or text generation. Their architecture is hierarchical, consisting of multiple layers, allowing for the creation of complex language representations. Models like GPT (Generative Pretrained Transformer) differ from other types of neural networks in several key aspects: GPT employs the transformer architecture, which is significantly more complex than traditional neural networks. Transformers use an attention mechanism that allows the model to focus on crucial parts of the text when processing long sequences. GPT is trained on massive datasets of textual data.

Despite the widespread interest in neural networks, in the context of wastewater treatment technology, the use of artificial neural networks remains a relatively uncommon approach to problem-solving [12].

In this study, an attempt was made to predict short-term wastewater inflow to the treatment plant using "deep" neural networks with LSTM (Long Short-Term Memory) layers. Neural networks are referred to as "deep" when they have multiple layers of neurons or hidden neurons. The appropriate number of layers and hidden neurons enables the creation of models with greater capacity and the ability to detect complex data dependencies. In practice, there is no specific number of layers or neurons that a network must have to be considered "deep." However, in literature and

practice, the term "deep neural network" often refers to networks with many hidden layers, especially in the case of Convolutional Neural Networks (CNN) and Recurrent Neural Networks (RNN).

LSTM networks are a type of recurrent neural network (RNNs) primarily used in sequence data processing contexts. They were introduced to address the vanishing gradient problem, which is a common issue in standard RNNs. The problem arises during backpropagation (the learning process) when gradients (i.e., derivatives of the cost function with respect to the network's parameters) become progressively smaller. In extreme cases, gradients can become so small that they do not introduce significant changes to the network's weights, making it extremely challenging or even impossible to train the neural network.

The cost function in the context of machine learning and artificial neural networks is a mathematical function that measures the difference between the model's predicted values and the actual data. In other words, the cost function evaluates how much the model's predictions deviate from the ground truth. The goal of the learning process is to minimize this cost function, which means striving to achieve minimal errors in the model's predictions. In the context of training artificial neural networks, the cost function is used as an indicator that tells the network how close or far it is from the correct answers. The network attempts to adjust its weights and parameters to minimize the value of the cost function, signifying an improvement in the quality of its predictions. The derivatives of the cost function with respect to the network's parameters represent the rate of change of this cost function concerning all the parameter values, including the connection weights ("synaptic weights") and network parameters. These derivatives indicate in which direction and by how much the network's weights and parameters should be adjusted to reduce the cost function value. In other words, these derivatives guide the optimization process in how to adapt the network's weights to reduce the error and improve the quality of predictions. Optimization algorithms, such as "gradient descent," utilize these derivatives to iteratively update the network's weights towards minimizing the cost function. This iterative approach allows for the fine-tuning of the neural network's weights until it reaches the minimum value of the cost function, which is equivalent to optimizing the model.

In summary, in the context of artificial neural networks, the cost function is a measure of the error between predicted and actual data. Derivatives of this cost function with respect to the network's parameters are used in the optimization process to adjust the network's weights to minimize the error and enhance the model's prediction quality.

The process of training neural networks relies on optimizing the network's weights to minimize the cost function, which quantifies the difference between predicted and actual data. When gradients vanish, it means that these updates are very small, causing the network to learn very slowly or even fail to learn meaningful patterns in the data. The vanishing gradient problem is particularly evident in recurrent neural networks (RNNs), which process sequential data and have a recurrent internal structure. During backpropagation in RNNs, gradients can exponentially decrease as they propagate backward in time, resulting from repeated multiplication by weights and activation functions at each time step.

To address the vanishing gradient problem, various techniques and types of neural networks that are more resilient to this issue have been introduced. Examples include:

1. Long Short-Term Memory (LSTM): LSTM networks employ special gating mechanisms that allow controlled information flow through the network over long time intervals. This makes them more resistant to the vanishing gradient problem and better at learning long-term dependencies in sequential data.
2. Gated Recurrent Unit (GRU): Another type of recurrent neural network with similar goals to LSTM and designed to handle the vanishing gradient problem. It is more streamlined compared to LSTM and has fewer parameters.
3. Skip Connections: In convolutional neural networks (CNNs) and deep neural networks with many layers, such as ResNet, skip connections (also known as residual connections) are used between layers. These connections enable more efficient gradient propagation through the network and help address the vanishing gradient problem.
4. Gradient-Vanishing-Resistant Activation Functions: Some activation functions, such as Rectified Linear Unit (ReLU) and its variants, can mitigate the vanishing gradient problem compared to traditional activation functions like sigmoid or hyperbolic tangent.

Those solutions indeed aid in training deep neural networks, particularly in the case of networks processing sequential data where the preservation of temporal information is crucial. LSTM networks are specifically designed to capture long-term dependencies in sequential data, making them suitable tools for forecasting time series data and other data types where historical context matters for future predictions.

In LSTM networks, several specific mechanisms and techniques are employed to facilitate working with time series data:

1. **Forget Gate:** The forget gate controls which information from previous time steps should be forgotten and which should be retained. These decisions are made based on the current input and the hidden state from the previous time step.
2. **Input Gate:** The input gate controls which new information should be incorporated into the update of the hidden state. It is computed based on the current input and the previous hidden state.
3. **Output Gate:** The output gate regulates which information will be passed as the hidden state to the output of the LSTM cell. This is controlled based on the hidden state and the current input.
4. **Hidden State:** LSTM has its own hidden state, which acts as long-term memory and is updated at each time step.

Through the gate mechanisms, LSTM networks can focus on capturing long-term dependencies in time series data. This enables a better understanding of changes over time and the incorporation of previous patterns into forecasts. The gate mechanism allows for the selective storage and updating of information in the LSTM cell's memory. This means that important information can be preserved while less significant information can be discarded, improving the quality of predictions.

LSTM networks are flexible and can process sequences of varying lengths, which is common in time series analysis where the number of available data points may differ over time. Thanks to their ability to model complex temporal dependencies, LSTM networks can effectively handle forecasting tasks involving data with more intricate and nonlinear patterns [7][5][16].

## **2. Subject of Research, Data Preparation**

The research utilized data from a wastewater treatment plant located in southwestern Poland. The measurements included flow rates, typically recorded at one-minute intervals (although there may be missing data for certain minutes), over a period of nearly 71 months (6 years and 11 months). To train neural networks effectively, preliminary data preparation was necessary.

Sample data is presented in the chart below.

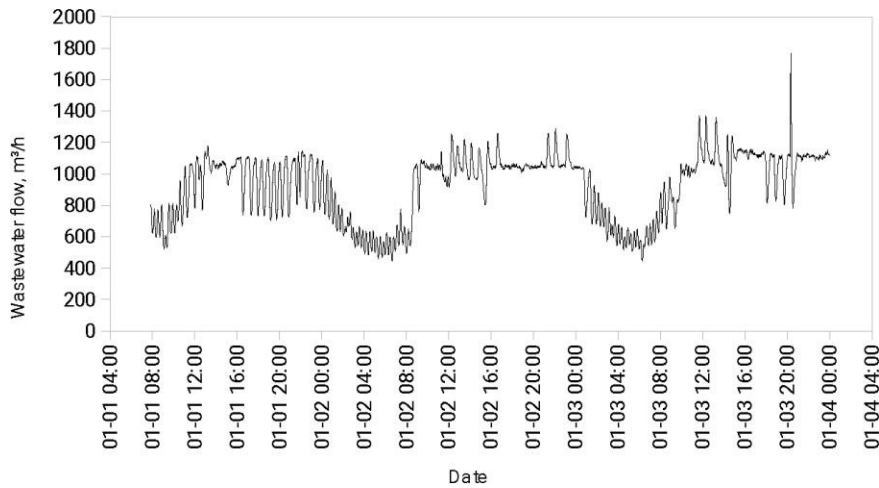


Fig. 1. A sample excerpt of unprocessed data representing the measurement of the raw wastewater flow intensity into the treatment plant is shown below. The oscillations are caused by the operation of the main pumping station

**Data Aggregation into Hourly Averages:** The first step in the data preparation process was to transform the raw wastewater treatment plant data into hourly average values. The purpose of this was to mitigate short-term flow fluctuations (pulsations) caused by the operation of the main pumping station, which were not indicative of the hydraulic load on the treatment plant. This processing was crucial because the neural network model needed to focus on learning long-term flow patterns rather than short-term fluctuations caused by technical infrastructure. This aggregation resulted in over 51,000 rows of data.

**Data Filtering:** After data aggregation, filtering was applied to remove days that did not contain a complete set of data (24-hour records). This step was essential to ensure a consistent and representative dataset for training. Eliminating incomplete data helped avoid modeling errors that could arise from incomplete or ambiguous information.

**Data Scaling:** Next, data scaling was performed, which is a standard practice in preparing data for neural networks. The purpose of scaling was to transform data values into a range that is more effectively processed by neural networks, increasing the stability and speed of the learning process. Scaling also allows for better comparison of features with different value ranges.

**Creation of Time Sequences:** The next step involved creating time sequences, which are essential for training LSTM models. LSTM networks are designed to work with sequential data, enabling them to efficiently learn and predict patterns in time-dependent data. These sequences were generated using a specified time window length, allowing the model to learn from a specific historical data interval.

The process of creating time sequence data occurs in several stages, which are essential for data preparation and modeling using recurrent neural networks such as LSTM (Long Short-Term Memory):

1. Determining the Length of the Time Window:

The length of the time window is defined as the number of consecutive time points that will be used in each sequence. This length determines the size of the window that encompasses the data. For example, setting the time window length to 24 hours allows for the analysis of data over a 24-hour period.

2. Sliding the Time Window in Time:

The process of creating sequences starts from the first data point and includes the next points within the specified time window. Then, the window is shifted forward by one time point, and the process is repeated. This way, each subsequent sequence contains data from the next time period, maintaining temporal continuity.

3. Assigning a Predicted Value to Each Sequence:



In the context of forecasting, each sequence is associated with a value to be predicted, such as the amount of wastewater flow in the next time unit. This value serves as the label for model training, allowing it to predict future values based on observations from a specific time window.

The primary goal of creating sequences is to enable recurrent models, such as LSTM networks, to efficiently learn and make predictions based on time-dependent data. This process transforms raw time-series data into a data structure compatible with the specific way these models operate. It provides the model access to historical information, which is crucial for accurate forecasting of future values.

Each sequence was assigned the average flow value for the next four hours as the flow prediction. This four-hour average served as the flow forecast. The neural network's task was to compute this forecast based on the 24 historical flow values.

**Division into Training and Testing Sets:** The final step in the data preparation process was to divide the sequences into training and testing sets. This division allowed for effective model training and its verification and evaluation on an independent dataset. This enabled the assessment of the model's ability to generalize and accurately predict on data that was not used during training.

The data was split into training and testing sets in an 80% to 20% ratio. Subsequently, the training set, comprising 80% of the total data, was shuffled and divided again into 80% for training and 20% for validation. This process enabled the monitoring and evaluation of the network's performance during training on data that it had not seen before, which is crucial for preventing overfitting.

During network training, using the validation set to assess its performance allowed for regular monitoring of the network's progress. The quality of predictions was evaluated based on the Mean Squared Error (MSE), calculated as the average of the squares of differences between expected values and values obtained by the network. After completing the training process, the model was tested on the remaining 20% of the data, which had been separated from the training set at the initial stage before the case shuffling procedure. This allowed for an assessment of how well the model performed in predicting data it had not been trained on, which is an important measure of its generalization ability.

In summary, careful data splitting into training, validation, and testing sets, along with their appropriate utilization in the training and evaluation process, enables the creation of an effective and reliable predictive model.

### 3. Hydraulic Load Forecast

The aim of the research was to determine the possibility of forecasting the amount of wastewater inflow to the wastewater treatment plant using modern neural network models, specifically LSTM (Long Short-Term Memory).

In the conducted research, Python programming language was used in conjunction with the Keras library, as well as the Keras Tuner tool for hyperparameter optimization of the neural network. The choice of these tools was driven by their specific features and benefits they offer in the context of time-series data modeling and working with neural networks.

Python is currently one of the most popular programming languages in the field of data science and machine learning. Keras is a high-level API for neural networks that operates on top of engines such as TensorFlow. Key features of Keras include an intuitive interface, modularity and flexibility, scalability, and performance. Keras Tuner is a tool for automated hyperparameter tuning of models built using Keras.

Keras Tuner, in addition to its primary role in hyperparameter optimization, also serves as an AutoML (Automated Machine Learning) tool. Its ability to automatically search the hyperparameter space and select optimal model configurations significantly simplifies and accelerates the process of building and tuning advanced neural network models. By employing Keras Tuner, the process of experimenting with different network structures and their parameters becomes more efficient and less time-consuming, which is particularly important when dealing with a large and complex hyperparameter space. This automation allows for quicker attainment of optimal solutions, which

is crucial in the rapidly evolving field of machine learning, where experiment time and efficiency are of great importance.

The neural network architecture for this project was defined as follows:

1. **LSTM Input Layer:** In the LSTM model, the first LSTM layer serves as the input layer. There is no dedicated "classical" input layer because the LSTM layer can directly take sequential data as input.
  - Parameters:
    - **Number of Units:** Ranging from 32 to 512. This range was chosen to balance the network's ability to learn complex dependencies in the data and the risk of overfitting. A higher number of units increases the model's learning capacity but also increases the risk of overfitting, requiring more data for effective training.
    - **L2 Regularization:** Ranging from  $1e-5$  to  $1e-2$ . L2 regularization is applied to prevent overfitting, especially in models with a large number of parameters, such as LSTM networks. Regularization in neural networks is a technique used to prevent overfitting, which occurs when the model becomes too closely fitted to the training data, losing the ability to generalize to new, unseen data. This is particularly important in complex models like deep neural networks, which are prone to memorizing training details at the expense of overall predictive ability. Regularization restricts the freedom with which the model can fit the training data, helping to maintain model simplicity, which, in turn, improves generalization.
2. **Second LSTM Layer:**
  - Parameters:
    - **Number of Units:** Same as in the first layer, ranging from 32 to 512. Repeating the same range for the number of units in both layers allows for flexible adjustment of the number of units in both layers during hyperparameter tuning. This provides the opportunity to explore different combinations of complexity in both LSTM layers based on the data's specifics.
3. **Dropout Layers (Dropout 1 and Dropout 2):** Ranging from 0 to 0.5. Dropout layers are placed after both the first and second LSTM layers. Their purpose is to prevent overfitting by randomly deactivating a portion of neurons during training. Choosing a range of dropout values allows for the exploration of different levels of this mechanism to find the optimal balance between the model's learning ability and generalization.
4. **Output Layer - One Unit:** The final layer of the network is a dense layer with one unit, which is a common choice for regression tasks. This layer aims to predict a single output value based on the features learned by the preceding layers of the network.
5. **Loss Function:** Mean Squared Error (MSE), a typical choice for regression tasks.

In each of these elements, the hyperparameter ranges were chosen to provide the model with sufficient flexibility to learn complex flow patterns in wastewater data while minimizing the risk of overfitting. Using two LSTM layers, each with independently tunable numbers of units, allows for in-depth modeling of sequential dependencies in the data.

During the network training, Keras Tuner used the defined model skeleton described in the previous sections as a base to construct and test various neural network variants. This process involved automatically selecting and modifying hyperparameters such as the number of neurons in the LSTM layers, regularization coefficient values, or dropout rates. The goal of Keras Tuner was to optimize these hyperparameters to identify a model that achieves the highest possible effectiveness in the forecasting task.

Keras Tuner, operating through an iterative exploration of hyperparameter space, conducted a series of training experiments. In each of them, based on a defined optimization algorithm, it selected different combinations of hyperparameters and evaluated the performance of the resulting model using metrics such as mean squared error (MSE). As a result, each subsequent attempt was directed towards improving the model by adapting to the specific characteristics of the data and the forecasting task.

During the hyperparameter optimization process, Keras Tuner not only examined individual parameter values but also analyzed how combinations of different hyperparameters influenced the model's performance. This allowed for the discovery of not only optimal values for individual hyperparameters but also the best combination of these parameters in the context of the entire model. Ultimately, the action of Keras Tuner led to the identification of a list of neural networks that provided the most accurate forecasts possible in the context of the amount of wastewater flowing into the treatment plant.

As a result of the experiment, 30 neural networks were obtained, each with varying prediction quality, from which the top five were selected. The parameters of these selected networks are presented in the tables below.

Table 1. Tabular representation of neural network 1.

Layer	Configuration
LSTM (Input)	batch_input_shape: (None, 24, 1); units: 512; activation: tanh; recurrent_activation: sigmoid; dropout: 0.0; recurrent_dropout: 0.0; kernel_regularizer: L2 (1.7403157471562736e-05)
Dropout	rate: 0.15
LSTM	units: 512; activation: tanh; recurrent_activation: sigmoid; dropout: 0.0; recurrent_dropout: 0.0
Dropout	rate: 0.0
Dense	units: 1; activation: linear

Table 2. Tasks performed by successive network layers.

Layer	Description
LSTM (Input)	The first LSTM layer, functioning as the input layer, processing time sequence data.
Dropout	Dropout layer, reducing the risk of overfitting by randomly deactivating certain connections.
LSTM	Second LSTM layer, continuing the processing of sequential data.
Dropout	Additional Dropout layer, providing extra protection against overfitting.
Dense	Output dense layer, transforming processed data into a single predicted value.

Table 3. Tabular representation of neural network 2.

Layer	Configuration
InputLayer	batch_input_shape: (None, 24, 1); dtype: float32
LSTM	units: 96; activation: tanh; recurrent_activation: sigmoid; dropout: 0.0; recurrent_dropout: 0.0; kernel_regularizer: L2 (5.717602834920399e-05)
Dropout	rate: 0.45
LSTM	units: 96; activation: tanh; recurrent_activation: sigmoid; dropout: 0.0; recurrent_dropout: 0.0
Dropout	rate: 0.4
Dense	units: 1; activation: linear

Table 4. Tabular representation of neural network 3.

Layer	Configuration
InputLayer	batch_input_shape: (None, 24, 1) dtype: float32

LSTM	units: 512 activation: tanh recurrent_activation: sigmoid dropout: 0.0 recurrent_dropout: 0.0 kernel_regularizer: L2 (0.00010070366261061281)
Dropout	rate: 0.3
LSTM	units: 512 activation: tanh recurrent_activation: sigmoid dropout: 0.0 recurrent_dropout: 0.0
Dropout	rate: 0.1
Dense	units: 1 activation: linear

Table 5. Tabular representation of neural network 4.

Layer	Configuration
InputLayer	batch_input_shape: (None, 24, 1) dtype: float32
LSTM	units: 352 activation: tanh recurrent_activation: sigmoid dropout: 0.0 recurrent_dropout: 0.0 kernel_regularizer: L2 (1.691463876341004e-05)
Dropout	rate: 0.0
LSTM	units: 352 activation: tanh recurrent_activation: sigmoid dropout: 0.0 recurrent_dropout: 0.0
Dropout	rate: 0.2
Dense	units: 1 activation: linear

Table 6. Tabular representation of neural network 5.

Layer	Configuration
InputLayer	batch_input_shape: (None, 24, 1) dtype: float32
LSTM	units: 256 activation: tanh recurrent_activation: sigmoid dropout: 0.0 recurrent_dropout: 0.0 kernel_regularizer: L2 (3.54105286533013e-05)
Dropout	rate: 0.0
LSTM	units: 256 activation: tanh recurrent_activation: sigmoid dropout: 0.0 recurrent_dropout: 0.0
Dropout	rate: 0.15
Dense	units: 1 activation: linear

The table below shows selected forecast parameters for the top five networks:

Table 7. Forecast parameters for the top five networks.

Network number	Parameter	Expected value	Calculated value	Error	Relative error	Square error
1	Average value	866,24	890,50	74,50 (MAE)	9,04% (MAPE)	13218,91(MSE) 114,97(RMSE)
	Standard deviation	226,96	192,99	87,56	10,49%	45 801,85
	Standard error	2,48	2,11	0,96	0,11%	501,02
2	Average value	866,24	899,47	74,50 (MAE)	9,04% (MAPE)	13774,27(MSE) 117,36(RMSE)
	Standard deviation	226,96	197,80	87,84	10,53%	45 470,34
	Standard error	2,48	2,16	0,96	0,12%	497,40
3	Average value	866,24	899,43	79,90 (MAE)	9,95% (MAPE)	13963,85(MSE) 118,17(RMSE)
	Standard deviation	226,96	187,82	87,05	10,69%	45 871,69

Network number	Parameter	Expected value	Calculated value	Error	Relative error	Square error
	Standard error	2,48	2,05	0,95	0,12%	501,79
4	Average value	866,24	892,56	75,34 (MAE)	8,95% (MAPE)	13428,90(MSE) 115,88(RMSE)
	Standard deviation	226,96	203,74	88,03	10,19%	45 492,91
	Standard error	2,48	2,23	0,96	0,11%	497,64
5	Average value	866,24	876,48	70,99 (MAE)	8,30% (MAPE)	13245,82(MSE) 115,09(RMSE)
	Standard deviation	226,96	205,90	90,57	10,18%	47 853,25
	Standard error	2,48	2,25	0,99	0,11%	523,46

Analyzing the obtained values for the top five neural networks, it's worth focusing on the Mean Absolute Percentage Error (MAPE) values, which ranged from 8.30% to 10.69%. It can be observed that all models exhibit a comparable level of accuracy. These values, although relatively low, need to be considered in the context of wastewater treatment plant operations. A low MAPE value indicates that the model is capable of generating forecasts that are a good approximation to the actual values. Typical flow measurement errors in sewage systems and wastewater treatment plants often fall within a range of a few percent. The MAPE values obtained in the study, while higher than typical measurement errors, should be considered acceptable, given the variability and unpredictability of wastewater flows. It's important to remember that no forecasting model will be perfect, especially in the context of such a variable and dynamic environment as a sewage system. MAPE values below 10% are therefore considered very good results in this context, suggesting that the models can effectively predict wastewater flows with sufficient operational accuracy.

In summary, the MAPE values obtained in the study indicate the high effectiveness of neural network models in predicting wastewater flow, which is crucial for efficient management of processes in treatment plants. These values, although higher than typical measurement errors, are sufficiently low to enable effective planning and response to changing operational conditions in the treatment plants.

In the study, the process of training neural networks was organized in a way that ensured their robust verification and evaluation of generalization abilities. Out of all the available data, 80% was used as the training set, while the remaining 20% constituted the test set, not participating in the training process. To provide a more accurate assessment of the model, the training set was further divided into two parts: 80% of the data were directly used for training the network, while the remaining 20% were used to validate the model during the training process. The purpose of validation was to monitor the model's performance on data that were not directly used for tuning the network's weights, thus avoiding the problem of overfitting.

After completing the training process, the top five networks were selected, evaluating their performance on the validation set. These networks were then used to predict wastewater flow based on an independent test set, which constituted the original 20% of data that were not used in any phase of training. This allowed for a precise evaluation of how the models performed in predicting data that had not been "seen" by the network before.

Interestingly, the fifth network, although not the best during validation in the training phase, turned out to be the most effective in predicting test data. This indicates its ability to generalize better compared to the other models. This observation underscores the importance of evaluating models not only on validation data but also on an independent test set to truly understand their ability to predict under real operational conditions.

In the chart below, sample flow prediction results are presented. Ten measurement days were selected during which atypical flow, associated with rainfall, was also recorded.

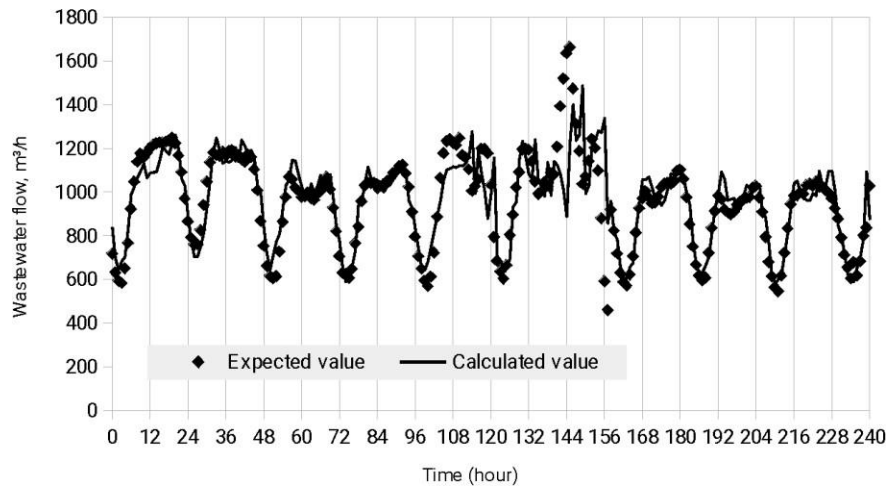


Fig. 2. Sample flow forecast results

The analysis of sewage flow forecast results indicates significant variations in the model's accuracy depending on weather conditions. During periods of stable, dry weather, the model achieves high forecast precision, reflected in low error values. This is due to the regularity and predictability of flow patterns under such conditions, where external factors have a lesser and more consistent impact on the sewage system. However, in rainy weather conditions, when sewage flows become more chaotic and variable due to additional influences like rainwater entering the sewage system, the model shows lower accuracy. This phenomenon results from the difficulty in modeling atypical and irregular flow patterns characteristic of rainy situations. Rainfall can cause abrupt and unexpected changes in sewage quantity, significantly complicating the forecasting task. From an operational perspective, the ability to forecast regular flows in dry weather conditions is still valuable as it allows for planning and optimizing wastewater treatment processes under typical operating conditions. For rainy conditions, where flows are more variable, it is important to develop methods for handling this variability, such as creating flow buffering or increasing the operational flexibility of systems. While models may not precisely predict flows in rainy conditions, the forecasted values in such situations can still provide useful information for operators. For example, detecting trends of increased flows can serve as an early warning of potential system overloads, enabling appropriate preventive actions. In summary, although rainy flows may exceed the current capabilities of precise modeling, MAPE values below 10% for forecasts in dry weather conditions demonstrate the high utility of neural network models for wastewater treatment management. The unpredictability of rainy conditions remains a challenge that requires further research and innovative modeling approaches.

#### 4. Conclusions

In summary, the application of deep LSTM neural networks in the analysis and forecasting of hydraulic loads in wastewater treatment plants has proven to be a promising approach. The study conducted on data from a Polish wastewater treatment plant showed that LSTM networks can effectively predict wastewater flows, especially during rainless periods. Data preparation involved aggregating hourly averages, filtering days with incomplete data, and then scaling and creating time sequences, which served as the basis for training and testing models.

The use of Keras Tuner allowed for efficient fine-tuning of network hyperparameters, leading to the selection of the five best models capable of forecasting with a relative error below 10%. Although the accuracy of forecasts decreased during rainy conditions due to increased irregularity and variability of flows, the obtained results are promising and indicate practical applications of neural networks in the control and optimization of wastewater treatment processes.

The conclusions of the study suggest that further research and model development may contribute to improving their performance and generalization abilities, especially under variable rain-induced loads. Additionally, these results can serve as a starting point for further exploration of the potential applications of artificial intelligence in urban and environmental infrastructure management.

## Acknowledgment

The work was carried out as part of statutory research.

## 5. References

- [1] Adhikari, R., & Agrawal, R. An Introductory Study on Time Series Modeling and Forecasting. ArXiv. <https://www.semanticscholar.org/paper/An-Introductory-Study-on-Time-Series-Modeling-and-Adhikari-Agrawal/0658264c335017587a906ceb202da417b5521a92>, (2013).
- [2] Benboubker, G., Kissani, D. I., & Mourhir, D. A. (2019). Comparative Analysis in Sales Forecasting: Classical Methods and Neural Networks.
- [3] Bhawe, P. P., Naik, S., & Salunkhe, S. D. (2020). Performance Evaluation of Wastewater Treatment Plant. *Water Conservation Science and Engineering*, 5(1–2), 23–29. <https://doi.org/10.1007/s41101-020-00081-x>
- [4] Dastres, R., & Soori, M. (2021). Artificial Neural Network Systems. *International Journal of Imaging and Robotics*, 21, 13–25.
- [5] Dhake, H., Kashyap, Y., & Kosmopoulos, P. (2023). Algorithms for Hyperparameter Tuning of LSTMs for Time Series Forecasting. *Remote Sensing*, 15(8), Article 8. <https://doi.org/10.3390/rs15082076>
- [6] Ehalt Macedo, H., Lehner, B., Nicell, J., Grill, G., Li, J., Limtong, A., & Shakya, R. (2022). Distribution and characteristics of wastewater treatment plants within the global river network. *Earth System Science Data*, 14(2), 559–577. <https://doi.org/10.5194/essd-14-559-2022>
- [7] Elsworth, S., & Güttel, S. (2020). Time Series Forecasting Using LSTM Networks: A Symbolic Approach (arXiv:2003.05672). arXiv. <https://doi.org/10.48550/arXiv.2003.05672>
- [8] Hewamalage, H., Bergmeir, C., & Bandara, K. (2021). Recurrent Neural Networks for Time Series Forecasting: Current Status and Future Directions. *International Journal of Forecasting*, 37(1), 388–427. <https://doi.org/10.1016/j.ijforecast.2020.06.008>
- [9] Icke, O., Van Schagen, K., Huising, C., Wuister, J., Van Dijk, E., & Budding, A. (2017). Flow intake control using dry-weather forecast. *Drinking Water Engineering and Science*, 10(2), 69–74. <https://doi.org/10.5194/dwes-10-69-2017>
- [10] Mannina, G., & Viviani, G. (2009). Separate and combined sewer systems: A long-term modelling approach. *Water Science and Technology*, 60(3), 555–565. <https://doi.org/10.2166/wst.2009.376>
- [11] Mehlig, B. (2021). Machine learning with neural networks. Publisher: Cambridge University Press. <https://doi.org/10.1017/9781108860604>
- [12] Qiu, X. (2023). The Application of Artificial Intelligence – Artificial Neural Networks – in Wastewater Treatment. *E3S Web of Conferences*, 393, 03003. <https://doi.org/10.1051/e3sconf/202339303003>
- [13] Salah, H., Hussein, M., & Zahran, I. (2021). Comparative Study between Classical Methods (CM) and Machine Learning Algorithms (MLA) for Time Series Forecasting. *Engineering Research Journal (Shoubra)*, 50(1), 29–40. <https://doi.org/10.21608/erjsh.2021.224658>
- [14] Shiruru, K. (2016). AN INTRODUCTION TO ARTIFICIAL NEURAL NETWORK. *International Journal of Advance Research and Innovative Ideas in Education*, 1, 27–30.
- [15] Velicer, W., & Fava, J. (2003). *Time Series Analysis (Vol. 2)*. <https://doi.org/10.1002/0471264385.wei0223>
- [16] Xiao, F. (2020). Time Series Forecasting with Stacked Long Short-Term Memory Networks (arXiv:2011.00697). arXiv. <https://doi.org/10.48550/arXiv.2011.00697>

# Application of walnut shells as a fuel and alternative reducer of slags from non-ferrous metallurgy industry

Lukasz Myćka<sup>1</sup>, Jerzy Łabaj<sup>2</sup>, Łukasz Kortyka<sup>3</sup>, Piotr Madej<sup>3</sup>, Tomasz Sak<sup>3</sup>, Rafał Michalski<sup>3</sup>, Piotr Palimąka<sup>4</sup>, Andżelika Bukowska<sup>5</sup>

<sup>1</sup>Lukasiewicz Research Network – Institute of non-Ferrous Metals  
email: lukasz.mycka@imn.lukasiewicz.gov.pl

<sup>2</sup>Silesian University of Technology

<sup>3</sup>Lukasiewicz Research Network – Institute of non-Ferrous Metals

<sup>4</sup>AGH University of Krakow

<sup>5</sup>Lukasiewicz Research Network – Krakow Institute of Technology

---

## Abstract

In this paper, research was carried out on the reduction of slags with biomass in the form of walnut shells. The reduction was realised at 1400 °C and a holding time of 2 h. The addition of bioreducer was 2, 5, 7 and 10 % by weight of the feedstock. The reduction efficiency was also compared with that of coke, which was added at 5 and 10 %. The best Cu and Pb yields were observed for a bioreducer addition of 10 %. Under the experimental conditions, coke proved to be a less effective reductant..

**Keywords:** biomass, walnut shells, slag, bioreduction

---

## 1. Introduction

One of the several energy sources developed and used on a large scale is biomass, which is an organic material that is biodegradable. This material includes different types of waste fractions from agriculture, forestry and industry (wood, woodworking industry). The most common biomass is plants or plant-based materials that are combusted to produce energy in the form of heat. Biomass on an industrial scale is produced from millet, hemp, maize, sugar cane, rapeseed, sunflower and many other plant species and trees. At present, it is mainly used to produce electricity and heat. The application attractiveness of biomass itself, as well as its derivatives, is the fact that the carbon it contains comes entirely from the atmosphere. As a result of the use (combustion) of biomass, carbon is released from it into the atmosphere and subsequently absorbed by the new crop through photosynthesis. Therefore, by using biomass, the CO<sub>2</sub> balance in the atmosphere is not altered, making it seen as a neutral source of CO<sub>2</sub> emissions and its very rapid renewability places it in the category of renewable raw materials (EU Parliament and Council Directives: 2018/2001, 2009/28WE, 2014/94). Another important advantage for the use of biomass compared to other renewable energy sources (wind, solar, water) is the possibility to locate biomass processing facilities close to biomass growing areas, which has a positive impact on reducing costs and facilitates the logistics of such projects [1-3]

One biomass material frequently found in the literature is walnut shells. In the work submitted here, it was decided to use this material as an alternative bioreducer to coke [4].

## 2. Characteristics of the experimental feedstock

Two materials were used in the experiments. The first was slag from non-ferrous metallurgy. The second material was crushed walnut shells.



## 2.1 Physical and chemical properties of slag

The slag used in this paper was metallurgical slag of industrial origin (copper metallurgy) with a significant content of such non-ferrous metals as Cu and Pb. Among other metals, the slag also contained significant amounts of Fe, small amounts of Zn, As, Co, Ni. The other components were typical slag-forming additives in the form of Si, Ca, Al, Mg compounds. A more detailed chemical analysis is presented in table 1.

Table. 1. Chemical composition of slag

Element	O	Cu	Pb	Si	Fe	Ca	C	Al	K	Mg	As	Zn	Co	Ni	Ti	Mn	Mo
Concentration [%]	25,08	17,25	14,10	13,15	11,70	5,57	3,36	2,43	1,55	1,22	1,16	0,92	0,55	0,29	0,18	0,15	0,12

In order to determine the reduction process parameters, it was necessary to determine physical properties such as softening onset temperature, softening temperature and melting point, and viscosity. The first three parameters were determined using the Bunte-Baum-Reerink method. The viscosity, in turn, was determined using a rotating viscometer.

Based on the study conducted and the results obtained, it was determined that the softening onset temperature ( $T_p$ ) was 788 °C, the softening temperature ( $T_m$ ) 857 °C and the melting temperature ( $T_t$ ) 891 °C.

A diagram of the viscosity of the slag as a function of its temperature is shown in the figure 1. Based on the test carried out and the results obtained, it was determined that the lowest viscosity values of the slag start to adopt from a temperature of about 1200 °C (1206 °C - 3285 cP). Below 1200 °C, the viscosity already changes significantly.

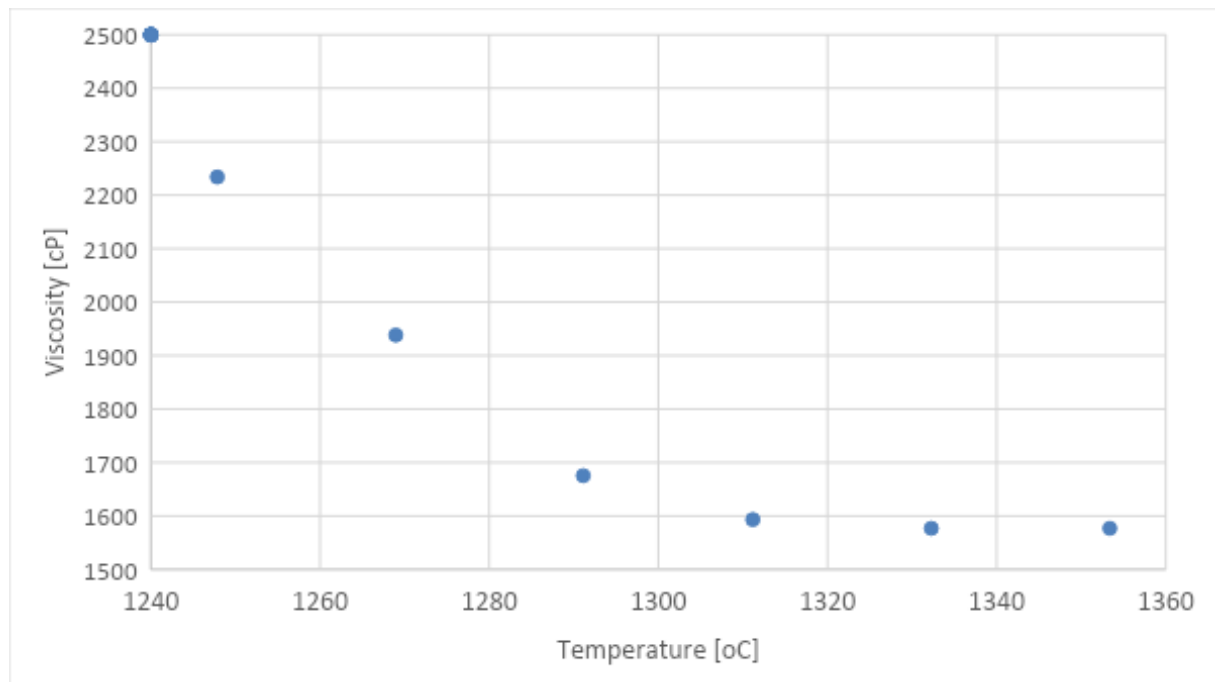


Fig. 1. Slag viscosity as a function of temperature

## 2.2 Walnut shells properties

Parameters such as chemical composition, heat of combustion, reactivity and proportion of fractions formed during their thermal decomposition at 25-600 °C were determined for them. The total is summarised in table 2.

Table. 2. Physico-chemical properties of walnut shells

Heat of combustion [j/g]	CO <sub>2</sub> reactivity [%]	Composition [%]		Proportion of fraction [%]		
		C	O	solid	liquid	gass
20154	99,53	45	54	26	41	33

Walnut shells represent a fuel with a relatively high heat of combustion compared to other biomass materials. Like most biomasses, they are characterised by very high reactivity. The C content of the submitted material is high at up to 45 % [5]. Anaerobic thermal decomposition of the material has shown that it contains significant amounts of volatile parts. It is probably these that are responsible for this high reactivity.

### 3. Conduct and results of experiments

Based on studies of the physico-chemical properties of the slag, i.e. composition, melting point and viscosity, it was determined that running the experiments at 1400 °C should allow satisfactory levels of metallic phase yield to be achieved. During the experiments, the reductant was placed at the bottom of the crucible and successively covered with slag and then placed in the furnace. The furnace was heated from about 20 °C with the sample to 1400 °C and held for 2 hr. After this time, the furnace was cooled spontaneously. On each occasion, the mass of the slag was about 200 g while the mass of the reductant was 2, 5, 7 and 10 % of the slag mass. For reference purposes, two experiments were carried out to reduce the slag with coke at 5 and 10 % relative to the slag mass. After the furnace had cooled, the solidified samples were removed from the furnace. The slag was separated from the reduced metallic phase and the products weighed. Subsequently, the slag was milled, the metallic phases were chipped and subjected to chemical analysis by XRF. The results of the experiments are shown in table 3.

Table. 3. Results of the experiments

Reducing agent	Reducing agent [%]	Reducing agent [g]	Slag [g]	Alloy [g]	Postreduction slag [g]
Walnut schells	2	4,03	200,01	-	-
	5	10,00	200,01	35,97	156,04
	7	14,01	200,00	40,46	149,69
	10	20,01	200,00	50,47	136,69
coke	5	5,00	200,06	22,31	150,90
	10	10,00	200,01	30,80	144,59

Basically, the indicator that determines the effectiveness of a particular reduction process is the mass of the metallic phase (alloy) obtained. The higher the mass, the better the reduction. For the bioreducer, in the case of an addition of 2 %, no metallic phase was obtained. For subsequent additions, the mass of the resulting alloy increased (36 g, 40 g and 50 g). In the case of coke addition (5 and 10 %), the mass of the alloy was 22 and 31 g, i.e. noticeably lower than for the same nut shell additives. In order to present the results more clearly, they have been summarised as a bar diagram (figure 2).

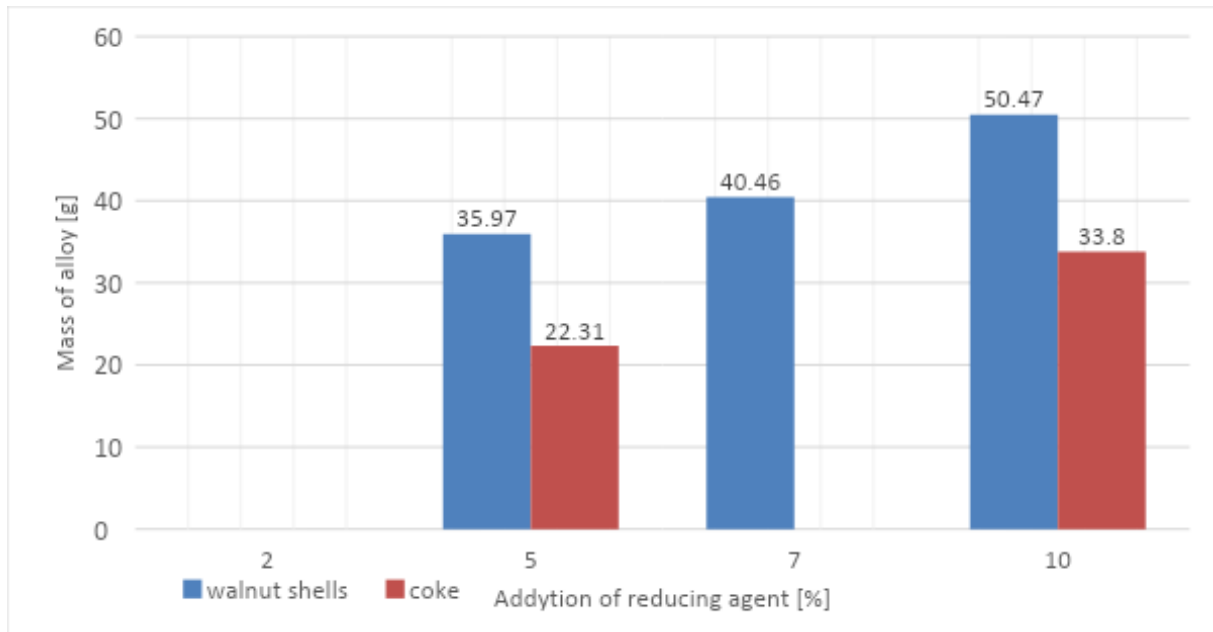


Fig. 2. Composition of alloys and obtaining Cu and Pb

The table 4. shows the results of chemical analyses for both alloys and slags. Based on these analyses and the weights of the charge and the individual products, the yields for Cu and Pb, the metals of most interest in these experiments from the point of view of non-ferrous metallurgy, have been determined.

Table. 4. Composition of alloys and obtaining Cu and Pb

Addition of reducing agent	Alloy						
	Composition [%]			Yield[g]		Yield [%]	
	Cu	Pb	Fe	Cu	Pb	Cu	Pb
5	76,91	20,56	0,19	27,66	7,40	80,18	26,22
7	70,7	26,89	0,03	29,49	9,96	85,47	35,31
10	66,6	29,4	0,58	33,61	14,84	97,43	52,62

The highest Cu yields were noted for Cu and Pb with the highest 10 % addition of walnut shells. Yields for Cu were close to 97.5 %, while for Pb they exceeded 52.5 %. The relatively low yield of Pb relative to Cu is due to the characteristics of this metal, i.e. its high vapour pressure. Small amounts of Fe were found in all the alloys obtained. In order to present the results more clearly, they have been summarised in the form of a bar diagram (Figure 3).

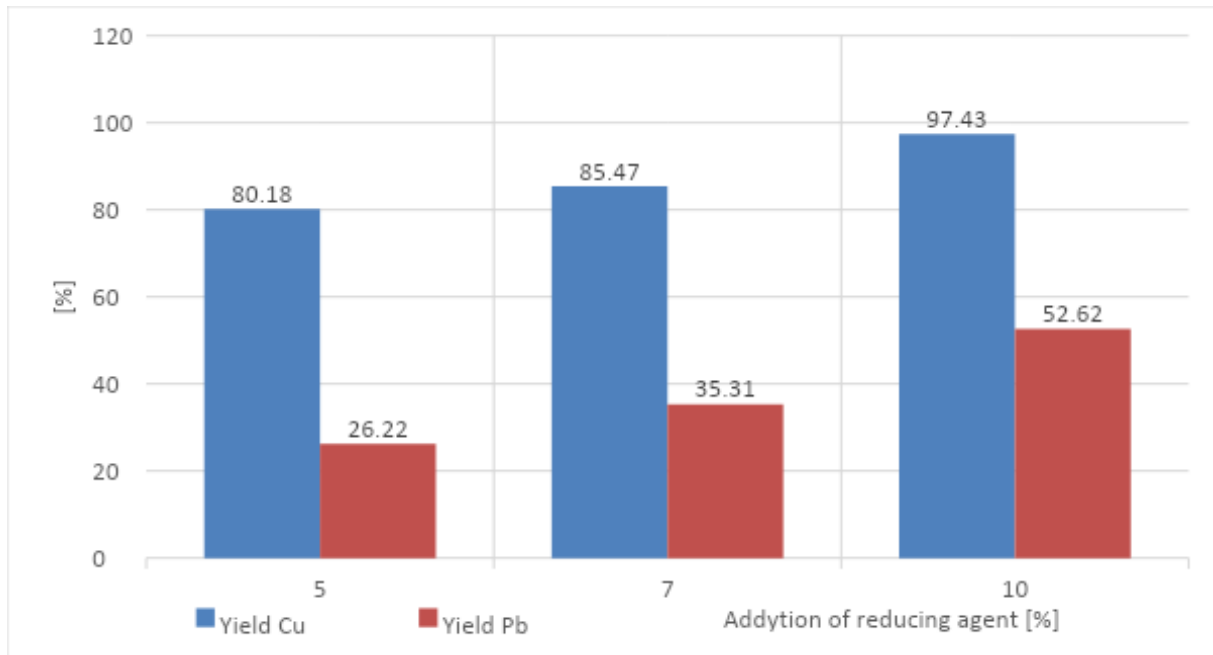


Fig. 3. Bar diagram of Cu and Pb yields

#### 4. Conclusions

- Walnut shells are a slag-reducing material.
- The highest Cu and Pb yields were noted with the addition of 10 % bioreducer (97,4 %, and 52,6 %).
- It is probable that a slight rise in the addition of bioreducer above 10 % will allow a higher yields of Cu and Pb.
- In the conditions of the experiments conducted, the bioreducer proved to be more effective than the coke (38 % in 5 % of reducing agent addition and in 33% in 10 % addition).

#### References

- [1] Magdalena Chmielowiec, *Biomasa jako źródło energii odnawialnej w Unii Europejskiej i w Polsce – zagadnienia ekonomicznoprawne*, Energia Gigawat - 5/2020, 2020.
- [2] Rozporządzenie Komisji (UE) nr 651/2014 z dnia 17 czerwca 2014 r. uznające niektóre rodzaje pomocy za zgodne z rynkiem wewnętrznym w zastosowaniu art. 107 i 108 Traktatu.
- [3] Produkcja biomasy na potrzeby własne energetyki. Forum Biomasy, 2012
- [4] Magdalena Dudek, Bartosz Adamczyk, Maciej Sitarz, Michał Śliwa c, Radosław Lach, Marek Skrzypkiewicz, Andrzej Raźniak, Magdalena Ziąbka, Jarosław Zuwała, Przemysław Grzywacz, *The usefulness of walnut shells as waste biomass fuels in direct carbon solid oxide fuel cells*, *Biomass and Bioenergy*, Volume 119, Pages 144-154, 2018.
- [5] Ł. Myćka, P. Madej, J. Łabaj, Ł. Kortyka, Ł. Jaworek, *Calorimetric research on selected types of biomass in the context of application in non-ferrous metallurgy*, Contemporary Problems of Environmental Protection and Energy 2022, Silesian University of Technology, Gliwice, 2023.

# Biodegradability and Kinetics of anaerobic co-digestion of coffee husk with food waste: Effect of mixing ratio and initial pH value

Mohammed Kelif Ibro\*<sup>1</sup>, Venkata Ramayya Ancha<sup>2</sup> and Dejene Beyene Lemma<sup>3</sup>

<sup>1</sup>Faculty of Mechanical Engineering, Jimma Institute of Technology, Jimma University, Jimma, Ethiopia, e-mail: mohamedkelifa@obu.edu.et

<sup>2</sup>Faculty of Mechanical Engineering, Jimma Institute of Technology, Jimma University, Jimma, Ethiopia, e-mail: dra.venkata@ju.edu.et

<sup>3</sup>Faculty of Civil and Environmental Engineering, Jimma Institute of Technology, Jimma University, Jimma, Ethiopia, e-mail: dejene.beyene@ju.edu.et

## Abstract

The optimization of operational parameters is crucial to maximizing biogas yield and quality. The impact of food waste (FW)/coffee husk (CH) ratios (100:0, 60:40, 50:50, 40:60, and 0:100) and initial pH values (5, 6, 6.5, and 7.5) on biogas yield and the biodegradability of the FW and CH co-digestion was studied under mesophilic conditions. First-order kinetic, modified Gompertz, and modified logistic models were also applied to fitting experimental results, to explain the kinetics of the co-digestion process. The findings showed that adding FW and increasing initial pH levels could greatly upgrade CH biogas production and biodegradability. The highest biogas yield was 540.78 ml/gVS and synergy of 1.46, with the highest biodegradability ( $BD_{fpc}$ ) and biodegradation degree ( $\eta_{BD}$ ) of 85.64 and 56.80%, respectively, for FW/CH ratio of 60:40 and pH 7, 164% raised compared to that 204.71 ml/gVS of the CH alone. A modified logistic model outperformed others with the best fitness. The synergistic effect evaluation disclosed that the synergy of the joint treatment of feedstocks might be the reason for the upgraded biogas yields. This study demonstrated the feasibility and attractiveness of co-digestion of FW and CH, affording a sound basis for cost-effective renewable energy recovery.

**Keywords:** Co-digestion, Biodegradability, Kinetic model, coffee husk, food waste, biogas

## 1. Introduction

Today, rapid population growth, and urbanization with industrialization, which require high-energy demand coupling waste management have emerged as major concerns challenging the world, which may result in global warming which is a call for sustainable solutions. The conversion of low-value biowastes into valuable products (biomethane and organic fertilizer) can be an interesting alternative due to providing clean energy [1] and meeting the requirements for waste management [2]. Burning of biogas produces less poisonous pollutants in addition to CO<sub>2</sub> and has a smaller acidification potential than other systems [3]. Apart from landfills, anaerobic digestion (AD) is a long-established bioenergy technology that is most cited for waste treatment and handling massive organic wastes, hereby ending the global bioenergy-supply gap. Biogas production leads to proper waste collection and management [4]. This practice decreases bio-waste disposal and management cost, which make it more competitive in a worldwide economy [5].

FW involves a larger constituent of municipal solid waste, which comprises restaurant, and canteen waste, household FW, and food-processing waste. Globally, 1.3 billion tons of edible food is wasted annually, and around 3.3 billion tons of greenhouse gas is released [6]. Owing to the high moisture level, the FW naturally decomposes quickly a few days after collection, posing health risks, social problems, and environmental issues [7]. However, in biological valorization processes, this kind of waste may be preferred. FW is composed of high levels of organic materials like proteins, carbohydrates, and lipids, making it a perfect renewable resource [8]. Despite the high potential of FW to produce biogas, it also has some constraints for AD, mainly the VFA production in high concentrations, which can affect the pH value and become poisonous for the growth of microorganisms [9]. Thus, AD of FW is bottlenecked due to the formation of an excessive volume of VFA, which will inhibit microbial actions and digestion rate. As per the reviewed study, this may lead to the failure of the AD process at a loading rate over 2.5 gVS/l.d, typically under thermophilic conditions. The joint treatment of FW with other waste delivers micro/macro-nutrients and alkalinity to overcome the instability faced in mono-digestion of FW [10]. Co-digestion optimizes the carbon-nitrogen (C/N) ratio, enhances nutrient balance [11], improves buffering capacity and subsequent digestion efficiency [12], and drops the free ammonia concentration [13]. As noted in advance, to resolve the system's instability, anaerobic co-digestion of food waste with compatible substrates like lignocellulose is an alternative to improve the system's performance and

products. In line with these benefits, FW is mainly co-digested with lignocellulosic materials [14], which may assist in neutralizing the toxic substance, improving hydrolysis kinetics, and boosting nutrient balance in the digesters [15]. Coffee husk is one of the lignocellulosic residue that compatible with food waste for effective biogas production.

Coffee is one of the world's leading agricultural products, mainly used for producing beverages that are consumed daily by millions of people. However, coffee processing from fruit to cup generates a large amount of coffee residues. For instance, it was reported that around 1 ton of pulp and husk was produced, where husks are about 50% of dry coffee cherries [16]. In Ethiopia, coffee husks are considered an economically no-value by-product and are discarded in streams and open dumps without important application or treatment. This improper disposal of coffee waste not only causes loss of biomass energy and land resources but also can cause environmental harm such as water eutrophication, salinization of soils, and toxic effects on some biological processes. These aspects have limited its application in agriculture [17]. In addition, caffeine and transition metals in coffee husks can cause DNA damage and present toxicity to aquatic organisms [18]. In contrast, the coffee husk is a lignocellulosic residue that is rich in carbohydrates (70%) with 7-29% of hemicellulose and 16-43% of cellulose as well as volatile matter evidences the existence of biodegradable organic contents meet the potential of biogas production [17]. However, due to lignin and imbalanced nutrient composition, the hydrolysis of this biomass is a rate-limiting step; the existence of easily biodegradable and good permeation of microbes past the surface does not occur. Lignin is a complex structure in nature that hinders both hydrolysis and the surface areas accessible for microbial action to degrade biomass. This drawback can be overcome by co-digestion with food waste. Food waste is applied to speed up hydrolysis and disintegrate lignin [11].

Operating factors (parameters) play a vital role in determining the efficiency and productivity of anaerobic digestion processes. These parameters include temperature, substrate composition, substrate mixing ratios, pH level, hydraulic retention time (HRT) [19], and organic loading rate (OLR). The composition of the feedstock being used can also have a key impact on biogas production. Different substrates have different nutrient content, biodegradability rates, and chemical characteristics, which can affect the microbial community and overall biogas production [12]. The role of mixing ratio optimization in co-digestion is to optimize the overall mixture of different types of organic materials with varying nutrient concentrations to maximize biogas production [20]. By combining easily degradable feedstocks like food waste to a digester with coffee processing residues like CH, the hydrolysis kinetics may be balanced, and biomethane production improved [21]. The initial pH level plays a significant role in desired biogas production as it affects the activity of microorganisms involved in the anaerobic digestion process. The optimum pH range for biogas production is between 6.5 and 7.5, which is somewhat alkaline [22]. At this range, the microorganisms responsible for breaking down organic matter into biogas are most active and efficient. If the initial pH is too low (acidic), it can inhibit the growth and activity of biomethane-producing microorganisms, resulting in a decrease in biogas production. On the other hand, if the pH value is too high (alkaline), it can lead to the growth of undesirable microbes that compete with biomethane-producing microbes, causing a decrease in biogas yield [11]. Co-digestion is significant for maintaining the optimal pH level in a digester, which is necessary for the health of anaerobic microorganisms [13]. Generally, adjusting these cooperating parameters is important for attaining maximum biogas production and quality.

Applying kinetic models is greatly important to estimate the system performance in the anaerobic co-digestion system that helps to predict the real-scale biogas plant [13]. Kinetic models might describe the feed degradation rate and microbial growth efficiency. The first-order kinetics equation determines the cumulative biogas production and hydrolysis kinetic constant;  $k$  is the crucial kinetic parameter, and it is deliberated as the rate-limiting step that governs the process. The modified Gompertz and Logistic equations are S-shape functions and are usually compared to elucidate exponential bacterial growth. Through these non-linear regression models, the biogas production rate, lag phase, and biogas potential were determined using experimental values. Although both models appear to be similar, the major difference between them is that the curve of the modified Gompertz equation is symmetrical, while that of the modified logistic model is asymmetric [23]. Both models fit gas production and assume that the gas production rate is directly proportional to the volume of produced gas and to the maximum gas production capacity [24].

Regarding the performance and kinetic analysis of the anaerobic co-digestion process, it is important to investigate the detailed interactive effect prompted by the digestion of FW with CH. There have been several studies exploring biogas generation from the anaerobic co-digestion of FW with lignocellulosic materials but no previous literature documented the co-digestion of cooked food waste with coffee husk at different initial conditions (mixing ratios and initial pH levels). Consequently, this research aimed to explore the synergistic effect of FW and CH co-digestion at different mixing ratios and initial pH values at a blend of FW/CH (1.5) on biogas production and biodegradation rates. The appropriate models reported in previous studies in simulating biogas yield, like first-order kinetic, modified Gompertz, and Logistic equations were also applied, which would be an important extension of their applicability for describing the methanogenesis process of co-digestion with a synergistic effect. This research will make available scientific information for bioenergy production via co-digestion of coffee husk and food waste.

## 2. Materials and methods

### 2.1 Substrates and inoculum

Coffee husk was collected from a dry coffee processing plant found in the Agaro, Jimma zone, Oromia Regional State. The collected sample was crushed using a coffee grinder for easy microbial degradation in the lab-scale biodigester. FW was collected from the student dining hall of the Jimma Institute of Technology. The FW mainly contained cooked food leftovers, including pasta, rice, meat, injera leftovers, and potato residue. The FW was homogenized after impurities such as bones were manually removed to achieve a uniform mixture of organic contents. They were transported to Addis Ababa University Biochemical Engineering Laboratory. The inoculum-containing consortium of anaerobes was collected from an active laboratory biodigester treating animal dung at mesophilic temperature. The inoculum was incubated in a water bath ( $37 \pm 1 \text{ }^\circ\text{C}$ ) under anaerobic conditions and degassed in line with the VDI guidelines before use [25]. All feeds were placed in plastic bags and stored at  $4 \text{ }^\circ\text{C}$  for later chemical analysis and use in a biogas digester.

### 2.2 Experimental procedure

A 500-ml plastic bottle was utilized as a bioreactor in a lab-scale batch experiment. The bioreactor was prepared in two sets and performed under mesophilic conditions for 40 days. The first set included five digesters that treated the FW/CH at different mixing ratios (i.e., 100:0, 60:40, 50:50, 40:60, 0:100). Second, the FW/CH mixing ratio of 60:40 was utilized for evaluation of the impact of varying initial pH levels (i.e., 5, 6, 6.5, and 7.5) on the performance of co-digestion (Table 2.1). A control with inoculum alone was carried out to subtract the biogas volume produced from the inoculum. The total amount of feedstocks added in each bottle was 10.75 grams volatile solid (VS) basis. To initiate a reaction and prevent inhibition in the fermentation, anaerobic inoculum was added to all bottles. After that the distilled water was added to get a total solid (TS) of digester less than 10% in all biodigesters as recommended by VDI 4630 guidelines [25]. The initial pH of the blended materials was checked and balanced to the desired target points using a pH meter. Then, they were placed inside a water bath to maintain the desired temperature. All tests were carried out in duplicate to confirm the reproducibility of data with average values reported. Biogas and methane were measured by water displacement method and gas analyzer (biogas 5000, geotechnical instruments (UK). Ltd) until biogas generation became insignificant and then standardized to the results at standard conditions (temperature ( $T$ ) = 273K and pressure ( $p$ ) = 1atm) according to VDI 4630 guidelines [25]. Biogas yield was expressed as the biogas volume produced per gram VS of substrate added to the bottle (i.e., ml/g VS), and gas contents were reported in percentage (%).

Table 2.1. Summary of operational parameters and initial conditions of the biodigester

Key parameters	FW/CH mixtures					Initial pH values			
Labeled	D <sub>1</sub>	D <sub>2</sub>	D <sub>3</sub>	D <sub>4</sub>	D <sub>5</sub>	pH-5	pH-6	pH-6.5	pH-7.5
FW/CH ratios	100:0	60:40	50:50	40:60	0:100	60:40			
pH	7					5	6	6.5	7.5
C/N	19.94	23.98	25.30	26.68	34.46	23.98			

### 2.3 Analytical methods

The cooked food waste (i.e., Injera leftovers, meat, potato, pasta, and rice) and coffee husks were analyzed for their total solids (TS), ash, moisture content, and volatile solids (VS) based on the Standard Methods [26]. The crude fiber determination was performed by gravimetric technique following chemical digestion and solubilization of other constituents available in the sample [27]. Total carbon was determined using the elemental analyzer, according to Kahassay and Bogale [28], whereas total nitrogen content was computed using the Kjeldahl method [29]. A protein percentage was calculated using the Kjeldahl nitrogen with the correction factor (6.25). The crude fat content was evaluated according to the standard method developed by the association of official analytical Chemists [30], and the carbohydrate content was calculated with the subtraction method according to Prentice and co-workers [31]. The lignocellulosic contents of the coffee husk were determined using procedure defined in the paper of Beshir et al.[32].

### 2.4 Biodegradability and synergistic index

The biomethanation rate is directly related to the biodegradability of the feedstock. Based on the concentration of carbohydrates(carb), proteins (p), and fat (f) in the substrates (TS basis), it is possible to calculate the maximum theoretical biogas potential ( $TBP_{fpc}$ ) under the assumption that the feedstock is completely converted into biogas as recognized by VDI guidelines with the help of eq. (1) [25].

$$TBP_{fpc} = \% (750 * carb + 1390 * f + 800 * p)/100 \quad (1)$$

Where TBP is the theoretical biogas potentials (ml/gVS) at standard conditions, thus, the  $BD_{fpc}$  of the substrate is calculated with this eq. (2).

$$BD_{fpc}(\%) = \frac{EBP}{TBP_{WH} * X_{WH} + TBP_{FW} * X_{FW}} * 100 \quad (2)$$

EBP = the biogas potentials of substrate or co-digester,  $TBP_{CH}$  = Theoretical biogas potential of CH, and  $TBP_{FW}$  = Theoretical biogas potential of FW that has been calculated based on the lipids, proteins, and carbohydrates compositions of the organic substrates,  $X_{CH}$  and  $X_{FW}$  represent the percentage of coffee husk and food waste in the co-digester, respectively. In addition, the organic matter biodegradation degree ( $\eta_{BD}$ ) of the complete anaerobic process was determined by dividing the measured biogas mass ( $m_B$ ) by the organic substrate added. The organic matter feeding was determined by the substrate mass (gVS basis) added (eq. (3))[33].

$$\eta_{BD} = \frac{M_B}{gVS \text{ added}} * 100 \quad (3)$$

The measured biogas mass ( $M_B$ ) was evaluated by the molar masses of the produced biogas compositions ( $M_{CH_4}$  – biomethane molar mass,  $M_{CO_2}$  – a molar mass of carbon dioxide,  $M_{O_2}$  – a molar mass of oxygen) with their respective compositions, supposing the produced biogas was composed of biomethane, carbon dioxide, and oxygen only (eq.(4)).

$$M_B = V_B \left( \frac{M_{CH_4} * cCH_4}{22400 * 100} + \frac{M_{CO_2} * cCO_2}{22400 * 100} + \frac{M_{O_2} * cO_2}{22400 * 100} \right) \quad (4)$$

Where 22400 ml/mol is the ideal gas molar volume,  $cCO_2$  – is the carbon dioxide content,  $cCH_4$  – is the methane content,  $cO_2$  – is the oxygen content, and  $V_B$  is the volume of the measured biogas. The synergistic and antagonistic effects may be found in the relationship between the experimental biogas yield and the weighted value (W), which is determined following eq. (5 and 6) according to [34].

$$CI = \frac{EBP_{co}}{W} \quad (5)$$

$$W = (X_{CH} * EBY_{CH} + X_{FW} * EBY_{FW}) / (X_{CH} + X_{FW}) \quad (6)$$

CI is the co-digestion synergistic index,  $EBP_{co}$  represents the experimental biogas potential (ml/gVS) of co-reactors, and  $EBP_{CH}$  and  $EBP_{FW}$  represent the experimental biogas potential of coffee husk and food waste alone, respectively.

## 2.5 Kinetic approaches

The experimental biogas were simulated with the First Order Kinetic equation (FOKE, eq. (9)), a modified Gompertz equation (MGE, eq. (8)) [35], and a modified logistic equation (MLE, eq. (9)) [36]. The kinetic parameters were used to forecast the biogas production potential.

$$\text{First Order Kinetic:} \quad B = B_o [1 - \exp(-k * t)] \quad (7)$$

$$\text{Modified Gompertz:} \quad B = B_o \exp \left\{ -\exp \left[ \frac{R_m}{B_o} (\lambda - t) + 1 \right] \right\} \quad (8)$$

$$\text{Modified Logistic Model:} \quad B = \frac{B_o}{1 + \exp \left[ \frac{R_m}{B_o} (\lambda - t) + 2 \right]} \quad (9)$$

Where B is cumulative specific biogas production (ml/gVS),  $B_o$  is the predicted maximum biogas production potential (ml/gVS),  $R_m$  is the maximum specific biogas production rate (ml/gVS d),  $e = 2.718282$ ,  $\lambda$  is the lag phase time in days, t is the duration of digestion (days), k (/d) is the hydrolysis rate constant. Simulation of the experimental data for the best-fit model determination was done, and the choice of the best-fitted equation was based on the biogas kinetic parameters that are  $R^2$ , Root mean square error (RMSE), and percentage of difference (%  $\gamma$ ) between the simulated biogas and experimental one.

## 2.6 Data analysis

Analysis of variance of the experimental data was determined by ANOVA (single one-way analysis of variance) using Microsoft Office Excel, with a p-value less than 0.05 being considered significant. The SPSS 26 software tool was used to simulate measured biogas yield.

## 3. Results and discussion

### 3.1 Characterization of substrates

Characteristics of substrates would provide essential information enabling a proper biogas production process. Table 3.1 shows the physiochemical compositions of the samples used in this study. In biochemical treatment, the amount of TS and VS is essential to determine the biodegradability of the samples. The total solids (TS) for CH and FW were 88.88% and 30.40%. The volatile solids (VS) for CH and FW were 89.82% and 90.25%, respectively. Volatile solids fractions contribute a rough approximation of the levels of biodegradable organic matter present in solid fractions of



the waste biomass [26]. A higher VS entails a higher organic component which is suitable for methane-rich biogas production. Both substrates have high VS, indicating the presence of enough organic content that might be converted to biogas yield. Additionally, FW contains a high amount of easily degradable organic fractions, such as carbohydrates, proteins, and fats, which can provide a readily accessible source of nutrients for the microorganisms to support the disintegration of the lignocellulosic materials in the CH.

Like other lignocelluloses, CH consists of cellulose, hemicelluloses, and lignin. CH contains a high content of lignin (23.16%), which could cause a low conversion rate of CH. The Lignin component of the material is not water-soluble; hence, microbes need more time to adhere to the material to start the hydrolysis [36]. Besides, FW assisted in the disintegration of lignin and depolymerization of lignocellulosic biomass without any acid pretreatments [11]. Thus, adding food waste augmented the quantities of VFA in the anaerobic bioreactor and improved the microbial activities to delignify lignocellulose. On the other hand, the carbon/nitrogen (C/N) ratio reflects the degree of nutrients available in samples for microbial growth, and it indicates process stability [11]. C/N ratios of approximately 20 to 30 were commonly appropriate for the digestion of lignocellulosic materials with food waste [12] to enhance digestibility and biogas yield with quality. However, the CH used for this study has a higher C/N ratio of 34.46 (Table 3.1), which could need to co-substrate with a fairly lower C/N ratio. FW has a C/N ratio (19.94), which is comparatively close to the optimal range better for biogas production in anaerobic conditions and is a preferable co-substrate for CH. The carbon concentration makes the CH and FW (Table 3.1) good materials for biogas production; but alarms like the lignin content and chemical concentration (like caffeine, tannin, and phenols) could prevent the effective biological processes of CH alone [18]. Thus, setting the reactors at different mixtures (C/N ratio) and initial pH values were performed to observing their effects on the co-digestion performances. The results are presented in the next sections.

Table 3.1. Characteristics of selected feedstocks

Parameters	Inoculum	FW	CH
Moisture (%)	91.39	69.60	11.10
VS (%)	73.98	90.25	89.82
TS (%)	8.6	30.40	88.88
Ash (%)	26	9.75	10.17
Total carbon	*	47.66	48.93
Kjeldahl Nitrogen	*	2.39	1.42
Hemicellulose	*	*	28.96
Cellulose	*	*	24.88
Lignin	*	*	23.16
Crude fiber (%)	*	*	32.67
Crude fat (%)	*	11.81	0.9
Crude protein (%)	*	14.93	8.56
Carbohydrate (%)	*	63.51	47.70

\*not determined

### 3.2 Influence of mixing ratios on biogas production

The produced biogas and its compositions were measured in intervals of 5 days. The cumulative biogas yields of FW and CH co-digestion at different mix ratios are presented in Table 3.2 and Fig. 3.1. As expected, at the end of the incubation period (Fig. 3.1a), CH showed the lowest EBP of 204.71 ml/gVS and average biomethane content of 49.8%, which lower than the report of Wang et al. [37], who reported 241.31 ml/gVS from the same material, which directs a fairly poor anaerobic process performance. The difference in biogas productivity could result from diverse growth conditions of the substrate, biochemical compositions of the substrate, and experimental conditions [38]. The result suggested that coffee husk is not appropriate for anaerobic conversion. The maximum recalcitrant (lignin)

concentration in the CH might be ascribed to the lowest EBP. In addition, this lowest EBP recovered from CH can correspond to the scarcity of trace elements, often causing a letdown in gas production owing to the failure of the process stability [37]. For this reason, real-scale AD of CH needs trace elements and easily degradable substrates to complement. On the other sides, since the CH ash content is relatively low, it could be proper for the thermochemical conversion technologies. The biogas yields of FW/CH mixture at ratios of 60:40, 50:50, and 40:60 were 540.78, 501.08, and 490.43 ml/gVS, respectively, which 2.6-, 2.4-, and 2.3-fold higher than that of pure CH (p-values < 0.02). The highest biogas yield was found at an FW/CH ratio of 60:40, highlighting the promising positive impact of co-digestion to biogas conversion. As in this work, Shitophyta et al. [39] observed the maximum biogas yield of 584.49 ml/gVS while increasing the food waste level to 20% in the co-digestion with corn stover. This might be attributed to the supplementing characteristics of FW and CH on the system performance parameters. The biogas profile indicates the increment of cumulative biogas yield and average biomethane concentration with increasing the FW portion in mixtures. This maximum EBP was improved by 164 % compared to the CH mono digestion. This intensification was caused by enhancing the metabolic conduit owing to proper nutritional condition (C/N). The calculated C/N ratio of the fed in treatments with the FW ratio of 60% was 23.98 in this experiment, which is reasonable with the decision that C/N of 20–30:1 had the best co-digestion performance [11]. Based on these findings, it can be decided that the FW addition on CH induced a multi-stage degradation process, which could stem from the enhancement of co-digestion in solubilization competence and co-substrates biodegradability.

Importantly, the FW and CH co-digestion performed in this study induced a much higher promotion in biogas recovery, which shows that co-digestion with FW might be an alternative line to boost bioenergy production from CH. These findings proved the statement described in the study of Hamrouni et al. [40] who described FW as a good catalyzer of co-digestion and accelerator of biogas production. The main reasons that might have contributed to the enhanced biogas in this work are: i) the easily biodegradable portion in FW, which was directly exposed to the successive acidification–methanogenesis process without the necessity of solubilization–hydrolysis first; nutrient balance and ii) the multiplied microbial species and their load, which stimulated the solubilization of CH cell wall structure and degradability [41].

The average CH<sub>4</sub> and CO<sub>2</sub> recorded from co-digestions are plotted in Fig.3.1. As shown in Fig. 3.1b, the maximum percentage of average CH<sub>4</sub> was observed from D<sub>2</sub>, 1.3 times higher than CH mono digestion, which illustrates a high enough calorific value in biogas to find use in several energy applications. These findings indicated that a stable digestion process may succeed by complimenting the nutrient characteristics of FW and CH in the co-digester. The observation showed that the average CH<sub>4</sub> content increased with increasing the level of FW concentration in the co-digestion, whereas the concentration of CO<sub>2</sub> decreased with increment of FW fraction. With the addition of CH, the average CH<sub>4</sub> content started to decline. The greater the CH composition ratio, the lower the moderate CH<sub>4</sub> content in the co-digestion system. The procedure with 100% CH had the lowest average CH<sub>4</sub> content of 49.8%. Like this work, Chen et al. [42] found CH<sub>4</sub> contents increments with an increase in food waste than lignocellulosic biomass. The CH<sub>4</sub>/CO<sub>2</sub> profile showed the highest CH<sub>4</sub>/CO<sub>2</sub> ratio of 2.47 at a C/N ratio of 23.98 (D<sub>2</sub>), followed by a C/N ratio of 25.30 (D<sub>3</sub>) with a respective value of 2.07, which displays the stimulated microbial activity responsible for the best CH<sub>4</sub> concentration. The lowest CH<sub>4</sub>/CO<sub>2</sub> ratio was observed for CH alone, illustrating the poor microbial activity responsible for the poor CH<sub>4</sub> content [43]. The reasons for the maximum biogas production presented in this work might also be accountable for the maximum percentage of CH<sub>4</sub> concentration.

Table 3.2. Summary of biogas potential and kinetic parameters

Setups	Parameters	FW/CH mixtures					Initial pH				
		100:0	60:40	50:50	40:60	0:100	5	6	6.5	7.5	
Types	Mix ratios (%)	100:0	60:40	50:50	40:60	0:100	5	6	6.5	7.5	
	Measure d value	EBP (ml/gVS)	480.74	540.78	501.08	490.43	204.71	347.44	448.54	478.23	518.75
		TBP (ml/gVS)	759.92	631.45	599.33	582.41	438.74	631.45	631.45	631.45	631.45
	CH <sub>4</sub> (%)	55.16	63.55	58.11	57.27	49.80	48.82	51.97	54.44	57.70	
	CPI	-	1.46	1.46	1.55	-	-	-	-	-	
	BD <sub>fpc</sub> (%)	63.26	85.64	83.60	84.20	46.66	55.02	71.03	75.73	82.15	
	η <sub>BD</sub> (%)	52.57	56.80	56.53	54.11	25.64	39.01	44.94	48.40	53	
Models											
FOKE	B <sub>o</sub> (ml /gVS)	530.97	592.87	537.42	525.54	225.15	382.64	498.22	520.04	578.61	
	k(/d)	0.042	0.05	0.052	0.05	0.043	0.042	0.041	0.041	0.04	
	γ (%)	10.44	9.63	7.25	7.15	9.98	10.13	11.07	8.74	11.53	

	R <sup>2</sup>	0.985	0.978	0.974	0.983	0.968	0.984	0.982	0.981	0.980
	RMSE	20.25	19.31	15.27	16.32	9.16	16.02	19.19	21.87	15.54
MGE	B <sub>o</sub> (ml/gVS)	523.81	565.52	510.43	501.57	214.12	380.51	489.84	499.50	570.22
	R <sub>m</sub> (ml/gVS d)	17.23	21.78	20.60	20.38	8.26	12.25	16.16	18.51	18.58
	λ (d)	1.4	2.23	2.10	1.6	2.65	1.3	1.7	1.8	1.9
	γ (%)	8.95	4.57	1.89	7.60	4.59	9.51	9.20	4.44	9.92
	R <sup>2</sup>	0.980	0.993	0.990	0.994	0.994	0.990	0.991	0.994	0.995
	RMSE	8.67	10.59	17.84	15.29	4.65	8.74	6.37	8.30	6.29
MLE	B <sub>o</sub> (ml/gVS)	489.52	536.07	490.5	478.22	202.75	355.05	456.51	472.48	528.90
	R <sub>m</sub> (ml/gVS d)	17.75	22.33	20.90	20.57	8.53	12.63	16.76	18.90	19.45
	λ (d)	2.5	3.1	2.8	2.3	3.6	2.3	2.9	2.7	3.17
	γ (%)	1.82	0.87	2.11	2.49	0.96	2.18	1.77	1.20	1.95
	R <sup>2</sup>	0.985	0.988	0.994	0.983	0.987	0.983	0.987	0.990	0.991
	RMSE	4.50	10.18	9.17	15.10	10.14	8.45	9.34	11.33	8.35

EBP-experimental cumulative biogas potential, TBP – theoretical biogas potential, B<sub>o</sub> – model predicted biogas yield, γ (%) –the difference between EBP and B<sub>o</sub>, i.e.,  $\gamma (\%) = |EBP - B_o| / EBP * 100$ , RMSE was calculated as defined by Yu et al. [13].

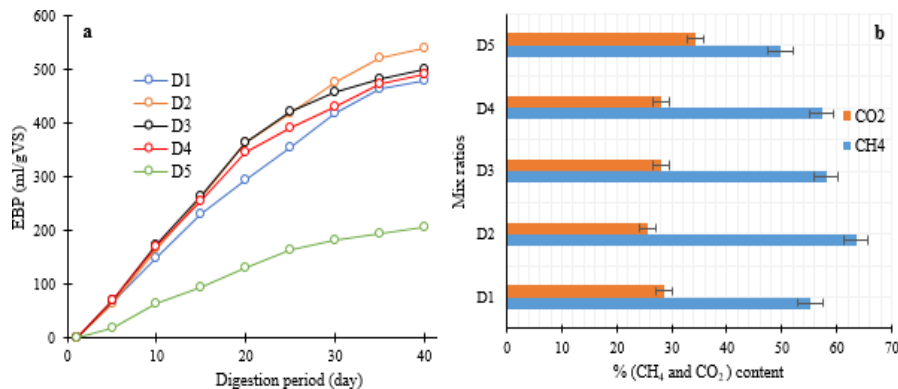


Fig. 3.1. a) Cumulative biogas production, b) percentages of CH<sub>4</sub> and CO<sub>2</sub> contents at different mixture ratios

### 3.3 Influence of Initial pH on biogas production

FW/CH mixing ratio of 60:40 was evaluated in the first set and applied for further study of the influence of the initial pH control (5, 6, 6.5, and 7.5) on the co-digestion of food waste and coffee husk performance. This ratio was picked because lignocellulose biomass had a low biogas yield. The total biogas production at different initial pH values of the co-treatments after 40 days are displayed in Table 3.2 and Fig. 3.2. The highest biogas yield of 518.75 ml/gVS was observed from the biodigester operated at a pH of 7.5 among all initial pH controls (5, 6, 6.5, and 7.5). At a pH value of 5.0, the cumulative biogas yield was 347.44 ml/gVS, 49 % below the highest result, which can be attributed to microbial activity inhibition. At this acidic condition, the microbial community may have been unable to function successfully, resulting in a decline in biogas production. The cumulative biogas production at different mix ratios and initial pH is shown in Fig. 3.3. As shown in Fig.3.3, at an initial pH of 7, the maximum biogas yield was produced, followed by the reactor treated at pH 7.5. The better biogas yield at an initial pH value of 7 and 7.5 can be attributed to the nutrient availability and the optimum conditions for microbial activity. At these pH points, the anaerobic microbes responsible for biogas production were able to work at their maximum efficiency, causing the maximum biogas yield.

Similar to previous studies, a clear increase in biogas production and substrate degradation was determined with increasing initial pH values [22]. As a result of an increase in initial pH values from 5.0 to 7.5, the cumulative biogas yields of the complete process increased by 55.6% at pH 7. The results indicate that the initial pH condition of the digester has a significant effect on biogas yield because it affects the activity of anaerobic microorganisms involved in the biogas production process, specifically biomethane-producing bacteria. Above all, the desirable initial condition for better biogas production was between pH 7 and pH 7.5, indicating resilient stability and buffering capacity for FW and CH co-digestion. Thus, to maximize biogas production and increase hydrolysis kinetics and hydrolysis to methanogenesis conversion efficiencies, an initial pH of 7 is recommended for the FW and CH fermentation under mesophilic ranges. The result revealed that a combination of a slowly degradable lignocellulosic substrate with easily degradable FW at around pH 7 assisted in balancing the digestion stages. Jijai et al. confirmed these results by observing a maximum biomethane volume of (311.2 mlCH<sub>4</sub>/gVS) with the highest percentage in co-digestion of chicken manure with rice husk and Thai rice noodle wastewater at pH 7[44]. This assumption is also consistent with Zhai et al. [22], who recommended that an initial pH of 7.5 was appropriate for obtaining maximum biogas production and digestion rate in anaerobic co-digestion of kitchen waste with cow manure.

The initial pH condition affects the process stability, biogas production potential, and quality. The CH<sub>4</sub> content recorded from co-digestions at varying initial pH conditions is shown in Table 3.2 and Fig. 3.2b. The maximum percentage of average CH<sub>4</sub> was observed at pH 7 (Table 3.2). However, for comparison of the digesters tested at a pH value (5, 6, 6.5, and 7.5), the maximum average CH<sub>4</sub> was attained at pH 7.5, while the low value was attained at pH-5. The onset of CH<sub>4</sub> formation with increasing pH values may be elucidated by the conversion of intermediate organic acids and this can be attributed to the optimum conditions for microbial action, leading to the maximum CH<sub>4</sub> yield. In contrast, the gaseous composition profile shows that the average CO<sub>2</sub> production reached the peak value at pH 5 (36.07 %). Similar to Lindner et al. [33], the lowest CO<sub>2</sub> concentration was detected at pH 7.5 (Fig. 3.2b ). Similarly, the higher CH<sub>4</sub>/CO<sub>2</sub> ratio of 2.09 was noticed at an initial pH of 7.5.

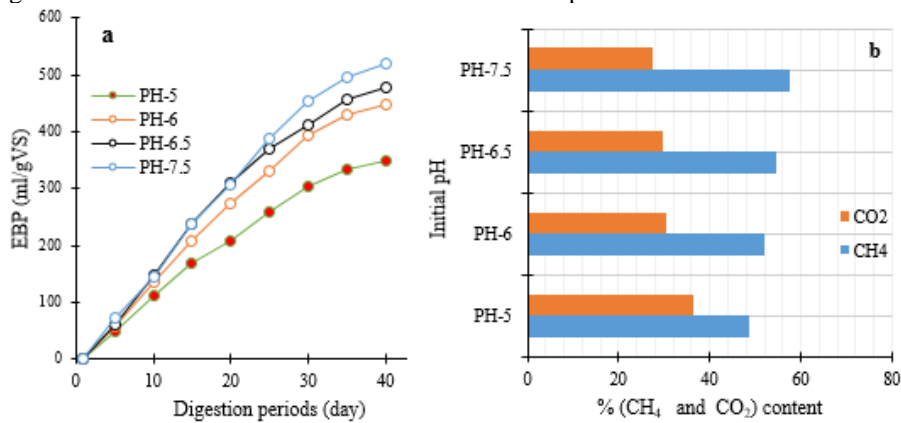


Fig.3.2. a) Cumulative biogas production and b) percentage of CH<sub>4</sub> and CO<sub>2</sub> at different initial pH values after the fermentation period

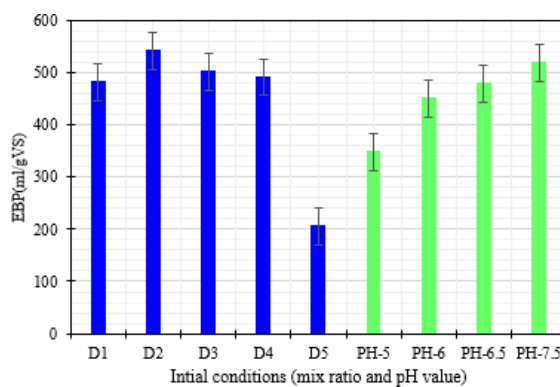


Fig. 3.3. Cumulative biogas production versus initial conditions

### 3.4 Synergistic effects estimation

The co-digestion synergistic impact during a combination of CH and FW was analyzed by comparing the experimental data and the weighted value calculated from eq. (6). As presented in Fig. 3.4, in all co-fermentation trials, the measured biogas profiles were greater than weighted values, which signifies the presence of positive synergistic effects. The increase in the actual biogas yield over the weighted one, because of a synergistic impact of co-treatments, varied between 46% and 55.6%, dependent upon the FW/CH ratios utilized (Fig.3.5). As in this experiment, Zhen and colleagues [41] reported a 54% increase while mixing FW and microalgae at a VS ratio of

0.5:0.5. Jason [45] also found a 24.0% increase with the VS-ratio of 0.75:0.25 in the co-treating of FW and microalgae. With this concept, co-substrates synergic effects can be assessed through eq. (5). Evaluation of CI proves that all co-digesters exhibited positive synergic effects (Table 3.2 and Fig. 3.4b), and the maximum CI value was obtained at a C/N ratio of 26.68 (D<sub>4</sub>) followed by a C/N ratio of 25.30 (D<sub>3</sub>) and 23.98 (D<sub>2</sub>) with a corresponding value of 1.55, 1.462 and 1.460, respectively, which reasonable the results of an increase in measured biogas volume over weighted one. This showed a reverse change trend for the cumulative biogas yield (Table 3.2). This finding proves the statement that suggested the maximum synergistic effect result is not always responsible for maximum biogas yield [11]. The comparable results were reported for the co-digestion of food wastes and *Sophora flavescens* residues co-digestion ( $0.97 < CI < 1.2$ ) (Table 3.3) and co-treating sewage sludge with cellulose, hemicellulose, and lignin ( $1.01 < CI < 3.59$ ) [46]. It appears that the FW/CH ratio of 60:40 was more capable of creating a better anaerobic environment (improved pH buffering capacity, alleviated toxicity and VFAs accumulation, as well as the development of specific microbial that can disrupt CH structure and elevated biochemical conditions for microbial growth to be enhanced the biodegradability of CH and consequent biogas conversion potential. Biogas production parameters of this current study are comparable to the previous one (Table 3.3).

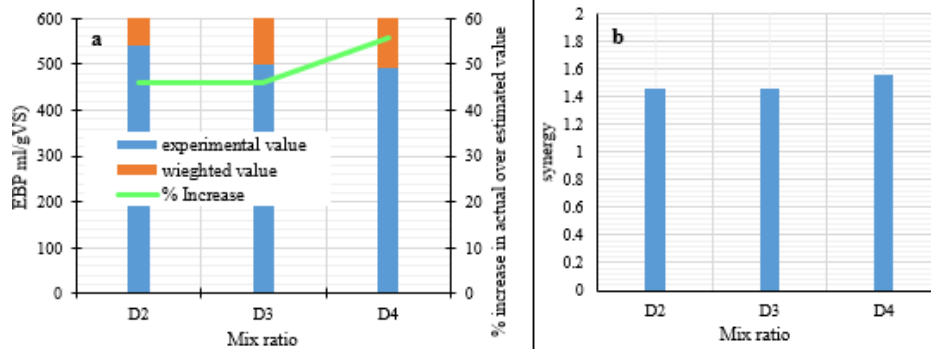


Fig.3.4. Increment of measured biogas yield over weighted one (a) and (b) co-digestion synergistic impact

### 3.5 Biodegradability

The biodegradability of organic matter during AcoD was established by calculating the theoretical biogas yield in terms of organic compositions (carbohydrate, protein, and fat) and produced gas compositions (CH<sub>4</sub>, CO<sub>2</sub>, and O<sub>2</sub>) as expressed in eq. (1) – (4). Adding FW into CH notably stimulated fermentation performance concerning the degradation of organic fractions, linking well with the outputs measured for biogas production. The BD rate trend was related to the biogas yield. The higher BD value was reached in the bioreactor with the greater biogas yield. Fig. 3.5 presents the effect of different substrate mixing ratios and initial pH values on biodegradability in the co-digestion of food waste and coffee husk. The maximum BD<sub>fpc</sub> was observed from D<sub>2</sub> with a corresponding value of 85.64%, while a low value was achieved from D<sub>5</sub> (46.66%). For the η<sub>BD</sub> profile, the minimum value was observed at D<sub>5</sub> (25.64%), while the highest value was observed at D<sub>2</sub> (56.80%). Low BD was expected from CH owing to the recalcitrant lignin contents that might be reasonable for the lowest biogas yield. With synergistic effects, the BD<sub>fpc</sub> was improved by 70 %, whereas η<sub>BD</sub> was improved by 120% compared with CH mono-digestion. Co-digestion with FW, in comparison, was competent to enhance the removal of degradable carbon, decreasing the quantity of the solid retained. It noted that it indicates that the more FW introduced, the greater the benefits for solids removal due to an FW enclosing an easily degradable organic fraction. In addition, based on the performed experiments, a clear effect of the initial pH value on the biodegradability rate was determined. Biodegradability increased with increasing the initial values of the pH of the bioreactor. Maximum biodegradability of 82.15% (BD<sub>fpc</sub>) and 53 % (η<sub>BD</sub>) was observed from the bioreactor operated at pH-7.5 among all tested pH with constant mix ratios of substrates, which shows the stability of the digester for microorganisms and their easy accessibility to the cell structure of biomass [11]. A low biodegradation rate of 55.02% (BD<sub>fpc</sub>) and 39.01 % (η<sub>BD</sub>) was obtained from the bioreactor performed at pH-5. This finding indicated that the initial pH value in the batch digester may affect the biodegradability of the substrate and the production of intermediate products. The low pH value can lead to a decrease in the stability of reactors, which causes microorganisms' inhibition and will be responsible for low digestibility. An increase in the initial pH value indicated biogas results similar to a two-phase process [33]. According to these findings for the anaerobic co-digestion of fiber-rich substrates with food waste, pH values between 7.0 and 7.5 look favorable.

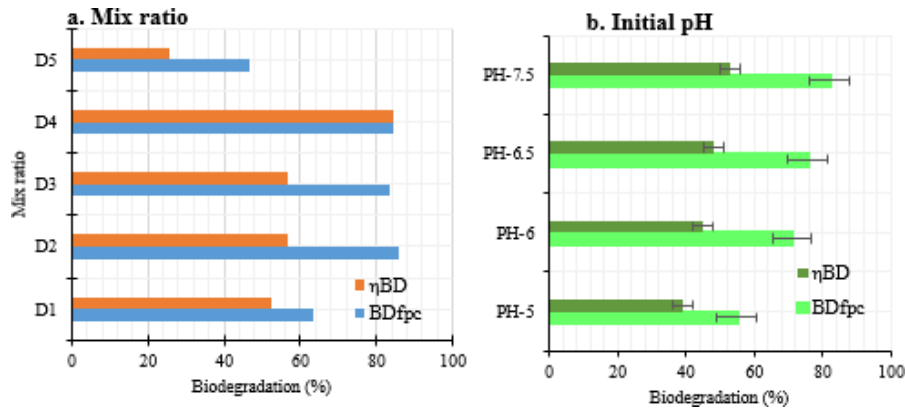


Fig.3.5. Biodegradability rate at various mixing ratios and initial pH

Table. 3.3. Comparison of the results of the current study with the literature.

Co-substrates	Initial pH	C/N	BD (%)	Synergy effect	Biogas yield (ml/gVS)	Reference
FW/SFR (7:3)		25.8	58.83	1.19	640	[47]
FW/MA(80:20)	7	-	-	-	639.8	[41]
FW/CC (64:36)	7.6	45	98	0.9	730.70	[48]
FW/CS(20:80)	6.3-7.4		-	-	584.49	[39]
FW/GW (60:40)	7.81	15.3		1.08	388.8	[42]
FW/CH (60:40)	7	23.68	85.64	1.46	540.78	This study

Where CM – cow manure, SFR – sophora flavescens residues, CC – cabbage and cauliflower, MA – microalgae, GW – green waste, CR – cow’s rumen, and CS – corn stover.

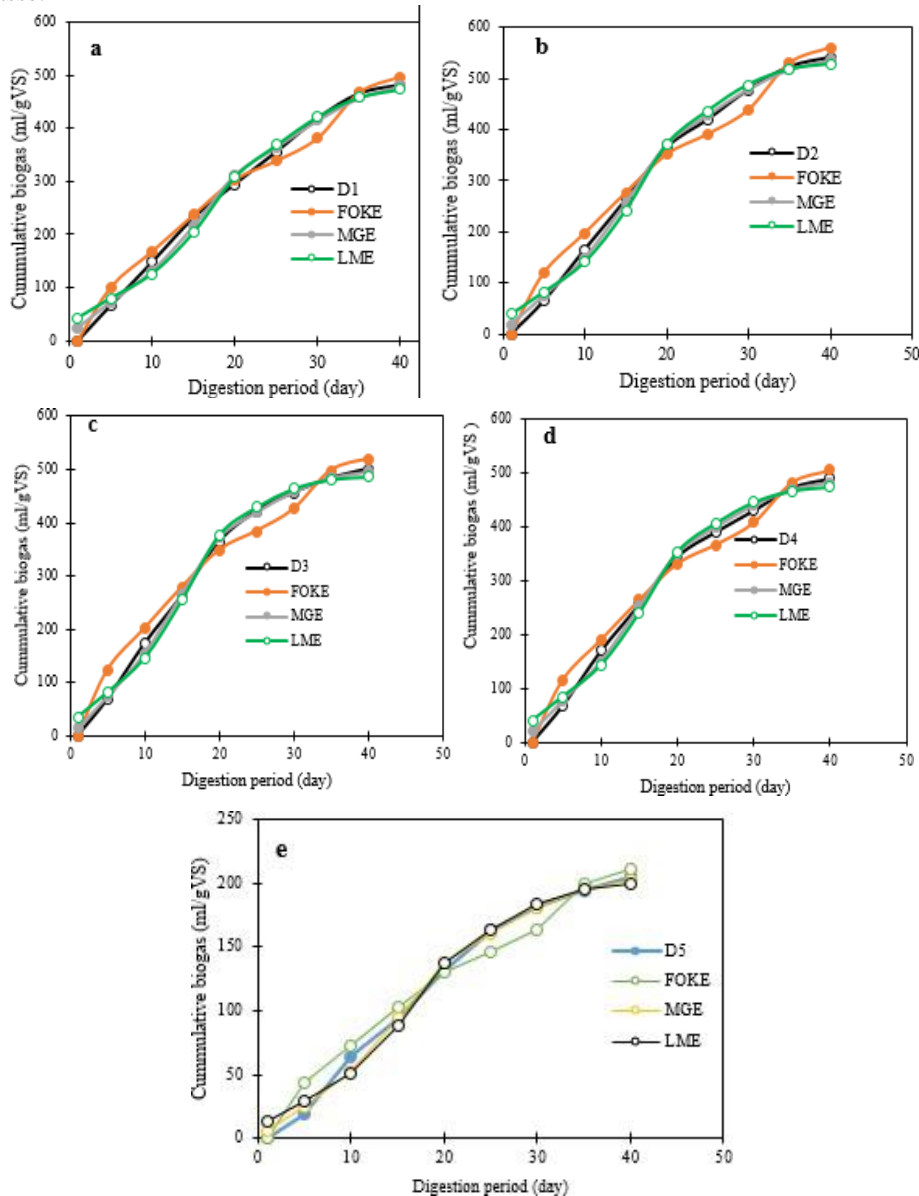
### 3.5 Kinetics of the co-digestion process

Biogas production was simulated using three kinetic models, including MGE, MLE, and FOKE, to estimate the performance of bio-kinetic parameters. Their corresponding kinetic values for different ratios and initial pH are shown in Table 3.2 and Fig. 3.6.  $R_{max}$  shows a similar trend as the estimated biogas yield.  $R_m$  projected for modified Gompertz and modified logistic model increased from 8.26 to 21.68 ml/g VS d and 8.53 to 22.33 ml/g VS d, apparently signifying that the co-digestion of CH with FW can facilitate the biogas production. These observations were in line with those of Zhen et al. [41], who highlighted that the joint treatment of FW with microalgae boosted the availability of organic materials in fermentation systems. The authors ascribed this to the robust microbial action in the favorable metabolism conditions promoted by the blending feedstock. Mono-digestion of CH and co-digestion test at pH 5 produced the lowest  $R_{max}$  for both models, linked to the complex lignocellulose structure, compositions, and microbial’ inhibition, which caused the difficulty and instability of reactors and slow degradability. The maximum  $R_{max}$  was achieved at 60:40 and an initial pH of 7. This result supports the calculated values of biodegradation rate and synergistic impact (Table 3.2).

Here, the lag phase ( $\lambda$ ) denotes the gradient of degradation and biogas generation rates [49]. The  $\lambda$  values raised as FW fractions increased in the mixtures. The maximum  $\lambda$  value was attained from CH alone and the minimum  $\lambda$  value was attained from FW alone for both models. It also increased with increasing an initial pH. These results did not support the experimental biogas that grew with increased FW fraction in the combinations and initial pH values. According to a reported study, the modified Gompertz model and Logistic model are regularly applied to obtain the biological parameters of AD [23]. They can fit the three phases of the digestion process (lag, exponential, and stationary phases) with a high fitting degree. In this study, both models over-predicted biogas at initial points (Fig. 3.6). These results support the statement that highlighted the limitation of both models in estimating the initial condition ( $B = 0$ ) [50]. FOKE is usually developed to simulate the exponential phase of biogas production. This may elucidate why it does not fit well with the real data [13]. The hydrolysis kinetic constant ( $k$ ) is an important indicator reflecting material digestibility and fermentation efficiency. Scholars believe that hydrolysis is the limiting step, leading to low solids biodegradation and constrained methanogenic production. Interestingly, the  $k$  values obtained in the current study exhibited a reverse change trend (Table 3.2). An increase of FW in the co-digestion produced higher EBP,  $B_0$ , and  $R_{max}$ . The  $k$  values experienced a variation trend as FW levels increased in the mixtures but almost increased from 0.042/d to 0.052/d. The  $k$  value slightly decreased as the initial pH increased from 5.0 to 6.0 and 6.5 to 7.5. This exhibited a reverse change trend with the cumulative biogas produced with increasing initial pH (Table 3.2). The current results imply that the enhancement in measured biogas and estimated  $B_0$  was independent of  $k$  and that the increased  $k$  does not always cause high biogas productivity. This statement agreed with Zhen et al. [41], who noticed that the introduction of FW considerably improved the overall degradability of microalgae; however, it

had a slight effect on the hydrolysis rate ( $k$ ). The cause for the low hydrolysis rate but high biogas output is yet well-known, and more work in investigating the actual role of the hydrolysis kinetic constant as well as other operational factors is still essential in future studies.

The soundness of the biogas kinetic model was decided by comparing its values with modeling values. As shown in Fig.3. 6 and Table 3.2, the experimental data for different mix ratios and initial pH values were well-fitted by the MGE ( $R^2 > 0.980$ ), MLE ( $R^2 > 0.985$ ), and FOKE ( $R^2 > 0.974$ ), respectively. The lower the  $\Upsilon$  and RMSE value is, the better the accuracy of the biogas model will be [36]. For the three models, differences in gas production between the estimated and measured one were 0.87– 4.9 % for MLE, 7.15–11.53% for FOKE, and 1.89–9.92% for MGE. In addition, the RMSE value ( $<17.84$  for MGE,  $<15.3$  for MLE, and  $< 22.8$  for FOKE) was obtained. Therefore, comparing these statistical values, the highest  $\Upsilon$  and RMSE were found for FOKE, followed by MGL, which may clarify that it does not fit well the experimental data. The lowest  $\Upsilon$  and RMSE observed for MLE directs the reliability to predict the co-digestion kinetics with a synergistic effect. Thus, a modified logistic model outperformed others with the lowest  $\Upsilon$  and RMSE value. These findings were comparable with those of Meraj et al. [36], who reported the good fitness of actual results to MLE compared to MGE results when co-digested rice straw, wheat straw, and sugarcane bagasse.



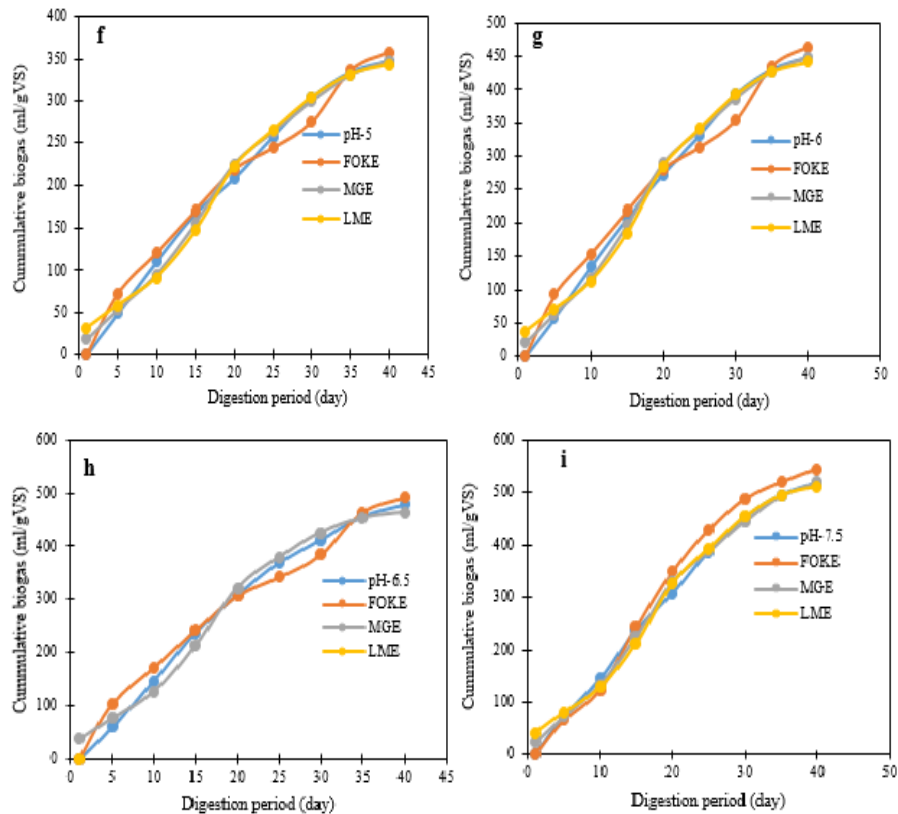


Fig.3.6. Regression fitting of EBP following MGE, MLE, and FOKE under different mix ratios (a-e) and initial pH values (f-i).

#### 4. Conclusions

The anaerobic co-digestion performances of coffee byproducts and food waste were studied under different initial conditions (blend ratios and initial pH). The corresponding biodegradation and kinetics were examined via model simulation. The supplementing food waste and increasing initial pH levels improved CH degradation efficiency with the highest biogas yield of 540.78 ml/gVS at a FW/CH ratio of 60:40 and pH-7.0, achieving 164% increment comparison with CH alone. In addition, a modified logistic function presented the best fitness to the actual results in both setups. It hence could elucidate the co-digestion kinetics of different initial pH settings more soundly. Additionally, parametric and synergistic impact analysis revealed that the enhancement in biogas productivity rather than in hydrolysis kinetic efficiency ( $k$ ) was responsible for the positive interaction involved in the co-digestion test, which upgraded biogas yield. The recent findings highlighted the need to increase the easily biodegradable materials in co-digestion to improve biogas production from CH. Results also show that a specific blend of FW/CH (60:40) can be feasible for real-scale applications for renewable bioenergy production and divert huge organic materials from landfills. Thus, renewable  $\text{CH}_4$ -rich bioenergy production through co-digestion of FW and CH would be an alternative to petroleum fuels for relieving the global energy crisis and mitigating the environment.

#### Acknowledgment

The researchers would like to express thanks JiT Center of Excellence, Jimma Institute of Technology, and Oda Bultum University for giving partial support for this study, as well as Addis Ababa Institute of Technology for technical support.

#### References

- [1] T. G. Berhe *et al.*, "Biogas Plant Distribution for Rural Household Sustainable Energy Supply in Africa Biogas Plant Distribution for Rural Household Sustainable Energy Supply in Africa," *Energy Policy Res.*, vol. 4, no. 1, pp. 10–20, 2017, doi: 10.1080/23815639.2017.1280432.
- [2] L. Espinoza, K. Ziegler-rodríguez, A. Teresa, E. Pérez, Ó. C. Vásquez, and I. Vázquez-rowe, "Closing the gap in the municipal solid waste management between metropolitan and regional cities from developing countries: A life cycle assessment approach," *Waste Manag.*, vol. 124, pp. 314–324, 2021, doi: 10.1016/j.wasman.2021.02.020.
- [3] O. S. Ananthu, "Small Scale Biogas Production by using Food Waste- Examples from three Restaurants," 2019.



- [4] N. E. Benti *et al.*, “The current status, challenges and prospects of using biomass energy in Ethiopia,” *Biotechnol. Biofuels*, vol. 14, no. 1, pp. 1–24, 2021, doi: 10.1186/s13068-021-02060-3.
- [5] M. A. Cusenza, S. Longo, F. Guarino, and M. Cellura, “Energy and environmental assessment of residual bio-wastes management strategies,” *J. Clean. Prod.*, vol. 285, p. 124815, 2021, doi: 10.1016/j.jclepro.2020.124815.
- [6] P. Roy, A. K. Mohanty, P. Dick, and M. Misra, “A Review on the Challenges and Choices for Food Waste Valorization: Environmental and Economic Impacts,” *ACS Environ. Au*, vol. 3, no. 2, pp. 58–75, 2023, doi: 10.1021/acsenvironau.2c00050.
- [7] K. R. Chew *et al.*, “Effects of anaerobic digestion of food waste on biogas production and environmental impacts: a review,” *Envir. Chem. Lett.*, vol. 19, no. 4, pp. 2921–2939, 2021, doi: 10.1007/s10311-021-01220-z.
- [8] C. Morales-Polo, M. del M. Cledera-Castro, and Y. M. Soria, “Reviewing the Anaerobic Digestion of Food Waste: From Waste Generation and Anaerobic Process to Its Perspectives,” *Appl. Sci.*, vol. 8, p. 1804, 2018, doi: 10.3390/app8101804.
- [9] J. Lin *et al.*, “Effects of mixture ratio on anaerobic co-digestion with fruit and vegetable waste and food waste of China,” *J. Environ. Sci.*, vol. 23, no. 8, pp. 1403–1408, 2011, doi: 10.1016/S1001-0742(10)60572-4.
- [10] O. S. Oladejo, S. O. Dahunsi, S. O. Ojo, R. A. Ibikunle, C. O. Osueke, and I. Evbuomwan, “Energy generation from anaerobic co-digestion of food waste, cow dung, and piggery dung,” *Bioresour. Technol.*, vol. 313, p. 123694, 2020, doi: 10.1016/j.biortech.2020.123694.
- [11] M. K. Ibro, V. R. Ancha, and D. B. Lemma, “Impacts of Anaerobic Co-Digestion on Different Influencing Parameters: A Critical Review,” *Sustainability*, vol. 14, no. 9387, pp. 10516–10523, 2022, doi: <https://doi.org/10.3390/su14159387>.
- [12] K. Hagos, J. Zong, D. Li, C. Liu, and X. Lu, “Anaerobic co-digestion process for biogas production: Progress, challenges, and perspectives,” *Renew. Sustain. Energy Rev.*, vol. 76, pp. 1485–1496, 2017, doi: 10.1016/j.rser.2016.11.184.
- [13] Q. Yu, S. Cui, C. Sun, R. Liu, Z. Guo, and R. Lai, “Synergistic Effects of Anaerobic Co-Digestion of Pretreated Corn Stover with Chicken Manure and Its Kinetics,” *Appl. Biochem. and Biotechnol.*, vol. 193, no. 2, pp. 515–532, 2021, doi: 10.1007/s12010-020-03445-0.
- [14] L. Mu, L. Zhang, K. Zhu, and A. Li, “Anaerobic co-digestion of sewage sludge, food waste, and yard waste: Synergistic enhancement on process stability and biogas production,” *Sci. Total Environ.*, vol. 704, p. 135429, 2019, doi: 10.1016/j.scitotenv.2019.135429.
- [15] S. Begum, T. Das, G. R. Anupoju, and N. E. i., “Solid-state anaerobic co-digestion of food waste and cardboard in a pilot-scale auto-fed continuous stirred tank reactor system,” *J. Clean. Prod.*, vol. 289, p. 125775, 2021, doi: 10.1016/j.jclepro.2020.125775.
- [16] N. Du, M. Li, Q. Zhang, M. D. Ulsido, R. Xu, and W. Huang, “Study on the biogas potential of anaerobic digestion of coffee husks wastes in Ethiopia,” *Waste Manag. Res.*, vol. 39, no. 2, pp. 291–301, 2021, doi: 10.1177/0734242X20939619.
- [17] A. C. Montoya, C. da S. Mazareli, and T. P. Delforno, “Hydrogen, alcohols and volatile fatty acids from the co-digestion of coffee waste (coffee pulp, husk, and processing wastewater) by applying autochthonous microorganisms,” *Int. J. Hydrog. Energy*, vol. 44, no. 39, pp. 21434–21450, 2019, doi: 10.1016/j.ijhydene.2019.06.115.
- [18] A. S. Fernandes *et al.*, “Impacts of discarded coffee waste on human and environmental health,” *Ecotoxicol. Environ. Saf.*, vol. 141, no. February, pp. 30–36, 2017, doi: 10.1016/j.ecoenv.2017.03.011.
- [19] M. A. Dareioti, K. Tsigkou, A. I. Vavouraki, and M. Kornaro, “Hydrogen and Methane Production from Anaerobic Co-Digestion of Sorghum and Cow Manure: Effect of pH and Hydraulic Retention Time,” *Fermentation*, vol. 8, p. 304, 2022, doi: <https://doi.org/10.3390/fermentation8070304>.
- [20] K. Bella and P. V. Rao, “Anaerobic digestion of dairy wastewater: effect of different parameters and co-digestion options — a review,” *Biomass Convers. Biorefinery*, vol. 13, pp. 2527–2552, 2023, doi: <https://doi.org/10.1007/s13399-020-01247-2>.
- [21] A. Rahman, H. B. Møller, C. Kumer, M. Alam, R. Wahid, and L. Feng, “Optimal ratio for anaerobic co-digestion of poultry droppings and lignocellulosic-rich substrates for enhanced biogas production,” *Energy Sustain. Dev.*, vol. 39, pp. 59–66, 2017, doi: 10.1016/j.esd.2017.04.004.
- [22] N. Zhai, T. Zhang, G. Yang, Y. Feng, X. Wang, and G. Ren, “Effect of initial pH on anaerobic co-digestion of kitchen waste and cow manure,” *Waste Manag.*, vol. 38, pp. 126–131, 2015, doi: 10.1016/j.wasman.2014.12.027.
- [23] H. Nie, H. F. Jacobi, K. Strach, C. Xu, H. Zhou, and J. Liebetrau, “Mono-fermentation of chicken manure: Ammonia inhibition and recirculation of the digestate,” *Bioresour. Technol.*, vol. 178, pp. 238–246, 2015, doi: 10.1016/j.biortech.2014.09.029.
- [24] P. Nguimkeu, “A simple selection test between the Gompertz and Logistic growth models,” *Technol. Forecast. Soc. Chang.*, vol. 88, pp. 98–105, 2014, doi: 10.1016/j.techfore.2014.06.017.
- [25] VDI 4630, “Fermentation of organic materials - Characterization of the substrate, sampling, collection of material data, fermentation tests,” *Gesellschaft Energietechnik*, p. 132, 2016.
- [26] E. W. Rice, R. B. Baird, and A. D. Eaton, *Standard Methods for the Examination of Water and Wastewater*,

23rd ed. APA, 2017.

- [27] E. O. Auma, "Anaerobic Co-Digestion of Water Hyacinth (*Eichhornia crassipes*) with Ruminant Slaughterhouse Waste under Mesophilic Conditions," *Ph. D. Thesis, Univ. Nairobi*, 2020.
- [28] T. Kahassay and W. Bogale, "Kinetic Modeling of Biogas from Food Waste: A Case Study of Ethiopian Airlines," *Thesis, Addis Ababa Inst. Technol.*, 2017.
- [29] M. R. Atelge, A. E. Atabani, C. Eskicioglu, G. Semaan, S. Unalan, and G. Kumar, "Anaerobic co-digestion of oil-extracted spent coffee grounds with various wastes: Experimental and kinetic modeling studies," *Bioresour. Technol.*, vol. 322, p. 124470, 2021, doi: 10.1016/j.biortech.2020.124470.
- [30] F. J. Baur and L. E. G., "The Association of Official Analytical Chemists (AOAC)," *J. Am. Oil Chem. Soc.*, vol. 54, no. 4, pp. 171–172, 1977.
- [31] P. Prentice, K. K. Ong, E. A. F. Van Tol, J. Vervoort, C. L. Acerini, and D. B. Dunger, "Breast milk nutrient content and infancy growth," *Acta Paediatr.*, vol. 105, pp. 641–647, 2016, doi: 10.1111/apa.13362.
- [32] J. Beshir, N. Gabbiye, V. Ramayya, and A. Seid, "Alkaline hydrogen peroxide pretreatment of cladodes of cactus (*Opuntia ficus-indica*) for biogas production," *Heliyon*, vol. 7, p. e08002, 2021, doi: 10.1016/j.heliyon.2021.e08002.
- [33] J. Lindner, S. Zielonka, H. Oechsner, and A. Lemmer, "Effect of different pH-values on process parameters in two-phase anaerobic digestion of high-solid substrates," *Environ. Technol.*, vol. 36, no. 2, pp. 198–207, 2015, doi: 10.1080/09593330.2014.941944.
- [34] O. Meneses-quelal, B. Velázquez-martí, D. De Ingeniería, and U. P. De València, "Effect of the co-digestion of agricultural lignocellulosic residues with manure from South American camelids," *Biofuels, Bioprod. Bioref.*, pp. 525–544, 2021, doi: 10.1002/bbb.2177.
- [35] J. Kim, H. Kim, G. Baek, and C. Lee, "Anaerobic co-digestion of spent coffee grounds with different waste feedstocks for biogas production," *W. Manag.*, vol. 60, pp. 322–328, 2017, doi: 10.1016/j.wasman.2016.10.015.
- [36] S. Meraj, R. Liaquat, S. R. Naqvi, and A. Zainab, "Enhanced Methane Production from Anaerobic Co-Digestion of Wheat Straw Rice Straw and Sugarcane Bagasse: A Kinetic Analysis," *Appl. Sci.*, vol. 11, no. 13, p. 6069, 2021, doi: <https://doi.org/10.3390/app11136069>.
- [37] M. D. Ulsido, G. Zeleke, and M. Li, "Biogas potential assessment from a coffee husk: an option for solid waste management in Gidabo watershed of Ethiopia," *Eng. Rural Dev.*, vol. 1, pp. 1348–1354, 2016, [Online]. Available: <https://www.tf.lbtu.lv/conference/proceedings2016/Papers/N270.pdf>.
- [38] B. Chala, H. Oechsner, S. Latif, and J. Müller, "Biogas Potential of Coffee Processing Waste in Ethiopia," *Sustainability*, vol. 10, no. 2678, pp. 1–14, 2018, doi: 10.3390/su10082678.
- [39] G. I. Budiarti, L. M. Shitophyta, Y. E. Nugroho, and D. Fajariyanto, "Biogas Production from Corn Stover by Solid-State Anaerobic Co-digestion of Food Waste," *JTKL*, vol. 4, pp. 44–52, 2020.
- [40] Y. M. B. Hamrouni and R. B. Cheikh, "Enhancing the energetic potential of Mediterranean food waste by anaerobic co-digestion with sewage sludge," *Env. Prog. Sustain. Energy*, pp. 1–10, 2020, doi: 10.1002/ep.13512.
- [41] G. Zhen, X. Lu, T. Kobayashi, G. Kumar, and K. Xu, "Anaerobic co-digestion on improving methane production from mixed microalgae (*Scenedesmus* sp., *Chlorella* sp.) and food waste: Kinetic modeling and synergistic impact evaluation," *Chem. Eng. J.*, vol. 299, pp. 332–341, 2016, doi: 10.1016/j.cej.2016.04.118.
- [42] X. Chen, W. Yan, K. Sheng, and M. Sanati, "Comparison of high-solids to liquid anaerobic co-digestion of food waste and green waste," *Bioresour. Technol.*, vol. 154, pp. 215–221, 2014, doi: 10.1016/j.biortech.2013.12.054.
- [43] Z. Guo *et al.*, "Synergistic ammonia and fatty acids inhibition of microbial communities during slaughterhouse waste digestion for biogas production," *Bioresour. Technol.*, vol. 337, p. 125383, 2021, doi: 10.1016/j.biortech.2021.125383.
- [44] S. Jijai, S. Muleng, L. Noynoo, and C. Siripatana, "Kinetic model of biogas production from co-digestion of Thai rice noodle wastewater with rice husk and different type of manure with ash supplement," *Earth Environ. Sci.*, vol. 463, p. 012008, 2019, doi: 10.1088/1755-1315/463/1/012008.
- [45] T. A. N. Zhi and N. A. N. Jason, "Co-Digestion of Food Waste and Microalgae," 2015.
- [46] P. Li, C. Cheng, C. He, R. Yu, D. Shen, and Y. Jiao, "Experimental study on anaerobic co-digestion of the individual component of biomass with sewage sludge: methane production and microbial community," *Biomass Convers. Biorefinery*, vol. 12, pp. 5045–5058, 2022, doi: <https://doi.org/10.1007/s13399-020-01049-6>.
- [47] X. Ma, M. Yu, M. Yang, M. Gao, C. Wu, and Q. Wang, "Synergistic effect from anaerobic co-digestion of food waste and *Sophora flavescens* residues at different co-substrate ratios," *Environ. Sci. Pollut. Res.*, vol. 26, pp. 37114–37124, 2019, doi: <https://doi.org/10.1007/s11356-019-06399-x>.
- [48] I. Beniche, J. Hungría, H. El Bari, J. A. Siles, A. F. Chica, and M. A. Martín, "Effects of C/N ratio on anaerobic co-digestion of cabbage, cauliflower, and restaurant food waste," *Biomass Conv. Bioref.*, vol. 11, no. 5, pp. 2133–2145, 2021, doi: 10.1007/s13399-020-00733-x.
- [49] G. Zhen, X. Lu, T. Kobayashi, Y. Li, K. Xu, and Y. Zhao, "Mesophilic anaerobic co-digestion of waste activated sludge and *Egeria densa*: Performance assessment and kinetic analysis," *Appl. Energy*, vol. 148, pp. 78–86, 2015, doi: 10.1016/j.apenergy.2015.03.038.
- [50] J. Shen and J. Zhu, "Development of General Gompertz Models and Their Simplified Two-Parameter Forms Based on Specific Microbial Growth Rate for Microbial Growth, Bio-Products and Substrate Consumption," *Adv. Biotechnol. Microbiol.*, vol. 4, no. 3, 2017, doi: 10.19080/aibm.2017.04.555640.



# Characterization of the properties of essential oils obtained by various distillation methods

<sup>1</sup>Michał Myszak, <sup>1</sup>Patryk Zdziobek, <sup>2</sup>Joanna Chmiel, <sup>3</sup>Marta Wójcik

<sup>1,3</sup>AGH University of Science and Technology, Faculty of Energy and Fuels, 30-059 Cracow, Poland, e-mail: zdziobek@agh.edu.pl

<sup>2</sup>AGH University of Science and Technology, Faculty of Energy and Fuels, 30-059 Cracow, Poland, Student's research circle "Bio-logika",

---

## Abstract

The presented analyses focus on examining the antioxidant properties of essential oils obtained under laboratory conditions. For this purpose, buds of clove, cumin seeds, fruits of common caraway, and needles of silver fir were utilized. The first step involved determining the moisture content in the plant material to assess the efficiency of the applied methods for obtaining hydrosols. Three different extraction methods—simple distillation, steam distillation, and percolation—were employed to obtain mixtures of water and essential oils. The purification of essential oils was carried out through extraction using methylene chloride and evaporation using a rotary membrane evaporator. To evaluate the antioxidant properties of the obtained essential oils, the DPPH and ABTS<sup>+</sup> methods were applied, based on the Equivalent Antioxidant Capacity of Vitamin C (VCEAC). Additionally, an FT-IR analysis was conducted by comparing the spectra of the obtained essential oils with reference spectra of substances present in the examined oils at the highest concentrations. The entire study aimed to define and compare the antioxidant properties of essential oils derived from different plant materials and using different extraction methods. The obtained results may be relevant to the cosmetic, pharmaceutical, or food industries, where antioxidant properties can be significant. Furthermore, the FT-IR (Fourier Transform Infrared Spectroscopy) analysis provided additional information regarding the chemical composition of the obtained essential oils.

**Keywords:** antioxidants, plant material, essential oil, distillation

---

## 1. Introduction

Essential oils are aromatic and volatile liquids extracted from plant materials such as flowers, roots, bark, leaves, seeds, fruits, and entire plants. Throughout history, these substances have garnered significant interest due to their wide-ranging applications in the cosmetic and food industries. The extraction of essential oils from plants involves the use of a diverse range of local household methods or more industrialized processes on a larger scale [1]. Estimate the antioxidant properties is possible with the help of DPPH and ABTS<sup>+</sup> methods, which measure the speed at which antioxidants capture synthetic free radicals. The samples are then analyzed spectrophotometrically to determine antioxidant activity.

Distillation is the most commonly employed technique for extracting essential oils. This process is relatively time-consuming, and the quantity of obtained oil depends on factors such as the type of plant material, temperature, pressure, and the duration of the process. The extraction method employed also influences the efficiency of obtaining essential oils because it is not possible to subject all plants to the same method under identical conditions. An example of such a phenomenon is the application of simple distillation, which, unlike steam distillation, proves to be more effective in extracting essential oil from smaller-sized raw materials [1, 2].

In addition to their distinctive aroma, essential oils are characterized by potent antioxidant properties. Due to the harmful effects of free radicals, there is a growing interest in natural sources of antioxidants. Essential oils exhibit varying levels of antimicrobial and antioxidative activities, as exemplified by rosemary oil, which has a stimulating effect on the sympathetic nervous system [3].

To assess the antioxidant properties of essential oils, two popular methods are commonly employed: the DPPH and ABTS+ methods, which involve measuring the impact of antioxidants on the rate of scavenging synthetic radicals. As a result of the reaction, the analyzed samples are examined spectrophotometrically, and the antioxidant activity is determined, for example, based on the equivalent of a reference substance possessing antioxidative properties [4].

These antioxidant properties can also be used to protect biofuels against aging.

## 2. Characteristics of analyzed essential oils

### 2.1 Clove - *Syzygium aromaticum*

The clove tree, scientifically known as *Syzygium aromaticum*, is a perennial tropical plant used for obtaining plant material to produce essential oil. The resulting clove oil is widely applied in the medical and cosmetic industries [5]. The raw material, comprising cloves, leaves, and stems of the clove tree, is typically sourced from regions such as Zanzibar, Indonesia, or Madagascar, with variations in the content of clove oil (see Figure 1) [6].

### 2.2 Cumin - *Cuminum cyminum L.*

Cumin (*Roman cumin, Cuminum cyminum L.*) is one of the most popular spices, used for its unique aroma. The taste of Roman cumin is assessed based on the content of volatile oil, which is responsible for its distinctive scent. *Cuminum cyminum L.* is an annual plant that grows to a height of 15-50 cm, featuring oval fruits, a bitter and sharp taste, and small 4-5 mm seeds [7, 8].

### 2.3 Common caraway - *Carum carvi L.*

Common caraway (*Carum carvi L.*) is a biennial plant native to Western Asia, Northern Africa, and Europe. It features feathery leaves that grow on stems measuring 20–30 cm and small, white flowers, with an overall height reaching up to 60 cm. The fruits of caraway are known for their pungent, anise-like aroma attributed to the presence of essential oil, making it a widely utilized spice in bread and various food items [9,10].

### 2.4 Fir Needle Oil- *Abies alba M.*)

The European silver fir (*Abies alba M.*) is a long-lived evergreen coniferous tree that can grow up to 60 meters in height. It is predominantly found in mountainous regions across Western, Eastern, Southern, and Central Europe. This plant holds significant economic and ecological value. The timber extracted from it is recognized for its robustness and lightness, making it widely employed in construction and furniture making. As a component of forest ecosystems, the European silver fir contributes to preserving biodiversity in wooded areas. It is distinguished by a deep and well-established root system that provides stability. Additionally, the fallen needle litter has a positive influence on forest management practices [11,12,13].

## 3. Materials and methods

### 3.1. DPPH method

Year after year, there is a growing interest in antioxidant substances that have the potential to protect the human body from the harmful effects of free radicals. Additionally, their impact on the degradation process of fats and other food components is increasingly studied. As a result of this trend, there is a simultaneous increase in methods used to assess the effectiveness of specific substances as antioxidants [14]. One of the more commonly employed methods is based on the use of a stable radical - 2,2-diphenyl-1-picrylhydrazyl (DPPH), which is characterized by an intense purple color due to the presence of a delocalized electron in its structure [14].

The methodology for assessing antioxidant activity through this approach involves combining an alcoholic DPPH solution with the substance under examination. In this reaction, the stable free radical captures electrons from the tested antioxidant, leading to a color shift from purple to yellow. The alteration in color is examined using spectrophotometry at a wavelength around 517 nm. The calculated indicator of antioxidant activity is the IC50 value, representing the concentration of the compound with antioxidative properties that results in a 50% reduction in the

initial DPPH radical concentration. An alternative method for evaluating oxidative potential is to use equivalent reference substances with demonstrated antioxidant effects, such as ascorbic acid [14, 15].

Due to the absorption occurring in the visible light range, spectrophotometric measurement can be performed using standard plastic cuvettes, and alcohol solvents such as methanol or ethanol, which do not interfere with the course of the reaction. The obtained basic DPPH solution is incubated at a temperature of about 25°C, but due to its progressive degradation, the measurement should be carried out within an hour. The result of the analysis is expressed as a percentage of scavenging free radicals, applying the following relationship or conducting a series of equivalent samples of a reference substance at increasing concentrations, such as ascorbic acid, using linear regression [42].

### 3.2. ABTS method

The use of the ABTS<sup>+</sup> cation radical [2,2'-azobis(3-ethylbenzothiazoline-6-sulfonic acid)] allows, similar to the DPPH method, the determination of the antioxidant activity of the substances under investigation. The analysis involves the prior preparation of this compound by conducting the oxidation reaction of ABTS (Fig. 1.), using, for example, potassium persulfate. The result is the formation of a solution of the ABTS<sup>+</sup> cation radical with an intense, bluish-green color [15,16,17].

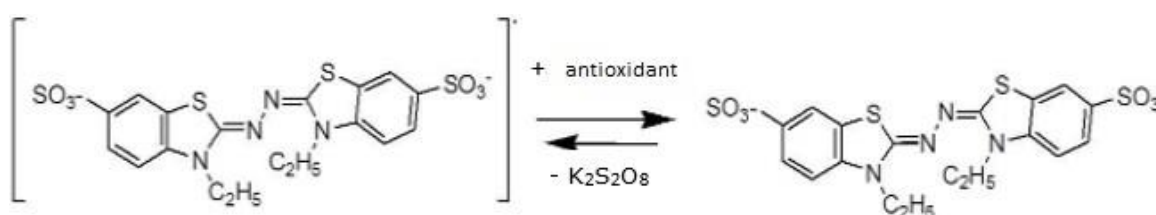


Fig. 1. The structure of the free and stable ABTS radical.

The addition of an antioxidant causes the reduction of the ABTS<sup>+</sup> cation radical to its stable form, resulting in the disappearance of the bluish-green color of the solution. The antioxidant activity is assessed spectrophotometrically at a wavelength of 734 nm, and the content of antioxidants is measured as the quantity of equivalent reference substance per unit volume or mass, similar to the DPPH method [15].

To calculate the VCEAC values, standard curves were prepared showing the relationship between absorbance and the concentration of ascorbic acid for DPPH and ABTS in the range of (100-1000 µg/mL). Based on these curves, linear regression equations were derived as follows:

- DPPH- Linear regression equation, Coefficient of determination ( $y=0.0019x+0.0748$ ,  $R^2=0.9928$ )
- ABTS- Linear regression equation, Coefficient of determination ( $y=0.0002x+0.0916$ ,  $R^2=0.9956$ )

### 3.3. FT-IR

The ATR (Attenuated Total Reflectance) technology is widely employed in Fourier Transform Infrared Spectroscopy (FT-IR) as one of the most frequently used sampling methods. This is because it allows for the convenient and swift measurement of various samples, including liquids, solids such as powders and pastes. In ATR sampling, infrared light passes through a crystal and undergoes total reflection at the point where the crystal contacts the sample. The reflected light is then partly directed towards the detector, while another part is absorbed by the sample [18].

For the analysis of liquid and paste samples, a few drops are typically applied to the ATR crystal, and the measurement is carried out. Subsequently, the crystal is cleaned, often using solvents like ethanol. Analyzing powders or other solid samples follows a similar procedure of applying the sample to the ATR crystal and using a rotating press to ensure optimal contact between the sample and the crystal. ATR analysis is extensively used in the pharmaceutical industry and academic settings, particularly for examining polymers utilized in pharmaceutical packaging.

The aim of the FT-IR study was to identify substances characteristic of the specific essential oils presented in the first chapter of the thesis. To achieve this, the obtained clove, cumin, caraway, and fir essential oils were examined for the presence of eugenol, carvone, cumin aldehyde, and bornyl acetate, respectively. This was done using the FT-IR

spectrometer PerkinElmer Frontier Spotlight 400 with an ATR accessory for liquids, equipped with MIR and DTGS detectors, and an additional wide-range MCT detector.

## 4. Experimental

### 4.1. Producing Clove Hydrosol - Percolation

To obtain clove hydrosol from clove bud using the percolation method, a setup for this process was prepared. The setup consisted of a round-bottom flask containing boiling stones and distilled water, occupying about half of the flask's volume. The round-bottom flask was then connected through its neck to a Hempel column with a joint, into which a weighed portion of cloves (65.52 g) was introduced, completely filling the percolation column. The upper outlet of the column was connected with a distillation adapter, which was sealed on one side with a glass stopper and on the other side connected to a condenser attached to the lower nozzle with a cold water tap. The final element of the setup was an extension with a prepared one-liter receiver. To ensure stability, the percolation setup was supported by a lift, on which a container for collecting the hydrosol was placed, and by two stands with attached clamps with a socket (Fig. 2. A).

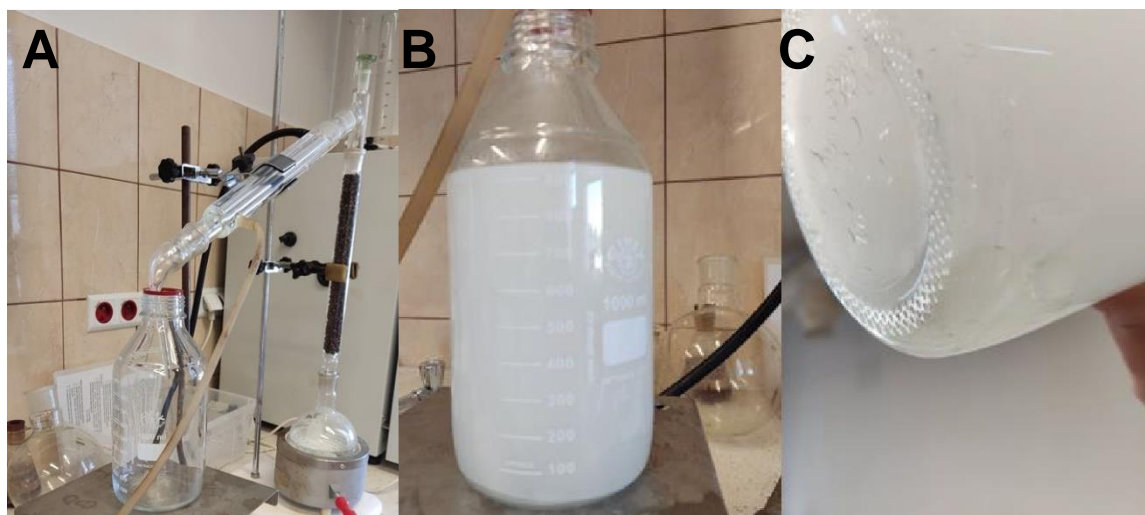


Fig. 2. Set to percolation (A) collected hydrosol (B) and aggregated droplets (C).

After confirming the airtightness of the percolation setup, the cold water supply to the condenser was activated, and the heater was turned on to initiate the percolation process. About 30 minutes into the boiling of water in the round-bottom flask, condensation occurred in the receiver, resulting in a pale white, sticky liquid with a pleasant clove fragrance. Furthermore, there was a noticeable change in the color of the contents in the flask – the distilled water took on a reddish-brown hue.

After 2-3 hours from that point, nearly half of the volume of clove hydrosol had been collected in the receiver, and the content of the round-bottom flask had turned black. At this juncture, a few drops of the obtained product were sampled onto a watch glass. Since the examined drops were not adhesive and did not release a clove aroma, the percolation process was halted. This involved turning off the heater, closing the water supply to the condenser, and removing the spent clove material from the process. Subsequently, the Hempel column was reloaded with "fresh" cloves weighing 65.08 g, and the distilled water in the flask was replaced. After reconfirming the system's airtightness, the water flow to the condenser was resumed, and the heater was switched on, initiating another round of extracting essential oil from cloves.

The second percolation was conducted until the receiver was fully filled. This process yielded approximately one liter of a blend of water and clove oil (Fig. 2. – B). Shortly thereafter, the emergence of a thin layer of clove oil at the container's bottom was noticed (Fig. 2. – C).

#### 4.2 Receiving Caraway and Cumin Hydrosol - Steam distillation

In the initial step, aimed at obtaining caraway and cumin hydrosol, the grinding of caraway seeds and common cumin fruits was carried out using a mill. The fragmentation of the plant material used in this process was essential to facilitate the extraction of essential oil by steam distillation.

In the next stage, a steam distillation setup was prepared, consisting of a single-neck round-bottom flask placed on a lift in a heater. The round-bottom flask containing boiling stones was filled to 2/3 of its volume with distilled water and connected with a single joint through a distillation head and an extension with a three-necked round-bottom flask. In the three-necked flask, ground plant material weighing 500 g was placed. The second joint of the flask was sealed with a glass stopper, and the third joint was connected to the condenser, similar to the steam distillation process discussed earlier. The endpoint of the condenser, as in the previously described process, was a attached liter receiver (Fig. 3. A).

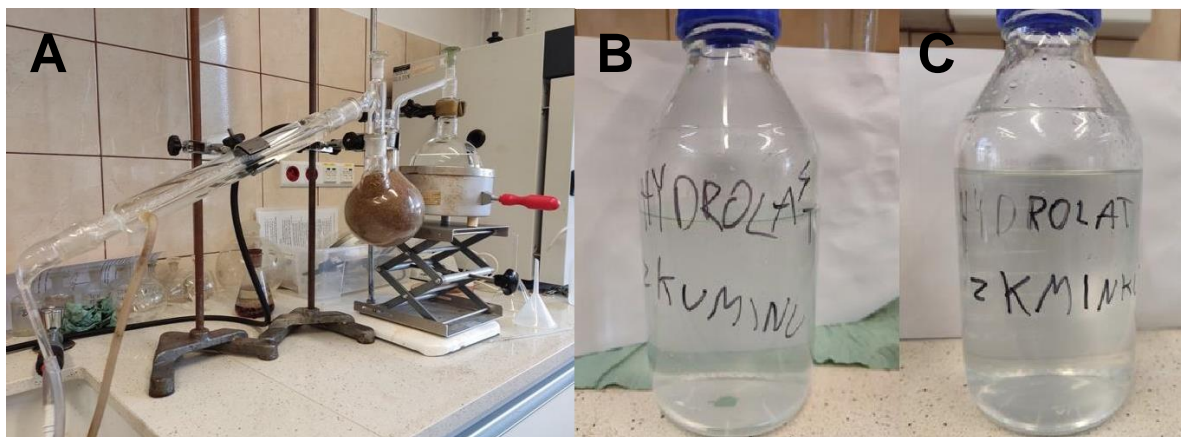


Fig. 3. Steam distillation setup (A), caraway hydrosol (B) and cumin hydrosol (C).

In a similar fashion to percolation, it was confirmed that the devised setup was airtight. Subsequently, the water supply to the condenser was activated, and the heater was switched on to commence the distillation process. Approximately 30 minutes later, noticeable changes in the color of the upper layer of the ground plant material in the three-necked flask were observed for both caraway and common cumin, indicating the infiltration of steam generated from the round-bottom flask. After 45 minutes, the condenser exhibited the condensation of initial droplets, forming a mixture of water and essential oil. Distillation was continued in both cases until the collection vessel was completely filled. This entire process spanned over 3 hours. Throughout this duration, efforts were made to agitate the ground plant material in the three-necked flask with a rod to enhance the interaction of steam with caraway and common cumin. Moreover, distilled water was periodically added to the round-bottom flask to sustain the driving force of the process, driven by the generated steam.

The outcome of this procedure yielded approximately 1 liter of hydrosol from caraway and common cumin. In both instances, the emergence of a delicate, pale-yellow upper layer, representing the essential oil, was evident (Fig. 3. A & B).

#### 4.3 Obtaining Fir Needle Hydrosol - Simple Distillation

In a manner similar to the procedures applied for cumin and caraway, the production of fir needle hydrosol commenced by fragmenting the plant material. Scissors were employed to cut the fir needles into smaller segments. Subsequently, a setup for simple distillation was arranged, comprising a round-bottom three-neck flask. This flask contained previously measured and cut silver fir needles, weighing 250 g, along with boiling stones. Distilled water was then poured over the entire mixture to completely submerge the plant material. The three-neck flask was positioned in a heater mounted on a lift, and one of the flask's necks was connected, much like in steam distillation, to a condenser linked with a faucet supplying cold water. The opposite end of the condenser was affixed to a liter receiver (Fig. 4. A).





Fig. 4. Set for atmospheric distillation with cut silver fir needles (A) and its hydrosol (B)

After confirming that the setup for simple distillation was properly arranged, the condenser's cold-water supply was connected, and the heater was activated to commence the extraction process. Approximately 2 hours into the simple distillation, just under a liter of silver fir needle hydrosol was produced. As observed in the previous instances, there was the emergence of a delicate, cloudy upper layer, indicative of the essential oil (Fig. 4. B).

#### 4.4 Extraction essential oils from hydrosol

Distillation with steam, percolation, and simple distillation allowed for obtaining water and essential oil mixtures from cloves, cumin seeds, common caraway fruits, and common spruce needles. To obtain pure essential oils, the water content was initially pipetted out from the vessels using a glass pipette with an attached pump, taking care not to remove the fine layer of essential oil. Next, 20 ml of dichloromethane was added to each of the liter-sized receivers. In the following step, the contents were shaken for several minutes. Periodically, the lids of the vessels were opened to equalize the pressure between the surroundings and the vessel interior. As a result of the extraction, two separate phases formed in each receiver: an upper inorganic layer consisting of water and a lower organic layer consisting of essential oil along with dichloromethane. After pipetting out the separated water layer, the residue was transferred to a separation funnel, to which an additional portion of dichloromethane was added. The separation funnel was closed with a stopper, and then the entire mixture was shaken, keeping the separation funnel with the valve up. The valve was opened every now and then to remove air and equalize pressure. Finally, the separation funnel was placed on a stand, and after observing the formation of two distinct phases after a few minutes, the lower layer was poured into a separate container, while the upper layer was discarded (Fig. 5.).



Fig. 5. Extraction of clove hydrosol

To clean the container that initially held the hydrosol from a specific plant, a third portion of dichloromethane was introduced into the collecting vessel. Following this, the remaining residue was divided using the pear-shaped separating funnel in a manner similar to the previous steps. This procedure yielded the organic phase, consisting of dichloromethane along with the essential oils, including clove, cumin, caraway, and spruce.

In order to separate methylene chloride from the desired essential oils, a rotary evaporator RV 10 digital V with vacuum pump was used. This apparatus includes a water bath and a spiral condenser. The process was conducted under reduced pressure, with the addition of a KNF Lab vacuum pump membrane to the setup.

To ensure that all methylene chloride was removed, the obtained essential oils were thoroughly rinsed using compressed nitrogen from a cylinder. Subsequently, their volume was determined using a measuring cylinder.

## 5. Results

Table. 1. The obtained results regarding the quantity of essential oils obtained through a specific method of hydrosol production.

The plant material	Clove buds	Cumin seeds	Simple caraway	Common fir needles
The method of hydrosol obtaining	Percolation	Steam distillation	Steam distillation	Atmospheric distillation
The total mass of plant material [g]	130.6	500	500	250
The volume of essential oil [ml]	15	10	5.50	0.70

Based on the above data (Tab.1.), it was determined that the steam distillation of cloves buds allowed for obtaining the highest amount of essential oil (15 ml) with the least amount of plant material utilized. The steam distillation process also yielded 10 ml of cumin oil and 5.5 ml of caraway oil using the same quantity of cumin seeds and caraway fruits. In the case of steam distillation of common fir needles, only 0.70 mL of essential oil was produced from 250 g of needles.

Table. 2. The data, along with the obtained results and calculated values of the yield of obtaining hydrosols from a given plant.

The plant material	Clove buds	Cumin seeds	Simple caraway	Silver fir needles
The method of hydrosol obtaining	Percolation	Steam distillation	Steam distillation	Dry distillation
Density of essential oil (25°C) [ $\frac{g}{mL}$ ]	1.040	0.925	0.910	0.909
The total mass of plant material [g].	130.6	500	500	250
The content of dry matter of plant material [g]	97.268	450.116	438.697	109.212
The yield of obtaining hydrosol. [%]	16.04	2.06	1.14	0.54

The efficiency of the clove bud percolation process, compared to the other methods, was the highest, reaching over 16%. The ability to obtain other hydrosols was significantly lower, ranging from 0.5% to approximately 2%. In the case of steam distillation, the distillation of cumin seeds was more effective, despite the higher dry mass of plant material compared to caraway fruits. The simple distillation process proved to be the least efficient. Distilling 250 g of common fir needles resulted in the smallest portion of essential oil, with a method efficiency of only 0.54%.

Table. 3. Results regarding the antioxidant activity of essential oils using the DPPH method.

Type of oil	Average VCEAC	
	DPPH method	ABTS method
Clove oil	600.684±0.091	946.2±4.60
Cumin oil	85.790±0.110	319.5±2.20
Caraway oil	578.05±0.180	640.17±0.76
Fir oil	583.53±0.130	702.33±0.58

Based on the obtained results (Tab. 3.), it was found that clove oil exhibits the strongest antioxidant properties among the investigated essential oils. The DPPH method, along with the use of an antioxidant equivalent in the form of ascorbic acid, allowed for determining the free radical scavenging value by clove oil at a level of 600.684±0.091. Fir oil and caraway oil showed similar antioxidant properties, with fir oil obtained from common fir needles being more effective (583.53±0.130). Cumin oil exhibited the lowest antioxidant activity, with a value of only 85.79±0.110.

The application of the ABTS method to the four essential oils revealed that clove oil exhibited the strongest antioxidant properties (946.2±4.60) among all the investigated oils (Tab. 3.). Common fir needle oil demonstrated a free radical scavenging ability at a level of 702.33±0.580. Caraway and cumin oils showed the weakest antioxidant properties, with values of 640.17±0.76 and 319.5±2.20, respectively.

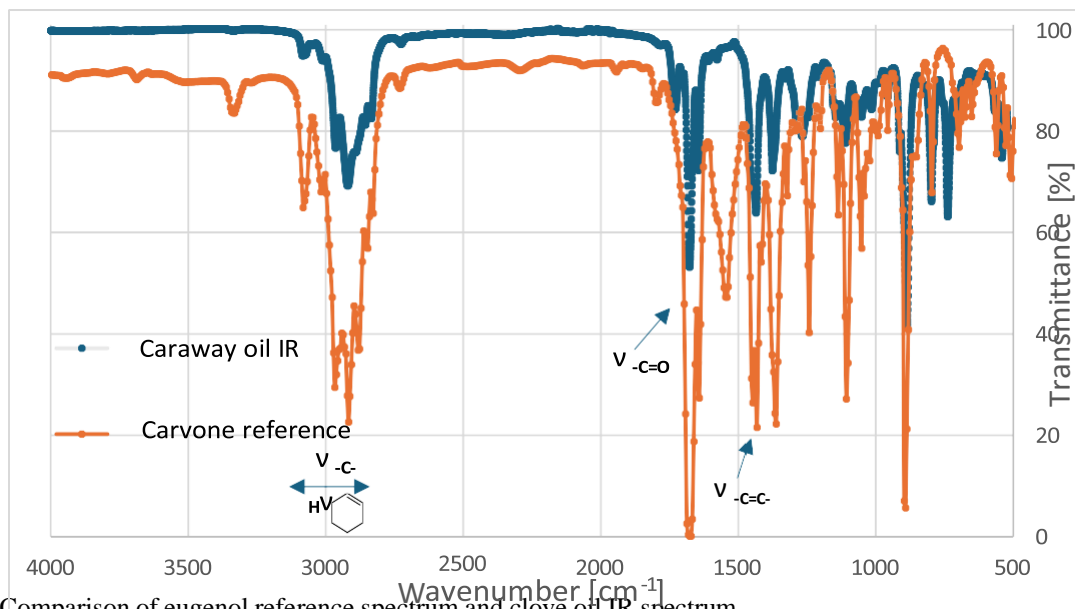


Fig. 6. Comparison of eugenol reference spectrum and clove oil IR spectrum

The comparison of the caraway oil spectrum with the reference spectrum of carvone (Fig. 6.) allowed for the identification of stretching vibrations (3000-2800 cm<sup>-1</sup>) associated with the presence of the alkyl group. Additionally, the presence of the characteristic cyclohexenyl group of carvone was observed in the range of 3100-

2800  $\text{cm}^{-1}$ . Finally, a prominent peak at 1670  $\text{cm}^{-1}$  indicated the presence of a ketone group, and a peak in the region of 1450-1430  $\text{cm}^{-1}$  suggested the presence of a double bond. Through this analysis, the participation of carvone in the examined essential oil was confirmed.

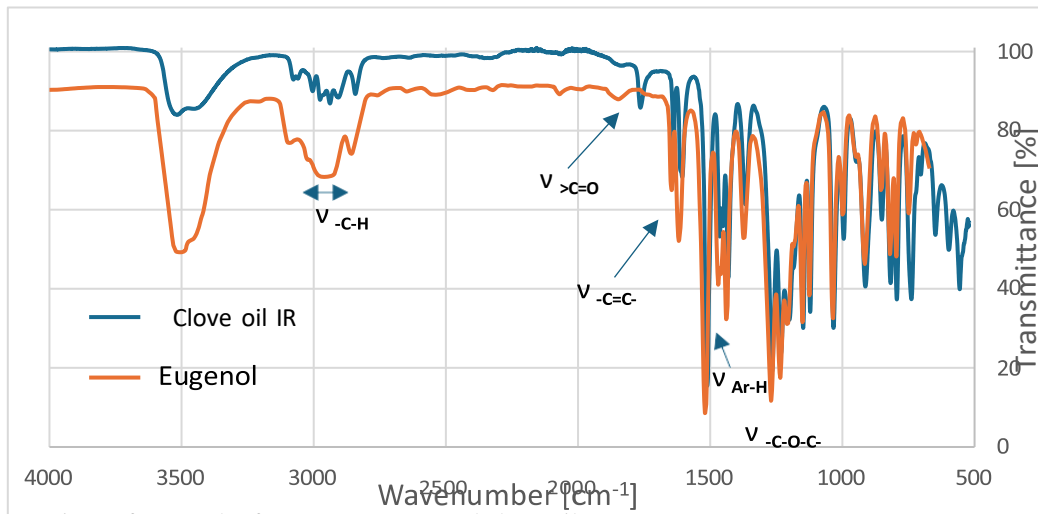


Fig 7. Comparison of eugenol reference spectrum and clove oil IR spectrum

By overlaying the spectrum of the laboratory-produced clove oil with the reference spectrum of eugenol (Fig. 7.), similarities in the range of 3700-3400  $\text{cm}^{-1}$  were observed. Within this range, absorption bands associated with the vibrations of the hydroxyl group were identified. Additionally, the region from 3000-2800  $\text{cm}^{-1}$ , related to the stretching vibrations of the alkyl group, was characteristic. The range of 1800-1600  $\text{cm}^{-1}$  confirmed the presence of the carbonyl group and the double bond characteristic of alkenes. Finally, the long absorption bands in the 1600-1400  $\text{cm}^{-1}$  range were attributed to the aromatic group, while the isolated peaks in the 1300-1200  $\text{cm}^{-1}$  range were associated with the ether group. In summary, the presence of the hydroxyl, carbonyl, aromatic, alkyl, ether, and double bond groups allowed for the identification of eugenol in the examined sample of clove oil.

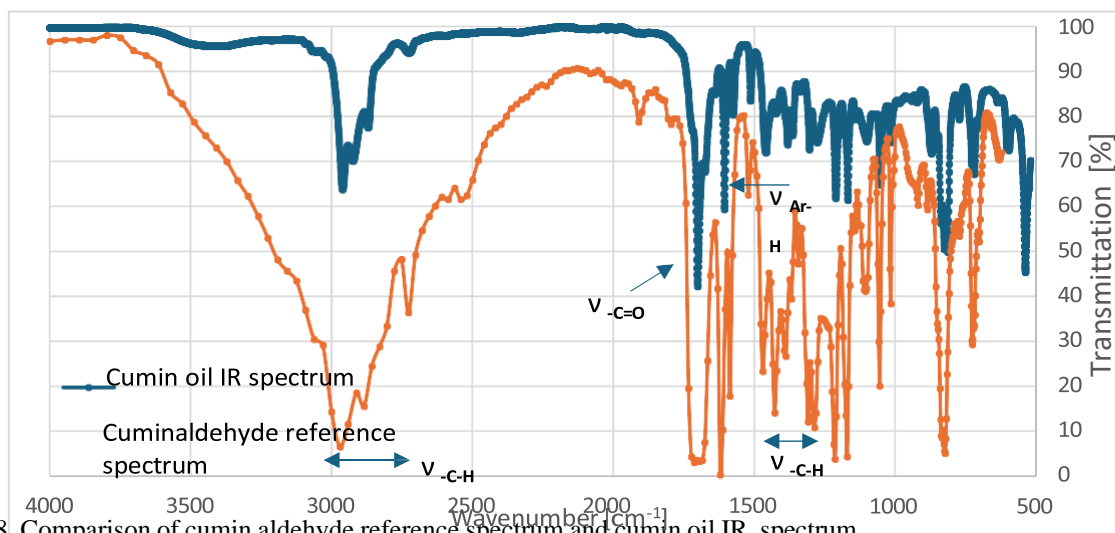


Fig. 8. Comparison of cumin aldehyde reference spectrum and cumin oil IR spectrum

In the analysis of cumin oil (Fig 8.) along with the spectrum of cumin aldehyde, similar to the previous case, the presence of bands characteristic of the alkyl group (3000-2800  $\text{cm}^{-1}$ ) was observed and confirmed by deformation vibrations (1485-1365  $\text{cm}^{-1}$ ). Additionally, a peak at 1730  $\text{cm}^{-1}$ , associated with stretching vibrations, confirmed the presence of the carbonyl group in aldehydes. The absorption band, similar to the clove oil spectrum in the range of 1600-1500  $\text{cm}^{-1}$ , allowed for the identification of the aryl group. The presence of an aromatic ring, the aldehyde group, and the alkyl group confirmed the presence of cumin aldehyde in the oil obtained from Roman cumin.

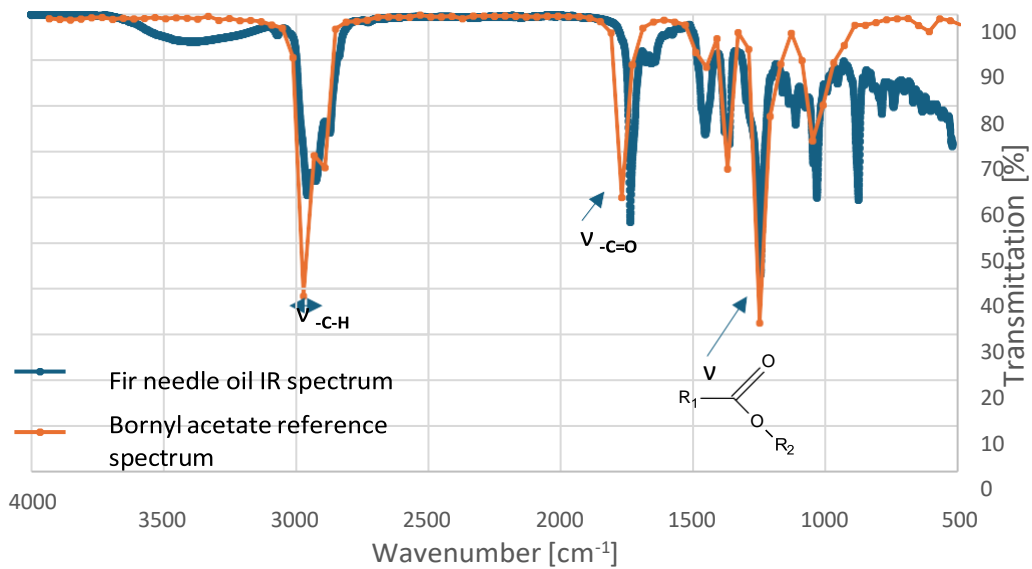


Fig. 9. Comparison of bornyl acetate reference spectrum and fir needle oil IR spectrum

The analysis (Fig. 9.) of fir oil and bornyl acetate allowed for the identification of similar stretching vibrations of C-H bonds in the range of 3000-2890  $\text{cm}^{-1}$ . Additionally, a distinctive long peak at 1250  $\text{cm}^{-1}$  was identified, associated with the presence of the divalent functional group found in esters. Confirmation of this was provided by the stretching vibrations of the carbonyl group at 1770  $\text{cm}^{-1}$ . Classifying the substance under investigation as an ester confirmed the presence of bornyl acetate in the fir oil.

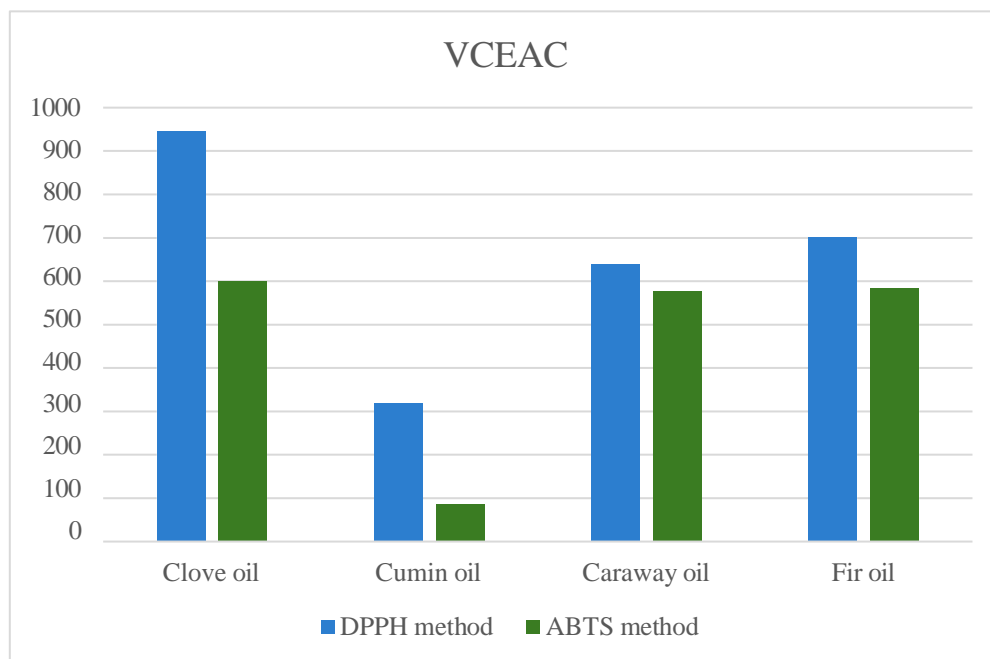


Fig. 10. Comparison of the antioxidant activity of essential oils using the DPPH and ABTS<sup>+</sup> methods.

## 6. Conclusions

The analysis of the antioxidant characteristics of essential oils derived from clove, cumin, caraway, and fir buds through the DPPH and ABTS<sup>+</sup> methods indicated that clove bud oil could be the most efficient in addressing the formation of free radicals in the body (Fig. 10.). In comparison, fir bud oil and caraway oil exhibited lower effectiveness in the assessed parameter, with cumin oil demonstrating the least antioxidant properties among the oils under investigation. The FT-IR examination of clove, cumin, caraway, and silver fir needle oil samples facilitated the recognition of eugenol, cumin aldehyde, carvone, and bornyl acetate, respectively. According to relevant literature, these components are acknowledged as the primary constituents of these oils. Furthermore, a comparison of the

essential oil spectra with reference spectra of substances most concentrated in each plant part from the NIST database demonstrated a significant resemblance in the positions of specific absorption bands. This provides evidence that clove, cumin, caraway, and fir oils were effectively derived. Importantly, the FT-IR analysis didn't reveal the presence of the methylene chloride used in extraction, and this was corroborated by obtaining pure essential oils.

The identification of aromatic substances in essential oils with antibacterial, analgesic, and anticancer properties served to validate the existence of antioxidant qualities in clove, cumin, caraway, and fir oils.

The antioxidant properties of essential oils can be used to compose anti-aging additives for biofuels alone [19] or in a matrix with other compounds, such as polyphenols.

## References

- [1] Preedy V. R., *Essential oils in food preservation, flavor and safety*, Department of Nutrition and Dietetics, Londyn, 2016.
- [2] Mahfud M., et al., *Extraction of essential oil from Bangle (Zingiber purpureum Roxb.) by hydrodistillation and steam distillation methods*, Journal of Chemical Technology and Metallurgy, 52, 5, 2017, 791-796, Indonezja, 2017.
- [3] Yang S., et al., *Radical Scavenging Activity of the Essential Oil of Silver Fir (Abies alba)*, J. Clin. Biochem. Nutr., 44, 253–259, Daegu, South Korea, 2009.
- [4] Flieger J., et al., *Antioxidants: classification, natural sources, activity/capacity measurements, and usefulness for the synthesis of nanoparticles*, MDPI, 2021.
- [5] Jirovetz L., et al., *Chemical composition and antioxidant properties of clove leaf essential oil*, Journal of agricultural and food chemistry, Vienna, 2006.
- [6] Mahulette A.S., et al., *Physico-chemical properties of clove oil from three forest clove accessions groups in Maluku*, IOP conf. Ser.:Earth Environ. Sci. 418 012028.
- [7] Boughendjioua H., *Characterization of aroma active compounds of cumin (Cuminum Cyminum L.) seed essential oil, modern applications of bioequivalence & bioavailability*, Sakikda, 2019.
- [8] Gotmare S. R., et al., *Chemical characterization of cumin seed oil (Cuminum Cyminum) by GCMS and its comparative study*, International journal of scientific research in biological sciences, Santa Cruz, Bombaj, 2018.
- [9] Preedy V. R., *Essential oils in food preservation, flavor and safety*, Department of Nutrition and Dietetics, Londyn, 2016.
- [10] Raal A., et al., *The content and composition of the essential oil found in Carum carvi L. commercial fruits obtained from different countries*, Journal of essential oil research, Londyn, 2012.
- [11] European Forest Genetic Resources Programme – jodła pospolita, <https://www.euforgen.org/species/abies-alba/>, Access: 03.04.2023.
- [12] Wolf, H. 2003. EUFORGEN Technical Guidelines for genetic conservation and use for silver fir (Abies alba). International Plant Genetic Resources Institute, Rzym, Włochy, 6 stron.
- [13] Konnerth M., Bergmann F., *The geographical distribution of genetic variation of silver fir (Abies alba, Pinaceae) in relation to its migration history*, Plant Systematics and Evolution, Austria, 1995.
- [14] Molyneux P., *The use of the stable free radical diphenylpicryl- hydrazyl (DPPH) for estimating antioxidant activity*, Songklanakar J. Sci. Technol., 2004, 26(2) : 211-219.
- [15] Wilczyńska A., *Metody oznaczania aktywności antyoksydacyjnej miodów pszczelich*, BROMAT. CHEM. TOKSYKOL. – XLII, 2009, 3, str. 870 – 874.
- [16] Drużyńska B., et al., *Składniki bioaktywne i właściwości przeciwrodnikowe wybranych owoców egzotycznych, Aparatura badawcza i dydaktyczna*, Warszawa, 2014.

- [17] Rayess Y. E., et al., *Analytical methods for wine polyphenols analysis and for their antioxidant activity evaluation*, *Wine: Phenolic Composition, Classification and Health Benefits*, lipiec, 2014.
- [18] *Akcesoria do pobierania próbek ATR do spektrometru Agilent Cary 630 FTIR*  
<https://www.agilent.com/cs/library/technicaloverviews/public/5991-6858EN.pdf>, Access: 02.02.2023.
- [19] Jeena K., Liju V.B. Kuttan R., *Antioxidant, anti-inflammatory and antinociceptive activities of essential oil from ginger*, *Indian Journal of Physiol Pharmacol.* 2013; 57(1):51-62

# Critical assessment of slagging and fouling indicators for animal derived biomass with the use of aluminosilicate additives.

Kamil Niesporek <sup>1</sup>, Izabella Maj <sup>1</sup>

<sup>1</sup>Politechnika Śląska/ IŚiE/KMiUE, Stanisława Konarskiego 18, 44-100 Gliwice,  
adres e-mail:kamil.niesporek@polsl.pl; izabella.maj@polsl.pl

---

## Abstract

In this study, the impact of aluminosilicate fuel additives on slagging, fouling and ash agglomeration was assessed using slagging indices. Two different types of animal-origin biomass, chicken litter and cattle manure, with significantly different chlorine contents in the ash, were investigated. Three most common fuel additives were examined: halloysite, kaolin and bentonite. It was observed that the use of aluminosilicate additives for low-chlorine cattle manure with high ash fusion temperatures does not positively influence the slagging indices results. Contrary, the addition of each additive increased the deformation temperatures of the high-chlorine chicken litter ash. Nevertheless, the results showed that the indices based on the composition of the ash are not suitable for evaluating biomass due to significant discrepancies. Instead, the assessment should be based on laboratory research and ash fusion temperature tests.

**Keywords:** biomass, waste, aluminosilicates, chicken litter, cattle manure, biomass ash, ash fusion temperature, slagging, fouling

---

## 1. Introduction

The limited availability of conventional fossil fuel reserves and the high emissions rates associated with their energy use are driving the search for more sustainable and environmentally friendly energy sources. Currently, there is a significant shift towards renewable energy sources like solar and wind power. However, the instability of these energy sources is a challenge, dependent on current weather conditions [1]. This necessitates the need for electrical energy storage. In this context, biomass, one of the oldest energy sources used by humanity, presents a promising alternative as an energy resource that can provide stable and CO<sub>2</sub> emission neutral energy. It has great potential as a bridge tool in the ongoing energy transformation, with the aim of replacing highly emitting coal-fired power plants. The application of carbon dioxide capture and storage (CCS) technology in biomass-fired energy systems (BECCS) offers the possibility of achieving negative carbon dioxide emissions [2], [3].

Despite its potential, the use of biomass as energy is not without drawbacks. Current boiler designs are not well suited for combustion of biomass as they were originally designed for fossil fuels with a different elemental composition. Biomass is characterised by a high content of unwanted elements such as K, Na, and Cl, leading to the formation of chlorides and alkali metal oxides in ash, which promotes ash fusion, agglomeration, and slagging [4], [5]. This leads to more frequent boiler maintenance, decreased process efficiency and increased operating costs. To mitigate the adverse effects of biomass ash on boiler operation, special fuel additives are used to influence the reactions within the combustion chamber and the chemical composition of the ash [6]. Essentially, the fuel additive is expected to reduce the concentration of problematic chemical compounds in the ash and result in an increase in the characteristic ash fusion temperatures. A group of prospective additives is aluminosilicate minerals such as kaolin, bentonite, or halloysite. In the literature, studies focus on the influence of aluminosilicate additives on the characteristics of biomass ash, primarily of plant origin, and their effect on ash fusion temperatures.

The authors of the study [7] conducted research in order to reduce agglomeration problems in fluidized bed boilers, which are commonly used for the combustion of biomass. In their research, they focused on the use of two additives:



dolomite and kaolin. They used biomass in the form of a mixture of miscanthus and wheat straw. In the case of kaolin, it was observed that it features the ability for potassium adsorption. This phenomenon allowed for the formation of high-melting-point alkaline aluminosilicates. Interestingly, the adsorption occurred at a significant depth within the kaolin structure, reaching around 60  $\mu\text{m}$ , although typically limited to about 20  $\mu\text{m}$ . Additionally, modelling the behaviour of fuel ash with the addition of kaolin using the FactSage software predicted a substantial reduction in the formation of molten phase as a result of the increased ash fusion temperatures.

In the study by Steenari and Lindqvist [8], research using dolomite and kaolin is presented. In this work, biomass in the form of various types of rapeseed, wheat, and barley straw was examined. The authors investigated the reactions between straw ash and kaolin,  $\text{Al}_2\text{Si}_2\text{O}_5(\text{OH})_4$ , or dolomite,  $\text{CaMg}(\text{CO}_3)_2$ . It was found that kaolin was a more effective additive. The reaction between kaolin and potassium salts in straw ash resulted in  $\text{KAlSiO}_4$  and  $\text{KAlSi}_2\text{O}_6$ . A laboratory study of reactions involving  $\text{K}_2\text{SO}_4$  or  $\text{KCl}$  and kaolin showed that various products are possible, including kalsilite ( $\text{KAlSiO}_4$ ). The capture of potassium by kaolin partly explained the higher ash fusion temperature of the ash-additive mixture. Contrary, no reaction between dolomite and potassium compounds was detected.

In the study by Roberts et al. [4] it was demonstrated that additives such as coal pulverised fuel ash (PFA) and kaolin positively affected the ash fusion temperatures of biomass ash, olive pit ash and white wood pellet ash. Kaolin was found to be more effective than PFA, raising the ash fusion temperatures. The additives also reduced the sintering tendency of white wood ash, which is beneficial during the combustion process. In the case of olive pit ash, kaolin completely inhibited the sintering process, making olive pit more suitable for combustion. Kaolin effectively bound potassium in the ashes, increasing the viscosity of the ashes and positively impacting the combustion conditions. These results suggest that kaolin can be used to improve the combustion of problematic biomasses, such as olive pits.

In the article by Wang et al. [9], a comprehensive review of fuel additives, including aluminosilicates, was conducted to reduce the problems related to biomass ash. The authors emphasise the need for research beyond the laboratory scale to thoroughly investigate the optimal dosage of additives in commercial units.

Research on the optimal dose of additives for Cl-rich biomass of various types was presented by Sobieraj et al. [6]. The authors suggest that costly and complex chemical analyses can be avoided when selecting an optimal additive dose. Instead, they propose a simple and less expensive method to determine the dose of halloysite based on the chlorine content in the fuel. Nevertheless, the method does not consider possible reactions of alkali metal sulfation or the loss of halloysite during combustion and improper mixing with the fuel. Based on the research conducted, it was concluded that for most types of biomass, a 1-2% halloysite weight dosage should suffice to reduce ash-related problems in biomass-fired boilers.

## 2. Purpose and scope of the analysis

This study presented the influence of kaolin, bentonite and halloysite additives on the slagging and fouling indices for animal-origin biomass. Two fuels are taken into account: chicken litter and cattle manure and the additive dosage of 8% is investigated.

## 3. Materials and methods

### 3.1. Animal-derived biomass

In this study, two fuels are taken into account: chicken litter and cattle manure. They have been collected from Polish farms and selected as representatives of animal-origin biomass. Both chicken litter and cattle manure are widely available around the World, in both urbanized and non-urbanized areas. The detailed characterization of animal-origin biomass has been presented in previous research [10], [11].

### 3.2. Additives

Aluminosilicate minerals, described by the general chemical formula  $\text{Al}_2\text{Si}_2\text{O}_5(\text{OH})_4$ , are commonly used in various industries due to their physicochemical properties and wide availability. Their high porosity and significant specific surface area allow them to adsorb elements on their surface. Furthermore, their high melting temperature makes them

attractive fuel additives. It is widely believed that their thermal processing does not reduce the efficiency of the process and is not a source of pollution [12]–[14]. In this study, three different aluminosilicate additives were applied: kaolin, halloysite, and bentonite, each in a dose of 8%. The additives feature a powdery structure as presented in Figure 1. The distinctive red colour of halloysite is attributed to the presence of iron compounds.



Fig. 1. Fuel additives used in powder form: a) halloysite; b) kaolin; c) bentonite.

### 3.3. Ash preparation and characterization

The fuels described in 3.1 were pre-dried and ground in a laboratory mill. The additives were admixed to ground fuels prior to incineration at a dose of 8%. Small batches of fuels with and without additives were placed in ceramic crucibles and incinerated in a constant temperature zone of 550 °C. As a result, chemically stable ash was obtained with a minimal amount of unburned carbon.

The ash oxide composition and ash fusion temperatures (AFT) were determined for both reference samples and those with additives. These parameters are the most common procedures for ash characterization in terms of slagging, fouling and other combustion-related issues. The ash composition was determined by Inductively Coupled Plasma-Optical Emission Spectroscopy (ICP-OES). The ash fusion temperatures were determined by the microscope-photographic method in accordance with PN-EN ISO 21404:2020-08, The procedure covers the identification and recording of shrinkage starting temperature (SST), deformation temperature (DT), hemisphere temperature (HT), and flow temperature (FT). The specific characteristic shapes of the ash cylinders were recorded by a digital system. The procedure took place at a maximum temperature of 1500 °C.

### 3.4. Slagging and fouling indices

In Table 1, the slagging and fouling indices, along with their evaluations are presented [15]–[17]. These indicators are based on the composition of ash and are commonly used to assess the risk of how a fuel may affect the heating elements of a boiler. Although in presented work the indices are applied to biomass fuels, most of them were initially developed for coals.

Table 1 Slagging and fouling indices.

INDEX	FORMULA	EVALUATION
BASE TO ACID RATIO	$\frac{B}{A} = \frac{Fe_2O_3 + CaO + MgO + Na_2O + K_2O}{SiO_2 + Al_2O_3 + TiO_2}$	<0.5 – low 0.5–1.0 – moderate 1.0–1.75 – high >1.75 – very high
BASE TO ACID RATIO SIMPLIFIED	$\frac{B}{A_{simplified}} = \frac{Fe_2O_3 + CaO + MgO}{SiO_2 + Al_2O_3}$	<0.5 – low 0.5–1.0 – moderate 1.0–1.75 – high >1.75 – very high
FOULING INDEX FU	$Fu = \frac{B}{A} \cdot (Na_2O + K_2O)$	<0.6 – low 0.6–40.0 – moderate >40.0 – high
QUOTIENT (SA) OF SILICA OXIDE AND ALUMINA OXIDE	$SA = \frac{SiO_2}{Al_2O_3}$	<1.87 – low 1.87–2.65 – moderate, high >2.65 – very high
CL RATIO	$Cl_{ratio} = \frac{Cl + K_2O + Na_2O}{SiO_2 + Al_2O_3}$	< 1.0 – low >2.4 – high
SILICA CONTENT IN THE ASH	$SiO_2$ [%]	<20 – low 20–25 – moderate >25 – high
BED AGGLOMERATION INDEX	$BAI = \frac{Fe_2O_3}{Na_2O + K_2O}$	>0.15 – low <0.15 – high
SLAG VISCOSITY INDEX	$S_R = SiO_2 \cdot \frac{100}{SiO_2 + Fe_2O_3 + CaO + MgO}$	>72 – low 65–72 – moderate <65 – high

#### 4. Effect of additives on ash composition

The chemical composition of the ashes and their AFTs are presented in Table 2 and Table 3

Table 2. Ash elemental analysis and ash fusion temperatures of chicken litter.

Parameter	Unit	Chicken litter	Chicken litter + halloysite	Chicken litter + kaolin	Chicken litter + bentonite
Cl	wt%	6,38	3,42	2,97	3,74
SO <sub>3</sub>	wt%	1,37	1,04	0,98	1,10
K <sub>2</sub> O	wt%	11,20	8,40	8,53	8,55
SiO <sub>2</sub>	wt%	59,20	56,20	58,90	58,90
Fe <sub>2</sub> O <sub>3</sub>	wt%	2,60	6,95	2,34	2,65
Al <sub>2</sub> O <sub>3</sub>	wt%	3,51	8,57	12,30	7,00
Mn <sub>3</sub> O <sub>4</sub>	wt%	0,12	0,21	0,09	0,11
TiO <sub>2</sub>	wt%	0,25	1,07	0,37	0,23
CaO	wt%	6,53	5,45	5,41	5,63
MgO	wt%	2,20	1,94	1,83	2,41
P <sub>2</sub> O <sub>5</sub>	wt%	5,02	4,19	4,06	4,06
Na <sub>2</sub> O	wt%	0,68	0,68	0,58	4,55
BaO	wt%	0,03	0,05	0,03	0,04
SrO	wt%	0,02	0,02	0,02	0,02
SST	[°C]	1040	1130	1100	1150

DT	[°C]	1170	1210	1270	1220
HT	[°C]	1330	1280	1330	1300
FT	[°C]	1370	1300	1380	1350

Table 3. Ash elemental analysis and ash fusion temperatures of cattle manure.

Parameter	Unit	Cattle manure	Cattle manure + halloysite	Cattle manure + kaolin	Cattle manure + bentonite
Cl	wt%	0,48	0,18	0,01	0,24
SO <sub>3</sub>	wt%	0,70	1,20	1,10	1,20
K <sub>2</sub> O	wt%	4,60	5,20	5,50	6,20
SiO <sub>2</sub>	wt%	77,70	72,80	75,00	76,10
Fe <sub>2</sub> O <sub>3</sub>	wt%	1,20	3,90	1,10	1,30
Al <sub>2</sub> O <sub>3</sub>	wt%	5,30	6,20	8,00	3,60
Mn <sub>3</sub> O <sub>4</sub>	wt%	0,06	0,13	0,06	0,07
TiO <sub>2</sub>	wt%	0,17	0,69	0,26	0,21
CaO	wt%	2,70	3,30	3,00	3,50
MgO	wt%	1,00	0,90	0,90	1,00
P <sub>2</sub> O <sub>5</sub>	wt%	<1.5	<1.5	<1.5	<1.5
Na <sub>2</sub> O	wt%	1,23	0,92	0,81	1,05
BaO	wt%	0,04	0,04	0,03	0,03
SrO	wt%	0,01	0,01	0,01	0,01
SST	[°C]	1240	1180	1150	1180
DT	[°C]	1290	1260	1270	1370
HT	[°C]	1440	1430	1470	>1500
FT	[°C]	>1500	>1500	1490	>1500

When comparing the data presented in Table 1 and Table 2, a noticeable difference in the composition of the ash can be observed for the reference samples. The cattle manure ash has significantly lower chlorine (0.48%), sulphur and potassium content, while the silica content is significantly higher. For comparison, the chlorine content in chicken litter ash is extremely high, reaching 6.38%. The chlorine content in the ash plays a crucial role in boiler corrosion due to excessive agglomeration of deposits during biomass combustion. Chlorine, along with alkali metals such as Ca, K, and Na, tends to form low-melting alkali metal oxides responsible for agglomeration and ash fusion [18], [19]. In particular, alkali metal chlorides such as NaCl and KCl are responsible for the high temperature corrosion of boiler heating elements [16], [18], [19].

The addition of aluminosilicate fuel additives reduced the percentage of chlorine in all samples. The lowest chlorine content was observed in the ashes with the addition of kaolin. The potassium oxide content in the ash decreased with the use of silicates only for chicken litter samples, and the values for all additives are similar. Ash fusion temperatures, particularly SST and DT are considered key temperature indicators for assessing ash fusion and agglomeration. As these temperatures increase, the risk of unwanted issues decreases. Characteristic ash fusion temperatures are lower for all chicken litter ash samples compared to cattle manure samples.

## 5. Slagging and fouling prediction

Based on the analysis of the ash composition and its fusion temperatures, slagging and fouling indices were determined according to the methodology presented in Table 1. The results for chicken litter and cattle manure ashes with and without additives, are presented in Table 4.

Table 4. Slagging and fouling indices of cattle manure and chicken litter ash with aluminosilicate additives.

Index	Chicken litter	Chicken litter + halloysite	Chicken litter + kaolin	Chicken litter + bentonite	Cattle manure	Cattle manure + halloysite	Cattle manure + kaolin	Cattle manure + bentonite
B/A	0,45	0,42	0,32	0,42	0,15	0,20	0,15	0,18
B/A <sub>simplified</sub>	0,18	0,22	0,13	0,16	0,06	0,10	0,06	0,07
FU	5,33	3,81	2,90	5,52	0,86	1,21	0,97	1,32
SA	16,87	6,56	4,79	8,41	14,66	11,74	9,38	21,14
Cl ratio	0,29	0,19	0,17	0,26	0,08	0,08	0,08	0,09
SiO <sub>2</sub> ash [%]	59,20	56,20	58,90	58,90	77,70	72,80	75,00	76,10
BAI	0,22	0,77	0,26	0,20	0,21	0,64	0,17	0,18
Sr	83,94	79,67	86,01	84,64	94,07	89,99	93,75	92,92

<b>Legend</b>	low	moderate	high	very high
---------------	-----	----------	------	-----------

Analysing the results presented in Table 4, a significant discrepancy can be observed in the risk assessment for various indices. Some indices, such as B/A, B/A<sub>simplified</sub>, Cl ratio, BAI, and Sr, indicate a low risk of slagging and fouling and the FU index indicates moderate risk for all samples. On the other hand, indices such as SiO<sub>2</sub> ash [%], and especially the SA index, suggest a high risk of slagging and fouling. It is worth noting that these indices were originally developed for analysing coal combustion, so their applicability to biomass fuels remains a matter of debate. Various authors in their studies have reported a lack of correlation between different indices and conflicting results [15], [17]. However, their research focused on plant-based biomass. By analysing the results in Table 4, it is possible to conclude that the same relationship exists for biomass of animal origin. Therefore, in order to predict the risk of ash agglomeration and sintering, the authors of papers [15], [17] recommend relying on ash fusion temperatures determined by laboratory tests. AFT-based indices more accurately reflect these phenomena, in particular the first two characteristic fusion temperatures: SST and DT. Generally, the higher these temperatures are, the lower the risk of ash slagging. A graphical interpretation of the effect of the different aluminosilicate additives on AFT is shown in Figures 2-5.

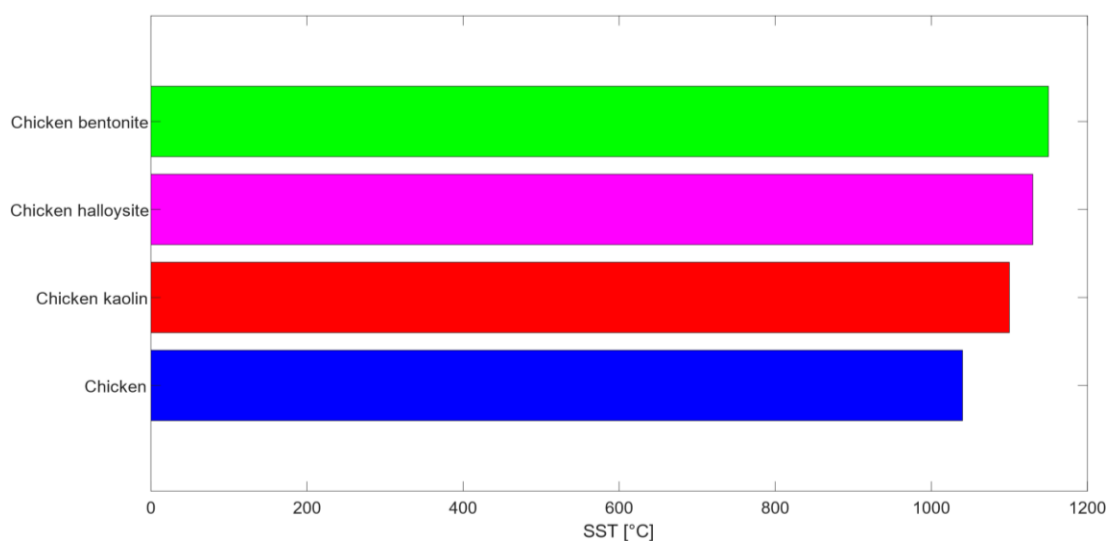


Fig. 2 Effect of aluminosilicate additives on shrinkage starting temperature for chicken litter ash.

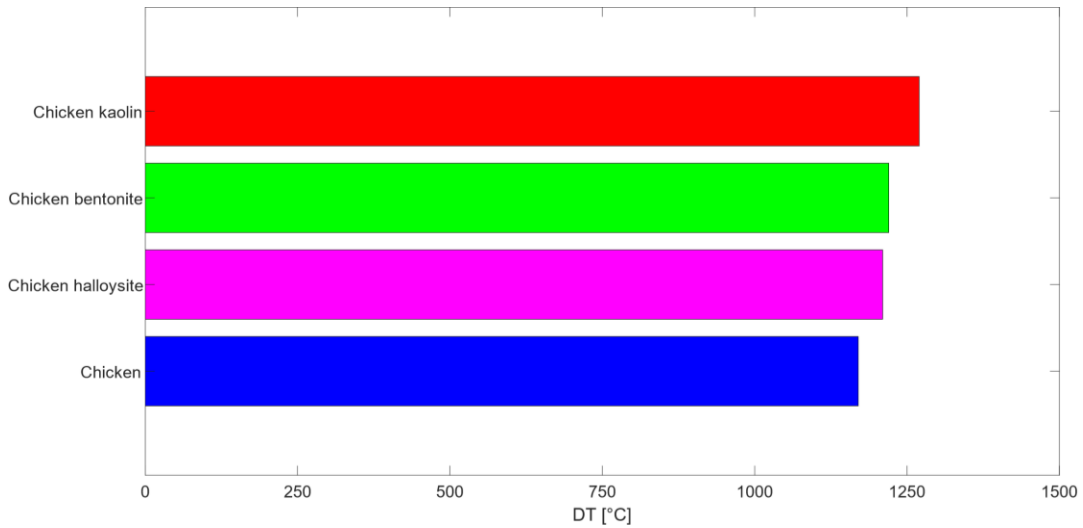


Fig. 3 Effect of aluminosilicate additives on deformation temperature for chicken litter ash.

The use of each aluminosilicate additive increases the shrinkage starting temperature and deformation temperature of the chicken litter ash. This translates into a reduced risk of ash agglomeration and sintering. In the case of SST, bentonite proves to be the most effective, as there is an increase in temperature from 1040°C to 1150°C. The least effective is the addition of kaolin, raising the temperature to 1100°C. For DT, kaolin increases the temperature to the greatest extent relative to the reference sample from 1170°C to 1270°C. The least effective DT increase was shown for halloysite - increasing the temperature to 1210°C

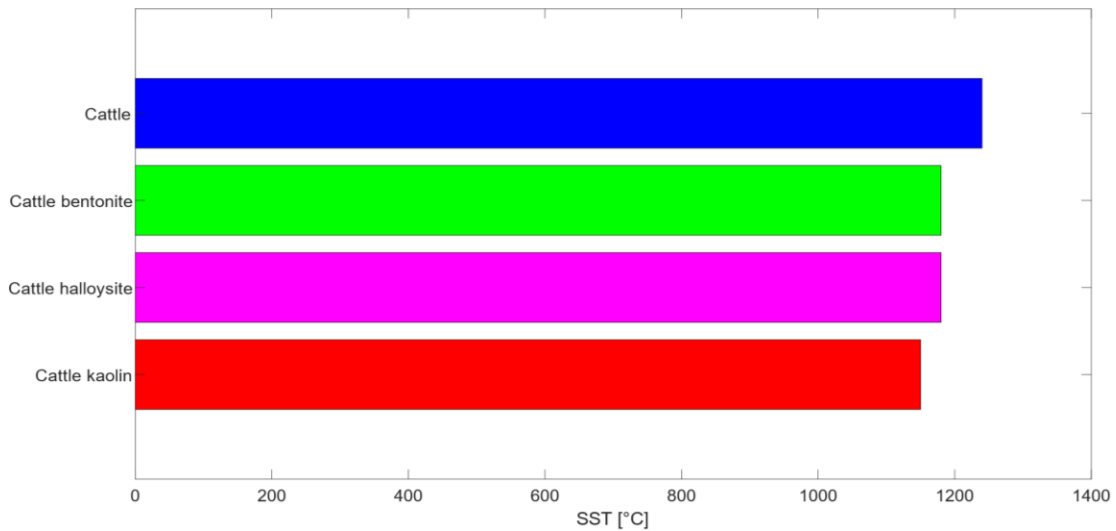


Fig. 4 Effect of aluminosilicate additives on shrinkage starting temperature for cattle manure ash.

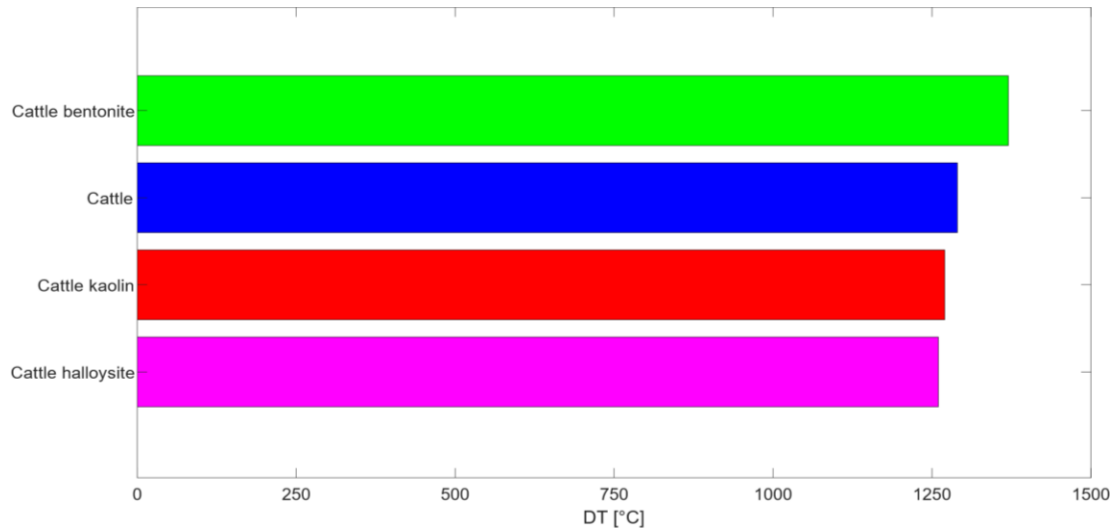


Fig. 5 Effect of aluminosilicate additives on deformation temperature for cattle manure ash.

In the case of cattle manure ash, there is no observed increase in the shrinkage starting temperature when aluminosilicate additives are applied. As shown earlier, cattle manure ash is characterized by low chlorine content. Therefore, the use of aluminosilicate additives does not significantly affect its composition. Furthermore, the SST of the reference sample of cattle manure ash is already high and equals 1240°C. An increase in deformation temperature is only observed in the sample with the addition of bentonite, raising it from 1290°C to 1370°C. Overall, both the SST and DT results obtained indicate a low risk of ash slagging when using this fuel.

## 6. Conclusions

Conventional coal power plants adapted for biomass combustion could play a significant role in the future energy sector. However, the utilization of biomass comes with a high risk of ash agglomeration, slagging, fouling and sintering, which not only reduces the energy efficiency of the boiler, but also intensifies high-temperature corrosion of its heating surfaces. To assess these hazards, various indicators are used, however, as demonstrated in this study, as well as by Lachman et al. [15] and Garcia et al. [17] there is a significant inconsistency in risk assessment between different indicators for biomass. Therefore, risk assessment should not be based on indicators based on ash composition, but rather on laboratory experiments and AFT tests [15].

For chicken litter ash with high chlorine content, it was found that the addition of aluminosilicates resulted in the increase in the shrinkage starting temperature and the deformation temperature. In particular, bentonite and halloysite significantly increased SST, reducing the risk of slagging. In the case of DT, the best effect was achieved with the addition of kaolin. Therefore, there is no specific correlation between the impact of individual additives on different ash fusion temperatures of the investigated ashes. Furthermore, there was only a slight increase in deformation temperature with the addition of bentonite and halloysite. However, the dose of 8% of aluminosilicates was investigated, and the selection of the optimal additive dose requires further research. The dose increase could potentially result in a more noticeable improvement in indicators based on AFT, nevertheless it may affect the economic feasibility.

The research also found that the ash composition has a significant impact on the effectiveness of aluminosilicate additives, with a particular focus on the chlorine content in the ash. In the case of cattle manure ash with relatively low chlorine content in the ash, no increase in SST was observed with the use of fuel additives. The action of aluminosilicates is based on adsorption and binding, especially of alkali metals, such as K and Na. On the other hand, the reference cattle manure ash exhibits high ash fusion temperatures, making the use of aluminosilicates unnecessary from the standpoint of raising deformation temperatures. In future research, it is planned to investigate the same types of fuels with varying chlorine content in the ash to understand its impact on AFT.

## Acknowledgments

This research was supported by National Science Centre, Poland, grant number 2021/43/D/ST8/02609 “The influence of aluminosilicate additives on high-temperature corrosion and ash properties of animal-origin biomass”.

## References

- [1] L. S. Paraschiv and S. Paraschiv, *Contribution of renewable energy (hydro, wind, solar and biomass) to decarbonization and transformation of the electricity generation sector for sustainable development*, Energy Reports, vol. 9, pp. 535–544, doi: 10.1016/J.EGYR.2023.07.024, Sep. 2023.
- [2] S. Bello, Á. Galán-Martín, G. Feijoo, M. T. Moreira, and G. Guillén-Gosálbez, *BECCS based on bioethanol from wood residues: Potential towards a carbon-negative transport and side-effects*, Appl Energy, vol. 279, p. 115884, doi: 10.1016/J.APENERGY.2020.115884, Dec. 2020.
- [3] M. Bui, M. Fajardy, and N. Mac Dowell, *Bio-energy with carbon capture and storage (BECCS): Opportunities for performance improvement*, Fuel, vol. 213, pp. 164–175, doi: 10.1016/J.FUEL.2017.10.100, Feb. 2018.
- [4] L. J. Roberts *et al.*, *The impact of aluminosilicate-based additives upon the sintering and melting behaviour of biomass ash*, Biomass Bioenergy, vol. 127, p. 105284, Aug. 2019, doi: 10.1016/J.BIOMBIOE.2019.105284, Aug. 2019.
- [5] M. Díaz-Ramírez, F. J. Frandsen, P. Glarborg, F. Sebastián, and J. Royo, *Partitioning of K, Cl, S and P during combustion of poplar and brassica energy crops*, Fuel, vol. 134, pp. 209–219, doi: 10.1016/J.FUEL.2014.05.056, Oct. 2014.
- [6] J. Sobieraj, W. Gądek, K. Jagodzińska, and S. Kalisz, *Investigations of optimal additive dose for Cl-rich biomasses*, Renew Energy, vol. 163, pp. 2008–2017, doi: 10.1016/J.RENENE.2020.10.061, Jan. 2021.
- [7] J. D. Morris, S. S. Daood, and W. Nimmo, *The use of kaolin and dolomite bed additives as an agglomeration mitigation method for wheat straw and miscanthus biomass fuels in a pilot-scale fluidized bed combustor*, Renew Energy, vol. 196, pp. 749–762, doi: 10.1016/J.RENENE.2022.06.151, Aug. 2022.
- [8] B. M. Steenari and O. Lindqvist, *High-temperature reactions of straw ash and the anti-sintering additives kaolin and dolomite*, Biomass Bioenergy, vol. 14, no. 1, pp. 67–76, doi: 10.1016/S0961-9534(97)00035-4, Mar. 1998.
- [9] L. Wang, J. E. Hustad, Ø. Skreiberg, G. Skjevraak, and M. Grønli, *A Critical Review on Additives to Reduce Ash Related Operation Problems in Biomass Combustion Applications*, Energy Procedia, vol. 20, pp. 20–29, doi: 10.1016/J.EGYPRO.2012.03.004, Jan. 2012.
- [10] I. Maj, *Significance and Challenges of Poultry Litter and Cattle Manure as Sustainable Fuels: A Review*, Energies (Basel), vol. 15, no. 23, p. 8981, doi: 10.3390/en15238981, Nov. 2022.
- [11] I. Maj, S. Kalisz, and S. Ciukaj, *Properties of Animal-Origin Ash—A Valuable Material for Circular Economy*, Energies (Basel), vol. 15, no. 4, doi: 10.3390/en15041274, Feb. 2022.
- [12] I. Maj and K. Matus, *Aluminosilicate Clay Minerals: Kaolin, Bentonite, and Halloysite as Fuel Additives for Thermal Conversion of Biomass and Waste*, Energies 2023, Vol. 16, Page 4359, vol. 16, no. 11, p. 4359, doi: 10.3390/EN16114359, May 2023.
- [13] R. Wejkowski, S. Kalisz, M. Tymoszuk, S. Ciukaj, and I. Maj, *Full-Scale Investigation of Dry Sorbent Injection for NO<sub>x</sub> Emission Control and Mercury Retention*, Energies 2021, Vol. 14, Page 7787, vol. 14, no. 22, p. 7787, doi: 10.3390/EN14227787, Nov. 2021.



- [14] S. Kalisz *et al.*, *Full-scale study on halloysite fireside additive in 230 t/h pulverized coal utility boiler*, Energy, vol. 92, pp. 33–39, doi: 10.1016/J.ENERGY.2015.03.062, Dec. 2015.
- [15] J. Lachman, M. Baláš, M. Lisý, H. Lisá, P. Milčák, and P. Elbl, “*An overview of slagging and fouling indicators and their applicability to biomass fuels*,” Fuel Processing Technology, vol. 217, p. 106804, doi: 10.1016/J.FUPROC.2021.106804, Jun. 2021.
- [16] A. Mlonka-Mędrała, A. Magdziarz, I. Kalemba-Rec, and W. Nowak, *The influence of potassium-rich biomass ashes on steel corrosion above 550 °C*, Energy Convers Manag, vol. 187, pp. 15–28, doi: 10.1016/J.ENCONMAN.2019.02.074, May 2019.
- [17] A. Garcia-Maraver, J. Mata-Sanchez, M. Carpio, and J. A. Perez-Jimenez, Critical review of predictive coefficients for biomass ash deposition tendency, Journal of the Energy Institute, vol. 90, no. 2, pp. 214–228, doi: 10.1016/J.JOEL.2016.02.002, Apr. 2017.
- [18] H. P. Nielsen, F. J. Frandsen, K. Dam-Johansen, and L. L. Baxter, *The implications of chlorine-associated corrosion on the operation of biomass-fired boilers*, Prog Energy Combust Sci, vol. 26, no. 3, pp. 283–298, doi: 10.1016/S0360-1285(00)00003-4, Jun. 2000.
- [19] H. P. Nielsen, L. L. Baxter, G. Schlippab, C. Morey, F. J. Frandsen, and K. Dam-Johansen, *Deposition of potassium salts on heat transfer surfaces in straw-fired boilers: a pilot-scale study*, Fuel, vol. 79, no. 2, pp. 131–139, doi: 10.1016/S0016-2361(99)00090-3, Jan. 2000.

# Determining the current-voltage characteristics of colored BIPV modules based on experimental research.

Paweł Nowak<sup>1,2</sup>, Tomasz Muskala<sup>1</sup>, Sabina Gawlik<sup>1</sup>, Dominik Leszczewski<sup>1</sup>, Patrycja Koszut<sup>1</sup>

<sup>1</sup>Faculty of Energy and Environmental Engineering, Silesian University of Technology,

<sup>2</sup>Helioenergia Sp. z o.o.

## Abstract

The article presents the results of conducted current-voltage analyses of colored BIPV (Building Integrated Photovoltaics) modules. The study evaluated photovoltaic modules manufactured using various coloring layers. The considered coloring elements include colored EVA (Ethylene-Vinyl Acetate) foils, TPU (Thermoplastic Polyurethane), and OWV (One Way Vision) foil. The aim of the analysis is to demonstrate the impact of different colorization technologies on the amount of electricity production.

**Keywords:** BIPV, Current-voltage characteristics, coloring foil, electroluminescence imaging

## 1. Introduction

Photovoltaic modules can be divided into two groups based on their installation method: modules designed for building-mounted installation and modules mounted on support structures. Currently, the most popular method of installing modules is on building rooftops, constituting over 30% of all modules [1]. The second mounting system, known as Building Integrated Photovoltaics (BIPV), involves integrating photovoltaic modules with the building facade elements. Modules installed in this way serve both as a building material, cladding the structure, and as an electro-energetic device. They can be also used in small architectural objects, such as bus shelters, or in autonomous facilities like informational banners.

These systems pose a challenge for both building designers and the manufacturers of such solutions due to the individual nature of each construction. The main advantage of these solutions lies in their aesthetic value resulting from the integration of the module with the building. There are various coloring techniques that contribute to increased visual appeal, though not without an impact on efficiency. The behavior of the current-voltage characteristics with respect to solar irradiance change is shown in Figure 1. [2].

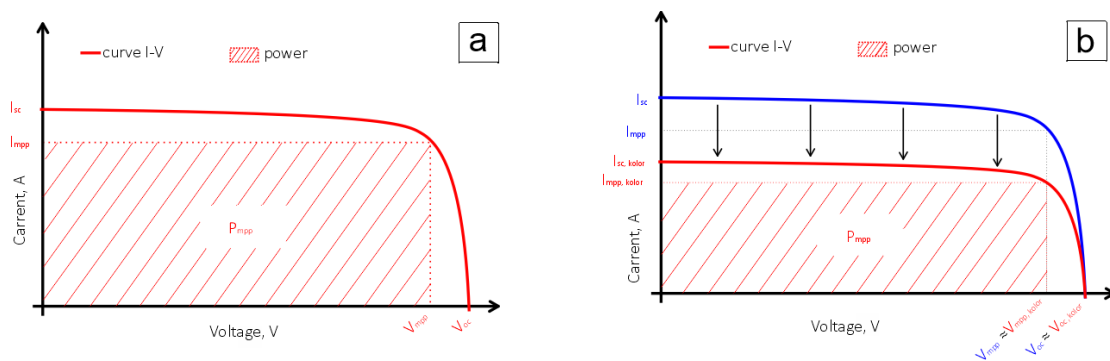


Fig. 1. Current-voltage characteristics: a) For modules without a coloring layer, b) With a coloring layer – decreased solar irradiance.

## 2. Research Methodology

To conduct the analysis, PV modules were produced using various colorization and masking methods for silicon cells. Additionally, a reference cell without colorizing foils was prepared. The study focused on three types of colorizations: the use of colored EVA foil, colored TPU foil, and the application of OWV foil on the module glass.

After the modules were produced, they underwent a study in which the current-voltage characteristics of each module were determined. These analyses were conducted using the PSS 8 Berger Lichttechnik device, which utilizes a solar light simulator to determine the maximum power point of the PV module. The study was performed under Standard Test Conditions (STC), meaning a temperature of 25 °C, solar radiation intensity of 1000 W/m<sup>2</sup>, and air mass 1.5 AM. [3] Adequate illumination was achieved using a xenon flash lamp located in the upper part of the measurement chamber. The internal walls of the measurement chamber were painted black to avoid disturbing the measurement results. In the lower part of the measurement chamber, there is a table allowing the module to be introduced into the chamber. The research space is equipped with heaters that maintain the temperature at the appropriate level. The chamber is additionally equipped with a light radiation intensity sensor, which allows measurement and correction of the flash generator settings to closely approach STC conditions. Additionally, a PT100-type thermocouple is attached to the module, measuring the module's temperature, and controlling the operation of the heaters. The entire current-voltage characteristic is recorded during a single flash.

Another study involved electroluminescence examination aimed at assessing the quality and condition of the modules. In this study, the module is placed in a dark chamber. Voltages are applied to the leads in the reverse manner compared to normal module operation. This results in the emission of light in the infrared range. Subsequently, the emitted radiation is recorded using the ZWO ASI183MM PRO camera with ATRONOMIK ProPlanet 742 filter. The image can reveal defects such as microcracks, shaded areas, mechanical damage, corrosion, or faults in the connections between module layers.[4]

## 3. Sample description

As part of the study, one reference module without colorizing foil was produced, along with three modules representing different colorization methods. Two of them utilize special pre-colored encapsulant foils applied directly to the PV cells instead of the usual clear foil. For this purpose, two types of foils were used: colored EVA and TPU foils. The third method involved applying OWV foil to the front of the PV module glass.

Each module was designed with 6 strings of 4 monocrystalline silicon cells each, type bifacial 10 BB half-cut. The strings were interconnected in a parallel-series configuration to optimize voltage and current in the module. Junction boxes were used to lead the wires out of the module, providing separate outputs for the positive and negative terminals. The connection diagram for the modules is shown in Figure 2.

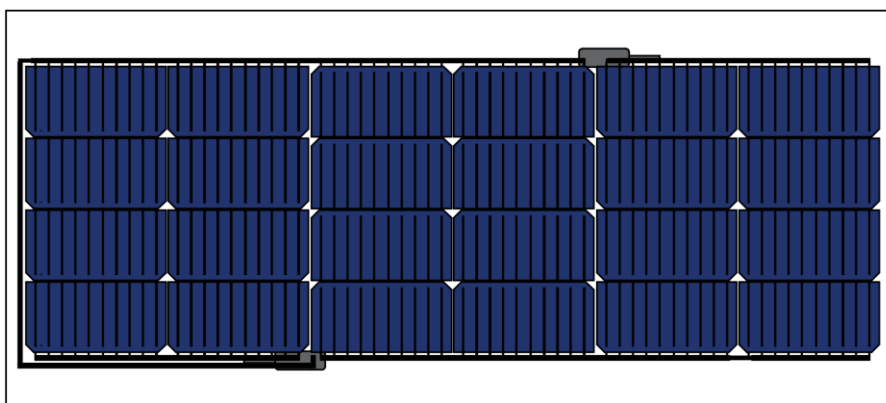


Fig. 2. connection diagram of solar cells.

In Table 1 a list of samples is presented, while in Table 2 the arrangement of layers in the samples is depicted.

Table. 1. Sample designation.

Sample designation.	Construction	Colorizing element
REF_GB	Glass-Backsheet	-
EVA_A_GB		Foil EVA vers A
EVA_B_GB		Foil EVA vers B
TPU_GB		Foil TPU
OWV_GB		Foil OWV

Table. 2. Description of sample layers.

Sample	REF_GB_X	EVA_GB	TPU_GB	OWV_GB
Front	Glass	Glass	Glass	Glass with OWV foil attached
Inter layer	EVA foil	Colored EVA foil	Colored TPU foil	EVA foil
	PV cell	PV cell	PV cell	PV cell
	EVA foil	EVA foil	TPU foil	EVA foil
Back	Backsheet	Backsheet	Backsheet	Backsheet

For the comparison of the quality of cell masking, images of selected fragments of the modules were taken. Modules colored using EVA foil feature a bright and vibrant color. All metal elements of the cell are visible through the colorizing foil. To achieve a better visual effect, additional masking of busbars can be applied with this foil. The interference nature of the dyes in the applied foils becomes apparent when viewing the modules at different angles. When observing the modules from the front, the color is most intense. As the viewing angle increases, the color gives way to the color of the cells. This effect also occurs when using TPU foil for colorization, whereas it does not occur when using OWV foil. In the case of a module colored with TPU foil, the visual effect is similar to modules using EVA foil. In the module using OWV foil, coloration is the most uniform and effectively masks the cells and busbars in the module. Coloring with OWV foil is based on a reflective mechanism of color impartation. The modules described in Table 3.1 are presented in figures 3-7.



Fig. 3. REF\_GB

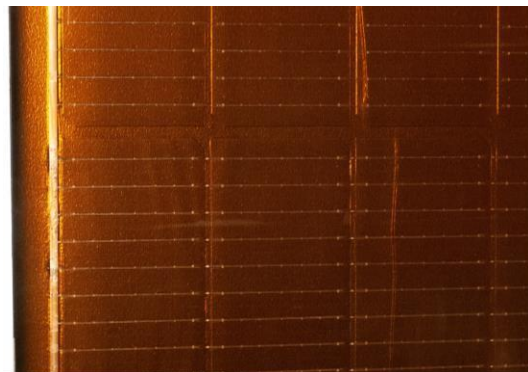


Fig. 4. EVA\_A\_GB

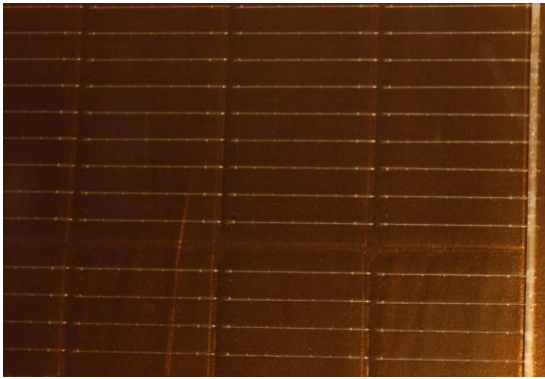


Fig. 5. EVA\_B\_GB

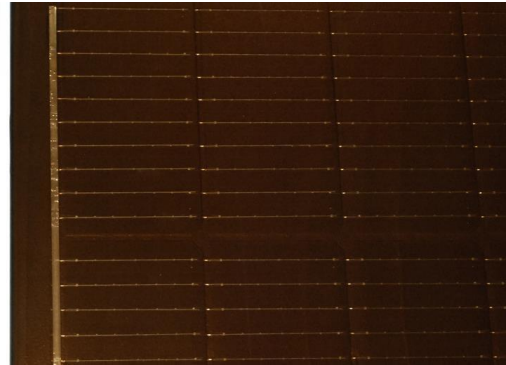


Fig. 6. TPU\_GB

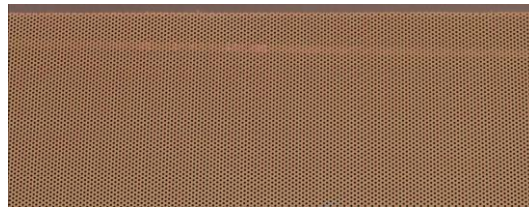


Fig. 7. OWV\_GB

#### 4. Results

Current-voltage characteristics were determined for all samples. Figure 8 shows the results obtained for the reference sample, while Table 3 presents the results for all samples.

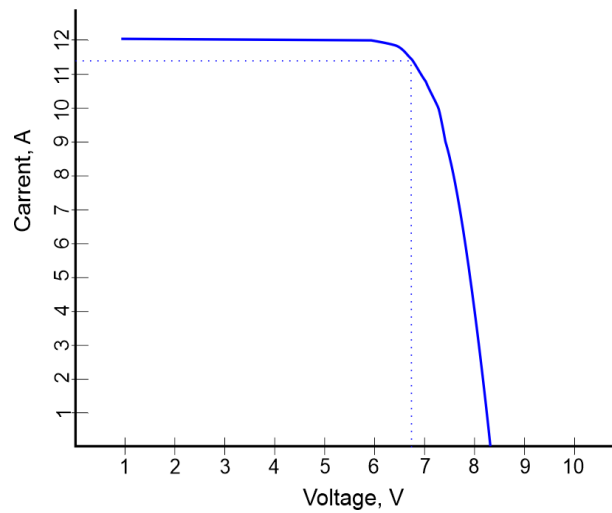


Fig 8. Current-voltage characteristics for the sample REF\_GB.

Table. 3. The obtained results for the GB samples.

	Units	REF_GB	EVA_A_GB	EVA_B_GB	TPU_GB	OWV_GB
Uoc	V	8,315	8,238	8,215	8,303	8,119
Isc	A	11,957	8,992	8,476	10,624	5,006
Ump	V	6,747	6,701	6,585	6,518	6,692

Imp	A	11,336	8,63	8,383	9,973	4,753
Pmax	w	76,484	58,557	55,207	65,006	32,678
FF	%	76,93	79,05	79,28	73,69	80,4
cell Eff	%	19,36	14,82	13,97	16,45	8,27
MOD EF	%	14,65	11,22	10,58	12,45	6,26

For a direct comparison of the samples to the reference, the obtained differences are presented in Table 4.

Table. 4 Percentage value in relation to the reference.

	EVA_A_GB	EVA_B_GB	TPU_GB	OWV_GB
Uoc	-1%	-1%	0%	-2%
Isc	-25%	-29%	-11%	-58%
Ump	-1%	-2%	-3%	-1%
Imp	-24%	-26%	-12%	-58%
Pmax	-23%	-28%	-15%	-57%
FF	3%	3%	-4%	5%
cell Eff	-23%	-28%	-15%	-57%
MOD EF	-23%	-28%	-15%	-57%

To verify the quality of the photovoltaic modules, electroluminescence imaging was used. This was done to check whether the power drop in the modules was not caused by errors in soldering the cells. Local, individual shadows are visible on all modules, but they do not have a significant impact on the obtained results. Such isolated deactivations on the cells, represented by rectangular areas, are also observed on commercial photovoltaic modules. Electroluminescence images have been presented in figures 9-13.

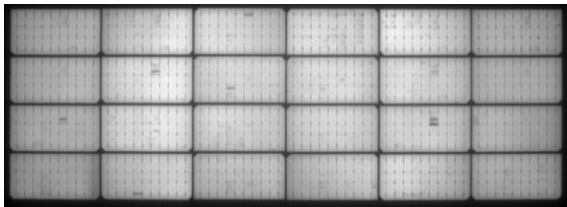


Fig.9. REF\_GB

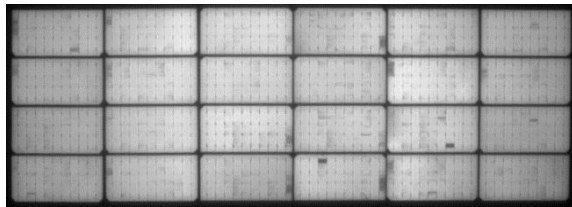


Fig.10. EVA\_A\_GB

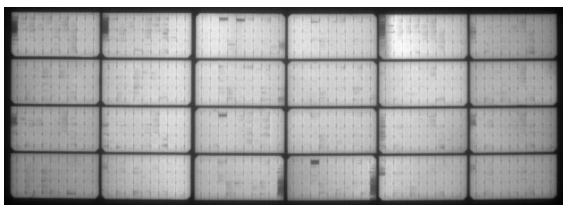


Fig.11. EVA\_B\_GB

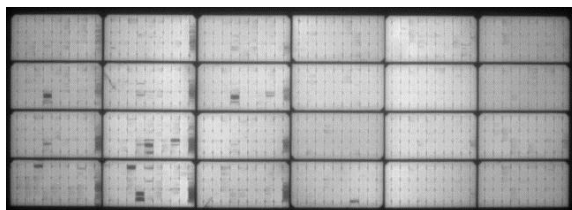


Fig.12. TPU\_GB

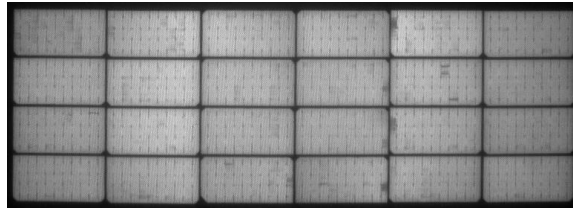


Fig.13. OWV\_GB

## Conclusions

During the conducted work, a series of photovoltaic modules were produced, and the correctness of the soldering and lamination process was verified using electroluminescence imaging. These modules do not exhibit significant defects, such as extensive cracks that would cause the deactivation of larger areas of cells. In the case of the module labeled as TPU\_GB, a cell crack was observed; however, this crack propagated in line with the crystallographic orientation of the cell, positioned at a 45-degree angle to the direction of the fingers on the cell. As a result, only a small area of the cell was disconnected. It is also worth noting that the obtained current-voltage parameters for such a module, with the elimination of the mentioned minor defects, could be further improved. The obtained results can be considered as extreme values, especially since similar defects were not observed in the case of the reference module.

Of all the examined colorized modules, the TPU\_GB module shows the smallest power drop at -15%. It should be noted that the lamination process using TPU foil differs from the more typical lamination of PV modules (using EVA foil). Furthermore, this foil is about 50% more expensive than EVA foil.

Modules made with EVA foil were produced in a typical PV module lamination process. Depending on the color intensity variant on the foil, power drops for these modules were achieved at levels of -23% and -28%. The process of making such modules is much easier, and therefore cheaper in industrial production.

The last colorization variant involving the use of OWV foil is the simplest process of all described here. However, this modification showed the largest power drop at -57%. This method, however, allows for graphic exchange on the module, making it particularly attractive in combination with small architectural objects. Such modules could serve as a backdrop for large-format advertising as well as a power source needed for its illumination.

## Acknowledgment

Funding for Project-Based Learning (PBL), under the Excellence Initiative - Research University programme

The authors of the article would also like to express their sincere thanks to Helioenergia sp. z o.o. for all the assistance provided in the collaboration and the conducted research.

## References

- [1] International Technology Roadmap for Photovoltaic (ITRPV). (2022). Results 2022. Fourteen edition, April 2023
- [2] Colorful photovoltaic modules, [online access: 30.11.2023]
- [3] EN IEC 61215-2:2021 Terrestrial photovoltaic (PV) modules – Design qualification and type approval – Part 2: Test procedures
- [4] Review on infrared and electroluminescence imaging for PV field applications, Report IEA-PVPS T13-10:2018, March 2018

# Energy transition and climate change in the opinion of Poles over the past few years.

Oliwia Baszczęńska<sup>1</sup>

<sup>1</sup>Faculty of Energy and Environmental Engineering, Silesian University of Technology,  
e-mail: oliwia.baszczeska@polsl.pl

---

## Abstract

The changing global climate situation in recent times has led to many transformations aimed at creating a sustainable economy. The most significant impact on the deteriorating environmental conditions comes from the very high emissions of harmful substances into the environment from the energy sector, transportation, and industry. The article presents surveys regarding how Poles perceive climate change and the energy transition over the past decade. More and more people are noticing that the poor climate situation is a real problem and a threat that needs to be addressed.

**Keywords:** Renewable Energy Sources, Energy transition, climate change.

---

## 1. Introduction

The recent years have brought significant challenges and changes in the energy sector in Poland and around the world. Growing concerns about adverse climate change and the depletion of traditional fossil fuel sources have contributed to taking steps toward energy transformation.

Conventional energy sources such as coal, natural gas, and oil have served as the backbone of the economy for decades. The global population growth has led to rapid advancements in technologies utilizing these fuels in the energy sector, resulting in increased emissions of carbon dioxide and other greenhouse gases. This has had a highly negative impact on the environment and has exacerbated the greenhouse effect. One of the most significant events that influenced the implementation of changes and stringent environmental restrictions was the United Nations Conference on Climate Change, which took place in November 2015 in Paris [1]. The culmination of the UN Conference was the Paris Agreement, which was ratified by 55 countries responsible for at least 55% of global greenhouse gas emissions released into the atmosphere [2]. There are also numerous documents that define the direction of actions aimed at energy transformation. Poland is a signatory to these documents, including:

- The Energy Policy of Poland until 2040 (EPP2040)
- The 2030 National Energy and Climate Plans (NECPs)
- Polish Hydrogen Strategy until 2030 with an outlook until 2040 (PHS)
- European Green Deal

The main goal of the green transformation is not only the previously mentioned reduction of greenhouse gas emissions and the mitigation of climate change but also the creation of a sustainable, efficient, and more independent energy system. Achieving this can be facilitated by increasing the use of renewable energy sources (RES). The transition to RES encompasses a wide range of technologies, including solar, geothermal, wind, and hydropower [3,4]. In recent years, there has been a highly dynamic development of these technologies and increasingly newer proposals for installations with more efficient thermodynamic and economic parameters. Furthermore, the energy transformation will lead to the creation of many new jobs and enhance the country's energy security.

## 2. Production changes in the energy mix in Poland

For years, the Polish energy sector has primarily relied on coal, both hard coal and lignite, due to the abundant coal reserves within our country. The combustion of coal and rapid population growth have led to significant emissions of carbon dioxide and other substances. Over the past several years, changes have been introduced to prevent environmental pollution from conventional energy sources. One of the most significant changes is the substantial



increase in the share of renewable energy sources in electricity production. Figure 1 illustrates electricity production in Poland from various sources between 2017 and 2022 [4-9].

In 2017, coal's share in the overall energy mix was 78.3%. Over the next 5 years, it decreased to 70.7%, primarily in favor of renewable energy sources (RES). In 2017, RES energy primarily came from onshore wind farms, accounting for 62% of the annual energy production from these sources. Photovoltaics was still a less developed source, contributing to just under one percent [4]. This situation changed over the next few years, and by 2022, the share of wind farms in energy generated from RES decreased to 52.4%. In contrast, the share of solar farms increased more than twentyfold and reached 21.8% [8]. The significant changes were driven by a series of support programs for companies and households that chose to install photovoltaic panels. The unfavorable changes in the so-called wind turbine law also played a role in slowing down the dynamic growth of wind farm shares. In 2022, there was also a decrease in the share of natural gas as a source of electricity production, primarily due to the outbreak of the war in Ukraine.

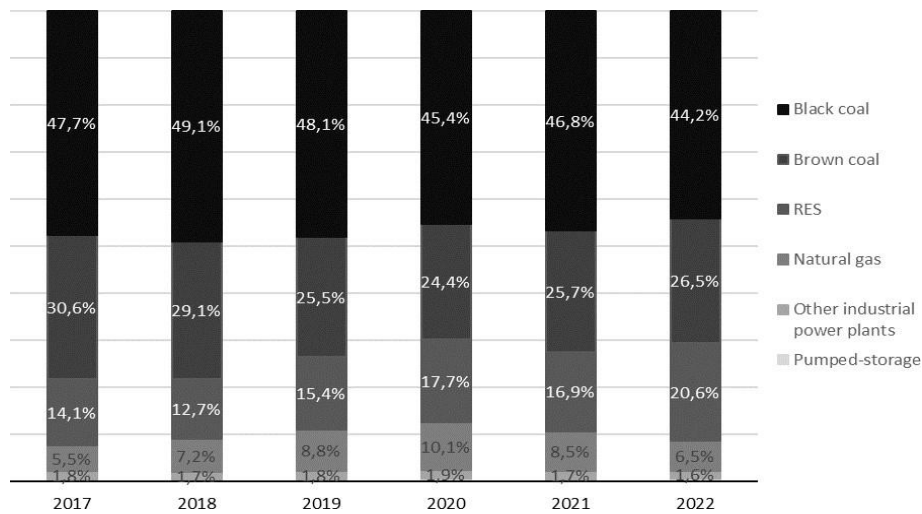


Fig 1. Electricity production in Poland from various sources between 2017 and 2022 [4-9].

### 3. Polish attitudes towards climate change.

The worsening climate situation is one of the most significant challenges our planet faces. The negative effects of these changes are becoming increasingly noticeable and affect our daily lives, from extreme weather events to threats to health and safety. The source of the problem is the emissions of a large amount of harmful substances into the atmosphere, which contribute to the deepening greenhouse effect. According to research conducted by the Center for Public Opinion Research (CBOS) over the past decade, significantly more than half of Poles believed that climate change is one of the greatest threats or poses a certain risk to modern civilization. Only one in four people considered climate change to be an insignificant threat, or that phenomena such as climate change do not exist. Among those surveyed, there were also individuals who could not determine whether climate change is a threat. From 2014 to 2018, there was an increase in the number of respondents who indicated awareness of climate change issues. In 2021, there was a slight decrease in these individuals, possibly due to the outbreak of the COVID-19 pandemic, which drew attention mainly to issues related to that aspect [10]. Figure 2 presents responses regarding how Poles perceive climate change worldwide from 2014 to 2021 [10].

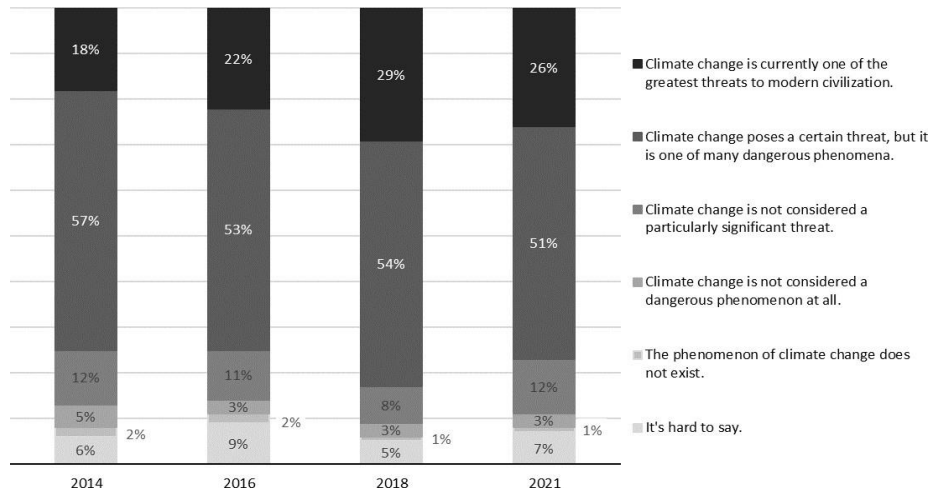


Fig 2. Responses regarding how Poles perceive climate change worldwide. [10].

In the face of the escalating climate crisis, it was necessary to create a series of documents aimed at defining actions to achieve climate neutrality by 2050. As mentioned in the introduction, one of the most important documents is the Paris Agreement, which sets the goal of limiting the increase in global average temperature to 1.5 °C compared to the pre-industrial era [11]. Alignment in actions is necessary not only at the national level but also at the European and global levels. In response to global threats and in the spirit of international cooperation, the European Union has established the European Green Deal. This is a package of political initiatives aimed at the green transformation of the economy [12].

Many countries pledge to achieve climate neutrality before 2050 and are rapidly adopting newer technologies aimed at reducing harmful emissions. The Center for Public Opinion Research conducted a survey in which it asked Poles who had previously expressed their views (data from 2021) about how quickly our country should achieve climate neutrality [10]. Three out of four people who had previously stated that climate change is currently one of the greatest threats to modern civilization believe that Poland should achieve climate neutrality before or by 2050. Only one in five individuals suggested that Poland should progress towards climate neutrality at its own pace. Among respondents who did not consider climate change to be a particularly significant threat or did not see it as a dangerous phenomenon, 70% and 76%, respectively, advocated for Poland to achieve climate neutrality on its own timeline, even if it extended beyond 2050. Only about one in five people in both cases believed that these changes should be implemented by 2050 or sooner. Figure 2 illustrates Polish responses regarding the pace at which Poland should achieve climate neutrality [10].

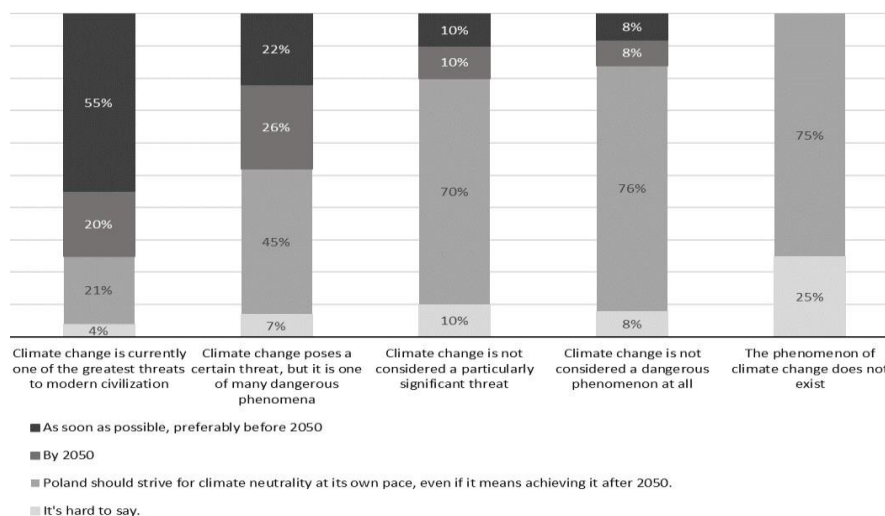


Fig 3. Responses regarding the pace at which Poland should achieve climate neutrality [10].

#### 4. Energy transition in the opinion of Poles

The primary challenge of energy transformation is increasing the share of renewable energy sources in the energy mix. Poland has mainly relied on coal for energy production, but increasingly, we can observe the emergence of new solar and wind farms. Considering the need to reduce harmful emissions into the atmosphere, it is crucial for the country to develop renewable energy sources and reduce the share of coal in the Polish energy sector. CBOS conducted a survey and asked Poles about what should be the source of energy generation in Poland over the next 10-20 years (from 2015 to 2018, they were asked about changes over a 20-30 year perspective) [13]. The overwhelming majority of respondents believe that Poland should gradually move away from coal-based energy and develop other methods of energy production. In 2014, 30% of respondents favored primarily relying on Poland's domestic hard coal resources, but in subsequent years (2018 and 2021), the percentage of these individuals decreased to 19%. In 2023, this number increased by 4 percentage points. Figure 3 illustrates responses regarding the source of energy generation in Poland over the next 10-20 years [13].

The next question pertained to the type of energy source that should currently be focused on. Figure 4 presents responses to this question [13]. The overwhelming majority of respondents believe that renewable energy sources such as solar farms, wind farms, hydroelectric power plants, etc., should be developed, or they are in favor of equal development of both non-renewable and renewable energy sources. Only 5% of individuals in 2015 and 2016 stated that the focus should be on nuclear, coal, oil, and natural gas. In 2023, this number increased by 3 percentage points. The research shows that most people believe that developing renewable energy sources will contribute to mitigating climate change.

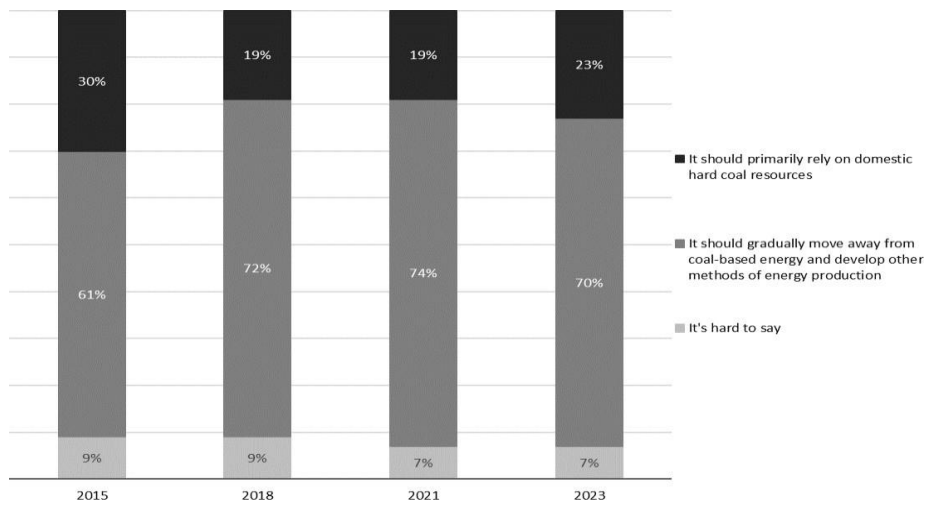


Fig 4. Responses regarding the source of energy generation in Poland in the next 10-20 years [13].

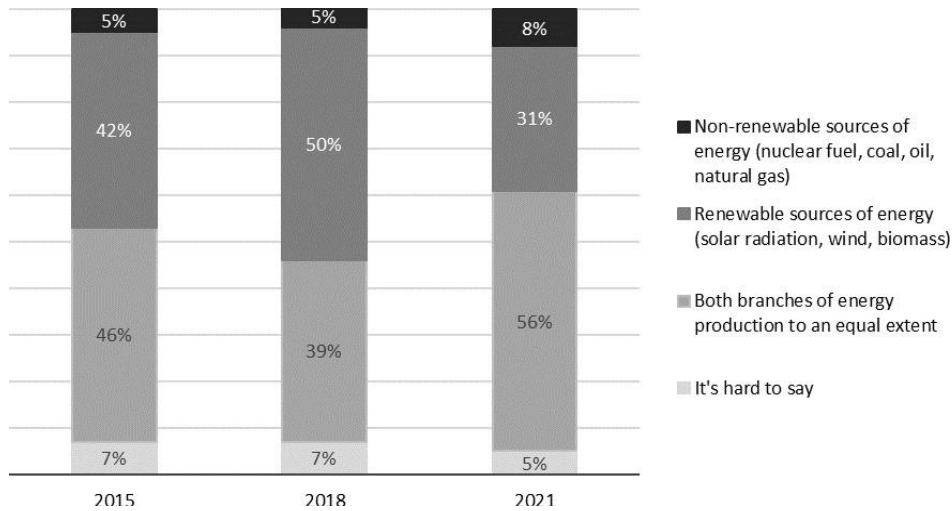


Fig 5. Responses regarding the type of energy source that should currently be focused on in Poland [13].

## 5. Conclusions

In response to the ongoing climate change and deteriorating environmental conditions, the answer lies in ensuring an energy transformation based on renewable energy sources. Over half of Poles are aware that climate change represents a significant threat to modern civilization, and they believe that Poland should strive to achieve climate neutrality by 2050. The key element of this energy transformation is increasing the share of renewable energy sources (RES) in the energy mix, enabling the utilization of low-emission sources such as wind and solar energy. The number of people who believe that Poland's energy sector should rely on coal in the next 10-20 years has decreased in recent years. Significant factors influencing respondents' answers may have been the onset of the COVID-19 pandemic in 2020 and the outbreak of the war in Ukraine on February 24, 2022. During the pandemic, attention shifted to other threats that could affect civilization, and issues related to Poland's energy economy took a backseat. Additionally, there were fluctuations in electricity demand and production during this time due to most companies transitioning to remote work or closing. The outbreak of the war in Ukraine had a significant impact on how energy sources were perceived, given the suspended gas supplies from Russia to our country. It demonstrated the need for greater energy independence in uncertain international relations. In the last decade, Polish society has increased its awareness of electricity generation sources, and the topic of energy transformation is increasingly discussed and becoming a reality.

## References

- [1] *Paris climate agreement - Consilium.*, [Published in polish], Accessed: Sep. 24, 2023. [Online]. Available: <https://www.consilium.europa.eu/pl/policies/climate-change/paris-agreement/>
- [2] *Energy transition in the perception of Poles and Europeans – IBRiS.*, [Published in polish], Accessed: Sep. 24, 2023. [Online]. Available: <https://ibris.pl/2022/07/28/transformacja-energetyczna/>
- [3] S. Mehmood, K. Zaman, S. Khan, Z. Ali, H. Ur, and R. Khan, *ARTICLE IN PRESS Energy and Built Environment xxx (xxxx) xxx The role of green industrial transformation in mitigating carbon emissions: Exploring the channels of technological innovation and environmental regulation*, 2023, doi: 10.1016/j.enbenv.2023.03.001.
- [4] *Poland's energy transition 2017 r.*, [Published in polish], Accessed: Sep. 28, 2023. [Online]. Available: [www.forum-energii.eu](http://www.forum-energii.eu)
- [5] A. Zieleniec and K. Koszniec, *Energy transition in Poland 2 march 2020*, [Published in polish]
- [6] *Energy transition in Poland | Edition 2021 – Energy forum*, [Published in polish], Accessed: Sep. 28, 2023. [Online]. Available: <https://www.forum-energii.eu/pl/analizy/transformacja-2021>

- [7] *Energy transition in Poland | Edition 2022 – Energy forum*, [Published in polish], Accessed: Sep. 28, 2023. [Online]. Available: <https://www.forum-energii.eu/pl/analizy/transformacja-2022>
- [8] “Energy transition in Poland | Edition 2023 – Energy forum.”, [Published in polish], Accessed: Sep. 28, 2023. [Online]. Available: <https://www.forum-energii.eu/pl/analizy/transformacja-2023>
- [9] *Energy transition in Poland | Edition 2019 – Energy forum*, [Published in polish], Accessed: Sep. 28, 2023. [Online]. Available: <https://forum-energii.eu/pl/analizy/transformacja-2019>
- [10] K. Z. Badań, *Reprinting and distribution of this publication in its entirety is permitted only with the permission of CBOS. Use of excerpts and empirical data requires acknowledgment of the source Energy Transformation-Expectations and Demands*, [Published in polish], Accessed: Sep. 25, 2023. [Online]. Available: <http://www.cbos.pl>
- [11] *The 6 most important demands of the Paris agreement*, [Published in polish], Accessed: Sep. 26, 2023. [Online]. Available: <https://www.teraz-srodowisko.pl/aktualnosci/Porozumienie-Paryskie-szesc-punktow-1668.html>
- [12] *European Green Deal - Consilium*. Accessed: Sep. 28, 2023. [Online]. Available: <https://www.consilium.europa.eu/en/policies/green-deal/>
- [13] K. Z. Badań, *Attitudes towards the energy transition*, [Published in polish] , Accessed: Sep. 27, 2023. [Online]. Available: <http://www.cbos.pl>

# Estimation of soil pollution from hydrocarbons in Vlora region

Blerina Beqaj <sup>1</sup>, Lira Aliaj<sup>2</sup>

<sup>1</sup>*Polytechnic University of Tirana, Faculty of Civil Engineering, Department of Environmental Engineering, Tirana, Albania e-mail: belabeqaj@gmail.com*

<sup>2</sup>*Polytechnic University of Tirana, Faculty of Civil Engineering, Department of Environmental Engineering, Tirana, Albania e-mail: lira.aliyaj2001@gmail.com*

---

## Abstract

Hydrocarbon pollution is one of the most important and worrying environmental problems. Hydrocarbons are organic compounds, composed of two main components of carbon and hydrogen. Hydrocarbons are found in the composition of petroleum, underground gas. Considering their nature, composition, structure, properties and specific characteristics, the impacts and consequences they cause are at extremely high and disturbing levels. The sources of hydrocarbon pollution are of several types, from which we would single out as one of the most important, the hydrocarbon pollution that comes from petroleum industry. In this article a small part of Vlora region is taken as the object of study where an old petroleum producing area is situated. The article highlights the main problems faced by this municipality as a result of the use of the oil industry and how pollution can be prevented and the area can be rehabilitated. In any case, environmental pollution from petroleum sector is a major problem, but even more so when this pollution endangers and directly affects ecosystems and natural resources, then the situation is very serious and urgent, which undoubtedly requires intervention and taking measures as soon as possible.

**Keywords:** soil pollution, hydrocarbons, environmental quality

---

## 1. Introduction

Land has traditionally been considered a place to dispose of waste, whether hazardous or non-hazardous. Humans have been dumping waste on the ground since ancient times, but pollution was not taken into account back then, as there were plenty of free spaces for dumping manufactured waste. The growth of the population and the revolution in industry and agriculture led to a high production of waste and other types of pollutants, in quantities and compositions of many types. Some of these wastes are difficult to destroy or decompose, therefore, they began to be processed by man. We classify the types of waste deposited on the ground into: - urban waste, - agricultural waste, - industrial waste, - nuclear waste. The discharges of the petroleum industry which are deposited on the ground are part of the industrial waste. Industrial waste also includes hydrocarbons, which in turn can be treated and degraded. This transformation depends on the influence of temperature, pressure, soil/air/water composition, etc. Crude oil, commonly known as petroleum, is a liquid found inside the earth and consisting of hydrocarbons, organic compounds and small amounts of metal. While hydrocarbons are usually the main component of crude oil, their composition can range from 50%-97% depending on the type of crude oil and how it was extracted. Organic compounds such as nitrogen, oxygen, and sulfur typically make up about 6%-10% of crude oil, while metals such as copper, nickel, iron, and vanadium are less than 1% of the total composition. Crude oil is created by heating and compressing organic materials over a long period of time. Oil, like all mining raw materials, is extracted from the underground at a depth of 300-5000m accompanied by mechanical impurities or those that participate in its molecular construction [1]. So from oil extraction, from the well to its processing, part of these impurities leave in the form of gases (H<sub>2</sub>S, SO<sub>2</sub>, NH<sub>3</sub>, CO, CO<sub>2</sub>) or liquids; while the rest after processing accompanies the products; example sulfur, nitrogen, oxygen, metals, etc. in the form of their compounds such as mercaptans, thiophenes, pyridines, phenols, naphthenic acids, etc.

All these impurities, such as during the extraction or oxidation processes of petroleum products, fuel combustion, pyrolysis, gasification, catalytic and thermal cracking, etc., are released in the form of gases, causing an irreparable damage to the environment. The various studies carried out previously show that soil pollution can occur during the usual works of petroleum and gas drilling, extraction, transportation or even processing of these products, such as

dumping of drilling waste in an inappropriate place, depositing pollutants emitted by the gas burning process, etc.[2]. However, in many studies carried out over the years, it has been concluded that: soil pollution is mainly caused by accidental spills, whether large or small, or by industrial activities, after objects have been abandoned. During the process of drilling - exploitation and contouring for oil and gas, the possibility of soil pollution is smaller. To drill a well, a larger area of land is dug, but the occupation time is less than in the case of oil extraction. The concentrated drilling of wells has reduced the surface of the land that is suitable for drilling or exploitation of an oil-bearing gas layer. During the process of concentrated drilling of wells, breakdowns also occur, which cause great pollution of the environment. With the introduction of new technologies, we see that the possibility of rehabilitating polluted areas and returning them to their previous state is increasing, such as bioventing a technology used for the elimination of pollutants, where air is injected at a relatively low speed into the polluted area to supply the sufficient amount of oxygen, thus degrading the hydrocarbons [3], [4]. In the case of a lack of oxygen, anaerobic conditions prevail. Nitrates  $\text{NO}_3^-$  or other oxygenated forms of nitrogen can serve as nutrients for some types of bacteria. Petroleum penetrates<sup>3</sup> the ground under the influence of gravity and capillary action. The rate of petroleum penetration into the soil depends on the type of petroleum and the type of soil [5]. The petroleum in the study area is included in the types of asphalt-resinous petroleum, therefore they are not expected to penetrate deep. Underground migration of oil pollutants can affect the population's exposure to these pollutants, such as volatile substances emitted from BTEX oil; volatile organic compounds VOCs, (benzene, toluene, ethylbenzene and xylene) that migrate towards residential areas and can seep into homes and be inhaled by inhabitants [6]. Migration of petroleum and hydrocarbons in general to residential areas where agriculture is developed can lead to the accumulation of pollutants in vegetables and other garden plants, which are then consumed by humans. For this reason, different scenarios should be built, regarding the exposure of the population to soil contaminated by petroleum hydrocarbons [7].

## 2. Case study of Gorrisht-Kocul oil-bearing source

The Gorrisht-Kocul oil deposit is one of the 12 known oil deposits in Albania. It is one of the 3 oil limestone deposits. This field was discovered in 1966. It currently has a production of about 925 barrels/day (147.1 m<sup>3</sup>/d). The source is used by Albpetrol company. Exploration and production of hydrocarbons includes a full cycle of seismic, geological, engineering, geophysical, research, extraction, processing and marketing of petroleum products. Conventional oil is extracted from underground reservoirs using traditional drilling and pumping methods. Conventional oil is a liquid at atmospheric temperature and pressure, so it can flow through a well and a pipeline – unlike bitumen, which is too thick to flow without being heated or diluted. It is easier and less expensive to recover and requires less processing after extraction. Unconventional oil cannot be recovered using conventional drilling and pumping methods.

Advanced extraction techniques are used to recover heavier oil that does not flow on its own. Oil found in such geological formations that make extraction more difficult is also called unconventional oil as non-traditional techniques are needed to extract the oil from the underground reservoir. This type of oil is found deep below the earth's surface, mostly within rock formations with low permeability. Horizontal drilling and hydraulic fracturing are used for this type of oil extraction.

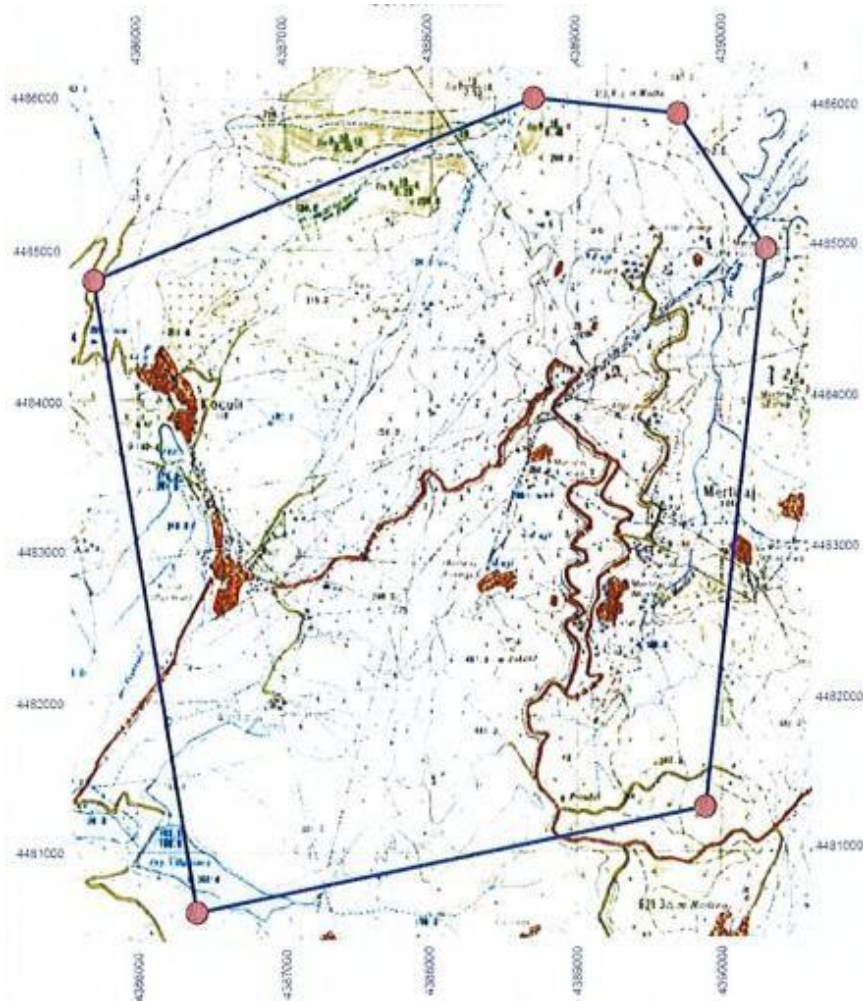


Fig. 1. Topographic map and site boundaries

### 2.1. Constituent elements and characteristics of petroleum in the study area

The main factors of environmental pollution in the oil extraction and processing industry include wells, collection site (groups), decantation plants, pumping stations, transport pipelines, oil processing plant and technological waste discharges. The oil of the area, as well as many mineral materials, are accompanied by dirt, where the high sulfur content is particularly noticeable, from 2-6% S. The chemical composition of the country's crude oil is as follows: C-85-90% ; H<sub>2</sub>-10-14%; S<sub>2</sub>-6%; O<sub>2</sub> -1.5%; N<sub>2</sub>-0.1%. Besides them, it contains metal impurities and trace halogens such as: vanadium, nickel, arsenic, sodium and chloride. General physico-chemical characteristics of oil from the Gorrish-Kocul area: density 0.823-0.961gr/cm<sup>3</sup>, asphaltenes 5.5-15.1%, ash 0.11-0.18%, NaCl 800-3100mg NaCl/kg, sulfur 3.2-6.1%S, coke 9.1-16.5% and viscosity in cst, at 20°C 1500-3100cst. Environmental pollution (land, water, air) from oil is in three states: liquid (oil, waste water, water+oil); gaseous (gases associated with oil, gases from evaporation, exhaust gases from processing); solids (solid residues associated with oil, catalysts from oil processing; solid particles from oil by-products processing).

### 2.2. Sources of oil pollution along the path it describes from the well (reservoir) to processing

First: during the extraction of oil from the well, due to the use of outdated techniques, spills are caused on the ground. Also, a part of the oil and formation water that comes out of the well spreads into the surrounding environment, while the rest passes into it.

Second: each well has its own pit, which is also used in cases of repair to collect the fluid. The number of pits is the same as the number of wells. These are simple pits, without any specific technology that limits discharges, filtration



or evaporation of the fluid in the environment; example during the rains, they are overfilled and the oil is discharged into the environment, or in the case of hot and sunny weather, the oil that is on the surface in the form of a thin layer evaporates.

Third: the transportation of oil from the well to the collection is done by surface or underground pipeline. Pipe leaks or cracks are also a source of environmental pollution with oil that seeps into the ground or is spread by water on the surface.



Fig. 2. View from the petroleum refinery of the case study

Fourth: the oil from the wells is collected in storage areas. Often times, their discharges or breakdowns become a source of environmental pollution with oil.

Fifth: the pre-collected oil is processed in the decanting plant, so that it is suitable for further processing in the refinery plants. Water with high oil content and other harmful wastes are not processed before they be discharged into the environment.

And the last process is the oil processing in the refinery, but since the Gorrisht-Kocul oil field does not have a refinery, the oil extracted from this area is processed in other refineries that are under the administration of the private company.

### 3. Results and discussions

In the case study oil fields, there is significant soil pollution from accidental oil discharges. This pollution is a condition inherited from the activity of a long time in the springs. This situation is more pronounced around oil extraction wells. The most important reasons for soil pollution are as follows:

- Damage to equipment and technological connections at the wellhead. In some cases, there is damage to the well nozzles and therefore there is an oil leak. It is necessary for the wells to be under a systematic control and to intervene in time for the elimination of breakdowns and various defects.
- Underground works of cleaning wells and replacement of equipment. This is a moment that deserves attention and treatment with due care. During the extraction of pipes and perches for technological operations, a significant amount of oil comes out with them, which must be collected in special pits in the well site. In the technological project, each well has one or more pits for the collection of oil and its reintroduction into the production cycle. Collecting and recycling this amount of oil has a double positive effect: environmental and economic.

- Replacement of oil pipelines and mains. In many low points of these pipelines, there is a significant amount of oil that must be carefully managed during this process.
- Power supply interruptions. The amount of oil found in the heating furnaces in the decanters must be discharged immediately to avoid coking. Oil can be found in the furnace in quantities of up to 5 m. Even this process must be carefully managed in order not to cause soil pollution.
- An ever-present danger is the landslide in areas where it can be favored by the broken relief. Experience so far has shown that landslides have been accompanied by cracks in oil pipelines, and as a result there has been soil pollution on a large surface. This risk is evident in the Gorisht reservoir.
- The high risk for the soil is pollution from the thinner (solar) where it is applied.

Its low viscosity favors quick distribution on the surface and deep in the soil. Soil pollution by hydrocarbons has direct negative consequences on the soil structure and vegetation. Evaporation of light oil fractions is an additional factor in air pollution. Soil pollution from oil greatly reduces the productivity of cultivated agricultural crops or spontaneous vegetation. The high presence of hydrocarbons in the soil is accompanied by a decrease in the amount of nutrients in the soil, especially nitrate. This is accompanied by the yellowing of plant leaves or the complete non-ripening of agricultural crops. Due to the properties of the petroleum, the high viscosity and high density and the structure of the soil, the contamination of the soil by oil, in the case studie's deposits, turns out not to have penetrated to a great depth. Soil pollution from oil represents a moderate risk for underground water, but a more pronounced risk for surface water. An area of approximately 250 m<sup>2</sup> around each well or 16,000 m<sup>2</sup> around each treatment station is considered oil-contaminated. The amount of oil in these lands is several times higher than the recommended rates; example the concentration of oil and crude oil in oil wells used with old technology results in 130-24000 mg of oil/kg of land, while in oil treatment stations (decantation) it fluctuates from 6200-165,000 mg of oil/kg of land, when the rates recommended by the EU are up to 5000 mg of oil/kg of soil. The presence of the compounds benzene, toluene, benzene ether and xylene (BTEX) in soil is very low, 0.2 mg BTEX/kg soil, against the recommended 206 mg BTEX/kg soil. This is related to the nature and type of our oils which are considered heavy oils with low content of volatile products.

#### 4. Conclusions

In the environments where oil extraction and processing activities are carried out, there have been persistent problems with environmental pollution. This pollution acts a lot in the air, surface water and soil, as a result of the use of technologies, which do not take into account the requirements for environmental protection. In the oil industry, the problem becomes more worrying, because its activity extends to very wide regions of the country. Thus, not only the workers of the oil sector are subject to the harmful effects, but also the population and the living world of the villages around them. The presence of oil pools on the surface of the earth in these areas is a panorama that the residents of the area face in their daily life. As a result of the many years that these wells have been in use and outdated technology, it is impossible to prevent soil contamination around the wells without an intervention plan. The location of wells near settlements and agricultural lands makes the situation even more serious and increases the need for an environmental intervention in the area. The heavy metal pollution in the lands around the industrial areas has proved destructive both for the agricultural land and for the forests and pastures. The biological method is the method that uses microorganisms as a cleaning agent. These methods include the use of biopreparations and biostimulants for the degradation of oil and its by-products in contaminated soils. The efficiency of this method depends a lot on the physico-chemical conditions of the soil in which this method will be applied. The main contribution in this method is made by microorganisms, which have hydrocarbons as the main source of organic matter and energy. A soil contaminated with oil can give satisfactory results during their treatment with the biological method, for a period of 3 years. The concentration of crude oil in contaminated soils can be reduced to 10-15% of the total mass of the soil. These percentages are acceptable to return the normal production of the lands. In the breakdown of oil in the soil, the functional activity of the complex of soil microorganisms, which ensure the complete mineralization of oil and oil products into carbon dioxide and water, is of primary and decisive importance. The main contribution to this process is given by microorganisms that are able to use hydrocarbons as the only source of organic matter and energy. The type of soil, its mineral and organic composition, moisture, aeration, temperature also affect the rate of degradation of petroleum hydrocarbons. From the use of biological methods in different countries of the world that have faced the same problem that the area under study is facing today, satisfactory results have been obtained for the recovery

of soil pollution. One of the aspects that makes this method more efficient and usable is the relatively low cost it has compared to other methods and does not require the creation of special infrastructures for use.

## References

- [1] [https://ec.europa.eu/eurostat/statistics-explained/index.php?title=Glossary:Crude\\_oil](https://ec.europa.eu/eurostat/statistics-explained/index.php?title=Glossary:Crude_oil)
- [2] Njuguna J., Siddique Sh., Kwroffie L.B., Piromrat S., Afoakwa K-A., Ekeh-Adegbotolu U., Oluyemi G., Yates K., Mishra A.K., Moller L. (2022). *The fate of waste drilling fluids from oil & gas industry activities in the exploration and production operations*. Waste Management. Volume 139, pp: 362-380, ISSN 0956-053X. <https://doi.org/10.1016/j.wasman.2021.12.025>.
- [3] Lee JH (2013) An overview of phytoremediation as a potentially promising technology for environmental pollution control. *Biotechnol Bioprocess Eng* 18:431–439. doi:10.1007/s12257-013-0193-8.
- [4] Rayner JL, Snape I, Walworth JL, Harvey PM, Ferguson SH (2007) Petroleum–hydrocarbon contamination and remediation by microbioventing at sub-Antarctic Macquarie Island. *Cold Reg Sci Technol* 48:139–153. doi:10.1016/j.coldregions.2006.11.001
- [5] Yue J I, Jiang P J. (2006). Characteristics and Environmental Behavior of Petroleum Pollutants. *Petrochemical technology and application*, 24(4):307-309.
- [6] Kamani H., Baniasadi M, Abdipour H., Mohammadi L., Rayegannakhost Sh, Moein H., Azaric A. (2023). Health risk assessment of BTEX compounds (benzene, toluene, ethylbenzene and xylene) in different indoor air using Monte Carlo simulation in zahedan city, Iran. *Heliyon*, Volume 9, Issue 9, <https://doi.org/10.1016/j.heliyon.2023.e20294>.
- [7] Chen, H.; Lang, M.; Liao, C.; Guo, X. (2022). Migration Behavior and Influencing Factors of Petroleum Hydrocarbon Phenanthrene in Soil around Typical Oilfields of China. *Processes*, 10, 1624. <https://doi.org/10.3390/pr10081624>.

# Experimental study on low-temperature combustion engine mode operations (RCCI)

Habtamu Deresso Disassa<sup>1</sup>, Ramesh Babu Nallamothe<sup>1</sup>, Venkata Ramayya Ancha<sup>2</sup>

<sup>1</sup>Department of Mechanical Engineering, Adama Science and Technology University, Adama, Ethiopia, E-Mail: [habtamu.deresso@astu.edu.et](mailto:habtamu.deresso@astu.edu.et), and [rbnallamothe@gmail.com](mailto:rbnallamothe@gmail.com)

<sup>2</sup>Department of Mechanical Engineering, Jimma University Institute of Technology, Jimma, Ethiopia, E-Mail: [dra.venkata@ju.edu.et](mailto:dra.venkata@ju.edu.et)

---

## Abstract

Research for better combustion technologies, and renewable and clean energy sources is driven by environmental contamination as well as the current energy crisis. Many low-temperature combustion (LTC) technologies have been proposed to increase engine combustion efficiency and lower emissions. To regulate the ignition and combustion process, the reactivity control compression ignition (RCCI) combustion mode had preferred to reduce smoke and oxide of nitrogen emissions, but it didn't get the best solution yet. The intake system is modified to use port injection in RCCI operations for controlling emissions, in-cylinder charge reactivity, and combustion phasing. The experimental investigation of a triple-fuel RCCI engine running on port-injected blends of gasoline and ethanol while diesel fuel is injected directly. The results of G25E75-RCCI engine operation modes have a maximum cylinder pressure of 88 bars at 3000 rpm and a minimum of 58 bars at 2600 rpm on baseline fuel represented D100G0E0. The maximum Heat Release Rate (HRR) of the engine is 62 J/deg at the engine speed of 3000 rpm when operating with the G25E75-RCCI engine and a minimum at G50E50-RCCI with an HRR of 10 J/deg. The engine operating with G25E75 fuel had a minimum of NO<sub>x</sub>, smoke, and CO<sub>2</sub>, which were maximum at the engine running with the baseline experiment. The brake power of the engine is maximum at maximum speed (3000 rpm), and the brake torque is maximum at about 2400 and 2500 rpm with the engine running on a G50E50-RCCI engine. The triple-fuel RCCI engine performs better in terms of thermal efficiency, brake power, brake torque, and minimum NO<sub>x</sub> emission at middle and higher engine speeds at 80% engine load, but stalls at lower engine speeds below 2200 rpm.

**Keywords:** LTC, Oxides of nitrogen, premixed ratio, RCCI, Speed.

---

## 1. Introduction

Research for better combustion technologies, and renewable and clean energy sources is driven by environmental contamination as well as the current energy crisis [1]. Many low-temperature combustions (LTC) technologies, including premixed charge compression ignition (PCCI) [2], partially premixed charge ignition (PPCI) [3], and homogenous charge compression ignition (HCCI) [4], have been proposed to increase internal combustion engine combustion efficiency and lower emissions. To regulate the ignition point and combustion process, the reactivity control compression ignition (RCCI) combustion mode [5] adjusts the ratio of two fuels with variable reactivity, one of which is injected through the port and the other directly [6]. Hence, the RCCI paradigm has drawn a lot of interest. One of the main problems with RCCI engines is that they have a propensity to knock when under heavy loads [7]. Compression ignition engines often have greater compression ratios [8][9], leaner charges [10], and smaller throttle losses [11][12] than spark ignition engines. However, compression ignition engines sharply increased particulate matter (PM) and nitrogen oxide (NO<sub>x</sub>) emissions. Vehicles must abide by severe regulations for both pollution and fuel efficiency under current and prospective legislation [13]. These issues necessitated the creation of cutting-edge engine technology as well as a fuel substitute for fossil fuels that is effective and generates very few pollutants [14]. To lower emissions in a cylinder while maintaining retaining or improved thermal efficiency, several front-line compression ignition combustion approaches have been researched [15],[16]. The majority of existing methods are categorized as low-temperature combustion engines to answer future demands for cleaner and more effective power plants [17][18]. It was discovered that RCCI combustion functions with low nitrogen oxide and soot emissions, though these emissions still require further study and higher suggested efficiencies. Unfortunately, the high-load

operation could not be accomplished with power outputs equivalent to those of a compression ignition engine because of load extension restrictions brought on by high-pressure rise rate (HPRR), high unburned hydrocarbon (HC), and carbon monoxide (CO) emissions in crevice volumes, and poor constituent load performance [19]. To increase fuel reactivity, an ethanol-gasoline blend fuel supply was employed in the experimental investigation of the basic engine and the modified RCCI engine, and diesel fuel was directly injected into the cylinder. It is demonstrated and investigated how fuel injection and premixed fuel ratios interact. The investigation's goal is to use indigenous bioethanol energy replacement with innovative RCCI engines to reduce further NOx and PM emissions.

## 2. Experimental setup and methodology

### 2.1. Experimental setup

The engine test rig had a data acquisition system with a dynamometer directly coupled to the engine output shaft that was found at the Jima University Institute of Technology (JIT), as shown in Fig 1., and a port fuel injection system (PFIS) controlling mechanism with an Arduino board microcontroller. The baseline experiments were conducted on a horizontally mounted, four-stroke, naturally aspirated, water-cooled, single-cylinder, indirectly injected diesel engine displacement of 0.309 liters with the detailed specifications as shown in Table 1. The second experiment was conducted on the same engine modified to the RCCI engines to improve efficiency and reduce emissions. Direct diesel injection is used to deliver fuel to the engine, while port fuel injection (PFI) is used to inject a hydrous bioethanol-gasoline fuel mixture into the intake manifold. Using a maximum load (80%), varying speed, and fuel ratios as a variable, the combustion, performance, and emission properties of blends and diesel fuel are examined to determine the combustion phase, at which efficiency is at its highest. The PFI fuel blend ratios of 20% port-injected fuel and 80% fuel provided by conventional injection were examined using the one-stage injection technique.



Fig. 1. The engine test rig setup, 1 – Fuel measuring tube, 2 – PFI(RCCI Engine), 3 – Dynamometer, 4 – Motor engine coupler, 5 – Exhaust manifold, 6 – Engine, 7 – Reactor, 8 – Air settling tank, 9 – Intake manifold, 10 - Computers for DAQ.

Table. 1 The engine specifications

Engine type, Company	EA300-E2-NB, Kubota
No cylinder and stroke	1 and 4-stroke
Bore*stroke	75.0 * 70.0 mm
Output power at 3,000rpm	5.1KW
Swept volume:	309cm <sup>3</sup>
Connecting rod ratio	0.25
Noise level	95 dB(A)
Speed (varies)	1600 - 3000 rpm
Compression ratio	23

Table 2. Physio-chemical properties of fuels

Properties	Ethanol	Gasoline	Diesel
Auto ignition temp(°C)	420	300	210
Flashpoint (°C)	13	45	93
Final boiling point (°C)	78.5	70	369.8
Density at 15°C	0.79	0.720	0.840
Adiabatic FT @(25°C)	2234	2289	2600
Molecular weight	46	(95-120)	198-202
Reid Vapor pressure, KPa	17	41-65	-
Cetane Number	7	17	54.6
Latent HOV (KJ/kg)	904	380-500	904
RON	106	Min 92	CN- 48
MON	89	81-89	-
LHV(MJ/kg)	26.sie	42.4	42.5
FBP in Fuel Temperature, °C	-	Max 225	380

Cylinder pressure versus crank-angle data over the compression and expansion strokes of the engine operating cycle can be used to obtain quantitative information on the progress of combustion. The HRR or rate of fuel burning is estimated from the cylinder pressure measurement by applying the first law of the single zone model. Data can be used to measure the rate at which fuel energy is released during the combustion process of a diesel engine. The optimal values for  $\gamma$  during combustion, which would provide the most accurate heat-release data, are not well defined. The AHRR during fuel combustion is estimated from the cylinder pressure measurement by applying the first law of the single zone model as stated in equation (1) [20][21].

$$HRR(\theta) = \left( \frac{K}{K-1} P(\theta) dV(\theta) \right) + \left( \frac{1}{K-1} V(\theta) dP(\theta) \right) \quad (Eq. 1)$$

Where  $\theta$  is the crank position, P is the cylinder pressure, and V is the instantaneous chamber volume,  $\gamma$  is the ratio of specific heats (cp/cv), with an appropriate range for diesel heat-release analysis of 1.3 to 1.35. More specifically, the expected diesel engine heat-release analysis to yield values that correspond to air temperatures at the end-of-compression-stroke before combustion ( $\approx 1.35$ ) is preferred in this study [22]. Experiments are performed at a constant 80% or maximum engine load, different engine speeds, and different premixed fuel ratios in both RCCI and baseline combustion. Due to excessive knocking during RCCI combustion at lower engine speed, the experiments were limited to medium to maximum speed only. The premixed fuel ratio ( $r_p$ ) is defined as the ratio of port fuel injection (PFI) energy to the total fuel (PFI+DI) energy injected, as shown in equation (2) [23].

$$r_p = \frac{m \cdot LHV_{GE}}{M \cdot LHV_D + m \cdot LHV_{GE}} \quad (Eq. 2)$$

Where M and m are the mass flow rates of primary and secondary fuels respectively, and LHV is the lower heating value of the respective fuels. The subscript  $D_{iesel}$  (diesel fuel) and G-E (gasoline-ethanol blend fuel) represent the primary and secondary fuels ( $r_p$ =G25E75, and G50E50); however, for baseline compression ignition combustion ( $r_p$  = 0). In all experiments, the start of injection (SOI) timing was maintained constant at 14°CA before the top dead center (bTDC) at all experiments.

### 3.1 Combustion analysis at the same fuel and different speeds

The combustion study of the baseline and reactivity control compression ignition diesel engine used the same fuel strategy at different engine speeds. Each fuel of the baseline (D100G0E0), G25E75 (RCCI), and G50E50(RCCI) fuel is separately used at various engine speeds. The results of the experiments showed the cylinder pressure of the baseline fuel at different speeds is almost similar with slightly greater at the engine speed increases. Maximum, medium, and low HRR are found at the speeds of 2200, 3000, and 2600 respectively as shown in Figs.6a and 6b [23]. The

combustion study of the RCCI-diesel engine uses the same fuel strategy at different engine speeds. The fuel used for port injection is G25E75 blended fuel and the diesel direct-injected fuel is separately used at various engine speeds. According to the results, the cylinder pressure, and heat release rate are maximum at the maximum engine speed and minimum at the speeds of 2600 rpm and intermediate at the engine speed of 2200 rpm as it is shown in Figs.1, 2 [28]. The engine running with the premixed fuel ratio of G50E50 reactivity control compression ignition (RCCI) and direct-injected conventional diesel fuel at different engine speeds has slightly greater cylinder pressure and heat release rate at the engine speeds of 3000rpm and minimum at 2200rpm but averages the engine speeds of 2600rpm as shown in Fig. 3. and 4.

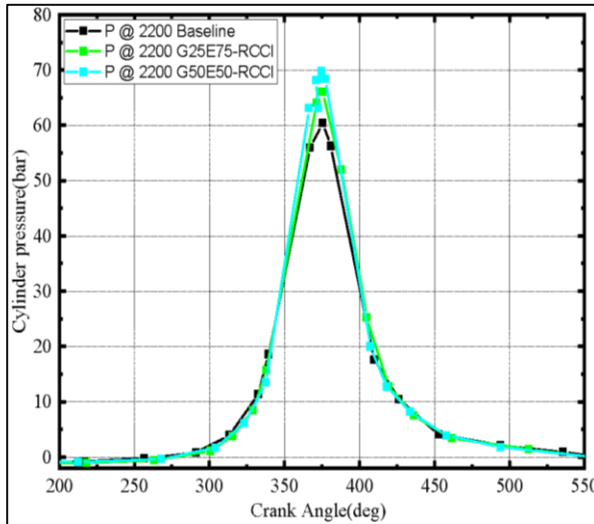


Fig. 2 Cylinder pressure

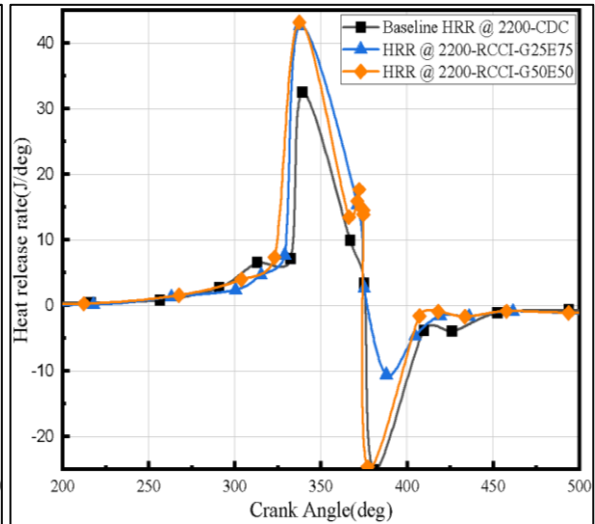


Fig. 3. HRR

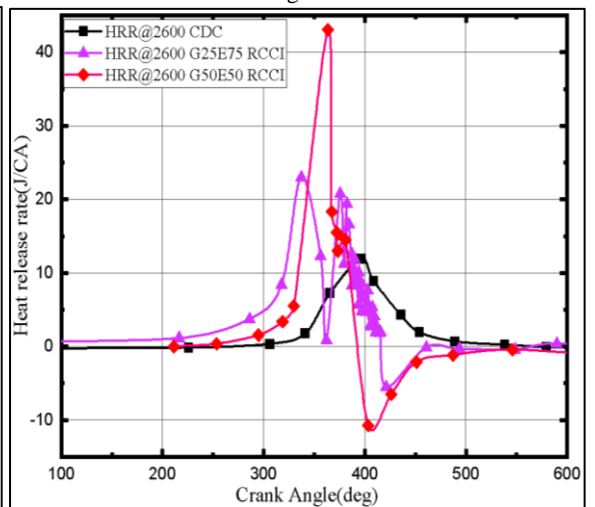
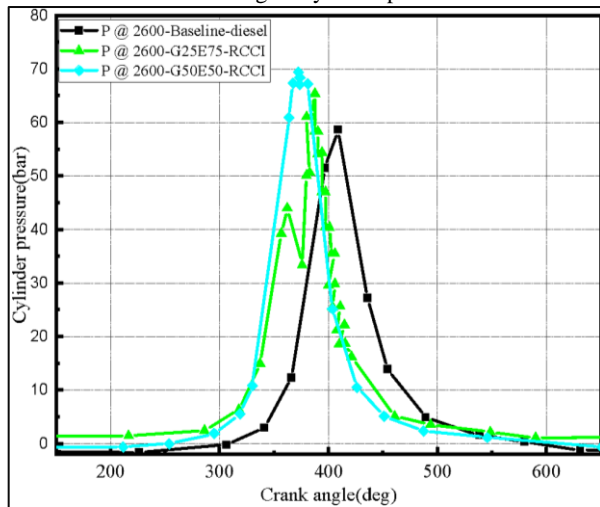


Fig. 4 Cylinder pressure

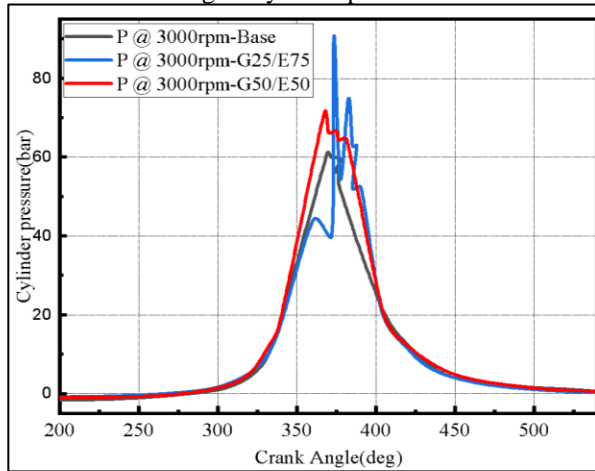


Fig. 6 Cylinder pressure

Fig. 5. HRR

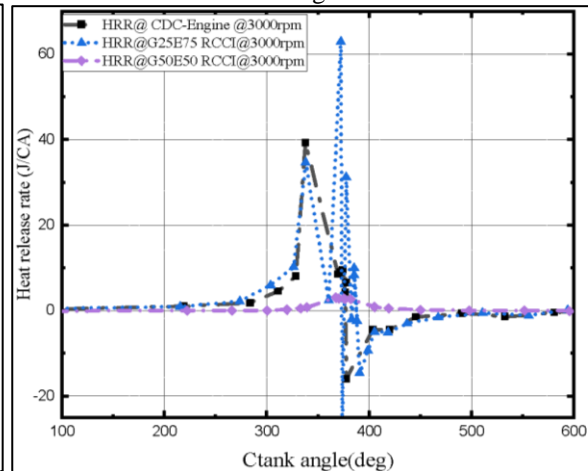


Fig. 7. HRR

According to the experiment's data result, it is possible to conclude that the engine running with the different fuel at a constant engine speed had greater variations in cylinder pressure and heat release rate as shown in Fig 2, 4, and 6 of the cylinder pressure and heat release rate of Fig 3, 5, and 7.

### 3.2 Combustion analysis at the same fuel and different speeds

The combustion study of the baseline and reactivity control compression ignition diesel engine used the same fuel strategy at different engine speeds. Each fuel of the baseline (D100G0E0), G25E75 (RCCI), and G50E50 (RCCI) fuel is separately used at various engine speeds. The results of the experiments showed the cylinder pressure of the baseline fuel at different speeds is almost similar with slightly greater at the engine speed increases. Maximum, medium, and low HRR are found at the speeds of 2200, 3000, and 2600 respectively as shown in Fig. 8. and Fig. 9. The combustion study of the RCCI-diesel engine uses the same fuel strategy at different engine speeds. The fuel used for port injection is G25E75 blended fuel and the diesel direct-injected fuel is separately used at various engine speeds. According to the results, the cylinder pressure, and heat release rate are maximum at the maximum engine speed and minimum at the speeds of 2600 rpm and intermediate at the engine speed of 2200 rpm as it is shown in Fig. 10. and Fig 11. [28]. The engine running with the premixed fuel ratio of G50E50 reactivity control compression ignition (RCCI) and direct-injected conventional diesel fuel at different engine speeds has slightly greater cylinder pressure and heat release rate at the engine speeds of 3000rpm and minimum at 2200rpm but averages the engine speeds of 2600rpm as shown in Fig. 12. and Fig. 13.



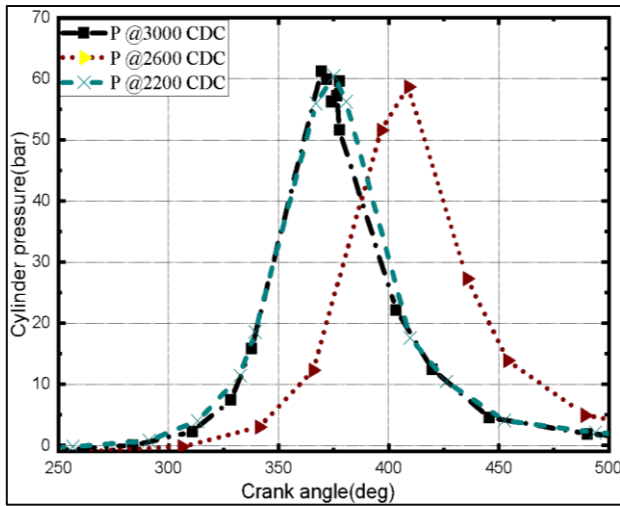


Fig. 8 Cylinder pressure

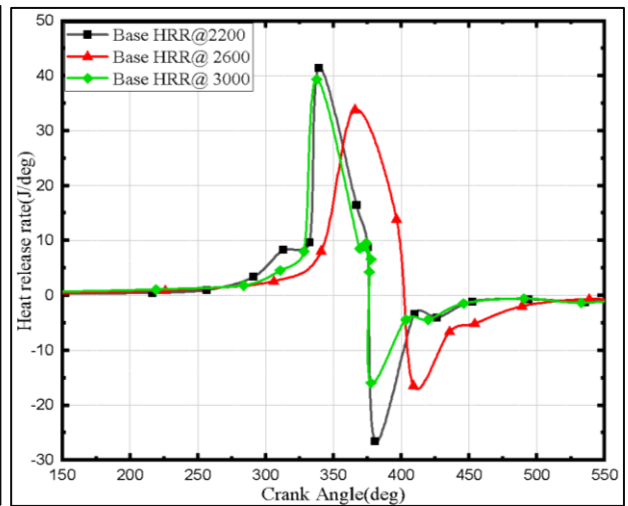


Fig. 9. HRR

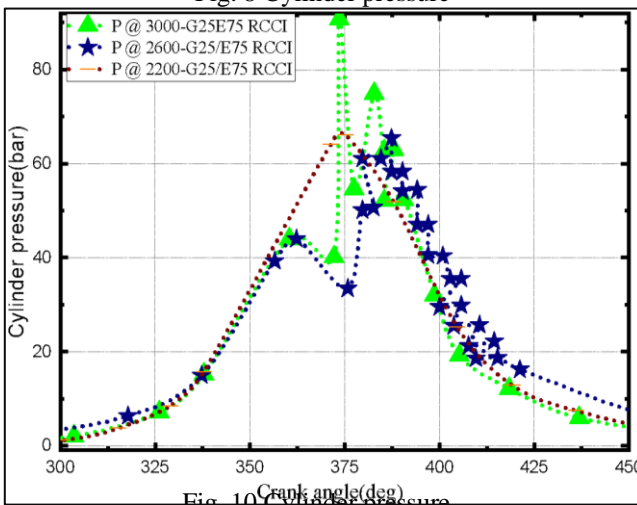


Fig. 10 Cylinder pressure

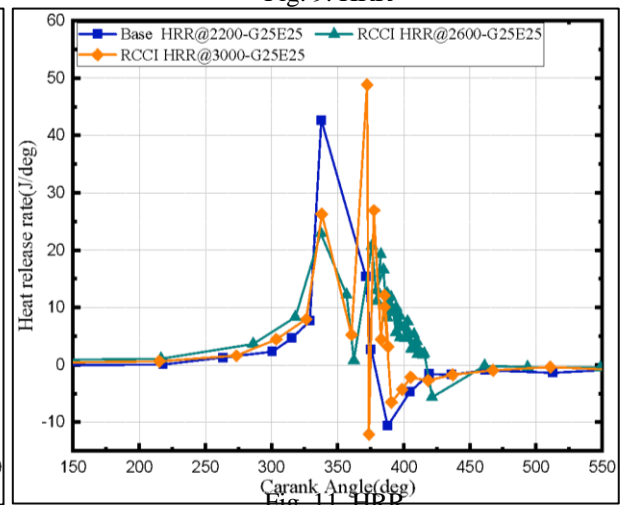


Fig. 11. HRR

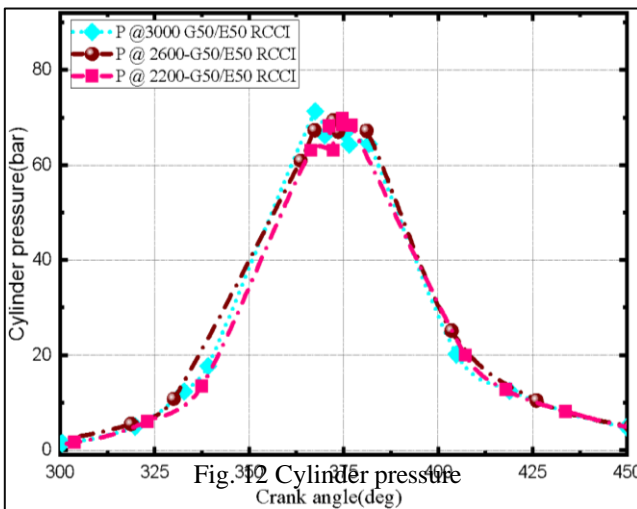


Fig. 12 Cylinder pressure

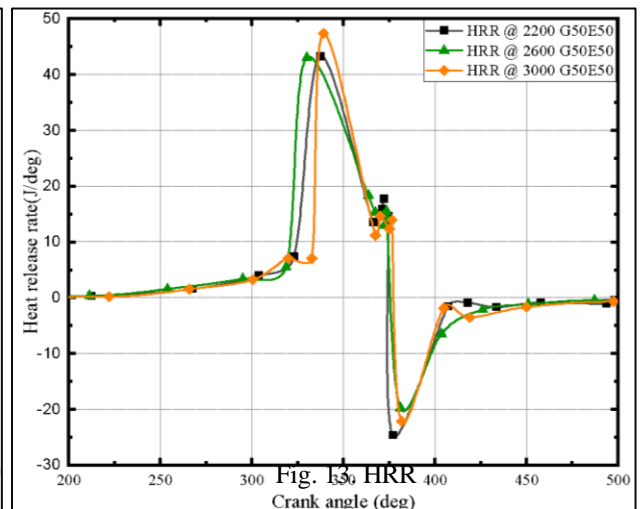


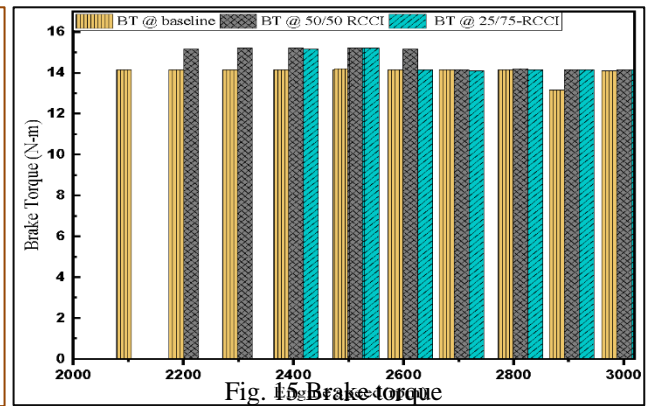
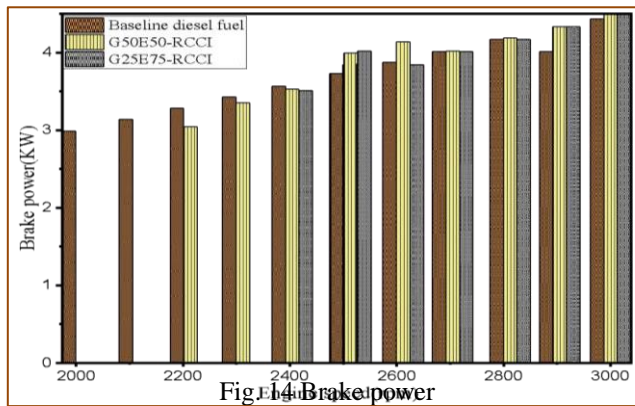
Fig. 13. HRR

According to the above-stated results, the engine running with the same fuel at different speeds has not or a slight change in cylinder pressure except when it is running with the higher ethanol content as shown in Fig 8., and had a great change in heat release rate as shown in all Fig. 9, Fig. 11, Fig. 13.

### 3.3 Engine performances

Using various fuel ratios of premixed ethanol-gasoline blends fuel with direct injection of a pure diesel fuel; experimental studies are carried out in a modified RCCI single-cylinder diesel engine. Engine various speeds are evaluated along with performance like brake power, brake torque, and brake thermal efficiency, brake specific fuel consumption. The baseline experiment performance took place by using pure diesel and the conventional diesel engine to compare with all other operating modalities used in the current advanced engine experiment.

**Brake power (kW):** The brake power in Fig 14. shows the brake power versus engine speed ranging from 1600 to 3000 rpm. The experiment showed the brake power with the premixed of G50E50 and G25E75 blended fuel of a PFI is higher than the baseline power at a speed greater than 2400–3000 rpm engine speed and low power than the baseline with speeds less than 2400rpm engine speed. As shown in the Fig below; power was continuously increasing as the engine speed increased, and the brake power was reduced at the low-speed engine speed[35]. The engine operations are stalled as the engine speed is below 2400 rpm for the engine running with the fuel blend of G25E75; stall for the engine speed below 2200rpm for the engine running with the fuel of G50E50 blend; but the engine is smoothly running with the baseline fuel until the engine speed falls to 1600rpm. From the result, it is possible to justify that the engine operating from middle to high speed at the maximum engine load showed better performances in brake power from 2500-3000rpm of RCCI than CDC.



**Brake torque (N-m):** Brake torque in Fig. 15. shows the brake torque versus engine speed with different premixed fuel ratios and engine speeds. Results below showed the higher brake torque with the G50E50 in the speed ranges of 2200-2600rpm and lower brake torque value with the engine running with the conventional diesel engine. This shows that as the amount of ethanol contents in the premixed fuel increases; the brake torques at 2400 and 2500 increased as shown in Fig. 15. and relatively the same amount with gasoline fuel. But the torques peak at about 2400 rpm and then begin to decline with more speed and become minimum at the highest speeds. The main factors affecting the engine brake torque are the lack of chemical energy conversion to mechanical energy, which is strongly related to volumetric efficiency, fuel mixing, net heat released rate, and cylinder pressure.

**Brake Thermal Efficiency ( $\eta_{b,th}$ ):** brake thermal efficiency is the ratio of the brake power obtained from the engine crankshaft to the fuel energy supplied. The BTE calculated how effectively heat is converted into useful work. The brake thermal efficiency purely depends on the engine design, type of fuel, and engine application. Fig. 16. shows the variation of brake thermal efficiency for different ethanol-gasoline blends and diesel fuel. The brake thermal efficiency slightly decreases with increasing ethanol content in a blend, as shown below. Among the different blends, the calorific values of ethanol, gasoline, and diesel fuel are 26,800, 42,400, and 42,500 J/kg, respectively. Since the fuel used for this investigation is not a pure diesel, G25/E75-RCCI, and G50/E50 blends of RCCI port injected fuel, it is a must to find out the calorific value of the blends to find their thermal efficiency as follows:

- The lower heating value of G25E75-RCCI engine combustion mode:

The LHV of the G25E75-RCCI engine combustion mode is shown in equation (Eq.4):

$$LHV_{G25E75} = (15\% LHV_E) + (5\% LHV_G) + (80\% LHV_D) \quad (Eq. 4)$$

Where:  $LHV_E=26800$ ,  $LHV_G=42,400$ , and;  $LHV_D=42,500$  KJ/kg, then the  $LHV_{25/75-RCCI}=40,140$  KJ/kg

- For the engine running with G50E50-RCCI mode operation, the LHV of the blends is found as shown in equation (Eq.5).

$$LHV_{G50E50} = (10\% LHV_E) + (10\% LHV_G) + (80\% LHV_D) \quad (Eq. 5)$$

So that, the  $LHV_{50/50-RCCI} = 40,920$ , and the  $LHV_{Diesel} = 42,500$  KJ/kg respectively.

After computing the calorific values of G25E75-RCCI, G50E50-RCCI, and diesel fuel, which are 40,140KJ/kg, 40,920KJ/kg, and 42,500 KJ/kg, respectively. The brake thermal efficiency of the engine running with each fuel computed from equation (Eq.6) is illustrated in Fig. 16.

Where  $Q_{LHV}$  is the lowest heating value of the fuel in KJ/kg and the mass flow rate of fuel flow is in kg/sec. Where:  $LHV_{eth}=26800$ ,  $LHV_{gas}=42,400$ , and;  $LHV_{Diesel}=42,500$  J/kg, then the  $LHV_{25/75-RCCI}=40,140$  J/kg. After computing the calorific values of G25E75-RCCI, G50E50-RCCI, and diesel fuel, which are 40,140J/kg, 40,920J/kg, and 42,500 J/kg, respectively, it is found that the brake thermal efficiency of the engine running with each fuel by using the equation (6) is illustrated as it is shown in Fig. 16.

$$\eta_{b.th} = \frac{BP}{\dot{m}_f Q_{LHV}} 100 \quad (Eq. 6)$$

Where  $Q_{LHV}$  is the lowest heating value of the fuel in J/Kg and the mass flow rate of fuel flow is in kg/sec. According to the experiment results, the average thermal efficiency of the engines running at G25/E75-RCCI, G50/E50-RCCI, and diesel engines is 27.7%, 27.8%, and 29%, respectively. So that the thermal efficiency of the engine with each parameter is almost equal to the other. The independent result showed a maximum thermal efficiency of 37% at 1900 rpm and a minimum of 25.139% at 2900 rpm when operating with G50/E50-RCCI; the maximum is 36% at 2600. The minimum is 24% at 3000 rpm engine speeds of the CDC; and the maximum is 29% at 2500 rpm engine speeds and the minimum is 26% at 2900 and 3000 rpm engine operations, as it is clearly shown in Fig. 16. The point that we have to see from the experiment at a maximum load engine set up is good for the engine running with diesel fuel from the higher engine speed to the lower even with the increasing engine thermal efficiency. However; the engine running with the G25E75 port-injected ethanol-gasoline blends is stalled as the engine speed becomes lower than 2200rpm at a maximum engine load (80%) and the engine running with the G50E50 port-injected fuel is stalled as it becomes lower than 1900 rpm engine speed respectively. This shows that the engine with more ethanol had a problem of working at high load and low engine speed and gasoline as well in agreement with findings from.

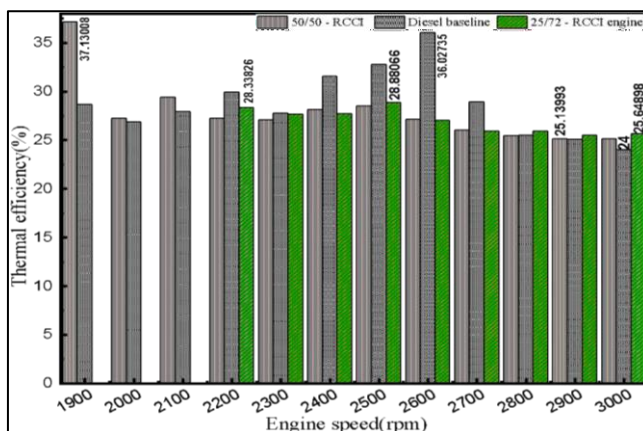


Fig.16 Brake thermal efficiency (%)

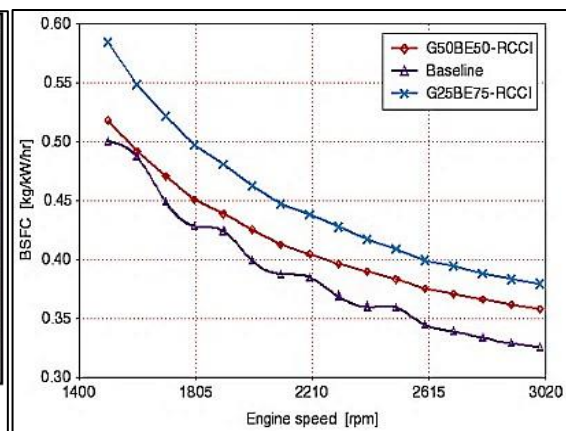


Fig.17 BSFC

*Brake-specific fuel consumption:* - Brake-specific fuel consumption is the ratio between the engine's effective power output and the rate of fuel consumption. Fig. 17. pinpoints the brake-specific fuel consumption (BSFC) characteristics versus engine speed. The investigation's result expressions indicate a minimum brake-specific fuel consumption at the blend ratio of the line experiment and a maximum at G25E75 premixing. Nevertheless, as the speed increases; brake-specific fuel consumption is decreased until the maximum engine speed of 3000 rpm. The brake-specific fuel consumption is minimum for the diesel fuel and maximum for the G25E75 but average for G50E50-RCCI as it is shown in Fig. 17.

### 3.4 Engine emissions

The emissions that need attention from the diesel engine are oxides of nitrogen and particulate matter. Unburned hydrocarbons and carbon monoxide are the main issues for the emissions from the RCCI-diesel engine mode of operation. Nitrogen oxides and smoke emissions from the engine with the highest percentage content of hydrous bioethanol (G25E75-RCCI) are the lowest at all engine speed ranges and the highest at the engine running with the baseline diesel fuel engine combustions. The G50E50 premixed blend ratio-fueled RCCI engine has a moderate value, which is an acceptable targeted result according to the study's objectives. The smoke from the engines is also reduced due to the lack of a rich region as fuel reactivity begins at the intake manifold, and nitrogen oxide is reduced due to the cooling effect of the hydrous bioethanol content. The carbon dioxide emissions in percentage volume in all speed ranges are maximum with conventional diesel combustion. Average with the pre-mixed blend ratio of G25E75 at 2200 and 3000 rpm engine speeds; average with the G50E50 pre-mixed blend ratio at 2600 rpm; and minimum with the G25E75 pre-mixed blend ratio at 2200 and 3000 rpm engine speeds, as shown in Fig.18. Because of the nature of the lean operations of the diesel engine, engine emissions of carbon monoxide in volume and unburnt hydrocarbon in ppm versus engine speed were lowest when the engine ran with conventional diesel combustion. The CO and UHC emissions of the diesel engines running with the G25E75 are the maximum and average for the engine operating with the G50E50-RCCI. The carbon monoxide and unburned hydrocarbon emission results from the experiment indicate that the RCCI engine operation mode has more CO and UHC emissions but low NOx, smoke, and carbon dioxide emissions when compared to the CDC engine in all engine speed ranges, as shown in Fig.3.18. below.

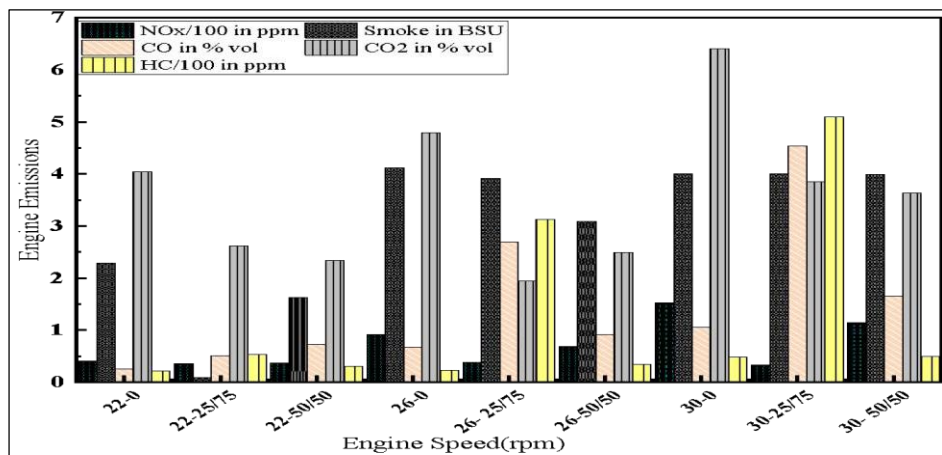


Fig. 18. NOx, smoke, HC, CO, and CO<sub>2</sub> emission of the CDC and RCCI engine

Where 22, 26, and 30 stand for 2200, 2600, and 3000 rpm engine speeds, respectively, and 0, G25/E75, and G50/E50 stand for the premixed ratios of gasoline and bioethanol blends, respectively.

## 4 Conclusions

In the current work, an experimental investigation of a triple-fuel RCCI engine running on port-injected hydrous bio-ethanol-gasoline blend and direct-injected diesel fuel was conducted. The following conclusions can be made on the findings:

- G25E75-RCCI engine operation modes have a maximum cylinder pressure of 88 bars at 3000 rpm and a minimum of 58 bars at 2600 rpm on baseline fuel. In addition, the maximum HRR of the engine is 62 J/deg at the engine speed of 3000 rpm when operating with the G25E75-RCCI engine and a minimum at G50E50-RCCI with an HRR of 10 J/deg.
- NO<sub>x</sub> increases in all cases as the engine speed increases. The engine operating with G25E75 fuel had a minimum of NO<sub>x</sub>, smoke, and CO<sub>2</sub>, which were maximum at the engine running with the baseline experiment.
- The brake power of the engine is maximum at maximum speed (3000 rpm), and the brake torque is maximum at about 2400 rpm with the engine running with G50E50-RCCI engine operation mode and minimum at maximum speeds.
- At 80% engine load operation, the RCCI engine had better thermal efficiency, brake power, brake torque, and minimum NO<sub>x</sub> emission at middle and higher engine speeds, but stalls at lower engine speeds below 2200 rpm.

### Acknowledgment

Supports from Adama Science and Technology University is gratefully acknowledged

### References

- [1] J. Li, D. Wang, C. Zhuang, S. Gong, and S. Li, *Numerical Investigation of the Knocking Combustion Characteristics of the N-Butanol/N-Octanol RCCI Engine, Processes*, vol. 10, no. 10, 2022, doi: 10.3390/pr10102142.
- [2] Y. Zhao, E. Weibo, T. Niu, and J. He, *Study on Combustion Processes of a Premixed Charge Compression Ignition (PCCI) Engine Fueled with DME/Diesel, J. Phys. Conf. Ser.*, vol. 1732, no. 1, 2021, doi: 10.1088/1742-6596/1732/1/012154.
- [3] B. Y. Habtamu Deresso, Venkata Ramayya Ancha, Ramesh Babu Nallamothe, Balkeshwar Singh, *Investigation of Partially Pre-mixed Charge Ignitions (PPCI) Engine Mode, J. Harbin Inst. Technol. (New Ser.)*, 2022, doi: 10.11916/j.issn.1005-9113.2022001.Review.
- [4] N. P. Komninos and C. D. Rakopoulos, *Modeling HCCI combustion of biofuels: A review,* *Renew. Sustain. Energy Rev.*, vol. 16, no. 3, pp. 1588–1610, 2012, doi: 10.1016/j.rser.2011.11.026.
- [5] U. Žvar Baškovič, R. Vihar, S. Rodman Oprešnik, T. Seljak, and T. Kutrašnik, *RCCI combustion with renewable fuel mix – Tailoring operating parameters to minimize exhaust emissions, Fuel*, vol. 311, Mar. 2022, doi: 10.1016/j.fuel.2021.122590.
- [6] J. S. Rosa, M. E. S. Martins, G. D. Telli, C. R. Altafini, P. R. Wander, and L. A. O. Rocha, *Exploring the effects of diesel start of injection and water-in-ethanol concentration on a reactivity controlled compression ignition engine Fuel*, vol. 281, no. July, p. 118751, 2020, doi: 10.1016/j.fuel.2020.118751.
- [7] J. Li, W. Yang, and D. Zhou, *Review on the management of RCCI engines, Renewable and Sustainable Energy Reviews*, vol. 69. Elsevier Ltd, pp. 65–79, Mar. 01, 2017, doi: 10.1016/j.rser.2016.11.159.
- [8] L. Finnegan, *Design of a Variable Compression Internal Combustion Engine By*, 2020.
- [9] K. K. Sadabadi, *Modelling and Control of Combustion Phasing of an RCCI Engine*, pp. 1–100, 2015, [Online]. Available: <http://digitalcommons.mtu.edu/etds/966>.

- [10] J. Benajes, S. Molina, A. García, E. Belarte, and M. Vanvolsem, *An investigation on RCCI combustion in a heavy-duty diesel engine using in-cylinder blending of diesel and gasoline fuels*, *Appl. Therm. Eng.*, vol. 63, no. 1, pp. 66–76, 2014, doi: 10.1016/j.applthermaleng.2013.10.052.
- [11] T. D. Nguyen, T. Tran Anh, V. T. Quang, H. B. Nhat, and V. N. Duy, *An experimental evaluation of engine performance and emissions characteristics of a modified direct injection diesel engine operated in RCCI mode*, *AIMS Energy*, vol. 8, no. 6, pp. 1069–1087, 2020, doi: 10.3934/energy.2020.6.1069.
- [12] E. Uherek *et al.*, *Transport impacts on atmosphere and climate: Land transport*, *Atmos. Environ.*, vol. 44, no. 37, pp. 4772–4816, 2010, doi: 10.1016/j.atmosenv.2010.01.002.
- [13] D. Splitter, R. Reitz, and R. Hanson, *High efficiency, low emissions RCCI combustion by use of a fuel additive*, *SAE Tech. Pap.*, vol. 3, no. 2, pp. 742–756, 2010, doi: 10.4271/2010-01-2167.
- [14] M. Mofijur, M. M. Hasan, T. M. I. Mahlia, S. M. A. Rahman, A. S. Silitonga, and H. C. Ong, “Performance and emission parameters of homogeneous charge compression ignition (HCCI) engine: A review,” *Energies*, vol. 12, no. 18, 2019, doi: 10.3390/en12183557.
- [15] T. J. Jacobs, C. Committee, J. A. Caton, and M. T. Holtzapple, “A HIGH EFFICIENCY AND CLEAN COMBUSTION STRATEGY FOR COMPRESSION IGNITION ENGINES : INTEGRATION OF LOW HEAT,” no. August, 2017.
- [16] S. L. Kokjohn, R. M. Hanson, D. A. Splitter, and R. D. Reitz, “Experiments and modeling of dual-fuel HCCI and PCCI combustion using in-cylinder fuel blending,” *SAE Int. J. Engines*, vol. 2, no. 2, pp. 24–39, 2010, doi: 10.4271/2009-01-2647.
- [17] B. Tekgül *et al.*, “Large-eddy simulation of split injection strategies in RCCI conditions,” 2022, doi: 10.1080/13647830.2022.2036372.
- [18] T. K. Sharma, G. A. P. Rao, and K. M. Murthy, “Homogeneous charge compression ignition (HCCI) engines: A review,” *Arch. Comput. Methods Eng.*, vol. 23, no. 4, pp. 623–657, 2016, doi: 10.1007/s11831-015-9153-0.
- [19] C. A. Buckner *et al.*, “We are IntechOpen , the world ’ s leading publisher of Open Access books Built by scientists , for scientists TOP 1 %,” *Intech*, vol. 11, no. tourism, p. 13, 2016, [Online]. Available: <https://www.intechopen.com/books/advanced-biometric-technologies/liveness-detection-in-biometrics>.
- [20] M. S. Gad, Z. He, A. S. El-Shafay, and A. I. El-Seesy, “Combustion characteristics of a diesel engine running with Mandarin essential oil -diesel mixtures and propanol additive under different exhaust gas recirculation: Experimental investigation and numerical simulation,” *Case Stud. Therm. Eng.*, vol. 26, no. May, p. 101100, 2021, doi: 10.1016/j.csite.2021.101100.
- [21] J. B. Heywood, *Internal Combustion Engine Fundamentals*. N. York: McGraw-Hill. 1988.
- [22] C. Guardiola, B. Pla, P. Bares, and A. Barbier, “applied combustion model applied to an RCCI engine engine,” *IFAC-PapersOnLine*, vol. 51, no. 31, pp. 119–124, doi: 10.1016/j.ifacol.2018.10.022.
- [23] V. B. Pedrozo, X. Wang, W. Guan, and H. Zhao, “The effects of natural gas composition on conventional dual-fuel and reactivity-controlled compression ignition combustion in a heavy-duty diesel engine,” *Int. J. Engine Res.*, vol. 23, no. 3, pp. 397–415, 2022, doi: 10.1177/1468087420984044.
- [24] L. Zhu, Y. Qian, X. Wang, and X. Lu, “Effects of direct injection timing and premixed ratio on combustion and emissions characteristics of RCCI (Reactivity Controlled Compression Ignition) with N-heptane/gasoline-like fuels,” *Energy*, vol. 93, pp. 383–392, 2015, doi: 10.1016/j.energy.2015.09.069.

- [25] M. A. Said, I. B. Dalha, Z. A. Abdul Karim, and M. El-Adawy, "Influence of biogas mixing parameters on the combustion and emission characteristics of diesel RCCI engine," *Alexandria Eng. J.*, vol. 61, no. 2, pp. 1479–1497, 2022, doi: 10.1016/j.aej.2021.06.052.
- [26] M. Elkelawy, E. A. El Shenawy, S. A. Mohamed, M. M. Elarabi, and H. Alm-Eldin Bastawissi, "Impacts of EGR on RCCI engines management: A comprehensive review," *Energy Convers. Manag.* X, vol. 14, p. 100216, May 2022, doi: 10.1016/j.ecmx.2022.100216.
- [27] M. Yıldız and B. A. Çeper, "A comparative study on gasoline/diesel-fueled RCCI combustion at different premixed ratios and high-EGR diesel CI combustion in an IC engine under low load conditions," *Fuel*, vol. 324, p. 124596, 2022.
- [28] A. K. Agarwal, A. P. Singh, and V. Kumar, "Particulate characteristics of low-temperature combustion (PCCI and RCCI) strategies in single cylinder research engine for developing sustainable and cleaner transportation solution," *Environ. Pollut.*, vol. 284, no. November 2020, p. 117375, 2021, doi: 10.1016/j.envpol.2021.117375.
- [29] S. Pan, X. Liu, K. Cai, X. Li, W. Han, and B. Li, "Experimental study on combustion and emission characteristics of iso-butanol / diesel and gasoline / diesel RCCI in a heavy-duty engine under low loads," *Fuel*, vol. 261, no. October 2019, p. 116434, 2020, doi: 10.1016/j.fuel.2019.116434.
- [30] Y. Jian-guang, Z. Wu-gao, and H. Zhen, "Effect of cetane number improver on heat release rate and emissions of high speed diesel engine fueled with ethanol – diesel blend fuel," vol. 83, no. 2004, pp. 2013–2020, 2020, doi: 10.1016/j.fuel.2004.05.003.
- [31] S. Pan *et al.*, "Experimental study on the cyclic variations of ethanol / diesel reactivity controlled compression ignition (RCCI) combustion in a heavy-duty diesel engine," *Energy*, vol. 237, p. 121614, 2021, doi: 10.1016/j.energy.2021.121614.
- [32] H. Liu, G. Ma, B. Hu, Z. Zheng, and M. Yao, "Effects of port injection of hydrous ethanol on combustion and emission characteristics in dual-fuel reactivity controlled compression ignition (RCCI) mode," *Energy*, vol. 145, pp. 592–602, 2018, doi: 10.1016/j.energy.2017.12.089.
- [33] A. B. Dempsey, S. Curran, and R. D. Reitz, "Characterization of Reactivity Controlled Compression Ignition (RCCI) Using Premixed Gasoline and Direct-Injected Gasoline with a Cetane Improver on a Multi-Cylinder Engine," *SAE Int. J. Engines*, vol. 8, no. 2, pp. 859–877, 2015, doi: 10.4271/2015-01-0855.
- [34] A. Weall and N. Collings, "Investigation into partially premixed combustion in a light-duty multi-cylinder diesel engine fuelled gasoline and diesel with a mixture of," *SAE Tech. Pap.*, no. 724, 2007, doi: 10.4271/2007-01-4058.
- [35] N. T. Nghia, N. X. Khoa, W. Cho, and O. Lim, "A Study the Effect of Biodiesel Blends and the Injection Timing on Performance and Emissions of Common Rail Diesel Engines," *Energies*, vol. 15, no. 242, 2022, doi: <https://doi.org/10.3390/en15010242> Academic.
- [36] J. R. Sodré and S. M. C. Soares, "Comparison of engine power correction factors for varying atmospheric conditions," *J. Brazilian Soc. Mech. Sci. Eng.*, vol. 25, no. 3, pp. 279–284, 2003, doi: 10.1590/S1678-58782003000300010.
- [37] E. Url, S. N. English, and U. Kingdom, "Experiment instructions," pp. 1–2, 2014.
- [38] R. Hanson, S. Curran, R. Wagner, and R. Reitz, "Effects of biofuel blends on RCCI combustion in a light-duty, multi-cylinder diesel engine," *SAE Int. J. Engines*, vol. 6, no. 1, pp. 488–503, 2013, doi: 10.4271/2013-01-1653.

- [39] E. Ansari, M. Shahbakhti, and J. Naber, "Optimization of performance and operational cost for a dual mode diesel-natural gas RCCI and diesel combustion engine," *Appl. Energy*, vol. 231, no. August, pp. 549–561, 2018, doi: 10.1016/j.apenergy.2018.09.040.
- [40] R. Willems, F. Willems, N. Deen, and B. Somers, "Heat release rate shaping for optimal gross indicated efficiency in a heavy-duty RCCI engine fueled with E85 and diesel," *Fuel*, vol. 288, no. September, p. 119656, 2021, doi: 10.1016/j.fuel.2020.119656.



# Impacts of Site Ambient Temperature and Wind Speed on Photovoltaic Performance with Varying Tilt Angles.

Ephrem Assefa Feyissa <sup>1</sup>, Endeshaw Alemu Bekele <sup>2</sup>, Mohammed Abdulkedir Alfeki <sup>3</sup>

<sup>1</sup>Collage of Engineering and Technology: Department of Mechanical Engineering, Bule Hora University, Ethiopia, ephrem.assefa@bhu.edu.et: ORCID: <https://orcid.org/0009-0006-2448-1525>:

<sup>2</sup>Department of Thermal Technology, Silesian University of Technology, Gliwice, Poland, ebekele@polsl.pl.

<sup>3</sup>Collage of Engineering and Technology: Department of Mechanical Engineering, Bule Hora University, Ethiopia, mohammed@bhu.edu.et: ORCID: <https://orcid.org/0009-0001-5284-9642>:

---

## Abstract

The exploitable daily reserve of solar radiation in Ethiopia is approximately 4-6 kWh/m<sup>2</sup>/day, but less than 1% of this potential is currently utilized. To address this, the Ministry of Water and Energy established the National Electrification Program 2 (NEP.2) to provide electricity to remote areas using photovoltaic systems. This study focuses on how site ambient temperature and wind speed impact photovoltaic performance in the Yaya Gulele district. The study combines the Faiman Model with the Angstrom-Prescott equation to analyse various factors affecting photovoltaic performance. Results indicate that tilt angle and ambient temperature significantly influence system performance. Specifically, an increase in ambient temperature from 291 K to 299 K, within a tilt angle range of 31.47° to 32.43°, leads to an average power loss of 32.83 W per module. Additionally, the study highlights the positive impact of wind speed on performance. As the wind speed ranges from 0.5 m/s to 2 m/s, temperature loss decreases from 37.51 W to 28.47 W, and performance increases from 21.76% to 22.39% within a tilt angle range of 34.91° to 42.44° at the mean ambient temperature of the study area. The optimal tilt angle for minimal losses and optimal performance is determined to be 41.96°, resulting in a temperature loss of 33.63 W and a performance of 22.12% in month of April which experiences the highest ambient temperature.

**Keywords:** Optimum tilt angle, Photovoltaic Performance, Site Ambient Temperature, Wind speed

---

## 1. Introduction

The daily falling exploitable reserve amount of solar radiation in Ethiopia is about 4-6 kWh/m<sup>2</sup>/day. Among these, only less than 1% of the resource is exploited [1] [2]. In 2019, the Ministry of Water and Energy (MoWE) of Ethiopia established National Electrification Program 2 (NEP.2) with the motto of “Lighting to all” to facilitate the electrification of remote areas [3] by recommending photovoltaics and other renewable energy conversion systems [4] [5]. However, the utilization of solar energy resource in specific site, needs further study related to the impacts of environmental weather condition on the performance of photovoltaic arrays to harness the required amount of power output effectively [6] [7]. The recent study [8], assessed the potential of solar energy resources with possible areas for photovoltaic installation in typical rural village of Ethiopia. However, the study did not investigate the impacts of weather conditions at the site. The working condition of photovoltaic modules can be affected by operating factors such as the ambient temperature, cloud, dust, weather condition, tilt angle, geographical location, types of photovoltaic material, cable thickness and shading effects [9] [10].

The performance and power output of a photovoltaic cell are primarily dependent on the variation of tilt angle, cell temperature, and wind speeds at the selected site [11] [12] [13]. Many researchers commonly use the “thumb rule” based on latitude for estimating the optimum tilt angle, which is “Latitude ±15°” [14]. However, solar radiation also varies with elevation of the selected site, and relying solely on latitude may not yield the best tilt angle value for different locations [15]. As previously proven in a prior researches [16] [17], lower tilt angles

causes more dust deposition due to low gravitational impact. Modules with tilt angles below 15 degrees showed increased water retention on the panels and creates a dust mixed sticky substance which causes the collection of extra dust particles that can't being blown off by the wind [18]. When comparing photovoltaic panels with tilt angles of 0°, 20° (the most common installation angle), and 33.5°, the solar panels installed at 33.5° exhibited over 50% reduced soiling losses than panels set at 0° [19].

The most relevant value of the optimum tilt angle ( $\beta_{opt}$ ) can be determined based on declination angle ( $\delta$ ) and day length of the site by using the correlations formulated as third-degree polynomial mathematical model [20].

$$\beta_{opt} = -0.00002(\delta)^3 - 0.0009(\delta)^2 - 1.0647(\delta) + 33.515 \quad (1)$$

Where:

declination angle ( $\delta$ ) is the function of the day length and sunshine hour in each months of the study area. For instance, sunshine hour and declination angle strongly depends on a location (Latitude) of the study area. Therefore the tilt angle is required to be adjusted twice a year which produce more energy than completely fixed module, while adjusting module more than four times will increase more power output [10]. In this study, the impact of cell temperature and wind speed on the performance of photovoltaic module with varying tilt angle was studied by analytical method. The Faiman-model equation (2) is used, which includes correlation of ambient temperature, irradiance and wind speed together [9].

$$T_c = T_a + \frac{H_c}{U_o + U_1 \cdot v_m} \quad (2)$$

Where:

$T_a$  is the ambient temperature,  $U_o$  is the constant heat transfer coefficient,  $U_1$  is the wind speed coefficient of heat transfer,  $v_m$  is the wind speed at the height of the modules. The value of  $U_o = 30.02 \text{ W/m}^2 \text{ K}$  and  $U_1 = 6.28 \text{ W/m}^3 \text{ K}$  are constant coefficient values.

The performance of solar cells decreases significantly as the temperature increases. On the contrary, lower temperatures are known to improve the efficiency and power output of the photovoltaic modules [21] [22]. Equation (3), (4) and (5) connects the parameters influencing efficiency and power output of photovoltaic modules.

$$P_{T_{loss}} = P_{STC} \times \left(\frac{H_c}{G_{STC}}\right) \times Q_{deg} \times C_{Temp} \times (T_{c,STC} - T_c) \quad (3)$$

Where:

$P_{T_{loss}}$  is Losses caused by the temperature,  $P_{STC}$  is the maximum power of the PV system at standard test condition (STC), ( $G_{STC}$  is the irradiance at  $STC$  which  $1000 \text{ W/m}^2$  and  $C_{Temp}$  is the temperature coefficient,  $Q_{deg}$  Module quality degradation coefficient and  $H_c$  is plane of array irradiance in  $\text{W/m}^2$ .

$$\eta = \eta_r [1 - C_{Temp}(T_c - T_{NOCT})] \quad (4)$$

Where  $\eta$  is the cell's monthly average efficiency,  $\eta_r$  is the module's efficiency at solar radiation flux of  $1 \text{ kW/m}^2$  and at reference temperature,  $C_{Temp}$  is the temperature coefficient which is dependent on the panel's material (e.g.  $0.004 \text{ K}^{-1}$  for crystalline silicon modules), and  $T_c$  is the monthly average temperature of the cell. Normally,  $C_{Temp}$  and  $T_{NOCT}$  are provided by the cell's manufacturer.

Therefore the power output is given by a relation:

$$P = H_c \times \tau_{pv} \times \eta_r \times A [1 - 0.0045 \times (T_c - 25)] \quad (5)$$

Where:

$H_c$  the irradiance on the cell ( $W/m^2$ ) is,  $\tau_{pv}$  is the transmissivity of the glass and A is the module's surface area ( $m^2$ ). For the most widely employed 3.2 and 4 mm thick glass, the visible light transmittance of sunlight is generally 90–92 % [23].

## 2. Methodology and Materials

### 2.1. Description of study area

Nano village is a rural community located at a Latitude of  $9^{\circ} 35' N$  and Longitude of  $38^{\circ}40'E$ , in Yaya Gulele district. It's located about 115 km North-West of the capital city, Addis Ababa [24] [25] [26].

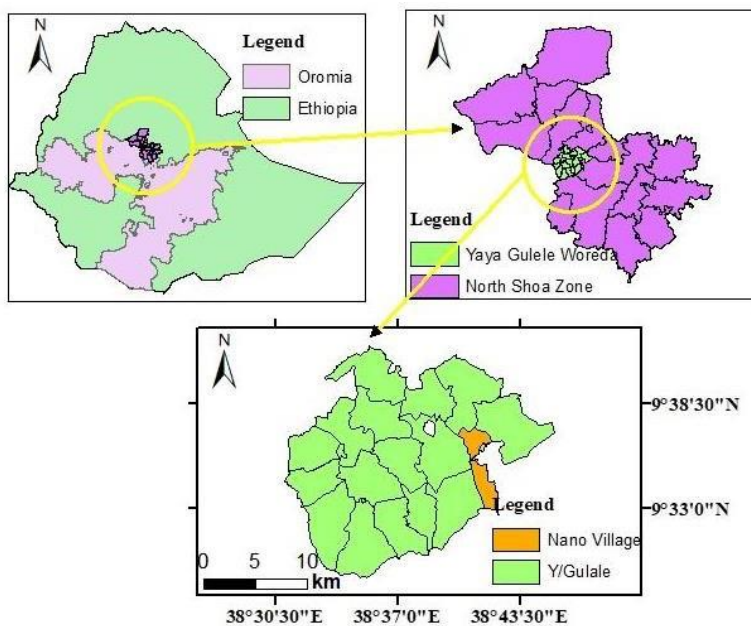


Fig.1. Location map of the study area

### 2.2. Solar energy resource, ambient temperature wind speed data of study area

To estimate available solar energy resource in the study area, the relevant sunshine hour data is collected from the National Meteorological Agency (NMA) of Ethiopia [27]. As shown in Figure 2., the study area's sunshine duration is increasing from October to May and slightly decreases in summer. It shows that the maximum of 8.59 sunshine hours is in November and a minimum of 5.26 hours in July.

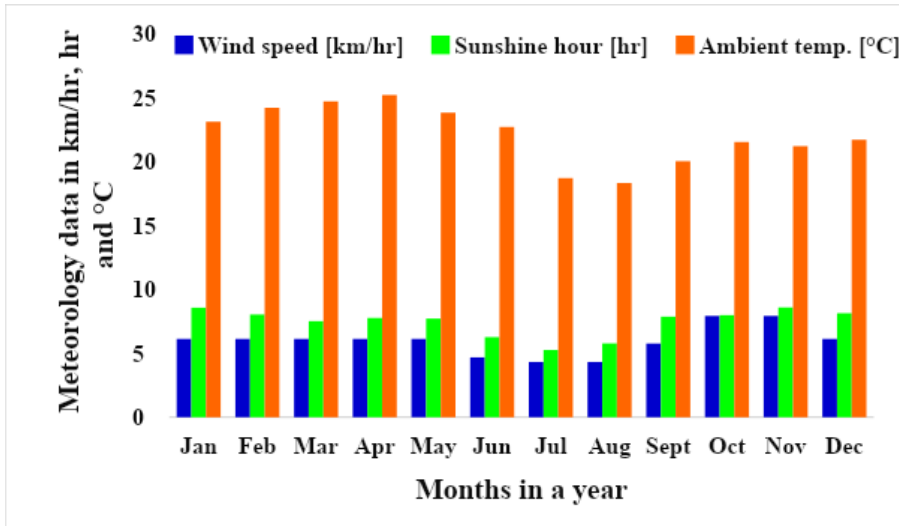


Fig.2. Variation of Sunshine hour, wind speed and ambient temperature in months of the year [27] [28].

The solar irradiance on a horizontal surface were estimated by Angstrom-Prescott linear model relating average horizontal radiation to clear day radiation and sunshine level [29] [30] [31].

$$\frac{K_T}{H_o} = \frac{H_h}{H_o} = (a + b \frac{\bar{u}}{N}) \quad (15)$$

Where:

$\bar{H}_h$  and  $\bar{H}_o$  are the horizontal terrestrial and horizontal extra-terrestrial radiation levels averaged for a month,  $K_T$  is clearness index,  $a$  and  $b$  are regression constants for a given site and  $\bar{u}$  and  $\bar{N}$  are the monthly average numbers of hours of bright sunshine and day length respectively. The wind speed data of the study area was obtained from New Local Climate estimator (New-LocClim) [28].

The obtained value of the solar radiation in this work was calculated from the ground data (sunshine hour data) collected directly from study area by National Meteorological Agency of Ethiopia (NMA). Since Ethiopia is located in a northern hemisphere, the recommended module orientation is also included as facing south to avoid panel self-shading effects [10] [32] [33].

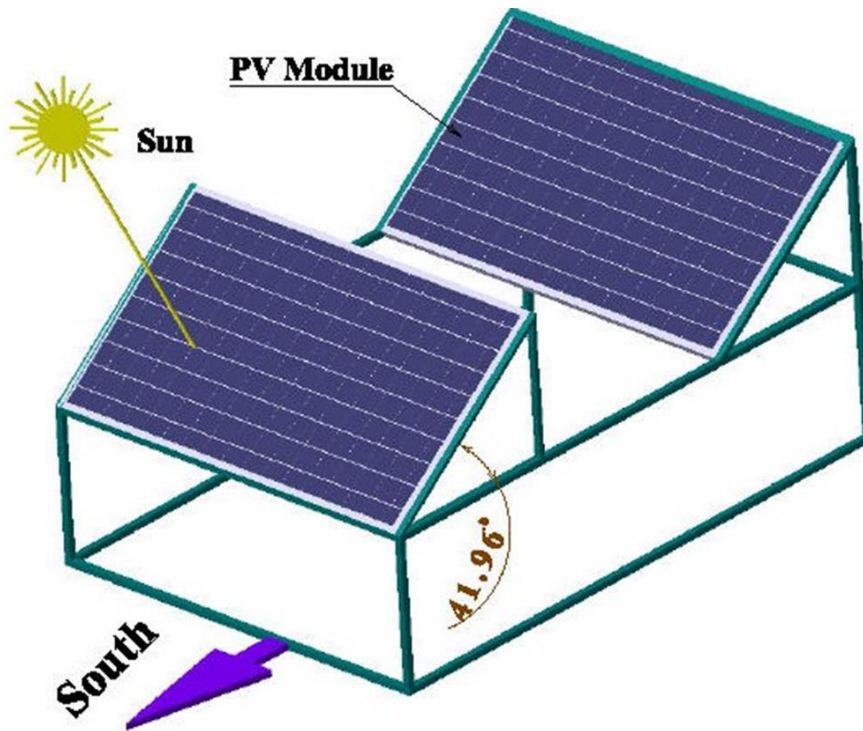


Fig.3. Module orientation model by CATIA V5.

The PV module produced by LONGI solar with model LR6-60-HPB-350 is also selected because of high efficiency and affordable cost in 2023 market. Their rated efficiency, capital cost, operation temperature and warranty year were 20.3 %, 0.6 USD /W, 47 °C and 25 year respectively [34].

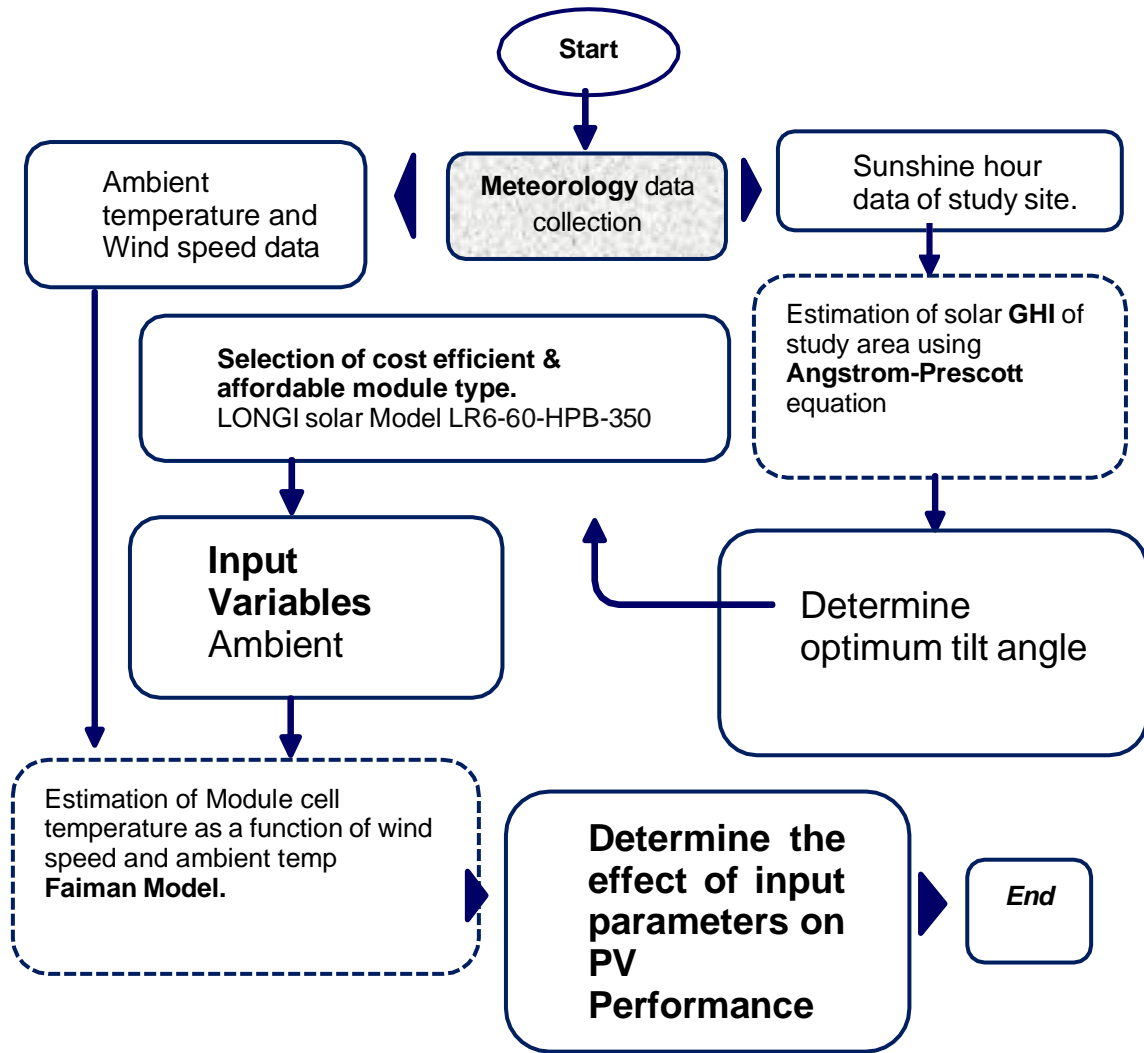


Fig.4. Flow chart of an overall analysis of the study.

### 3. Results and Discussions

#### 3.1. Impacts of ambient temperature and wind speed on photovoltaic performance

The ambient temperature in the study area varies from 291.3 K in August to 298.2 K in April. The highest solar radiation is received in the months of January. Tilt angle values ranging from 0° to 80° were considered in this study. At a constant ambient temperature of 291 K, the power output of the module reaches a maximum of 350.6 W at a tilt angle of 41.8°, and it starts decreasing as the tilt angle increases. Additionally, the power output decreases as the ambient temperature increases from 291 K to 299 K, as depicted in Fig.5. The maximum power output per module of 350.6 W was achieved at ambient temperature of 291 K, as an optimum tilt angle ranges from 40.44° to 43.16°. However, when the ambient temperature rises to 299 K, the maximum power output decreases to 336.5 W, as the optimum tilt angle spans from 40.76° to 43.16°.

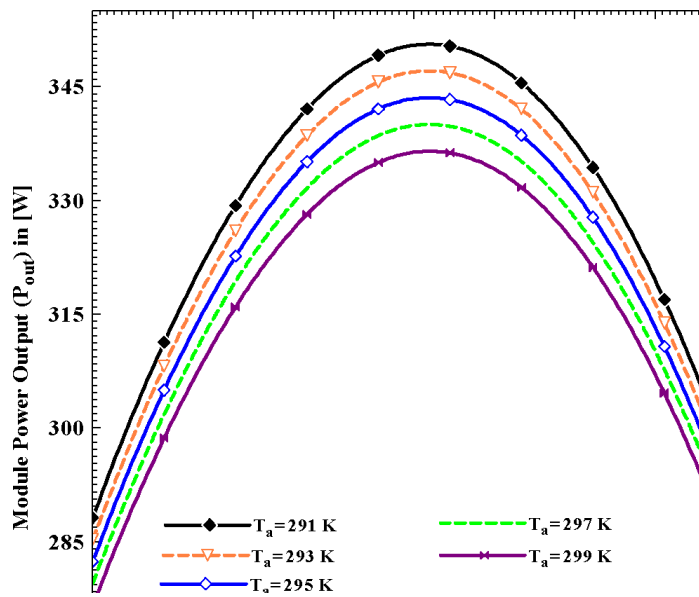


Fig.5. The module power output with variation of tilt angle at constant ambient temperature.

The power output of a photovoltaic system is influenced by the variation of tilt angle and cell temperature. Improper selection of the optimum tilt angle at a specified site can result in power losses in the photovoltaic array. The magnitude of these losses increases as the ambient temperature of the study site rises. Specifically, when the ambient temperature is at 291 K, the power loss increases and reaches a maximum of 30.04 W, between the tilt angle interval of 28.03° and 29.07°. However, the power loss starts decreasing as the tilt angle passes this point, as illustrated in Fig.6. When the ambient temperature rises to 299 K, the power loss becomes 39.67 W at tilt angle values ranging from 28.99° to 30.67°.

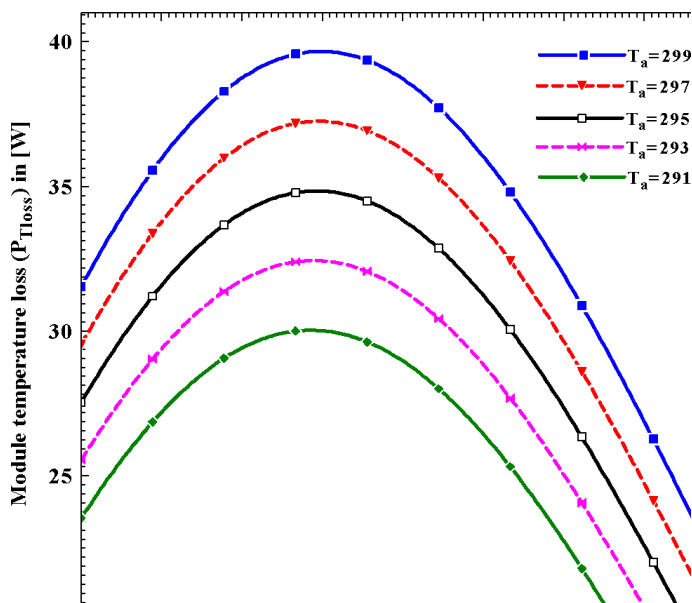


Fig.6. The effects of Cell temperature on module power output at constant ambient temperature in a month of April.

The temperature loss decreases as the wind speed in the study area increases. When the wind speed varies from 0.5 m/s to 2 m/s, the temperature loss reduces from peak value of 37.51 W to 32.24 W respectively, as tilt angle varies from 38.04°-39.4°. Despite the convective loss caused by wind on the photovoltaic panel during the cold season, the results demonstrate that wind speed has a positive impact on the performance of photovoltaic power plants. Fig.7. illustrates the effects of wind speed on photovoltaic power loss as the tilt angle varies from 0° to 80°.

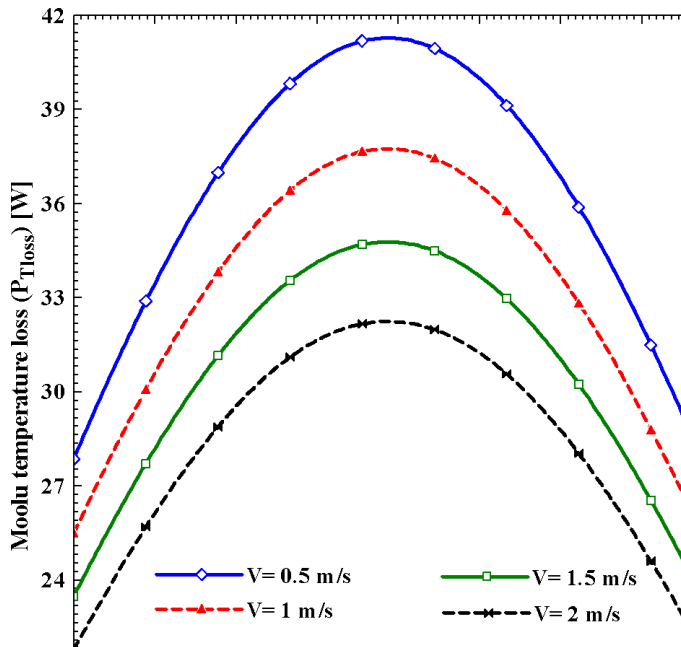


Fig.7. Module temperature loss with variation of wind speed.

In this study the effects of wind speed on the performance of photovoltaic module was considered in relation to cell temperature. The wind speed has positive effects on the performance, except soil particles and dust depositions on the module due to wind effect (negative effect). The wind speed of study area is not more than 2 m/s through year round. As the wind speed of the study area varies from 0.5 m/s -2 m/s, the photovoltaic module efficiency increases from an average value 21.76% to 22.39% between a tilt angle range of 34.91° - 42.44°. Therefore it's observed that the wind speed increases the performance of the PV module by decreasing it's the cell temperature. Fig.8. depicts the positive impacts of wind speed at a mean ambient temperature of the study area (295.1 K).



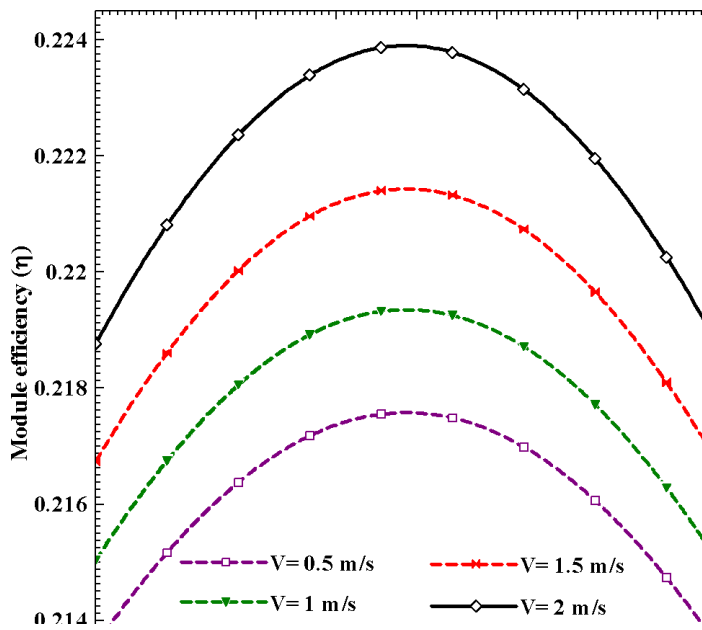


Fig.8. Variation effect of wind speed on module performance.at mean ambient temperature.

The tilt angle at which the maximum power of 336.5 W obtained were varies between 40.76° to 43.16° when ambient temperature of the study area was 298.2 K in April. When the optimum tilt angle is estimated according to thumb rule ( $Latitude \pm 15^\circ$ ) it becomes 24.35° for study area. At this angle, the temperature loss was 36.71 W when the wind speed of study area is 1.7 m/s in April with efficiency and power output of 22.07% and 336.2 W. In this work the best operating optimum tilt angle were found to be 41.96 ° with an optimum module efficiency of 22.12 % and reduced temperature loss of 33.63W. At this point the photovoltaic module operates at optimum condition with the reduced cell temperature of 325.6 K and the maximum power output of 343.3 W in months of April as shown in Fig. 9.

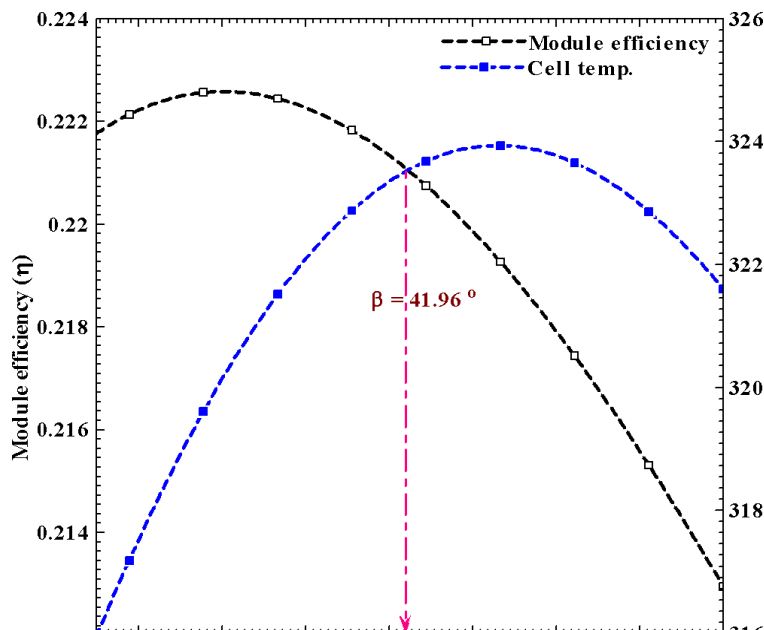


Fig.9. Optimum tilt angle at optimum operating condition.

Solar radiation distribution in the study area was mapped to assess solar radiation intensity and to select possible areas of photovoltaic installation. According to the analysis result, the areas located in lower elevation have low intensity of solar radiation due to shading of terrain and low altitude. Figure 10. shows the possible areas for photovoltaic array installation in the study area. The maximum and minimum amount of solar radiation in Nano kebele spans from 3.43 kWh/m<sup>2</sup>/day to 6.78 kWh/m<sup>2</sup>/day.

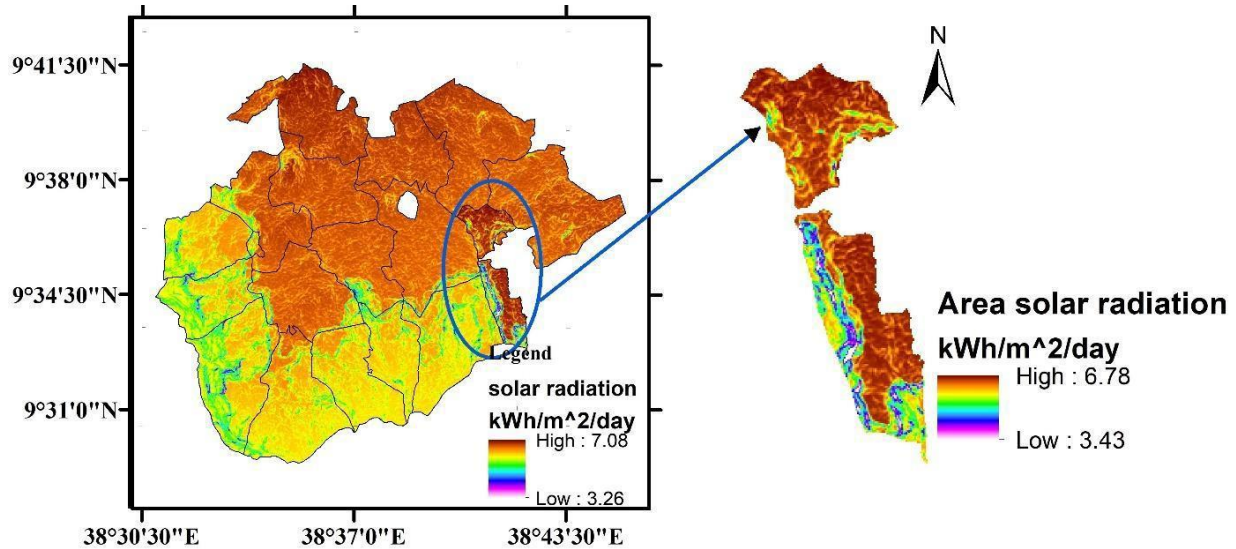


Fig.10. Area solar radiation of Nano kebele

#### 4. Conclusions

This study highlights the underutilization of solar radiation in Ethiopia and the efforts made through the National Electrification Program 2 (NEP.2) to address this issue using photovoltaic systems. The research focuses on the impact of ambient temperature and wind speed on photovoltaic performance in the Yaya Gulele district. The findings emphasize the significant influence of tilt angle and ambient temperature on system performance. Additionally, wind speed was found to positively affect performance. The optimal tilt angle for minimal losses and optimal performance was determined to be 41.96 °. It results in the reduction of temperature loss by 8.39 % and an increase in photovoltaic performance up to 22.12% in month of April which experiences the highest ambient temperature in the study area. These insights can be expected to guide the design and operation of photovoltaic systems by supporting environmental friendly and sustainable energy solutions in remote areas of Ethiopia.

#### References

- [1] Belay Kassa, A., *Current Status, Future Potential and Barriers for Renewable Energy Development in Ethiopia*. Iranian (Iranica) Journal of Energy & Environment, 2019. **10**(4): p. 269-274.
- [2] Hailu, A.D. and D.K. Kumsa, *Ethiopia renewable energy potentials and current state*. Aims Energy, 2021. **9**(1).
- [3] Bekele, S., *National Electrification Program 2 Integrated Planning for Universal Access. Technical report*. . 2019: Addis Ababa, Ethiopia.
- [4] Bekele, S., *Building the Market for Rural Electrification in Ethiopia; A report of mini-grid productive use assessment*. 2020, Ethiopian Ministry of Water and Energy (MoWE), Ethiopia Electric Authority (EEA) and Ethiopia Electric Utility (EEU): Addis Ababa, Ethiopia.
- [5] Bekele, S., *Off-Grid Solar Market Assessment Ethiopia: Technical report*. 2019, Power Africa and USAID: Addis Ababa, Ethiopia.
- [6] Farahmand, M.Z., et al., *The simultaneous impacts of seasonal weather and solar conditions on PV panels electrical characteristics*. Energies, 2021. **14**(4): p. 845.

- [7] Jathar, L.D., et al., *Comprehensive review of environmental factors influencing the performance of photovoltaic panels: Concern over emissions at various phases throughout the lifecycle*. Environmental Pollution, 2023: p. 121474.
- [8] Feyissa, E.A., et al., *Energy Potential assessment and techno-economic analysis of micro-hydro-photovoltaic hybrid system in Goda Warke village, Ethiopia*. Clean Energy, 2023, <https://doi.org/10.1093/ce/zkad080>.
- [9] Koehl, M., et al., *Modeling of the nominal operating cell temperature based on outdoor weathering*. Solar Energy Materials and Solar Cells, 2011. **95**(7): p. 1638-1646.
- [10] Vidyanandan, K., *An overview of factors affecting the performance of solar PV systems*. Energy Scan, 2017. **27**(28): p. 216.
- [11] Salimi, H., et al., *Effect of dust concentration, wind speed, and relative humidity on the performance of photovoltaic panels in Tehran*. Energy Sources, Part A: Recovery, Utilization, and Environmental Effects, 2019. **45**(3): p. 7867-7877.
- [12] Ebhota, W.S., *Impact of Photovoltaic Panel Orientation and Elevation Operating Temperature on Solar Photovoltaic System Performance*. International Journal of Renewable Energy Development, 2022.
- [13] Kaldellis, J.K., M. Kapsali, and K.A. Kavadias, *Temperature and wind speed impact on the efficiency of PV installations. Experience obtained from outdoor measurements in Greece*. Renewable energy, 2014. **66**: p. 612-624.
- [14] Darhmaoui, H. and D. Lahjouji, *Latitude Based Model for Tilt Angle Optimization for Solar Collectors in the Mediterranean Region*. Energy Procedia, 2013. **42**: p. 426-435.
- [15] Ashetehe, A.A., B.B. Gessesse, and F. Shewarega, *A generalized approach for the determination of optimum tilt angle for solar photovoltaic modules with selected locations in Ethiopia as illustration examples*. Scientific African, 2022. **18**.
- [16] Rudnicka, M. and E. Klugmann-Radziemska, *The issue of shading photovoltaic installation caused by dust accumulation on the glass surface*. Ecological Chemistry and Engineering S, 2021. **28**(2): p. 173-182.
- [17] Chiteka, K., R. Arora, and V. Jain, *CFD Prediction of dust deposition and installation parametric optimisation for soiling mitigation in non-tracking solar PV modules*. International Journal of Ambient Energy, 2021. **42**(11): p. 1307-1320.
- [18] Qasem, H., et al., *Dust-induced shading on photovoltaic modules*. Progress in Photovoltaics: Research and Applications, 2014. **22**(2): p. 218-226.
- [19] Afridi, M.A., et al., *Determining the effect of soiling and dirt particles at various tilt angles of photovoltaic modules*. International Journal of Engineering Works, 2017. **4**(8): p. 143-146.
- [20] Sharma, A., et al., *Correlation formulation for optimum tilt angle for maximizing the solar radiation on solar collector in the Western Himalayan region*. Case Studies in Thermal Engineering, 2021. **26**.
- [21] Hashemi, B., et al., *Systematic photovoltaic system power losses calculation and modeling using computational intelligence techniques*. Applied Energy, 2021. **284**: p. 116396.
- [22] Tanaka, A.M., *Investigation of Efficiency Loss of Distributed Solar Power Due to Soiling and Efficiency Recovery by Rainfall*. 2019, University of Nevada, Las Vegas.
- [23] Karasu, B., et al., *Solar glass panels: A review*. Avrupa Bilim ve Teknoloji Dergisi, 2020(20): p. 548-565.
- [24] Shaita, S.S., *Socio-Economic Benefits and Challenges of Energy Efficient Cook Stoves Utilization for Women and Children in Yaya Gulele District, North Western Ethiopia; Ph.D thesis*, in School of Social Work. 2014, Indra Gandhi National Open University.

- [25] *World Vision, Yaya Gulele Area Development Programme, Ethiopia*. Available from: <https://www.worldvision.org.sg/en/about-us/global-presence/ethiopia-yaya-gulele> ( 29 June 2023, date last accessed).
- [26] Meng, S.S. *Annual report; Going Further Than We Can Imagine*. Available from: <https://www.worldvision.org.sg/en/about-us/global-presence/ethiopia-yaya-gulele> ( 29 June 2023, date last accessed).
- [27] *Ethiopia National Meteorology Agency (NMA) Weather Report-2023*. Available from: <http://www.ethiomet.gov.et/stations/information> (3 July 2023, date last accessed).
- [28] *Local Climate Estimator (New\_LocClim): Land, Water, Food and Agriculture Organization of the United Nations* Available from: <https://www.fao.org/land-water/land/land-governance/land-resource-planning-toolbox/category/details/en/c/1032167/> (16 January 2023, date last accessed).
- [29] Kalogirou, A., *Solar Energy Engineering Processes and Systems*. 2nd ed., London: Elsevier Inc, 2014.
- [30] John A. Duffie, W.A.B., Nathan Blair, *Solar Engineering of Thermal Processes, Photovoltaics and Wind*. 5th ed., New Jersey, USA: John Wiley & Sons Inc, 2020.
- [31] Bekele, E.A. and V.R. Ancha, *Transient performance prediction of solar dish concentrator integrated with stirling and TEG for small scale irrigation system: A case of Ethiopia*. Heliyon, 2022. **8**(9).
- [32] Hasan, K., et al., *Effects of different environmental and operational factors on the PV performance: A comprehensive review*. Energy Science & Engineering, 2021. **10**(2): p. 656-675.
- [33] Aslam, A., et al., *Advances in Solar PV Systems; A Comprehensive Review of PV Performance, Influencing Factors, and Mitigation Techniques*. Energies, 2022. **15**(20).
- [34] Neumeister, K. *Top 5 Best Cheap Solar Panels in 2023 -Affordable Solar System Guide*. Available from: <https://www.ecowatch.com/solar/cheap-solar-panels> (17 March 2023, date last accessed).

# Integrated emergency response and telehealth systems for enhanced crisis management- A cross-sectorial approach

Ayesha Amjad<sup>1</sup>, Katarzyna.Markowska<sup>2</sup>

*Faculty of Transport and Aviation Engineering, The Silesian University of Technology, Krasińskiego 8 Street, 40-019 Katowice, Poland, Corresponding email: ayesha.amjad@polsl.pl*

---

## Abstract:

We evaluated the effectiveness of telehealth in enhancing the decision-making processes of medical coordinators involved in aeromedical retrievals at the Jinnah Hospital in Lahore. The study primarily focused on aspects such as timing, destination, mode of transport, and escort level. Medical coordinators stationed at the Northern Operations site of the emergency retrieval service in Lahore were surveyed to gather insights into the impact of telehealth on their decision-making processes. The survey covered six key areas: diagnosis, severity of the medical condition, priority of transfer, crew considerations, mode of transport, and destination selection.

Over a 6-month period, the Jinnah Hospital received 603 emergency referrals from various sites. Among these, 200 patient referrals were eligible for analysis, with 300 not undergoing teleconsultations. The most common reasons for the lack of teleconsultations were the medical coordinator being occupied with other tasks or forgetting to follow the new procedure (39 cases, 43%) and the remaining does not have the knowledge about teleconsultation. The remaining 46 patients underwent teleconsultations during the trial, and data from 100 consultations were available for analysis.

In 100 cases, some aspect of the decision-making process was influenced by the use of telehealth, with significant alterations observed in nine cases. The most common changes were related to the severity of the patient's condition, followed by modifications in diagnosis and the priority of transfer. Telehealth was perceived as beneficial in confirming the original decision in 30 cases. However, in seven cases, telehealth did not provide assistance in the decision-making process.

---

## 1. Introduction:

Ambulance retrieval stands as a vital component within the emergency health system, particularly crucial for providing timely access to definitive care for patients residing in the extensive and diverse urban landscape of Lahore. The city, with its varied neighborhoods and population, emphasizes the necessity of a robust ambulance retrieval system to ensure that patients are transported to hospitals equipped with resources tailored to their specific healthcare requirements [1]. Lahore, situated in the northeastern part of the Punjab province in Pakistan, serves as the capital and the most populous city. Ranking as the second-largest city in Pakistan, following Karachi, and holding the 26th position globally, Lahore boasts a population exceeding 13 million. Positioned along the banks of the River Ravi, it stands as a significant urban center in the region [2]

In Lahore, a sprawling city with dynamic healthcare needs, the significance of ambulance retrieval is underscored by the need for patients to receive the appropriate level of care during transport. The healthcare landscape of Lahore demands a well-coordinated and clinically supervised approach to ambulance retrieval to ensure the safe and efficient utilization of transport and clinical retrieval services.

Clinical coordination, a pivotal aspect of ambulance retrieval, entails direct supervision by medical specialists during the transport or retrieval of at-risk patients. This oversight guarantees the availability of high-level clinical advice throughout the transportation process, optimizes the use of transport and retrieval services, and directs

patients to the most suitable receiving facility in a timely manner. In Lahore, where healthcare resources are spread across a wide geographical area, effective clinical coordination becomes paramount in delivering optimal care to patients in transit [3].

The collaboration between Jinnah Hospital in Lahore and the Edhi ambulance service exemplifies a synergistic partnership in the realm of emergency medical services. Serving as a pivotal healthcare institution, Jinnah Hospital engages with the Edhi ambulance service to enhance the efficiency of emergency response and patient transfers. Medical professionals at Jinnah Hospital act as key contacts for referring cases to the Edhi Ambulance service, which specializes in swift and effective ambulance services. In this collaborative effort, patients in need of urgent medical attention are seamlessly transferred, and upon referral, a medical coordinator from the hospital evaluates the patients' condition, assigns a working diagnosis, and determines the most suitable mode of transport. This partnership not only ensures a prompt and coordinated response but also reflects a commitment to providing optimal emergency medical care to the diverse population served by Jinnah Hospital and Edhi ambulance in Lahore [4]. Both Jinnah Hospital in Lahore and the Edhi Ambulance service leverage advanced telecommunications for clinical coordination and patient transfers in the region. Telehealth plays a crucial role in this collaborative effort, aiding in the acute resuscitation of critically ill patients referred to the service. This technology facilitates real-time support and guidance for healthcare practitioners in remote areas until the arrival of the retrieval team. In the Lahore region, numerous sites, including 34 in the Northern Operations area, are equipped with telehealth connections to ensure seamless communication with Jinnah Hospital [5]. The primary objective of our study was to evaluate the effectiveness of telehealth in supporting decision-making processes for emergency medical coordinators, with a specific emphasis on determining its impact on timing, destination selection, mode of transport, and escort level.

## 2. Methodology:

The study encompassed five selected sites within the Lahore Health Service District: Lahore, areas: Kareem Market, Faisal Town, Mustafa Town, Barkat Market, Naseer Abad east. The examination focused on analysing the decisions made by the Retrieval Services Jinnah Hospital (RSJH) medical coordinator to ascertain the impact of telehealth on transport emergency, mode of transport (road, helicopter), escort level (doctor, paramedic, nurse), and the designated destination hospital for referred patients.

Eligible participants for the study were adult patients with transport priorities categorized as immediate (0–1 hour), semi-immediate (1–3 hours), or urgent (3–6 hours). These patients either met the early notification guidelines for trauma inter-facility transfer or were at the discretion of the medical coordinator. The study was exclusively conducted during periods of on-site staffing at the emergency centre, specifically from 06:00 to 22:30 on Mondays to Fridays, and 06:00 to 20:30 on Saturdays and Sundays.

Data collection spanned a 6-month period starting from January, 2022. A structured survey, administered over telehealth, gathered information across six key areas: diagnosis, severity, priority, crew, mode of transport, and destination. The survey employed a binary response question to determine the influence of telehealth on transport tasking, followed by a modified Likert scale to quantify this impact. The Likert scale excluded a neutral option, ensuring responses either indicated a positive contribution or no effect.

Information was collected from RSJH medical coordinators following teleconsultations, and the records identified cases where a telehealth consultation did not occur. Written consent was obtained from coordinators at the outset, acknowledging the routine use of telehealth as part of their duties. Ethics approval was secured, with individual patient consent sought, when possible, for the utilization of telehealth in the clinical coordination process.

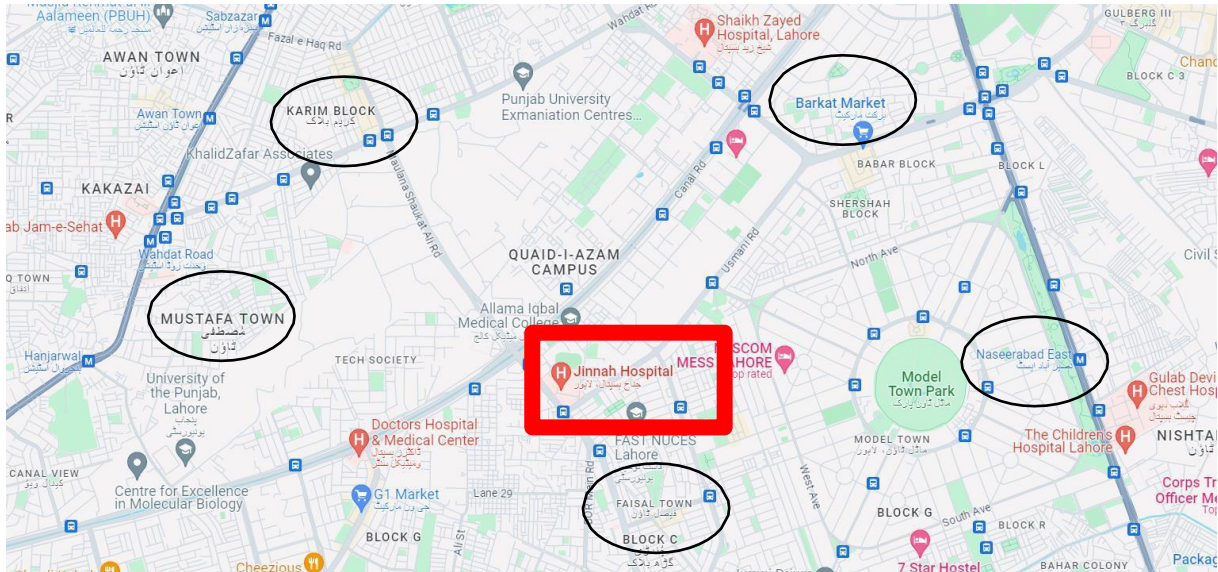


Fig. 1.

### 3. Results and Discussion:

In this study involving 604 patients, a total of 604 referrals were received. It is estimated that 398 patients did not meet the study criteria, leaving 206 eligible patient referrals for analysis. Among those eligible, reasons for not having teleconsultations were identified. Approximately 64 patients were excluded because the medical coordinator was too busy, 36 patients due to the new procedure being forgotten, and 59 patients with unspecified reasons. Consequently, 47 patients had teleconsultations during the trial, with 44 data sheets available for subsequent analysis. The common diagnoses for telehealth usage mirrored those observed in the original summary, including cases related to trauma, sepsis or infection, ischaemic heart disease, suspected subarachnoid haemorrhage, and acute shortness of breath due to fog.

Changes in patient transfer priority and destination were simulated, with a similar percentage of cases exhibiting alterations. The decision-making process was examined, indicating that in 21 cases, some aspect was influenced by the use of telehealth. Of these, telehealth significantly altered decisions in nine cases, particularly regarding the severity of patient condition, diagnosis, and priority of transfer. In 30 cases, telehealth was considered beneficial in confirming the original decision, and significant assistance was provided in 12 cases.

Furthermore, a simulation suggested that 48% of cases reported changes to patient care as a result of teleconsultation. These changes included further clinical assessment, medication or procedural advice, and recommendations for additional investigations.

By applying a chi-square test to the data. A chi-square test can be used to assess the independence between categorical variables. In this case, we can use it to examine whether the reasons for not having teleconsultations are independent of the type of diagnosis. Let's assume you have the following contingency table:

Tab. 1.

	Busy Coordinator	Forgotten Procedure	Unspecified Reasons	Total
Had Teleconsultation	20	25	X	45X
No Teleconsultation	15	30	X	45X
Total	45	45	x	90X

The null hypothesis (H0) is that the reasons for not having teleconsultations are independent of the type of diagnosis.

The chi-square test statistic is calculated as [6]:

$$X^2 = \sum \frac{(O_{ij} - E_{ij})^2}{E_{ij}}$$

Where:

- $O_{ij}$  is the observed frequency in each cell of the table.
- $E_{ij}$  is the expected frequency in each cell of the table, calculated as  $\frac{\text{row total} \times \text{column total}}{\text{grand total}}$ .

Fig. 2.

The degrees of freedom for a chi-square test in this context are given by

$$=(\text{Number of Rows}-1) \times (\text{Number of Columns}-1)$$

You would then compare the computed chi-square test statistic with a critical value from the chi-square distribution table to determine if the result is statistically significant.

In the current investigation, telehealth was utilized across a broad spectrum of referrals to the RSJH, intending to enhance both patient care and the safety of emergency transportation. This approach offers numerous potential advantages, encompassing improved appropriateness of transport, enhanced care during transportation, and early identification of the most suitable destination. The emphasis is particularly on positively impacting patient outcomes and optimizing the efficiency in the utilization of valuable resources. Additionally, the integration of telehealth may contribute to a reduction in secondary transports, instances where patients are initially relocated to inappropriate medical centres. This reduction is achieved by augmenting the information accessible to the medical team, thereby enhancing decision-making processes and overall patient care.

Table 1. presents responses to the query on whether the use of telehealth influenced decision-making. Out of the total 22 surveys, 19 respondents indicated that telehealth had an impact, while 3 respondents reported no influence. The breakdown of responses is detailed in the table below:

Table 2. responses to the question did the use of telehealth alter your decisions? Yes – 19 (see table below for detail provided by all 19); No – 3 (detail in table provided by 03); Total surveys – 22 (detail provided in table by 16)

Tab.2.

Number	Significantly variation	Light variation	No Variation	Surely No Variation
Treatment	10	8	11	13
Emergency	5	15	11	02
High Priority	3	4	18	12
Staff	2	4	19	12
Platform	6	8	8	15
Local Destination	5	9	13	10



Table 3. Responses to the question if your decisions were not altered, did telehealth assist you to confirm your original choices? Yes – 3 (see table below for detail provided by 13); no 7 (detail in table provided by 5); total responses – 22.

Tab. 3.

Number	Significantly variation	Light variation	No Variation	Surely No Variation
Treatment	11	7	13	10
Emergency	11	5	14	5
High Priority	18	14	11	3
Staff	19	14	10	2
Platform	8	7	5	6
Local Destination	13	9	15	5

The involvement of a medical coordinator during the referral process is particularly crucial, especially for the families of patients who often travel separately. This approach enables them to embark on the journey directly to the correct destination, thus avoiding the added costs and inconveniences associated with secondary transfers.

The findings from the study suggest that the application of telehealth in a broader scope of patient referrals to RSJH yields benefits, either by influencing the decisions of medical coordinators or by validating pre-existing decisions. Telehealth proves most valuable in decisions related to diagnosis, severity, and priority, both for altering and confirming decisions. Conversely, its impact is least pronounced in decisions regarding, mode of transport, or destination. Despite a demand for its utilization, the telehealth service was underutilized. To unlock its full potential and extend the service to more sites across the state, increased support for telehealth use is deemed necessary. This may entail additional medical coordinators during peak periods and improved integration of telehealth technology into standard communication systems, given that the current telehealth equipment is situated in separate rooms.

#### 4. Conclusion:

The present study posits that the utility of the telehealth process may have been underestimated. All medical coordinators, possessing extensive experience as emergency physicians and, in many cases, as doctors, may have limited potential for telehealth to significantly impact their decisions. The benefits of telehealth may potentially be more pronounced for less-experienced staff or those new to the coordination process. Furthermore, the study underscores the significance of knowledge and trust in local staff at referral centres, emphasizing their capabilities and available resources built over many years of collaboration to facilitate patient movement to higher levels of care.

#### Acknowledgement:

The author acknowledges the support provided by Jinnah Hospital staff during investigation.

#### References:

- [1] Sterud, T., Ekeberg, Ø., & Hem, E. (2006). Health status in the ambulance services: a systematic review. *BMC health services research*, 6, 1-10.
- [2] Hussain, J. S., & Naz, A. A. (2015). Public Perception towards Punjab Emergency Service Rescue 1122 in Lahore. *Pakistan Vision*, 16(2), 164.
- [3] Rehman, F. A. R. A. H., Janjua, A. R., & Shahzad, H. U. M. E. R. A. (2015). Client Satisfaction Regarding Family Planning Services in Reproductive Center at Jinnah Hospital, Lahore. *Pak J Med Health Sci*, 9(3), 1048-50.

- [4] Zia, N., Shahzad, H., Baqir, S. M., Shaukat, S., Ahmad, H., Robinson, C., ... & Razzak, J. A. (2015). Ambulance use in Pakistan: an analysis of surveillance data from emergency departments in Pakistan. *BMC emergency medicine*, 15, 1-6.
- [5] Kamran, T. (2020). 7 Abul Sattar Edhi. *The Dynamics of Conflict and Peace in Contemporary South Asia: The State, Democracy and Social Movements*.
- [6] Franke, T. M., Ho, T., & Christie, C. A. (2012). The chi-square test: Often used and more often misinterpreted. *American journal of evaluation*, 33(3), 448-458.

# Numerical Model of Solar Pond in Simulink Environment to Use Pond as Energy Storage

Magdalena Borowska<sup>1</sup>, Jakub Szykowski<sup>1</sup>, Grzegorz Wiciak<sup>2</sup>, Leszek Remiorz<sup>2</sup>, Kamila Szykowska<sup>2</sup>, Katarzyna Janusz-Szymańska<sup>2</sup>

<sup>1</sup>Silesian University of Technology

<sup>2</sup>Department of Power Engineering and Turbomachinery, Silesian University of Technology, e-mail: grzegorz.wiciak@polsl.pl, leszek.remiorz@polsl.pl, kamila.szykowska@polsl.pl, katarzyna.janusz-szymanska@polsl.pl

---

## Abstract

The paper presents a model of a solar pond developed in the Matlab® Simulink® environment and its evolution from a basic to an advanced version. In addition, the necessary environmental, technical, ecological, and social aspects for the utilization and revitalization of brownfield sites for use as solar energy storage facilities using available post-mining brines are discussed. Post-mining waters containing various types of brine in large quantities are an environmentally hazardous waste, which can be a cheap and readily available carrier of brine waters for use in energy storage, which we can treat as a renewable energy source in this view. The data compiled were obtained through research conducted with a group of students as part of the PBL project.

**Keywords:** solar pond, numerical model, matlab

---

## 1. Introduction

Solar ponds are low-temperature heat reservoirs that use stratified brine, e.g. NaCl, MgCl<sub>2</sub> and clean water for energy storage. They are used in a variety of industrial installations, in seawater desalination processes as bottom sources for heat pumps and others. The history of this technology dates back to the beginning of the 20th century, when the literature reported unusual temperature phenomena observed in several naturally occurring lakes in Hungary. At the end of September, the water temperature at the surface of the lake is close to the ambient temperature, while already at a depth of about 1 meter it reaches 65°C. Measurements by Kalecsinsky [1], Rozsa [2] revealed a strong gradient in salt concentration as a function of depth. It has been suggested that the effective suppression of natural convection caused by the salinity gradient and the absorption of solar radiation in the brine is responsible for the high temperatures that persist below the water table. This was confirmed by later studies [1-10].

The first artificial solar ponds were built in Israel in 1958. Near the Dead Sea, shallow reservoirs used to evaporate brine water (salinas) were converted into solar ponds. These solutions had no characteristic convective layer, and the salt density gradient ran through the entire depth of the pond. The best results were obtained with MgCl<sub>2</sub> as the salt, where a pond of 625 m<sup>2</sup> reached a maximum temperature of 96°C. The largest pond had a surface area of 1375 m<sup>2</sup> and was not a successful design, because as the temperature increased, to about 74°C, bacterial decomposition gases in the soil below the pond floated up making it impossible to maintain the necessary salinity gradient [1].

Current studies of this technology are being conducted for climatic zones similar to Polish conditions, including in the UK.

### 1.1 Principle

There are many types of solar collectors for extracting thermal energy from solar radiation. A solar pond is also a type of solar collector, combining the function of simultaneously extracting and accumulating thermal energy. A typical solar pond is divided into three conventional layers, as shown in Fig.1 [4,10,11]. The upper zone is called the convection layer and is formed by pure water whose salinity is close to 0%. This zone is stabilized by introducing fresh water at the height of the pond surface and providing cover from excessive wind. The temperature in this zone is close to the ambient temperature. The second is the non-convective or gradient zone. It is responsible for keeping the solar pond warm. If the salinity gradient is large enough, convection in this layer is suppressed despite the absorption of heat and temperature rise at the bottom of the pond. In order for the layer to work properly and convection to be suppressed, the condition must be met that the change in density due to the change in water temperature is less than the change in density due to the salinity gradient. Solar radiation also reaches the lowest layer, is absorbed there and can only be lost by conduction to the ground or a higher layer. Due to the low thermal conductivity of water, the non-convective zone acts as an insulator and prevents conduction toward higher layers. The last layer is the lower convective zone, which accumulates heat Energy. This layer is characterized by an almost constant level of salinity density, which is high enough to keep the accumulated heat at the bottom of the pond while avoiding the process of convection to the upper layers of the pond. Salinity in the lower layer varies from 20% to 30%. The achieved temperature in the accumulation zone generally oscillates between 50°C and 90°C. The thermal efficiency of a pond depends on various factors, such as the stability of the salinity gradient layer, water clarity, insulation of the pond relative to the ground and others. However, the key parameter for maintaining high solar pond efficiency is maintaining the correct salinity gradient profile [4-11].

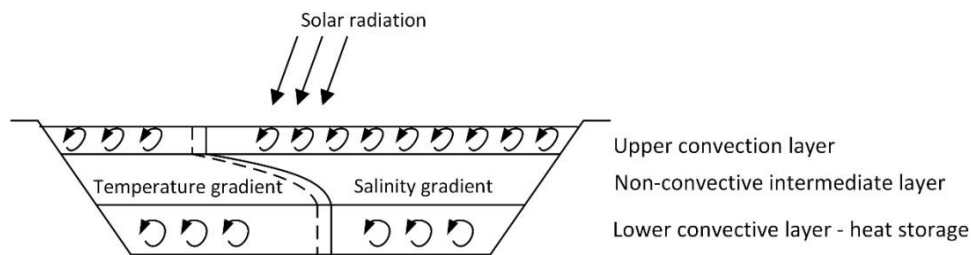


Fig. 1. Schematic of the solar pond with temperature and salinity gradient marked

## 2. The energy system model

The following structure of an energy system integrating solar pond technology with hybrid photovoltaic cells was adopted for the study, where the thermal energy extracted from PV panels is stored in the storage layer of the pond. A block diagram of the solution is shown in Figure 2. The model incorporates averaged insolation data for areas in southern Poland. The pond model consists of three main phases. The upper layer, called the convective layer, absorbs solar radiation reaching the surface of the pond. The water in the upper layer has a temperature close to the ambient temperature, and the salinity is close to zero. Heat loss to the environment is also considered here, including through the process of water evaporation and heat exchange with the environment - air and ground. The intermediate layer is further divided into 5 areas with linearly varying salinity concentrations. The second layer is called the non-convective layer or gradient layer. It ensures the maintenance of thermal energy in the pond. Due to the appropriate salinity gradient, convection between the layers of this the zone is suppressed. Solar radiation also reaches this layer, but the upper and lower layers of the solar pond also interact. The last layer stores thermal energy. This is the convective zone. It is characterized by an almost constant level of salinity density, which is high enough to keep the stored heat at the bottom of the pond while avoiding the process of convection to the higher layers of the pond. The salinity in the lower convection zone is high between 20% and 30%, and the temperature generally varies between 50°C and 90°C. In addition, each of these zones of the solar pond is affected by the ground, or more precisely, by the temperature and conduction coefficient, which vary depending on the ambient parameters, as shown in the block diagram in Figure 2. A combination of the solar pond system and the heat discharge of the photovoltaic system was also modeled, where the heat obtained in the PV system can be

introduced into both the intermediate layer and the lower storage layer, depending on the thermal parameters obtained from the PV panels. The Matlab® - Simscape® environment was used as the computational platform.

### 2.1 Solar pond model in Matlab simulink® environment

The basic model consists of an ambient model, then models of three layers with varying degrees of salinity and different locations (farther or closer to the sun), and scope© blocks displaying the time dependence of temperature and power of each model component. Which is shown in Figure 3, Figure 4 and Figure 5. In the ambient model, the ambient and ground temperatures were assumed to be constant, i.e., the pond has no effect on their temperatures. In this model, the heat source - the sun - was modeled as the positive part of a sinusoidal function. And the block labeled "Measurement" is used to measure the temperature and heat flow of the energy provided by the sun. These are passed to the part of the model that displays all the output data..

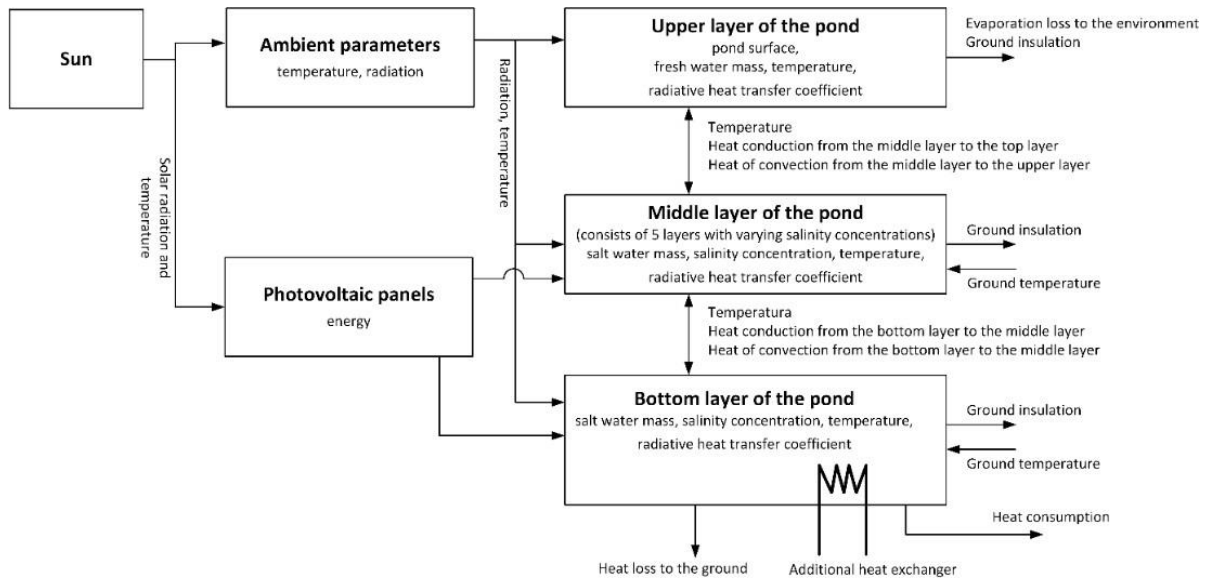


Fig. 2. Block diagram of the adopted energy structure using a solar pond

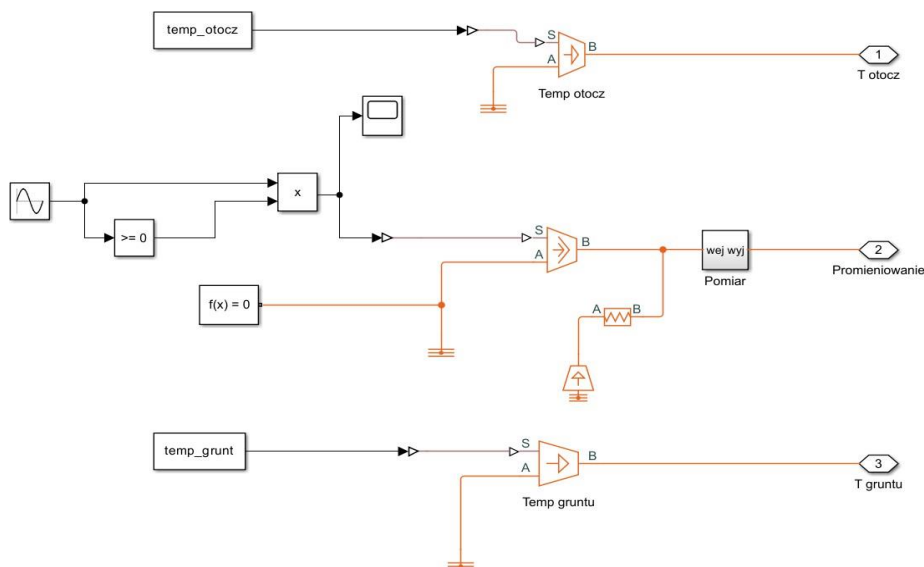


Fig. 3. Schematic of the environment model

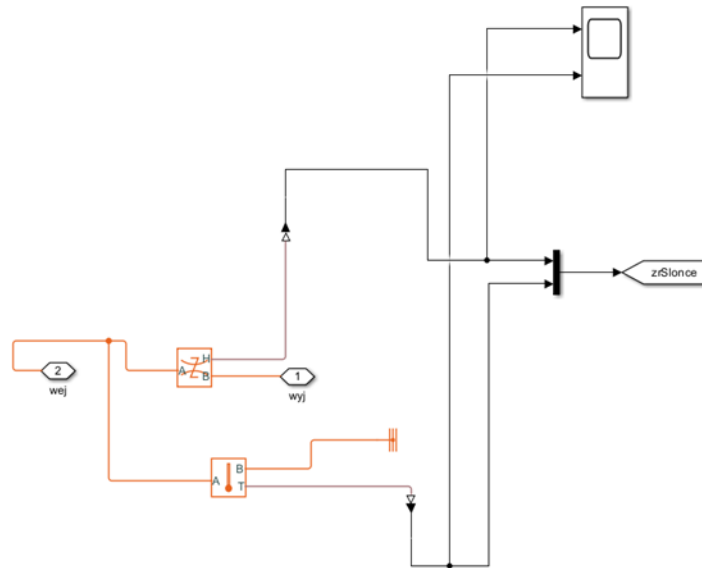


Fig. 4. "Measurement" block

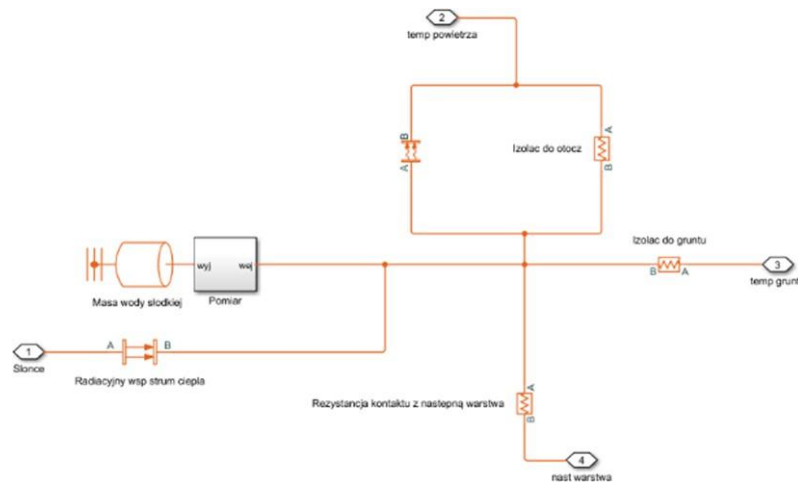


Fig. 5. Schematic of the construction of the top layer in the SIMULINK® environment

Next, layer models are presented, starting with the top layer, which is the least saline surface layer. This is the layer closest to the water surface and is affected by a number of factors, such as:

- air temperature,
- ground temperature,
- temperatures of the layer (water)
- and the sun itself.

The next layer is the intermediate layer, the so-called convection-free layer, in which, according to the model, a multiple number of measurements should take place, where the results of the measurements will be influenced by both the parameters obtained from the previous layer and the next. In operation it resembles a surface layer, however, there is limited influence of factors leaving only the sun, ground temperature and the influence of neighboring layers.

At the bottom of the pond will be the bottom layer, also known as the storage layer. The factors affecting this layer will be the sun, the layer above and the ground. This is the layer furthest from the surface and has the highest level

of salinity, it is needed to include the slope caused by its location, which will affect the results obtained during the measurement.

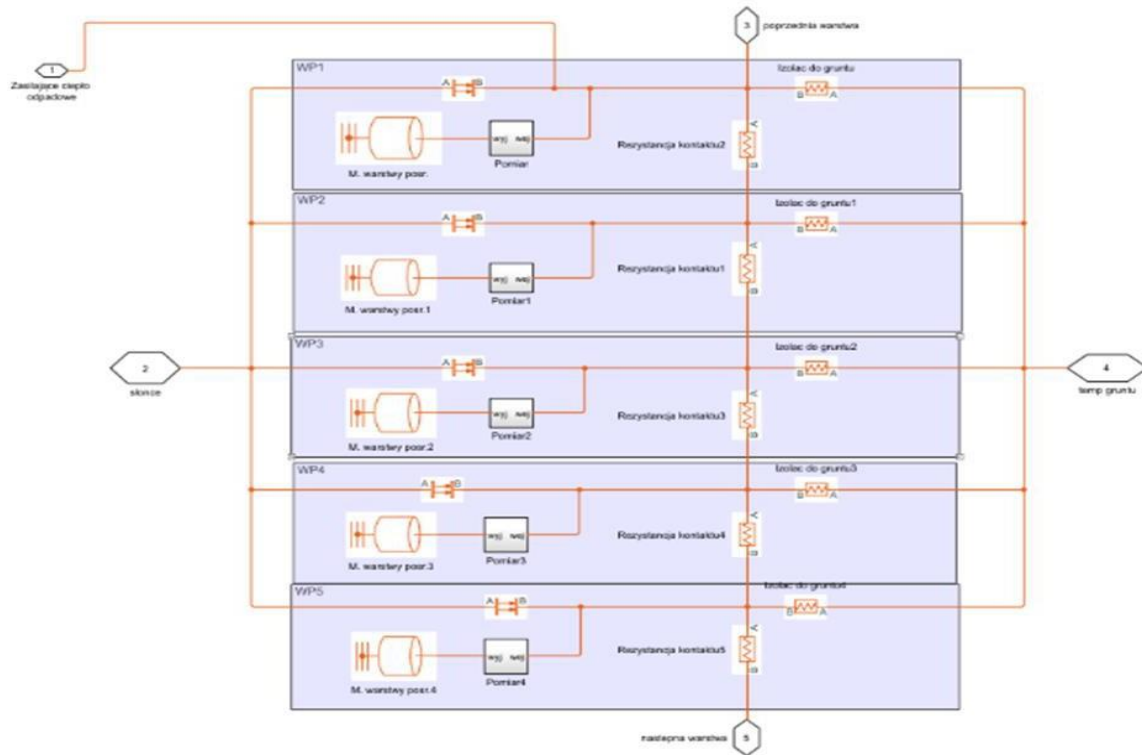


Fig. 6. Schematic of the intermediate layer construction in the SIMULINK® environment

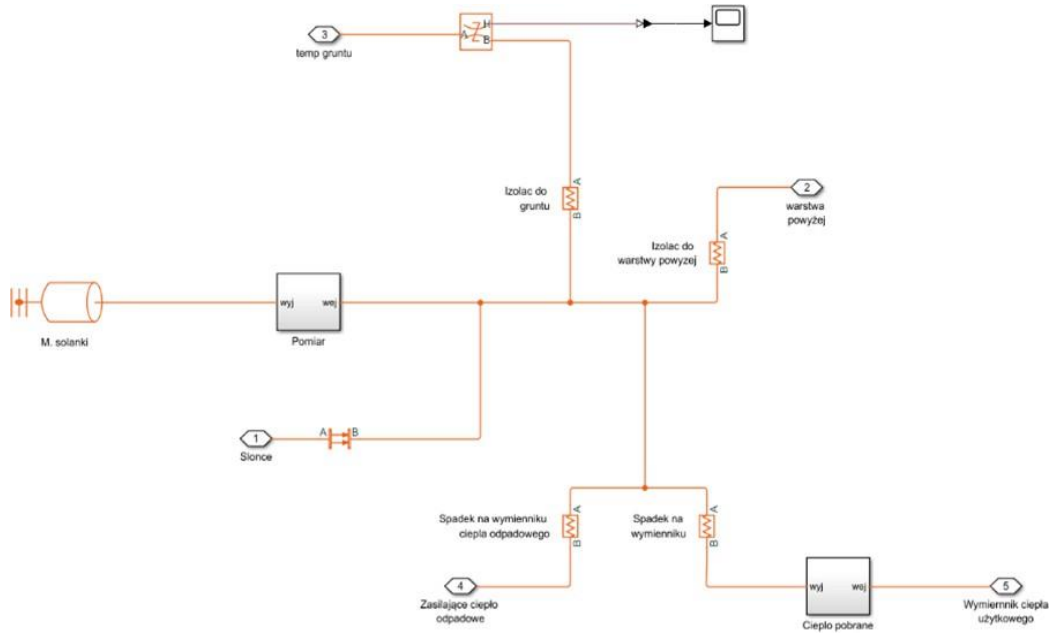


Fig. 7. Schematic of the bottom layer construction in the SIMULINK® environment

### 3. The model - preliminary results

Based on the temperatures obtained from the environment, especially the ground temperature, we are able to obtain a heat flow diagram for the lower layer - Fig. 8., 9. Preliminary results for the solar pond model suggest that in our climate, the occurrence of large temperature oscillations (both daily and throughout the year) is generally unfavorable, but nevertheless the temperature of the storage layer can rise to about 70°C. It is then possible to store more than 2,000 W of heat in a solar pond with an area equal to 9 m<sup>2</sup> and the assumptions made. In the case of using the pond as a heat accumulator for storing waste energy from other installations, paradoxically, lowering the temperature in winter improves the conditions for receiving waste heat, due to the increased available temperature difference.

The results and characterizations presented in the article are preliminary and require further research work to better understand the processes involved.

The presented energy structure of integrating a solar pond with a PV plant and an additional heat exchanger seems interesting for systems with larger capacities due to solar ponds, which are economically justified in the larger issue.

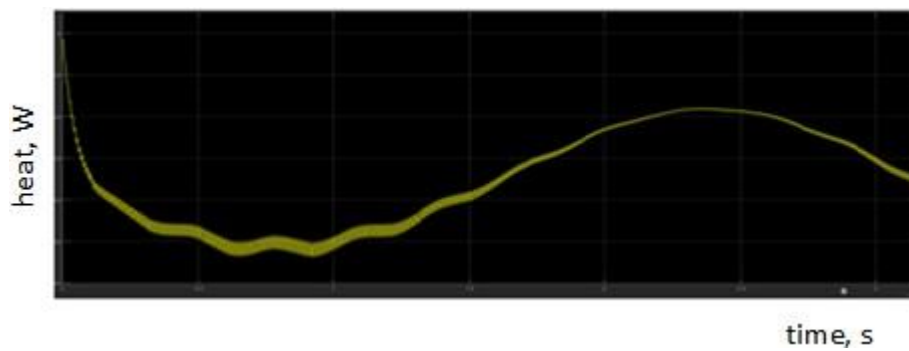


Fig. 8. Heat flow characteristics for the bottom layer over time

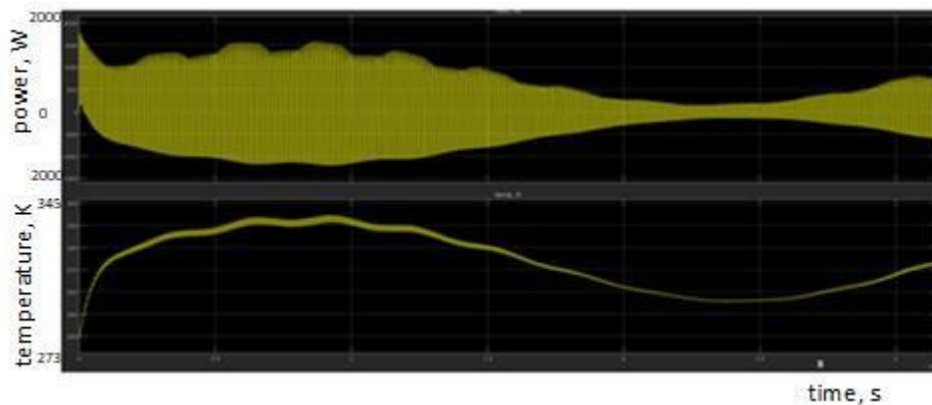


Fig. 9. Characteristics of power and temperature produced by the bottom layer

### 4. Summary and conclusions

- Solar pond technology has high application potential. A one-hectare pond is capable of converting 0.1 GWh/day of thermal and electrical energy (solar pond located in Israel).
- Use of thermal energy from the solar pond: heating or cooling of buildings; heating of domestic hot water; heating of industrial hot water; generation of electricity through the Rankine cycle.



- The project has not yet been fully implemented; it is continuing. Expansion of the model is planned. The advanced model represents a more expanded basic model, to which additional elements have been introduced to reflect the measurement results that would be obtained in a real environment. Elements have been added to represent the environment in which the measurements will be taken and the use of PV panels. A year-round test run was included, along with the change of seasons and the light source model.
- Negative values have been included in the power graph. They may appear if the brine temperature reaches a lower value than the initial reference temperature, since the power depends directly proportional to the temperature difference (between the current brine temperature and the reference temperature). The phenomenon of negative power can occur on very cold nights if the tank is not sufficiently insulated or if any of the salinity levels are incorrect, which also has the effect of reducing the insulation of the brine from the environment. This will be a negative indication that the model or salinity needs to be improved.
- Integrating the specifics of solar pond technology with the process of mine brine disposal seems not only possible, but also profitable and useful. Such a combination can address a number of challenges facing modern man. Moreover, the solution in question does not seem to generate any serious negative consequences. It is worth mentioning that the average increase in groundwater temperature as a function of depth is about 25 °C/1000 m [7], which also has a positive effect on the whole configuration.
- The thermal energy accumulated in a solar pond can be used for various purposes, but an important principle in designing a solar pond is to consider the specific use. Regardless of the purpose, a solar pond will absorb and store solar radiant energy in the form of low-grade thermal energy.

### References

- [1] A. V. Kalecsinsky "Ueber die ungarischen warmen und heissen Kochsalzseen als natuerlich Waermeaccumulatoren", Ann. Physik vol. IV, pp. 408, 1902.
- [2] M. Rozsa, Physik. Zeitachr. vol.1, pp. 108, 1915.
- [3] J. R. Hull "Physics of the solar pond". Retrospective Theses and Dissertations, 1979
- [4] Faqehaa, H., Bawahaba, M., Veta, Q. L., Faghihd, A., Datea, A. I Akbarzadah, A.: An experimental study to establish a salt gradient solar pond (SGSP). 2nd International Conference on Energy and Power, (2018).
- [5] Abu-Eishah, S.: Economic Feasibiliy of Salinity-Gradient Solar Ponds (SGSP) for Production of Fresh Water and Pure Salt(s) from Saline and Hypersaline Waters. The 2011 Int. Conf. on Water, Energy and Environment, (2011).
- [6] Mitko, K. i Turek, M.: Membrane-Based Solutions for the Polish Coal Mining Industry (2021).
- [7] Chowaniec, J., Ciężkowski, W., Dowgiałło, J., Kucharski, M., Nowicki, Z., Rudzińska-Zapaśnik, T., Szczepański: A. Hydrogeologia regionalna Polski Tom II. Wody mineralne, lecznicze i termalne oraz kopalniane, (2007).
- [8] Kanan, S.: A Simple Heat and Mass Transfer Model for Salt Gradient Solar Ponds.
- [9] Bawahab M. H. Faqeha, Q. L. Ve, A. Faghih, A. Date, and A. Akbarzadah: Industrial Heating application of a Salinity gradient solar pond for salt production, Energy Procedia 160 (2019), pp. 231–238
- [10] Ines M. et al.: Experimental studies on the effect of using phase change material in a salinity-gradient solar pond under a solar simulator, Solar Energy 186 (2019), pp. 335-346
- [11] Beika A. J. G., Assarib M. R., Tabriz H. B: Transient modeling for the prediction of the temperature distribution with phase change material in a salt-gradient solar pond and comparison with experimental data. Journal of Energy Storage 26 (2019), 101011

# On MILD: The Future of Hydrogen Combustion

Endeshaw A. Bekele<sup>1\*</sup>, Andrzej Szlęć<sup>1</sup>, Sławomir Śladek<sup>1</sup>

<sup>1</sup>Department of Thermal Technology, Silesian University of Technology, Konarskiego 18A, 44-100, Gliwice, Poland

---

## Abstract

The shift from traditional fossil fuels to cleaner, renewable sources of energy in combustion systems is an imperative step towards addressing the challenges posed by climate change. Hydrogen fuel promotes clean energy pathways while mitigating greenhouse gas (GHG) emissions. This work presents an overview of hydrogen combustion in moderate or intense low-oxygen-diluted (MILD) conditions, its role in future combustion systems, and challenges due to its unique physical properties, reaction mechanism, and heat transfer mechanism. Additionally, the paper explores the features of MILD combustion and its potential applications, highlighting its potential for uniform temperature distribution, ultra-low emissions, high combustion efficiency, and flexible fuel consumption. Hydrogen combustion holds great promise to revolutionize conventional combustion systems, but its high flame temperature results in high NO<sub>x</sub> emission and intricate radiative heat transfer. Hydrogen MILD combustion offers promising as it can achieve uniform temperature distribution, ultra-low emissions, high combustion efficiency, and flexible fuel consumption.

**Keywords:** Hydrogen combustion, MILD, Clean combustion, Heat transfer

---

## 1. Introduction

Currently, addressing environmental concerns has become an urgent matter. The growing global demand for energy, driven by population growth, has sparked interest in finding clean energy solutions to minimize emissions and strive towards carbon neutrality [1]. Fluctuating fuel prices, increased energy consumption, and clear indications of climate change have led to the development of new technology that produces and stores clean energy. Hydrogen fuel holds great promise with the potential to revolutionize our energy system, offering versatility and widespread application in various sectors, as depicted in Figure 1. Hydrogen fuel has emerged as a promising and versatile option to decarbonize multiple sectors, such as industrial, transportation, power generation, and building [2–6]. Furthermore, it plays a pivotal role in addressing the climate crisis, stabilizing energy costs, ensuring energy reliability, and shaping global political dynamics as its projected to constitute of 5% of global energy mix by 2050 [2]. The demand for hydrogen is projected to increase eight times in 2050, with transportation accounting for 28.57%, industrial energy for 20.77%, and power generation for 11.68% of the total demand, as shown in Figure 2 [7]. Hydrogen has the potential to be the most significant fuel source in the future due to its availability and its ability to achieve high efficiency without causing any adverse effects on the environment [8].

---

<sup>1\*</sup> Corresponding author: [ebekele@polsl.pl](mailto:ebekele@polsl.pl)

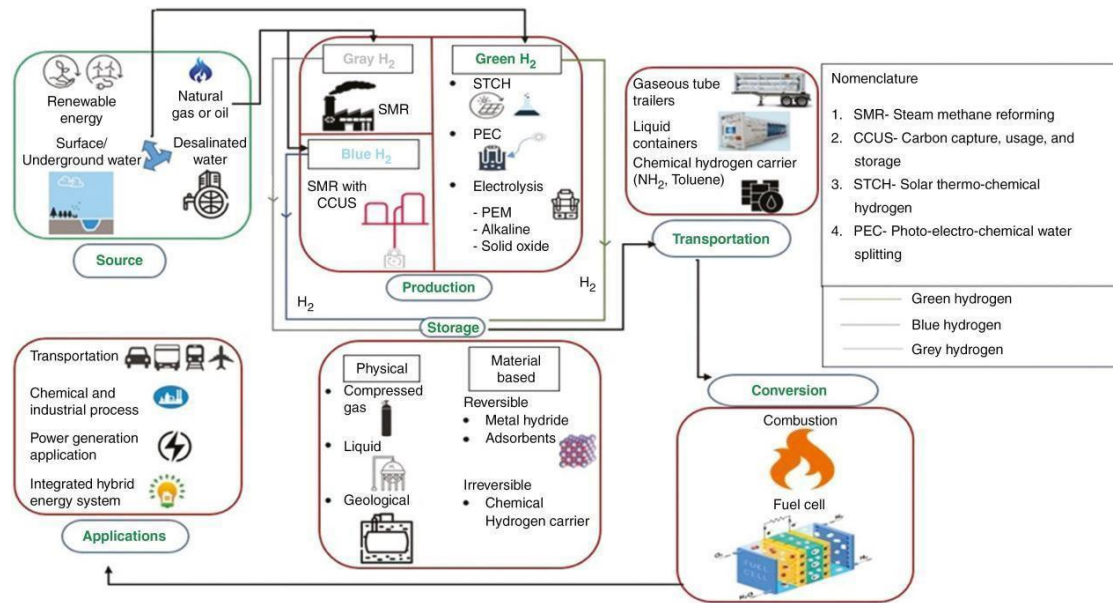


Fig. 1. Supply chain of hydrogen (Reprinted with permission from Ref.[9]. Copyright 2023, Oxford University Press)

## 2. Features of MILD Combustion

New combustion technologies have been further developed to improve combustion efficiency and emission reduction. MILD (Moderate or Intense Low Dilution) combustion is a promising combustion technology, as it can achieve high reactant temperatures and very low NO<sub>x</sub> emissions. In MILD combustion, small amounts of fuel are injected into the pre-mixture of air and recirculated exhaust gases at high temperatures, resulting in a low-oxygen and low-temperature environment, minimizing NO<sub>x</sub> emissions and maintaining high thermal efficiency [10]. Moreover, burning fuels in MILD combustion systems can also overcome the issues of combustion efficiency, fuel consumption, heat transfer problems, flame stability, and emissions [10].

In several studies, MILD combustion has been referred to as FLOX (Flameless Oxidation) [11,12], HITAC (High-Temperature Air Combustion) [13,14], HITOC (High-Temperature Oxidation Combustion) [15,16], and CDC (Colorless Distributed Combustion) [17–20]. Figure 2a provides a summary of their combustion regime. To achieve the MILD condition, certain conditions must be met, such as a higher pre-combustion temperature than the mixture's autoignition temperature [14]. In addition, the inlet temperature of the reactant mixture must be higher than its self-ignition temperature. However, it is essential to ensure that the maximum allowable temperature increase during combustion remains lower than the self-ignition temperature relative to the inlet temperature, as emphasized by [10]. MILD combustion is categorized into two types based on the recirculation ratio and oxygen mole fraction: unconditional and conditional [21]. Unconditional MILD combustion occurs when the recirculation ratio exceeds the critical recirculation ratio, and the oxygen mole fraction falls below the critical oxygen mole fraction.

On the contrary, conditional MILD combustion is characterized by a recirculation ratio below the critical recirculation ratio and an oxygen mole fraction exceeding the critical oxygen mole fraction [22]. The recirculation ratio measures the degree of dilution of the reactant by the flue gas. The MILD combustion regime occurs at a recirculation ratio of no less than 2.5 and a furnace temperature higher than 750 °C [23].

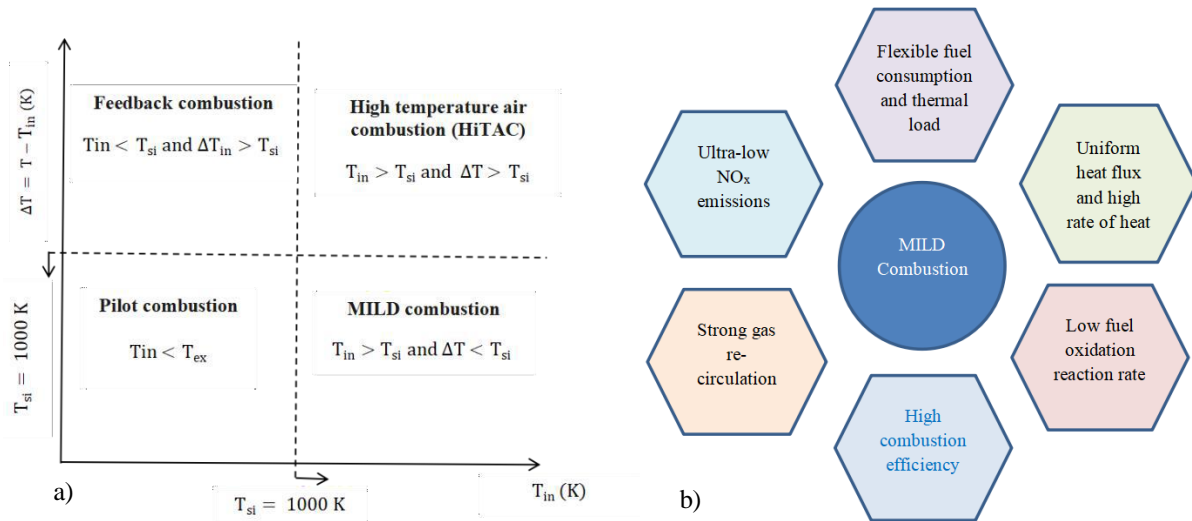


Fig. 2. a) Criteria of different types of combustion regimes ( $T_{si}$  is self-ignition temperature,  $T_{ex}$  is extinction temperature  $T_{in}$  is inlet temperature, and  $\Delta T$  is temperature increase at  $T_{in}$ ), b) Features of MILD combustion.

MILD combustion exhibits several distinct characteristics, as depicted in Figure 2b. It is characterized by strong gas recirculation [24] and uniform thermal heat flux [25,26], ensuring efficient and effective combustion [10]. The combustion process in MILD combustion occurs at a low fuel oxidation reaction rate, resulting in ultralow  $NO_x$  emissions and high combustion efficiency [10,27]. The broader reaction zone allows for more extensive combustion while the heat is homogeneously distributed, ensuring constant heat flux and facilitating high heat transfer rates [10,12,28]. Furthermore, MILD combustion demonstrates flexibility in fuel consumption and achieves high efficiency, enabling energy savings of up to 30% [14]. Moderate or Intense Low-oxygen Dilution combustion is a versatile technique with applications in various fields, as shown in Figure 3. MILD combustion offers various industrial applications, including high intensity combustion systems, heat utilization processes, thermal waste destruction, and power generation [28–31].

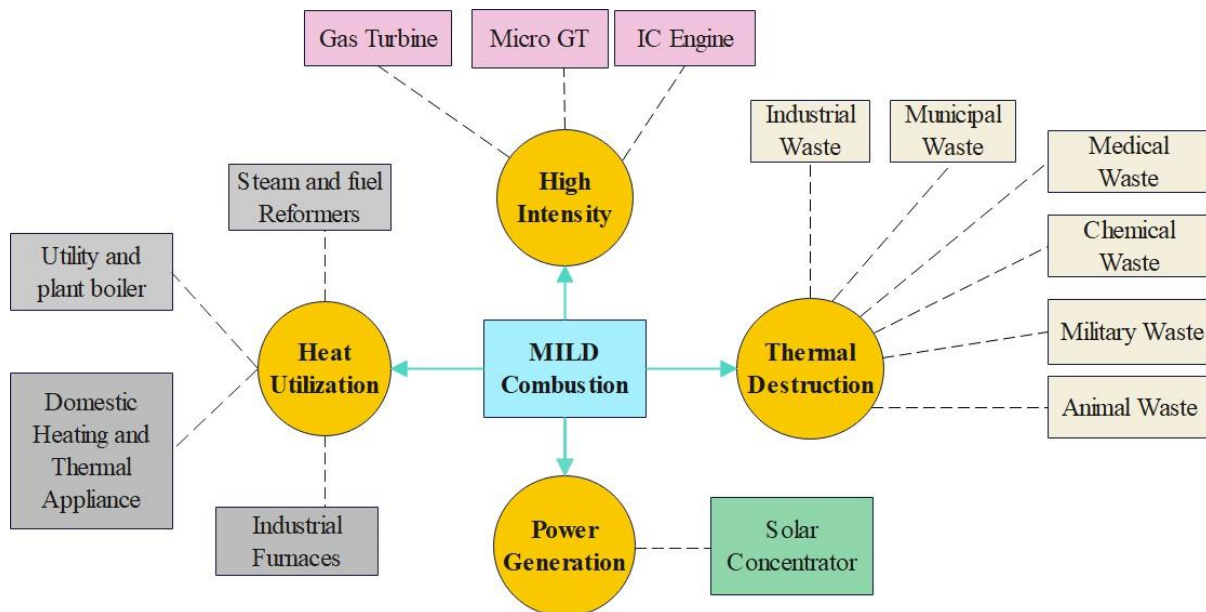


Fig. 3. Potential application of MILD combustion (Redrawn based on the data from Ref.[28–30])

### 3. Role of Hydrogen in Future Clean Combustion

Over recent decades, fossil fuels have played a pivotal role as the dominant energy source in combustion systems, driving economic progress and the industrial revolution. Unfortunately, our reliance on fossil fuels has significant environmental consequences that endanger our planet. Climate change is worsening, and 89% of CO<sub>2</sub> emissions are generated from combustion and industrial processes [32]. Transitioning from fossil fuels to clean energy in combustion systems is crucial to overcome climate impacts and energy demands. Hydrogen fuel is renowned for its thermophysical properties, making hydrogen combustion a promising solution to address environmental issues and achieve a greener future [33]. With zero carbon emissions and only water vapor as a by-product, hydrogen combustion offers a sustainable and efficient solution to various energy requirements. Hydrogen combustion is widely applied in internal combustion engines, gas turbines, industrial furnaces, marine engines, and cooking stoves, as illustrated in Figure 4.

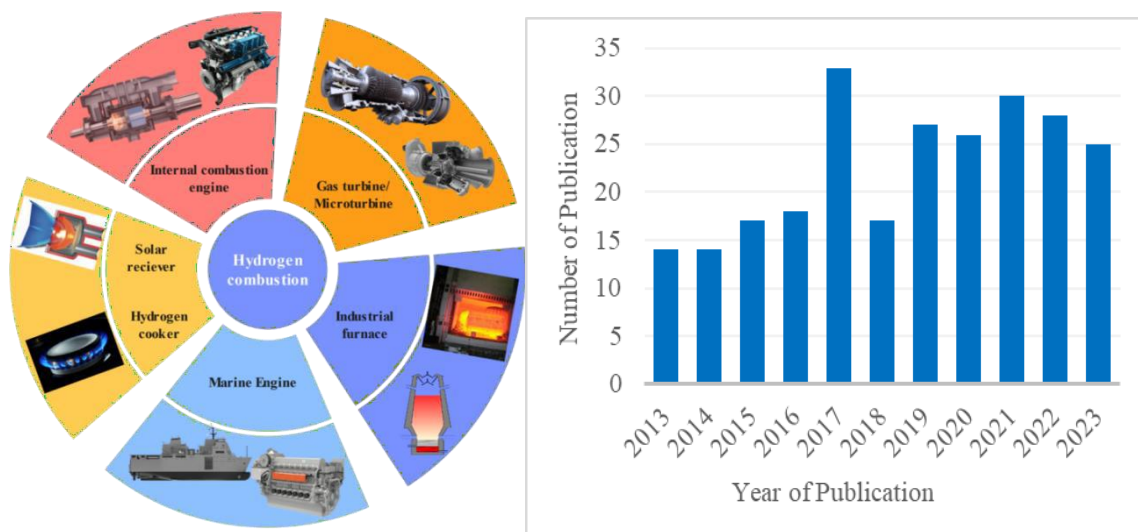


Fig. 4. An overview of hydrogen combustion in various applications and number of publications over the past decades (Keywords: "Hydrogen combustion chambers" OR "Hydrogen MILD combustion" OR "Hydrogen-air combustion" OR "Hydrogen-oxygen combustion" OR "Moderate and intense low-oxygen dilution.")

Hydrogen is characterized by its higher laminar burning velocity [34–36], higher molecular diffusion [37], lower activation energy [38], and higher autoignition temperature than common hydrocarbon fuels. Hydrogen has eight times more flame velocity than methane, three times the lower heating value (LHV) of gasoline, and six times the flammability range of methane, as summarized in Table (1). The flame speed measures how quickly a flame propagates through a reactant mixture, which is essential in determining the heat transfer rate in combustion chambers. In hydrogen combustion, due to the increase in flame propagation speed, a high rate of heat is released and more stable flame occurs in combustion chambers [39]. The flame temperature increases due to rapid combustion processes, which are also influenced by the specific heat of combustion and the stoichiometry of the combustion reaction. The energy required to ignite hydrogen is exceptionally very low (0.02MJ) and is about 1/14<sup>th</sup> of the energy needed to ignite methane [40].

Tab. 1. Physical properties of hydrogen and its comparison with common fuels used in combustion [41–43]

Property	Hydrogen (H <sub>2</sub> )	Methane (CH <sub>4</sub> )	Gasoline (C <sub>8</sub> H <sub>18</sub> )	Diesel (C <sub>12</sub> H <sub>23</sub> )	Ammonia (NH <sub>3</sub> )
Carbon content (mass%)	0	75	84	86	0
Lower heating value (MJ/kg)	120	45.8	44.8	42.5	18.6
Density <sup>a,b</sup> (kg/m <sup>3</sup> )	0.089	0.72	730-780	830	0.769
Molecular weight (gmol <sup>-1</sup> )	2.016	16.043	~110	170	17.031
Boiling point <sup>a</sup> (K)	20	111	298–488	453-633	240
Auto-ignition temperature (K)	844	723	573	503	924
Minimum ignition energy in air <sup>a,d</sup> (mJ)	0.02	0.29	0.24	0.24	8
Stoichiometric air/fuel mass ratio	34.5	17.2	14.7	14.5	6.1
Stoichiometric volume fraction in air (%)	29.53	9.48	~2	-	21.8
Quenching distance <sup>a,c,d</sup> (mm)	0.64	2.1	~2	-	7
Laminar flame speed in air <sup>a,c,d</sup> (m/s)	1.85	0.38	0.37–0.43	0.37-0.43	0.07
Flammability limits in air (vol%)	4–75	5.3-15	1-7.6	0.6-5.5	15-28
Adiabatic flame temperature <sup>a,c,d</sup> (K)	2480	2214	2580	2300	2090

<sup>a</sup> at 1 bar, <sup>b</sup> at 273 K, <sup>c</sup> at 298 K, <sup>d</sup> at stoichiometry

### 3.1. Challenges and Opportunities of Hydrogen Combustion

An attempt has been made to replace hydrocarbon fuels in combustion technology with pure hydrogen fuels, but challenges remain due to their physical properties [40,44]. With its wider ranges of flammability, high flame speed, high flame temperature, and low ignition energy, hydrogen combustion is prone to combustion instability, NO<sub>x</sub> formation, and flashback incidents, leading to increased concerns about environmental and safety aspects [42,45,46]. The hydrogen flame can be sustained in a low flammability range (4% by volume in air), leading to efficient combustion and high heat release rates. However, the wide flammability range of hydrogen (75% by volume in air) increases the flame propagation speed and poses challenges to flashback in combustion systems. The high reactivity and fast flame speed of hydrogen affect the shape of the flame and the stabilization mode, with direct consequences on peak temperature, combustion efficiency, and pollutant emissions [25,47–50]. A higher adiabatic flame temperature leads to overheating combustion systems and increases the formation of NO<sub>x</sub> (thermal and prompt NO<sub>x</sub>) in combustion chambers [51]. Lean combustion and partially premixed combustion have been found to be effective in reducing NO<sub>x</sub> emissions. Dilution of H<sub>2</sub>O in combustion systems. However, hydrogen flames in the lean combustion process exhibit intrinsic flame instabilities and flashback, which significantly affect the heat transfer rate, flame dynamics, and shapes [33,52].

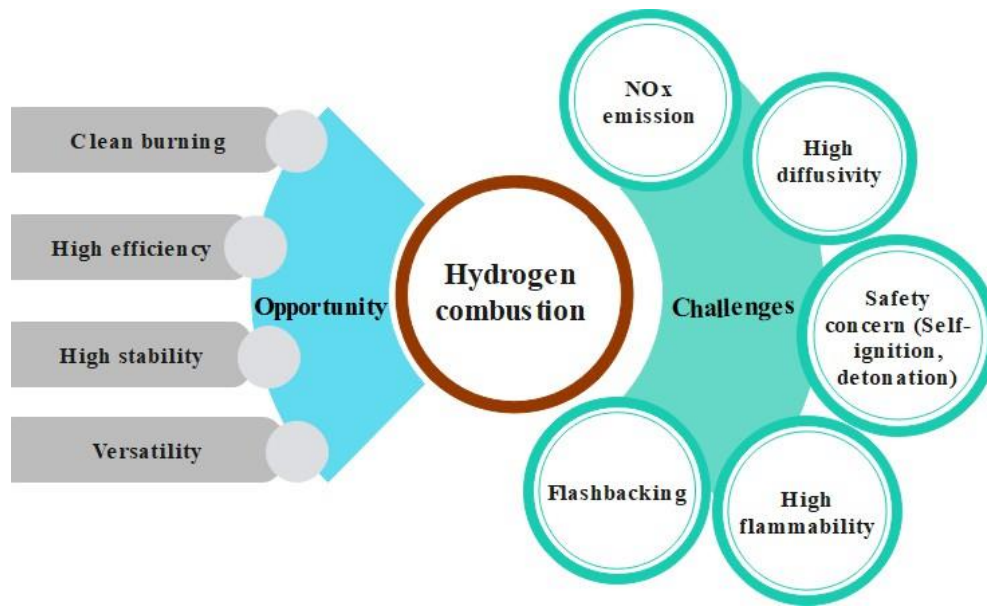


Fig. 5. Challenges and opportunities of hydrogen combustion

Hydrogen combustion exhibits hydrodynamic and thermodiffusive instability due to the density jumps across the flame front and the low Lewis number, respectively [53,54]. Hydrodynamic instability (Darrieus-Landau) occurs due to the density jumps across the flame front, which are always destabilizing. Thermodiffusive instability originates from the strong differential diffusion of hydrogen because of its low Lewis number, which leads to variations in the local equivalence ratio and reaction rates along the flame front. It significantly influences flame dynamics by quadrupling the flame speed in laminar flames and doubling the stretch factor [53]. Proper control of the fuel-air mixture, optimization of the ignition system, effective flame stabilization, and proper flow control techniques have shown promise in overcoming combustion instability [55]. However, there is also a problem associated with increasing the risk of spontaneous ignition and flashback in premixed combustion [33,46,56–59]. Non-premixed flame shows better performance, with some challenges in flame stability [60,61].

Utilizing pure hydrogen in combustion chambers poses technical challenges, such as controlling combustion temperature and managing the risk of combustion instability, which require further research and development. Using a hydrogen-air mixture in MILD combustion chambers significantly reduces harmful emissions, such as nitrogen oxide (NO<sub>x</sub>), while increasing the overall efficiency of the combustion process [62–64]. Xu et al. [63] numerically investigated the effect of pressure variation and H<sub>2</sub>O dilution on NO formation and reduction pathways in opposed-flow pure hydrogen MILD combustion. The study found that NO formation reaches its peak at 6 atm pressure and reduces as pressure increases, while H<sub>2</sub>O dilution results in a reduction of NO formation. Mixing hydrogen with conventional fuels in MILD conditions improves combustion stability, increases reactivity, reduces flame length, and reduces emissions [25,45,47–50,65].

Numerous experimental and numerical investigations have been carried out, providing valuable insights into various aspects of hydrogen's behavior in MILD combustion, including its effects on combustion parameters, emissions, and performance. Mayrhofer et al. [66] presented a modeling approach and experimentally validated flameless combustion of pure hydrogen in highly preheated air. Their study aimed to understand the dynamics of the combustion process and validate the accuracy of the numerical models with experimental data.

The findings indicated that the nonpremixed Steady Flamelet Model (NP-SFM) model exhibited the best results, aligning closely with the experimental data and accurately predicting the heat losses associated with the combustion process. Pashchenko [50] conducted a comparative study focusing on hydrogen-air premixed combustion, examining the differences between simulations of the three-dimensional (3D), two-dimensional (2D) and two-dimensional axisymmetric (2D) axes. The study shows a 25% higher temperature distribution in 3D simulations without a significant change in the hydrogen mass fraction. Additionally, the study highlighted substantial differences in velocity contours between 2D and 3D simulations. Yilmaz et al. [67] numerically investigated hydrogen/air mixtures using the microcombustor to establish colorless distributed combustion conditions. It has been found that combustion performance and emissions improved significantly when the mixture inlet temperature reached 1000 K with an O<sub>2</sub> concentration of 9% under the desired colorless distributed condition. Chemical reaction mechanisms are essential for understanding, controlling, and improving combustion processes. In addition, they played a great role in estimating the flame characteristics, such as the adiabatic flame temperature, auto-ignition delay time, and laminar flame speed, in combustion systems. Planke et al. [68] performed a numerical simulation, concentrating on the combustion of hydrogen jet flames under MILD conditions. The study incorporated six chemical reaction mechanisms and the eddy dissipation concept (EDC) combustion modelling to investigate a lifted jet flame. The research underscored that the flame lift-off height decreased as the co-flow temperature decreased, and identified the chemical reaction proposed by Li et al. [69] as yielding the most accurate results. Some of the recently developed theoretical and experimental chemical reaction mechanisms of pure hydrogen and its mixtures with other hydrocarbon fuels are provided in Table 2. The Konnov mechanism [70] accurately predicts laminar flame speed and NO concentrations, demonstrating good agreement with experimental results among recent chemical reaction mechanisms [71].

Tab. 2. Hydrogen chemical reaction mechanism over the past decades

Mechanism	Species	Reaction	Fuel and oxidizer	Types of mechanism
Skeletal Boivins 2010 [72]	9	12	H <sub>2</sub> +O <sub>2</sub>	Global
NUIG-NGM-2010 [73]	11(293)	21(1593)	H <sub>2</sub> +Syngas, Air	Reduced
Hong, 2011 [74]	10	31	H <sub>2</sub> +O <sub>2</sub>	Global
SanDiego 2011[75]	11(50)	21(244)	H <sub>2</sub> +Syngas, Air	Reduced
BURKE 2012 [76]	11	27	H <sub>2</sub> +O <sub>2</sub>	Global
CRECK-2012 [77]	11(14)	21(34)	H <sub>2</sub> +CO	Reduced
Keromnes-2013 [78]	12 (17)	33 (49)	H <sub>2</sub> +Syngas, Air	Reduced
Alekseev 2015 [79]	15	75	H <sub>2</sub> +O <sub>2</sub> +N <sub>2</sub>	Detailed
Varga-2015 [80]	12	30	H <sub>2</sub> +Syngas, Air	Reduced
Konnov 2019 [70]	15	75	H <sub>2</sub> +Air	Detailed
CRECK 2020 [77]	21	62	H <sub>2</sub> +CO	Detailed



### 3.2. Heat Transfer in Hydrogen MILD Combustion

Combustion modeling plays a crucial role in designing and optimizing industrial processes. Developing efficient combustion for hydrogen flames is essential for achieving flexible fuel consumption, reduced emissions, and improved combustion performance. In hydrogen combustion, radiation heat transfer is typically dominant due to the high flame temperature. MILD combustion involves various heat transfer interactions, including gas-to-gas, gas-to-wall, and wall-to-wall interactions [81]. Radiation heat transfer plays an important role in accurately predicting the behavior of the combustion system, the temperature of the flames, and the emission of pollutants [82,83]. Due to strong turbulence-radiation interactions (TRI), high computational costs, and a high spectral dependence of the radiative properties of combustion products, accurately modeling RHT in combustion systems is challenging. Various methods have been used to solve radiative heat transfer problems in combustion applications, including the Zonal method, the spherical harmonic method, the discrete transfer method (DTM), the discrete coordinates method (DOM), the finite-volume method (FVM), and the statistical Monte Carlo method (MC) [84]. The modeling of gas radiation in combustion systems is crucial to predicting the structure of the flame, the temperature distribution, and the heat transfer. Estimating the spectral properties of combustion products is tedious due to their dependence on wavelength, temperature, partial pressure, and total pressure of mixture fuels [85]. Different approaches, such as line-by-line, spectral band, and global models, have been employed to estimate these properties using the spectral database, such as HITRAN, HITEMP, and CDSD-1000 [86]. The weighted sum of gray gases (WSGG) model is commonly used due to its simplicity, accuracy, and computational efficiency over more sophisticated models like NBCK, spectral-line WSGG (SLW), full-spectrum correlated k-distribution (FSCK), and absorption distribution function (ADF) methods [87].

Heat transfer in hydrogen combustion chambers is often measured using calorimeter methods, heat flux sensors, and infrared cameras. For instance, Zhukop and Suslov [88] used calorimeter techniques to investigate heat flux in a rocket combustion chamber with a porous injector head using cryogenic oxygen and hydrogen. Using the same techniques, Tanneberger and Stathopoulos [89] studied a swirl-stabilized hydrogen-oxygen combustor and found that heat transfer to cooling air increased with swirl intensity and thermal power. Jones et al. [90] used coaxial thermocouple heat flux gauges to measure local heat flux with single-element coaxial injectors, while Droppers et al. [91] studied experimental measurements of injector face and chamber wall heat flux in a gaseous hydrogen-liquid oxygen rocket combustor. Schastlivtsev and Borzenko [92] investigated the distribution of heat flux in a hydrogen-oxygen steam generator with a thermal capacity of 25 MW. Heat flux sensors, such as contact type and convective sensors, are embedded in the heat transfer surface to measure the overall heat flux density through the furnace wall. Thermal radiative type sensors are suspended heat flux sensors that measure the distribution of the heat flux density within combustion chambers. Zhen et al. [93] estimated the heat flux on a flame impingement plate, and Wu et al. [94] used a water-cooled heat flux sensor to measure the total and radiative heat flux of the flame along the wall of the combustion chamber enclosure. These techniques help researchers understand the distribution of heat fluxes and the behavior of heat transfer in hydrogen combustion chambers.

#### 4. Conclusions

The increasing global demand for energy and environmental concerns have led to a growing interest in clean energy solutions, with hydrogen fuel emerging as a promising option for decarbonizing various sectors. This paper presents an overview of hydrogen MILD combustion, a promising approach to improving efficiency, flexibility, and emission control. The features of MILD combustion, the significance of hydrogen in forthcoming combustion technology, challenges and prospects, reaction mechanisms, and heat transfer analysis are discussed. MILD combustion is a cutting-edge technology capable of enhancing combustion efficiency and reducing emissions, offering applications in high-intensity combustion systems, heat utilization, and thermal waste destruction. Hydrogen combustion is environmentally friendly, producing only water vapor as a byproduct. However, because of its wide flammability range, high flame speed, high adiabatic temperature, and low ignition energy, it is prone to combustion instability, NO<sub>x</sub> formation when burning with air, and flashback incidents. Accurate modeling of radiative heat transfer in hydrogen combustion systems is challenging due to strong turbulence-radiation interactions, high computational costs, and spectral dependence. The weighted sum of gray gases (WSGG) model is commonly used to model gas radiation due to its simplicity, accuracy, and computational efficiency. Experimental techniques like calorimeter methods, heat flux sensors, and infrared cameras are used to measure heat transfer in hydrogen combustion. The study emphasizes the need for further research and development to address those challenges and ensure the safety and sustainability of hydrogen combustion.

#### References

- [1] IEA. Net Zero by 2050: A Roadmap for the Global Energy Sector. Int Energy Agency 2021:224.
- [2] IEA. The Future of Hydrogen. Futur Hydrog 2019. <https://doi.org/10.1787/1e0514c4-en>.
- [3] Sharma S, Ghoshal SK. Hydrogen the future transportation fuel: From production to applications. *Renew Sustain Energy Rev* 2015;43:1151–8. <https://doi.org/10.1016/j.rser.2014.11.093>.
- [4] Hauglustaine D, Paulot F, Collins W, Derwent R, Sand M, Boucher O. Climate benefit of a future hydrogen economy. *Commun Earth Environ* 2022;3:1–14. <https://doi.org/10.1038/s43247-022-00626-z>.
- [5] Nižetić S, Barbir F, Djilali N. The role of hydrogen in energy transition. *Int J Hydrogen Energy* 2019;44:9673–4. <https://doi.org/10.1016/j.ijhydene.2019.02.174>.
- [6] Nastasi B. Hydrogen policy, market, and R&D projects. Elsevier Inc.; 2019. <https://doi.org/10.1016/B978-0-12-814853-2.00002-3>.
- [7] McKinsey & Company. Hydrogen Roadmap Europe. 2019. <https://doi.org/10.2843/249013>.
- [8] Chakraborty S, Dash SK, Elavarasan RM, Kaur A, Elangovan D, Meraj ST, et al. Hydrogen Energy as Future of Sustainable Mobility. *Front Energy Res* 2022;10:1–23. <https://doi.org/10.3389/fenrg.2022.893475>.
- [9] Sedai A, Dhakal R, Gautam S, Kumar Sedhain B, Singh Thapa B, Moussa H, et al. Wind energy as a source of green hydrogen production in the USA. *Clean Energy* 2023;7:8–22. <https://doi.org/10.1093/ce/zkac075>.
- [10] Cavaliere A, De Joannon M. Mild combustion. vol. 30. 2004. <https://doi.org/10.1016/j.pecs.2004.02.003>.
- [11] Mancini M, Weber R, Bolletini U. Predicting NO<sub>x</sub> emissions of a burner operated in flameless oxidation mode. *Proc Combust Inst* 2002;29:1155–63. [https://doi.org/10.1016/s1540-7489\(02\)80146-8](https://doi.org/10.1016/s1540-7489(02)80146-8).
- [12] Wüning JA, Wüning JG. Flameless oxidation to reduce thermal no-formation. *Prog Energy Combust Sci* 1997;23:81–94. [https://doi.org/10.1016/s0360-1285\(97\)00006-3](https://doi.org/10.1016/s0360-1285(97)00006-3).

- [13] Hiroshi Tsuji, Ashwani K. Gupta, Toshiaki Hasegawa, Masashi Katsuki, Ken Kishimoto MM. High Temperature Air Combustion. 1st Editio. Boca Raton: CRC Press; 2002.
- [14] Katsuki M, Hasegawa T. The science and technology of combustion in highly preheated air. Symp Combust 1998;27:3135–46. [https://doi.org/10.1016/S0082-0784\(98\)80176-8](https://doi.org/10.1016/S0082-0784(98)80176-8).
- [15] Peters N. Principles and Potential of HiCOT Combustion. Proc Forum High-Temperature Air Combust Technol 2001:109–28.
- [16] Coelho PJ, Peters N. Numerical simulation of a mild combustion burner. Combust Flame 2001;124:503–18. [https://doi.org/10.1016/S0010-2180\(00\)00206-6](https://doi.org/10.1016/S0010-2180(00)00206-6).
- [17] Arghode VK, Gupta AK, Bryden KM. High intensity colorless distributed combustion for ultra low emissions and enhanced performance. Appl Energy 2012;92:822–30. <https://doi.org/10.1016/j.apenergy.2011.08.039>.
- [18] Khalil AEE, Gupta AK. On the colorless distributed combustion regime. AIAA SciTech Forum - 55th AIAA Aerosp Sci Meet 2017:1–13. <https://doi.org/10.2514/6.2017-1060>.
- [19] Khalil AEE, Gupta AK. Towards colorless distributed combustion regime. Fuel 2017;195:113–22. <https://doi.org/10.1016/j.fuel.2016.12.093>.
- [20] Arghode VK, Gupta AK. Development of high intensity CDC combustor for gas turbine engines. Appl Energy 2011;88:963–73. <https://doi.org/10.1016/j.apenergy.2010.07.038>.
- [21] Cardona LF, Alvarado PN. Numerical study of MILD Combustion of Ammonia/hydrogen Mixtures. Chem Eng Trans 2023;98:21–6. <https://doi.org/10.3303/CET2398004>.
- [22] Luan C, Xu S, Shi B, Tu Y, Liu H, Li P, et al. Re-Recognition of the MILD Combustion Regime by Initial Conditions of Tin and XO<sub>2</sub> for Methane in a Nonadiabatic Well-Stirred Reactor. Energy and Fuels 2020;34:2391–404. <https://doi.org/10.1021/acs.energyfuels.9b04177>.
- [23] Wang F, Li P, Wang G, Mi J. Moderate and Intense Low-Oxygen Dilution (MILD) Combustion of Liquid Fuels: A Review. Energy and Fuels 2022;36:8026–53. <https://doi.org/10.1021/acs.energyfuels.2c01383>.
- [24] Sabia P, Sorrentino G, Ariemma GB, Manna M V., Ragucci R, de Joannon M. MILD Combustion and Biofuels: A Minireview. Energy and Fuels 2021;35:19901–19. <https://doi.org/10.1021/acs.energyfuels.1c02973>.
- [25] Liu Z, Xiong Y, Zhu Z, Zhang Z, Liu Y. Effects of hydrogen addition on combustion characteristics of a methane fueled MILD model combustor. Int J Hydrogen Energy 2022;47:16309–20. <https://doi.org/10.1016/j.ijhydene.2022.03.132>.
- [26] Weber R, Orsino S, Lallemand N, Verlaan A. Combustion of natural gas with high-temperature air and large quantities of flue gas. Proc Combust Inst 2000;28:1315–21. [https://doi.org/10.1016/S0082-0784\(00\)80345-8](https://doi.org/10.1016/S0082-0784(00)80345-8).
- [27] Adamczyk WP, Bialecki RA, Ditaranto M, Gladysz P, Haugen NEL, Katelbach-Wozniak A, et al. CFD modeling and thermodynamic analysis of a concept of a MILD-OXY combustion large scale pulverized coal boiler. Energy 2017;140:1305–15. <https://doi.org/10.1016/j.energy.2017.03.130>.
- [28] Weber R, Gupta AK, Mochida S. High temperature air combustion (HiTAC): How it all started for applications in industrial furnaces and future prospects. Appl Energy 2020;278:115551. <https://doi.org/10.1016/j.apenergy.2020.115551>.
- [29] Chinnici A, Nathan GJ, Dally BB. Hybrid Solar-MILD Combustion for Renewable Energy Generation. Front Mech Eng 2019;5:1–11. <https://doi.org/10.3389/fmech.2019.00061>.
- [30] Lim JH, Nathan GJ, Hu E, Dally BB. Analytical assessment of a novel hybrid solar tubular receiver and combustor. Appl Energy 2016;162:298–307. <https://doi.org/10.1016/j.apenergy.2015.10.048>.
- [31] Li PF, Mi JC, Dally BB, Wang FF, Wang L, Liu ZH, et al. Progress and recent trend in MILD combustion. Sci China Technol Sci 2011;54:255–69. <https://doi.org/10.1007/s11431-010-4257-0>.

- [32] CO<sub>2</sub> Emissions in 2022. CO<sub>2</sub> Emiss 2022 2023. <https://doi.org/10.1787/12ad1e1a-en>.
- [33] Tingas Efsthathios-AI. Green Energy and Technology Hydrogen for Future Thermal Engines. 2023.
- [34] Milton BE, Keck JC. Laminar burning velocities in stoichiometric hydrogen and hydrogenhydrocarbon gas mixtures. *Combust Flame* 1984;58:13–22. [https://doi.org/10.1016/0010-2180\(84\)90074-9](https://doi.org/10.1016/0010-2180(84)90074-9).
- [35] Halter F, Chauveau C, Djebaili-Chaumeix N, Gökalp I. Characterization of the effects of pressure and hydrogen concentration on laminar burning velocities of methane-hydrogen-air mixtures. *Proc Combust Inst* 2005;30:201–8. <https://doi.org/10.1016/j.proci.2004.08.195>.
- [36] Huang Z, Zhang Y, Zeng K, Liu B, Wang Q, Jiang D. Measurements of laminar burning velocities for natural gas-hydrogen-air mixtures. *Combust Flame* 2006;146:302–11. <https://doi.org/10.1016/j.combustflame.2006.03.003>.
- [37] Bouvet N, Halter F, Chauveau C, Yoon Y. On the effective Lewis number formulations for lean hydrogen/hydrocarbon/ air mixtures. *Int J Hydrogen Energy* 2013;38:5949–60. <https://doi.org/10.1016/j.ijhydene.2013.02.098>.
- [38] Sánchez AL, Williams FA. Recent advances in understanding of flammability characteristics of hydrogen. *Prog Energy Combust Sci* 2014;41:1–55. <https://doi.org/10.1016/j.pecs.2013.10.002>.
- [39] Evans MJ, Proud DB, Medwell PR, Pitsch H, Dally BB. Highly radiating hydrogen flames: Effect of toluene concentration and phase. *Proc Combust Inst* 2021;38:1099–106. <https://doi.org/10.1016/j.proci.2020.07.005>.
- [40] Levinsky H. Why can't we just burn hydrogen? Challenges when changing fuels in an existing infrastructure. *Prog Energy Combust Sci* 2021;84:100907. <https://doi.org/10.1016/j.pecs.2021.100907>.
- [41] Erdemir D, Dincer I. A perspective on the use of ammonia as a clean fuel: Challenges and solutions. *Int J Energy Res* 2021;45:4827–34. <https://doi.org/10.1002/er.6232>.
- [42] Yip HL, Srna A, Yuen ACY, Kook S, Taylor RA, Yeoh GH, et al. A review of hydrogen direct injection for internal combustion engines: Towards carbon-free combustion. *Appl Sci* 2019;9:1–30. <https://doi.org/10.3390/app9224842>.
- [43] Ma F, Guo L, Li Z, Zeng X, Zheng Z, Li W, et al. A Review of Current Advances in Ammonia Combustion from the Fundamentals to Applications in Internal Combustion Engines. *Energies* 2023;16. <https://doi.org/10.3390/en16176304>.
- [44] Fischer M. Safety aspects of hydrogen combustion in hydrogen energy systems. *Int J Hydrogen Energy* 1986;11:593–601. [https://doi.org/10.1016/0360-3199\(86\)90126-6](https://doi.org/10.1016/0360-3199(86)90126-6).
- [45] Mihăescu L, Stanciu D, Lăzăroiu G, Pișă I, Negreanu G. Comparative analysis between methane and hydrogen regarding ignition and combustion in diffusive mode. *E3S Web Conf* 2021;327. <https://doi.org/10.1051/e3sconf/202132701001>.
- [46] Onorati A, Payri R, Vaglieco BM, Agarwal AK, Bae C, Bruneaux G, et al. The role of hydrogen for future internal combustion engines. *Int J Engine Res* 2022;23:529–40. <https://doi.org/10.1177/14680874221081947>.
- [47] Huang M, Zhang Z, Shao W, Xiong Y, Lei F, Xiao Y. MILD combustion for hydrogen and syngas at elevated pressures. *J Therm Sci* 2014;23:96–102. <https://doi.org/10.1007/s11630-014-0682-x>.
- [48] Mardani A, Karimi Motaalegh Mahalegi H. Hydrogen enrichment of methane and syngas for MILD combustion. *Int J Hydrogen Energy* 2019;44:9423–37. <https://doi.org/10.1016/j.ijhydene.2019.02.072>.
- [49] Riahi Z, Hraiech I, Sautet JC, Ben Nasrallah S. Numerical investigation of turbulent combustion with hybrid enrichment by hydrogen and oxygen. *Int J Hydrogen Energy* 2020;45:3316–26. <https://doi.org/10.1016/j.ijhydene.2019.11.151>.
- [50] Pashchenko D. Comparative analysis of hydrogen/air combustion CFD-modeling for 3D and 2D computational domain of micro-cylindrical combustor. *Int J Hydrogen Energy* 2017;42:29545–56. <https://doi.org/10.1016/j.ijhydene.2017.10.070>.

- [51] Kozhukhova AE, du Preez SP, Bessarabov DG. Catalytic hydrogen combustion for domestic and safety applications: A critical review of catalyst materials and technologies. *Energies* 2021;14. <https://doi.org/10.3390/en14164897>.
- [52] Skottene M, Rian KE. A study of NO<sub>x</sub> formation in hydrogen flames. *Int J Hydrogen Energy* 2007;32:3572–85. <https://doi.org/10.1016/j.ijhydene.2007.02.038>.
- [53] Berger L, Kleinheinz K, Attili A, Pitsch H. Characteristic patterns of thermodiffusively unstable premixed lean hydrogen flames. *Proc Combust Inst* 2019;37:1879–86. <https://doi.org/10.1016/j.proci.2018.06.072>.
- [54] Berger L, Attili A, Pitsch H. Intrinsic instabilities in premixed hydrogen flames: parametric variation of pressure, equivalence ratio, and temperature. Part 2 – Non-linear regime and flame speed enhancement. *Combust Flame* 2022;240:111936. <https://doi.org/10.1016/j.combustflame.2021.111936>.
- [55] McManus KR, Poinot T, Candel SM. A review of active control of combustion instabilities. *Prog Energy Combust Sci* 1993;19:1–29. [https://doi.org/10.1016/0360-1285\(93\)90020-F](https://doi.org/10.1016/0360-1285(93)90020-F).
- [56] Cheng RK, Oppenheim AK. Autoignition in methanehydrogen mixtures. *Combust Flame* 1984;58:125–39. [https://doi.org/10.1016/0010-2180\(84\)90088-9](https://doi.org/10.1016/0010-2180(84)90088-9).
- [57] Dryer FL, Chaos M. Ignition of syngas/air and hydrogen/air mixtures at low temperatures and high pressures: Experimental data interpretation and kinetic modeling implications. *Combust Flame* 2008;152:293–9. <https://doi.org/10.1016/j.combustflame.2007.08.005>.
- [58] Lieuwen T, McDonell V, Petersen E, Santavicca D. Fuel flexibility influences on premixed combustor blowout, flashback, autoignition, and stability. *J Eng Gas Turbines Power* 2008;130:1–10. <https://doi.org/10.1115/1.2771243>.
- [59] Ebi D, Clemens NT. Experimental investigation of upstream flame propagation during boundary layer flashback of swirl flames. *Combust Flame* 2016;168:39–52. <https://doi.org/10.1016/j.combustflame.2016.03.027>.
- [60] Pitts WM. Assessment of theories for the behavior and blowout of lifted turbulent jet diffusion flames. *Symp Combust* 1989;22:809–16. [https://doi.org/10.1016/S0082-0784\(89\)80090-6](https://doi.org/10.1016/S0082-0784(89)80090-6).
- [61] Lyons KM. Toward an understanding of the stabilization mechanisms of lifted turbulent jet flames: Experiments. *Prog Energy Combust Sci* 2007;33:211–31. <https://doi.org/10.1016/j.peccs.2006.11.001>.
- [62] Parente A, de Joannon M. Editorial: MILD Combustion: Modelling Challenges, Experimental Configurations, and Diagnostic Tools. vol. 7. 2021. <https://doi.org/10.3389/fmech.2021.726633>.
- [63] Buczyński R, Uryga-Bugajska I, Tokarski M. Recent advances in low-gradient combustion modelling of hydrogen fuel blends. *Fuel* 2022;328:125265. <https://doi.org/10.1016/j.fuel.2022.125265>.
- [64] Sabia P, de Joannon M. Critical Issues of Chemical Kinetics in MILD Combustion. *Front Mech Eng* 2020;6:1–10. <https://doi.org/10.3389/fmech.2020.00007>.
- [65] Xiao J, Travis JR, Kuznetsov M. Numerical investigations of heat losses to confinement structures from hydrogen-air turbulent flames in ENACCEF facility. *Int J Hydrogen Energy* 2015;40:13106–20. <https://doi.org/10.1016/j.ijhydene.2015.07.090>.
- [66] Mayrhofer M, Koller M, Seemann P, Bordbar H, Prieler R, Hochenauer C. MILD combustion of hydrogen and air – An efficient modelling approach in CFD validated by experimental data. *Int J Hydrogen Energy* 2022;47:6349–64. <https://doi.org/10.1016/j.ijhydene.2021.11.236>.
- [67] Yilmaz H, Cam O, Yilmaz I. Effect of micro combustor geometry on combustion and emission behavior of premixed hydrogen/air flames. vol. 135. Elsevier B.V.; 2017. <https://doi.org/10.1016/j.energy.2017.06.169>.
- [68] Planke K, Farisco F, Grimm F, Huber A. A Numerical Study on Hydrogen Jet Flame Combustion in MILD Conditions 2023:1–13. <https://doi.org/10.2514/6.2023-1098>.
- [69] Li J, Zhao Z, Kazakov A, Dryer FL. An updated comprehensive kinetic model of hydrogen combustion. *Int J Chem Kinet* 2004;36:566–75. <https://doi.org/10.1002/kin.20026>.

- [70] Konnov AA. Yet another kinetic mechanism for hydrogen combustion. *Combust Flame* 2019;203:14–22. <https://doi.org/10.1016/j.combustflame.2019.01.032>.
- [71] Giacomazzi E, Troiani G, Di Nardo A, Calchetti G, Cecere D, Messina G, et al. Hydrogen Combustion: Features and Barriers to Its Exploitation in the Energy Transition. *Energies* 2023;16. <https://doi.org/10.3390/en16207174>.
- [72] Boivin P, Jim C. An explicit reduced mechanism for h<sub>2</sub>-air autoignition and partially premixed combustion 2009:2009.
- [73] Healy D, Kalitan DM, Aul CJ, Petersen EL, Bourque G, Curran HJ. Oxidation of C1-C5 alkane quinary natural gas mixtures at high pressures. *Energy and Fuels* 2010;24:1521–8. <https://doi.org/10.1021/ef9011005>.
- [74] Hong Z, Davidson DF, Hanson RK. An improved H<sub>2</sub>/O<sub>2</sub> mechanism based on recent shock tube/laser absorption measurements. *Combust Flame* 2011;158:633–44. <https://doi.org/10.1016/j.combustflame.2010.10.002>.
- [75] Mechanical and Aerospace Engineering (Combustion Research) U of, Combustion C at SD. *Chemical-Kinetic Mechanisms for Applications*. San Diego Mech 2011.
- [76] Burke MP, Chaos M, Ju Y, Dryer FL, Klippenstein SJ. Comprehensive H<sub>2</sub>/O<sub>2</sub> kinetic model for high-pressure combustion. *Int J Chem Kinet* 2012;44:444–74. <https://doi.org/10.1002/kin.20603>.
- [77] CRECK. Hydrogen/CO Mechanism Version 1201. n.d.
- [78] Kéromnès A, Metcalfe WK, Heufer KA, Donohoe N, Das AK, Sung CJ, et al. An experimental and detailed chemical kinetic modeling study of hydrogen and syngas mixture oxidation at elevated pressures. *Combust Flame* 2013;160:995–1011. <https://doi.org/10.1016/j.combustflame.2013.01.001>.
- [79] Alekseev VA, Christensen M, Konnov AA. The effect of temperature on the adiabatic burning velocities of diluted hydrogen flames: A kinetic study using an updated mechanism. *Combust Flame* 2015;162:1884–98. <https://doi.org/10.1016/j.combustflame.2014.12.009>.
- [80] Varga T, Nagy T, Olm C, Zsély IG, Pálvölgyi R, Valkó, et al. Optimization of a hydrogen combustion mechanism using both direct and indirect measurements. *Proc Combust Inst* 2015;35:589–96. <https://doi.org/10.1016/j.proci.2014.06.071>.
- [81] Ceriello G, Sorrentino G, Cavaliere A, Joannon M de, Ragucci R. Mini-Review: Heat Transfer Mechanisms in MILD Combustion Systems. *Front Mech Eng* 2021;7:1–8. <https://doi.org/10.3389/fmech.2021.505923>.
- [82] Siegel R, Howell JR. *Thermal Radiation Heat Transfer III* 1971;III.
- [83] Modest MF. *Radiative Heat Transfer*. Second edi. New York: McGraw-Hill; 1993.
- [84] Modest MF. Radiative heat transfer in fire modeling. vol. 31. 2008. <https://doi.org/10.2495/9781845641603/07>.
- [85] Bordbar H, Coelho FR, Fraga GC, França FHR, Hostikka S. Pressure-dependent weighted-sum-of-gray-gases models for heterogeneous CO<sub>2</sub>-H<sub>2</sub>O mixtures at sub- and super-atmospheric pressure. *Int J Heat Mass Transf* 2021;173:121207. <https://doi.org/10.1016/j.ijheatmasstransfer.2021.121207>.
- [86] Gordon IE, Rothman LS, Hargreaves RJ, Hashemi R, Karlovets E V., Skinner FM, et al. The HITRAN2020 molecular spectroscopic database. *J Quant Spectrosc Radiat Transf* 2022;277:107949. <https://doi.org/10.1016/j.jqsrt.2021.107949>.
- [87] Modest MF. The treatment of nongray properties in radiative heat transfer: From past to present. *J Heat Transfer* 2013;135:1–12. <https://doi.org/10.1115/1.4023596>.
- [88] Zhukov VP, Suslov DI. Measurements and modelling of wall heat fluxes in rocket combustion chamber with porous injector head. *Aerosp Sci Technol* 2016;48:67–74. <https://doi.org/10.1016/j.ast.2015.10.021>.

- [89] Tanneberger T, Stathopoulos P. Heat transfer measurements in a hydrogen-oxyfuel combustor. *Exp Heat Transf* 2021;34:620–38. <https://doi.org/10.1080/08916152.2020.1798564>.
- [90] Jones G, Protz C, Bullard B. Local Heat Flux Measurements with. *Engineering* 2006:1–11.
- [91] Droppers LJ, Schuff R, Anderson WE. Study of heat transfer in a gaseous hydrogen liquid oxygen multi-element combustor. *Collect Tech Pap - 43rd AIAA/ASME/SAE/ASEE Jt Propuls Conf* 2007;5:5214–26. <https://doi.org/10.2514/6.2007-5550>.
- [92] Schastlivtsev AI, Borzenko VI. Investigation of the distribution of heat fluxes in the combustion chamber of a hydrogen-oxygen steam generator. *J Phys Conf Ser* 2018;1128. <https://doi.org/10.1088/1742-6596/1128/1/012077>.
- [93] Zhen HS, Cheung CS, Leung CW, Choy YS. Effects of hydrogen concentration on the emission and heat transfer of a premixed LPG-hydrogen flame. *Int J Hydrogen Energy* 2012;37:6097–105. <https://doi.org/10.1016/j.ijhydene.2011.12.130>.
- [94] Wu L, Kobayashi N, Li Z, Huang H. Experimental study on the effects of hydrogen addition on the emission and heat transfer characteristics of laminar methane diffusion flames with oxygen-enriched air. *Int J Hydrogen Energy* 2016;41:2023–36. <https://doi.org/10.1016/j.ijhydene.2015.10.132>.

# Polymeric approaches to the removal of endocrine disrupting compounds from water: a comprehensive review

Tomasz Fronczyk, Anna Mielanczyk

Department of Physical Chemistry and Technology of Polymers, Faculty of Chemistry, Silesian University of Technology, Gliwice, Poland, e-mail: tomasz.fronczyk@polsl.pl, anna.mielanczyk@polsl.pl

## Abstract

The study comprehensively reviews the presence and impact of Endocrine Disrupting Compounds (EDCs) in the environment, particularly focusing on their presence in water sources due to widespread industrial, agricultural, and consumer product use. Recognizing the urgent need to mitigate the adverse health and ecological impacts of EDCs, this review primarily explores the application of polymeric materials in EDC removal. Two primary methods—adsorption using polymeric adsorbents and membrane filtration with polymer-based membranes—are investigated for their effectiveness in EDC removal. The review evaluates various polymer types, including molecularly imprinted polymers, cyclodextrin-based adsorbents, biodegradable polymers, and polymeric microfibers for adsorption, as well as polymers like polyamide, polyethersulfone, cellulose acetate, and polysulfone for membrane filtration. The advantages, challenges, and future research needs of using these polymeric methods are discussed, highlighting their potential in addressing this significant environmental issue.

**Keywords:** EDC, polymers, adsorption, membranes, water purification

## 1. Introduction

Endocrine Disrupting Compounds (EDCs) are chemicals that interfere with the normal function of the endocrine system, which regulates the production and activity of hormones in the body. Hormones are essential for maintaining homeostasis, reproduction, development, and behavior in humans and animals. Exposure to EDCs can cause adverse effects such as reproductive disorders, developmental abnormalities, metabolic diseases, immune dysfunction, and cancer.[1,2]

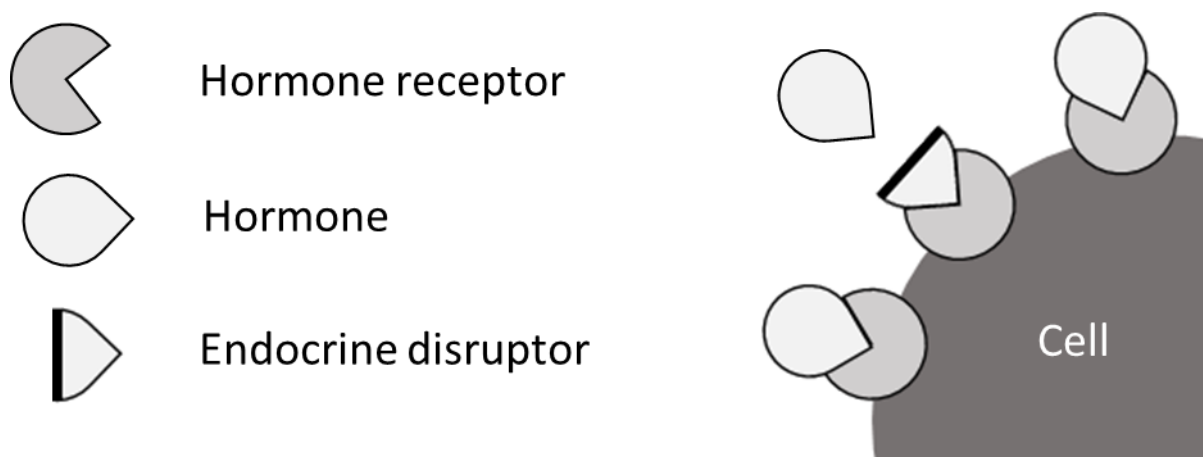


Fig. 1. Scheme of action of endocrine disruptors.

EDCs are widely present in the environment due to their use in various industrial, agricultural, pharmaceutical, and personal care products. They can enter the water cycle through wastewater effluents, runoff, leaching, or atmospheric deposition. [3,4]



Some of the most common and well-studied EDCs are:

- **Bisphenol A (BPA):** BPA can mimic estrogen and bind to estrogen receptors in the body. BPA exposure has been linked to reduced fertility, altered development of reproductive organs, increased risk of breast and prostate cancer, obesity, diabetes, and cardiovascular disease.[5–7]
- **Phthalates:** Phthalates can interfere with testosterone synthesis and action in males. Phthalate exposure has been associated with reduced sperm quality and quantity, cryptorchidism (undescended testes), testicular cancer, obesity, insulin resistance, and asthma.[8–10]
- **Per- and polyfluoroalkyl substances (PFAS):** PFAS can disrupt thyroid hormone production and action. PFAS exposure has been linked to thyroid dysfunction, reduced immune response, increased cholesterol levels, liver damage, kidney cancer, testicular cancer, and preeclampsia (a pregnancy complication characterized by high blood pressure).[11–13]
- **Atrazine:** Atrazine is one of the most commonly applied herbicides in the world. Atrazine can affect the synthesis and secretion of gonadotropins (hormones that regulate reproductive function) in both males and females. Atrazine exposure has been related to menstrual cycle disruption, reduced sperm count and motility, ovarian and testicular atrophy, impaired sexual behavior, and increased risk of breast cancer.[14–16]
- **Dioxins:** Dioxins are a byproduct of certain manufacturing processes. Dioxins can bind to the aryl hydrocarbon receptor (AhR), which regulates genes involved in detoxification, inflammation, cell cycle, and apoptosis. Dioxin exposure has been implicated in endometriosis (a condition where uterine tissue grows outside the uterus), altered thyroid function, immune suppression, skin lesions, and various types of cancer.[17–19]

Therefore, there is an urgent need to develop efficient and cost-effective techniques to remove EDCs from water sources and protect the aquatic ecosystems and human health. To protect the environment and public health, it is essential to remove EDCs from water effectively and efficiently. Among the various methods of EDC removal, such as flocculation, precipitation, adsorption, membrane treatment, oxidation, chemical degradation, photocatalytic degradation, biological degradation, transformation, and volatilization, chemical coagulation, and electro-coagulation, polymeric approaches have attracted considerable attention due to their advantages of high selectivity, stability, reusability, and low cost. Polymeric methods involve the use of synthetic or natural polymers as adsorbents or catalysts to capture or degrade EDCs from water.[20–24]

Polymeric materials are a class of synthetic organic adsorbents that have attracted considerable attention for the removal of EDCs from water. Polymeric materials have several advantages over other types of adsorbents, such as high surface area, tunable pore structure, adjustable functional groups, easy modification, good mechanical strength, and low cost. Polymeric materials can be classified into three categories based on their structure: linear polymers, cross-linked polymers, and polymer-based nanomaterials. Linear polymers are long-chain molecules that can be dissolved or swollen in water. Cross-linked polymers are network-like structures that are insoluble but can absorb water. Polymer-based nanomaterials are nano-sized particles or structures that are composed of or derived from polymers. Each category of polymeric materials has its own advantages and disadvantages for the removal of EDCs from water.[24–26]

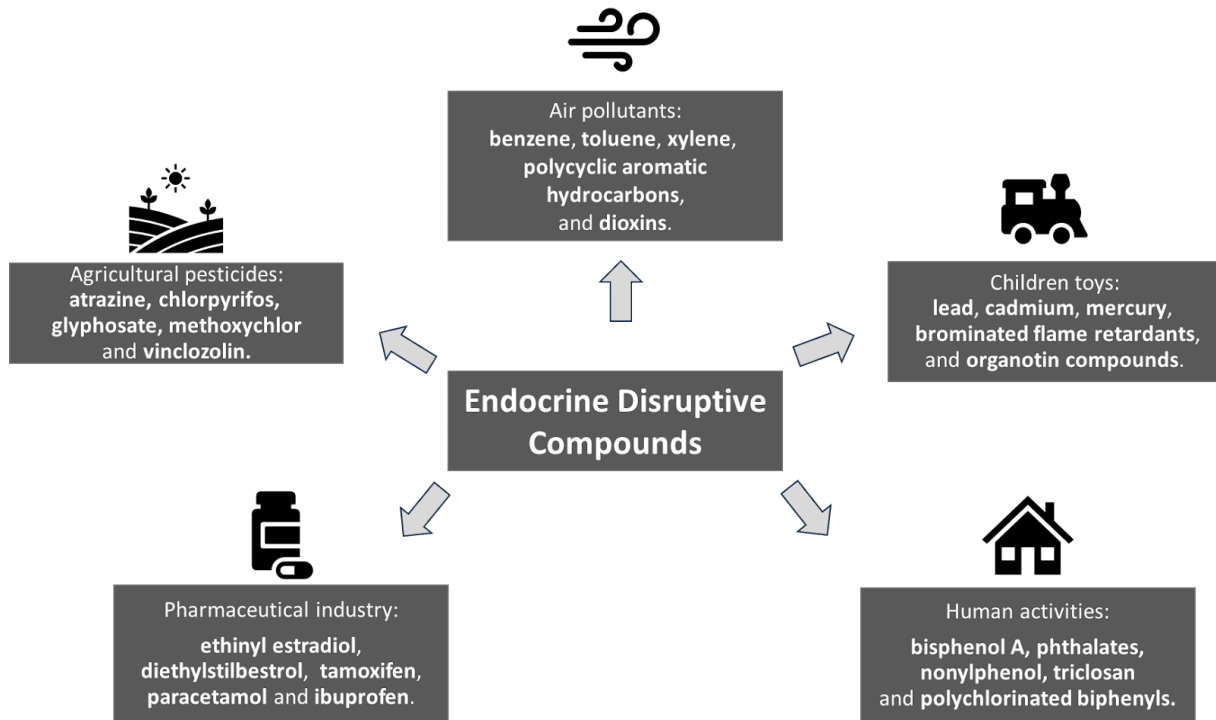


Fig. 2. Scheme of the presence of EDCs in various areas.

## 2. Application of polymers in removing EDCs

### 2.1 Adsorption

Adsorption is a surface-based process where molecules from a fluid phase accumulate onto a solid material's surface, leading to a concentration of these molecules at the interface. It is a physical process that does not generate harmful by-products and can be easily regenerated and reused. Among the various types of adsorbents, polymers have attracted much attention due to their high surface area, tunable properties, and low cost.

Some examples of polymers that have been used for EDCs adsorption are:

- **Molecularly imprinted polymers (MIPs):** These are synthetic polymers that have specific recognition sites for target molecules, such as EDCs, based on molecular imprinting technology. MIPs can selectively adsorb EDCs from water and have high adsorption capacity, stability, and reusability. For example, MIPs have been used to remove efficiently bisphenol A, progesterone, estrogens, and alkylphenols from water.[27,28]
- **Cyclodextrin (CD)-Based Adsorbents:** These specialized adsorbents have been developed with a focus on treating wastewater. They are particularly effective against a spectrum of pollutants, including heavy metals, dyes, and a range of organic contaminants such as pharmaceuticals and endocrine disruptor chemicals. The synthesis of CD-based adsorbents represents a significant advancement in targeting specific contaminants in wastewater treatment.[29]
- **Biodegradable polymers:** These are polymers that can be degraded by biological processes, such as enzymatic hydrolysis or microbial action. Biodegradable polymers can be used as eco-friendly adsorbents for EDCs removal from water, as they do not generate secondary pollution. For example, biodegradable polymers such as chitosan, starch, cellulose, and alginate have been used to remove bisphenol A, estrone,  $17\beta$ -estradiol, and  $17\alpha$ -ethinylestradiol from water.[30]
- **Poly(butyleneadipate-co-terephthalate) (PBAT) Microfibers:** These microfibers are created using the advanced electrospinning technique. They have been specifically tested and found effective in the adsorption of three kinds of EDCs: estrone,  $17\beta$ -estradiol, and  $17\alpha$ -ethinylestradiol from water-based solutions.[31]

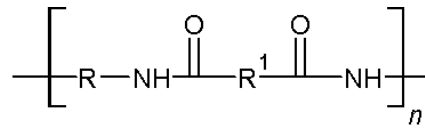
In conclusion, polymers are versatile and effective adsorbents for EDCs removal from water. Polymers can be tailored to achieve high adsorption capacity, selectivity, and recyclability for EDCs, by varying their composition, structure, and functionality. Polymers can also be combined with other techniques, such as membrane filtration or biodegradation, to achieve synergistic effects and enhance the overall efficiency of EDCs removal. However, there are still some challenges and limitations that need to be addressed, such as the optimization of the synthesis and modification methods, the evaluation of the environmental impact and toxicity of the adsorbents and their desorption products, and the scale-up and application of the adsorbents in real water systems. Therefore, further research and development are needed to explore the full potential of polymers as adsorbents for EDCs removal.

## 2.2 Membranes

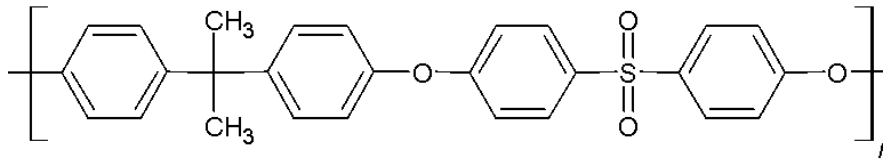
Membrane filtration is a physical separation process that uses a semi-permeable membrane to retain or reject certain molecules, such as EDCs, from a feed solution. Membrane filtration can be classified into four main categories, based on the pore size and operating pressure of the membrane: reverse osmosis (RO), nanofiltration (NF), ultrafiltration (UF), and microfiltration (MF). Membrane filtration has several advantages over conventional treatment methods, such as high efficiency, low energy consumption, and minimal environmental impact.[32,33]

Polymers are widely used as membrane materials for EDCs removal, due to their versatility, availability, and affordability. Polymers can be synthesized or modified to achieve desired properties, such as permeability, selectivity, stability, and fouling resistance. Polymers can also be blended, coated, or grafted with other materials, such as nanoparticles, metal-organic frameworks, or biopolymers, to enhance their performance and functionality. Some examples of polymers that have been used for EDCs removal by membrane filtration are:

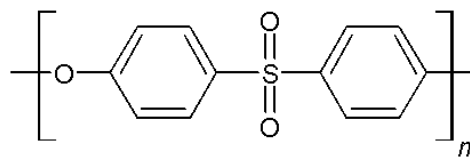
- Polyamide (PA): PA is a synthetic polymer that is commonly used as the active layer of thin-film composite (TFC) membranes for RO and NF applications. PA has high rejection of EDCs, such as bisphenol A, estrone, and 17 $\beta$ -estradiol, due to its dense and hydrophilic structure. However, PA is also prone to fouling and degradation by chlorine and other oxidants.[34]
- Polyethersulfone (PES): PES is a synthetic polymer that is widely utilized as the porous support layer of Thin-Film Composite (TFC) membranes, as well as the material for UF and MF applications. PES exhibits commendable mechanical strength, thermal stability, and chemical resistance, making it suitable for various filtration processes, including the removal of EDCs. PES membranes, especially when modified with hydrophilic coatings functionalized by amide groups, can significantly enhance the adsorption of EDCs like 17 $\beta$ -estradiol from water, achieving adsorption efficiencies of over 60%. However, PES is inherently hydrophobic and susceptible to fouling by organic and biological matter, which can be a limitation in its application for EDC removal unless appropriate modifications are made to improve its hydrophilicity and fouling resistance.[35]
- Cellulose acetate (CA): CA is a natural polymer that is derived from cellulose, which is the main component of plant cell walls. CA is one of the oldest and most widely used membrane materials for RO, NF, and UF applications. CA has good biocompatibility, biodegradability, and antifouling properties. However, CA also has low thermal stability, low chemical resistance, and low rejection of EDCs, especially those with low molecular weight and high hydrophobicity. To improve its performance, CA can be blended or coated with other polymers, such as chitosan.[36,37]
- Polysulfone (PSF): PSF is a synthetic polymer that is similar to PES, but has a lower degree of sulfonation. PSF is mainly used as the membrane material for UF and MF applications. PSF has high mechanical strength, thermal stability, and chemical resistance. However, PSF is also hydrophobic and prone to fouling by organic and biological matter. To enhance its hydrophilicity and antifouling properties, PSF can be modified by grafting or blending with other polymers, such as polyacrylic acid, polyethyleneimine, or polyvinylpyrrolidone. Polysulfone membranes have been incorporated in combined processes like ozone oxidation and ultrafiltration, which have proven effective in the removal of EDCs from water.[38]



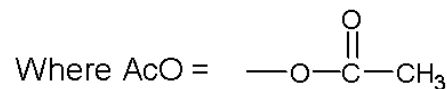
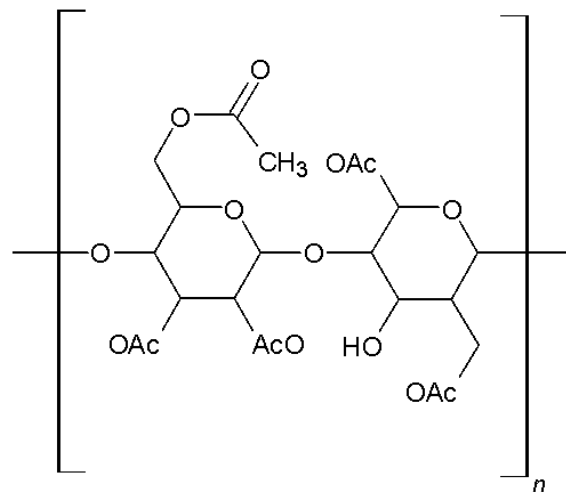
Polyamide



Polysulfone



Polyethersulfone



Cellulose acetate

Fig. 3. Schemes of polymers used in membrane filtration.

In summary, polymers are effective and versatile membrane materials for EDCs removal from water. Polymers can be tailored to achieve high permeability, selectivity, stability, and fouling resistance for EDCs, by varying their composition, structure, and functionality. Polymers can also be combined with other materials, such as nanoparticles, metal-organic frameworks, or biopolymers, to improve their performance and functionality. However, there are still some challenges and limitations that need to be addressed, such as the optimization of the synthesis and modification methods, the evaluation of the environmental impact and toxicity of the membranes and their permeates, and the scale-up and application of the membranes in real water systems. Therefore, further research and development are needed to explore the full potential of polymers as membrane materials for EDCs removal.

### 3. Conclusions

The extensive review of polymeric methods for the removal of Endocrine Disrupting Compounds EDCs from water sources highlights their significant potential in environmental remediation. Polymeric adsorbents, such as molecularly imprinted polymers, cyclodextrin-based adsorbents, biodegradable polymers, and poly (butyleneadipate-co-terephthalate) microfibers, demonstrate high adsorption capacity, selectivity, and recyclability. These materials can be engineered to target specific EDCs, offering a promising solution for mitigating the adverse health effects of these compounds. Similarly, polymer-based membrane materials, including polyamide, polyethersulfone, cellulose acetate, and polysulfone, have been effective in EDC removal through membrane filtration techniques. These polymers can be tailored for enhanced permeability, selectivity, and fouling resistance. However, challenges such as optimizing synthesis methods, evaluating environmental impacts, and scaling up for practical applications remain. Further research is essential to harness the full potential of polymers in EDC removal and to develop sustainable, efficient solutions for protecting public health and the environment.

### Acknowledgment

This research was funded by the Polish Budget Funds for Scientific Research in 2023 as core funding for R&D activities at the Silesian University of Technology-funding for young scientists, grant number BKM-545/RCH4/2023 (04/040/BKM23/0259).

### References

- [1]. La Merrill, M.A.; Vandenberg, L.N.; Smith, M.T.; Goodson, W.; Browne, P.; Patisaul, H.B.; Guyton, K.Z.; Kortenkamp, A.; Coglian, V.J.; Woodruff, T.J.; et al. Consensus on the Key Characteristics of Endocrine-Disrupting Chemicals as a Basis for Hazard Identification. *Nat. Rev. Endocrinol.* 2020, *16*, 45–57, doi:10.1038/s41574-019-0273-8.
- [2]. Kumar, M.; Sarma, D.K.; Shubham, S.; Kumawat, M.; Verma, V.; Prakash, A.; Tiwari, R. Environmental Endocrine-Disrupting Chemical Exposure: Role in Non-Communicable Diseases. *Front. Public Heal.* 2020, *8*, 1–28, doi:10.3389/fpubh.2020.553850.
- [3]. Metcalfe, C.D.; Bayen, S.; Desrosiers, M.; Muñoz, G.; Sauvé, S.; Yargeau, V. An Introduction to the Sources, Fate, Occurrence and Effects of Endocrine Disrupting Chemicals Released into the Environment. *Environ. Res.* 2022, *207*, doi:10.1016/j.envres.2021.112658.
- [4]. Wee, S.Y.; Aris, A.Z.; Yusoff, F.M.; Praveena, S.M. Occurrence of Multiclass Endocrine Disrupting Compounds in a Drinking Water Supply System and Associated Risks. *Sci. Rep.* 2020, *10*, 1–12, doi:10.1038/s41598-020-74061-5.
- [5]. Gao, H.; Yang, B.J.; Li, N.; Feng, L.M.; Shi, X.Y.; Zhao, W.H.; Liu, S.J. Bisphenol A and Hormone-Associated Cancers: Current Progress and Perspectives. *Med. (United States)* 2015, *94*, e211, doi:10.1097/MD.0000000000000211.
- [6]. Cimmino, I.; Fiory, F.; Perruolo, G.; Miele, C.; Beguinot, F.; Formisano, P.; Oriente, F. Potential Mechanisms of Bisphenol a (BPA) Contributing to Human Disease. *Int. J. Mol. Sci.* 2020, *21*, 1–22, doi:10.3390/ijms21165761.
- [7]. Xing, J.; Zhang, S.; Zhang, M.; Hou, J. A Critical Review of Presence, Removal and Potential Impacts of Endocrine Disruptors Bisphenol A. *Comp. Biochem. Physiol. Part - C Toxicol. Pharmacol.* 2022, *254*, 109275, doi:10.1016/j.cbpc.2022.109275.
- [8]. Meeker, J.D.; Sathyanarayana, S.; Swan, S.H. Phthalates and Other Additives in Plastics: Human Exposure and Associated Health Outcomes. *Philos. Trans. R. Soc. B Biol. Sci.* 2009, *364*, 2097–2113, doi:10.1098/rstb.2008.0268.
- [9]. Wang, Y.; Ni, C.; Li, X.; Lin, Z.; Zhu, Q.; Li, L.; Ge, R.S. Phthalate-Induced Fetal Leydig Cell Dysfunction Mediates Male Reproductive Tract Anomalies. *Front. Pharmacol.* 2019, *10*, 1–11, doi:10.3389/fphar.2019.01309.
- [10]. Monisha, R.S.; Mani, R.L.; Sivaprakash, B.; Rajamohan, N.; Vo, D.V.N. Remediation and Toxicity of Endocrine Disruptors: A Review. *Environ. Chem. Lett.* 2023, *21*, 1117–1139, doi:10.1007/s10311-022-01455-4.
- [11]. Kim, M.J.; Moon, S.; Oh, B.C.; Jung, D.; Ji, K.; Choi, K.; Park, Y.J. Association between Perfluoroalkyl Substances Exposure and Thyroid Function in Adults: A Meta-Analysis. *PLoS One* 2018, *13*, 1–17, doi:10.1371/journal.pone.0197244.
- [12]. Ducatman, A.; LaPier, J.; Fuoco, R.; DeWitt, J.C. Official Health Communications Are Failing PFAS-Contaminated Communities. *Environ. Heal. A Glob. Access Sci. Source* 2022, *21*, 1–18, doi:10.1186/s12940-022-00857-9.

- [13]. Blake, B.E.; Fenton, S.E. Early Life Exposure to Per- and Polyfluoroalkyl Substances (PFAS) and Latent Health Outcomes: A Review Including the Placenta as a Target Tissue and Possible Driver of Peri- and Postnatal Effects. *Toxicology* 2020, *443*, 152565, doi:10.1016/j.tox.2020.152565.
- [14]. Wirbisky, S.E.; Freeman, J.L. Atrazine Exposure and Reproductive Dysfunction through the Hypothalamus-Pituitary-Gonadal (HPG) Axis. *Toxics* 2015, *3*, 414–450, doi:10.3390/toxics3040414.
- [15]. Stradtman, S.C.; Freeman, J.L. Mechanisms of Neurotoxicity Associated with Exposure to the Herbicide Atrazine. *Toxics* 2021, *9*, doi:10.3390/toxics9090207.
- [16]. Pathak, R.K.; Dikshit, A.K. Atrazine and Human Health. *Int. J. Ecosyst.* 2012, *1*, 14–23, doi:10.5923/ije.20110101.03.
- [17]. Bruner-Tran, K.L.; Yeaman, G.R.; Crispens, M.A.; Igarashi, T.M.; Osteen, K.G. Dioxin May Promote Inflammation-Related Development of Endometriosis. *Fertil. Steril.* 2008, *89*, 1287–1298, doi:10.1016/j.fertnstert.2008.02.102.
- [18]. Epidemiol, J. Effects of Dioxins on Human Health : A Review Shaw Watanabe , Kimiyoshi and Masahito Nagahashi Polychlorinated Dibenzo-p-Dioxins and Dibenzofurans ( PCDD / PCDF ) Occur as Unwanted by-Products of Thermal Processes , so the Major Part of Their Environmenta. 1998, *9*, 1–13.
- [19]. Kogevinas, M. Human Health Effects of Dioxins: Cancer, Reproductive and Endocrine System Effects. *Hum. Reprod. Update* 2001, *7*, 331–339, doi:10.1093/humupd/7.3.331.
- [20]. Yang, B.; Ying, G.G.; Zhao, J.L.; Liu, S.; Zhou, L.J.; Chen, F. Removal of Selected Endocrine Disrupting Chemicals (EDCs) and Pharmaceuticals and Personal Care Products (PPCPs) during Ferrate(VI) Treatment of Secondary Wastewater Effluents. *Water Res.* 2012, *46*, 2194–2204, doi:10.1016/j.watres.2012.01.047.
- [21]. Gao, X.; Kang, S.; Xiong, R.; Chen, M. Environment-Friendly Removal Methods for Endocrine Disrupting Chemicals. *Sustain.* 2020, *12*, 1–16, doi:10.3390/su12187615.
- [22]. Imparato, C.; Bifulco, A.; Silvestri, B.; Vitiello, G. *Recent Advances in Endocrine Disrupting Compounds Degradation through Metal Oxide-Based Nanomaterials*; 2022; Vol. 12; ISBN 3908176859.
- [23]. Azizi, D.; Arif, A.; Blair, D.; Dionne, J.; Fillion, Y.; Ouarda, Y.; Pazmino, A.G.; Pulicharla, R.; Rilstone, V.; Tiwari, B.; et al. A Comprehensive Review on Current Technologies for Removal of Endocrine Disrupting Chemicals from Wastewaters. *Environ. Res.* 2022, *207*, 112196, doi:10.1016/j.envres.2021.112196.
- [24]. Murray, A.; Örmeci, B.; Lai, E.P.C. Removal of Endocrine Disrupting Compounds from Wastewater Using Polymer Particles. *Water Sci. Technol.* 2016, *73*, 176–181, doi:10.2166/wst.2015.481.
- [25]. Pan, B.; Pan, B.; Zhang, W.; Lv, L.; Zhang, Q.; Zheng, S. Development of Polymeric and Polymer-Based Hybrid Adsorbents for Pollutants Removal from Waters. *Chem. Eng. J.* 2009, *151*, 19–29, doi:10.1016/j.cej.2009.02.036.
- [26]. Al Sharabati, M.; Abokwiek, R.; Al-Othman, A.; Tawalbeh, M.; Karaman, C.; Orooji, Y.; Karimi, F. Biodegradable Polymers and Their Nano-Composites for the Removal of Endocrine-Disrupting Chemicals (EDCs) from Wastewater: A Review. *Environ. Res.* 2021, *202*, 111694, doi:10.1016/j.envres.2021.111694.
- [27]. Cáceres, C.; Bravo, C.; Rivas, B.; Moczko, E.; Sáez, P.; García, Y.; Pereira, E. Molecularly Imprinted Polymers for the Selective Extraction of Bisphenol A and Progesterone from Aqueous Media. *Polymers (Basel)*. 2018, *10*, 1–16, doi:10.3390/polym10060679.
- [28]. Matějčiček, D.; Grycová, A.; Vlček, J. The Use of Molecularly Imprinted Polymers for the Multicomponent Determination of Endocrine-Disrupting Compounds in Water and Sediment. *J. Sep. Sci.* 2013, *36*, 1097–1103, doi:10.1002/jssc.201200992.
- [29]. Syeda, S.E.Z.; Nowacka, D.; Khan, M.S.; Skwierawska, A.M. Recent Advancements in Cyclodextrin-Based Adsorbents for the Removal of Hazardous Pollutants from Waters. *Polymers (Basel)*. 2022, *14*, doi:10.3390/polym14122341.
- [30]. Al Sharabati, M.; Abokwiek, R.; Al-Othman, A.; Tawalbeh, M.; Karaman, C.; Orooji, Y.; Karimi, F. Biodegradable Polymers and Their Nano-Composites for the Removal of Endocrine-Disrupting Chemicals (EDCs) from Wastewater: A Review. *Environ. Res.* 2021, *202*, 111694, doi:10.1016/j.envres.2021.111694.
- [31]. Bertoldi, C.; Cercena, R.; Dal-b, A.G.; Soares, R.M.D.; Fernandes, A.N. Colloids and Surfaces A : Physicochemical and Engineering Aspects Adsorption of Endocrine Disrupting Compounds from Aqueous Solution in Poly ( Butyleneadipate-Co-Terephthalate ) Electrospun Microfibers. *Colloids Surfaces A Physicochem. Eng. Asp.* 2020, 125800.
- [32]. Cevallos-Mendoza, J.; Amorim, C.G.; Rodríguez-Díaz, J.M.; Montenegro, M. da C.B.S.M. Removal of Contaminants from Water by Membrane Filtration: A Review. *Membranes (Basel)*. 2022, *12*, 1–23, doi:10.3390/membranes12060570.
- [33]. Physicochemical, A.; Processes, T. *Advanced Physicochemical Treatment Processes*; 2006; ISBN 1588293610.

- [34]. Katibi, K.K.; Yunos, K.F.; Man, H.C.; Aris, A.Z.; bin Mohd Nor, M.Z.; binti Azis, R.S. Recent Advances in the Rejection of Endocrine-Disrupting Compounds from Water Using Membrane and Membrane Bioreactor Technologies: A Review. *Polymers (Basel)*. 2021, *13*, 1–52, doi:10.3390/polym13030392.
- [35]. Niavarani, Z.; Breite, D.; Prager, A.; Abel, B.; Schulze, A. Estradiol Removal by Adsorptive Coating of a Microfiltration Membrane. *Membranes (Basel)*. 2021, *11*, 1–13, doi:10.3390/membranes11020099.
- [36]. Islam, M.D.; Uddin, F.J.; Rashid, T.U.; Shahruzzaman, M. Cellulose Acetate-Based Membrane for Wastewater Treatment—A State-of-the-Art Review. *Mater. Adv.* 2023, 4054–4102, doi:10.1039/d3ma00255a.
- [37]. Ghaee, A.; Shariaty-Niassar, M.; Barzin, J.; Matsuura, T.; Fauzi Ismail, A. Preparation of Chitosan/Cellulose Acetate Composite Nanofiltration Membrane for Wastewater Treatment. *Desalin. Water Treat.* 2016, *57*, 14453–14460, doi:10.1080/19443994.2015.1068228.
- [38]. Basile, T.; Petrella, A.; Petrella, M.; Boghetich, G.; Petruzzelli, V.; Colasuonno, S.; Petruzzelli, D. Review of Endocrine-Disrupting-Compound Removal Technologies in Water and Wastewater Treatment Plants: An EU Perspective. *Ind. Eng. Chem. Res.* 2011, *50*, 8389–8401, doi:10.1021/ie101919

# Production of bioethanol from apple pomace and its suitability as a fuel

Krzywda N<sup>1</sup>, Czmajduch K<sup>1</sup>, Krent M<sup>1</sup>, Kubik M<sup>1</sup>, Mendrela P<sup>2</sup>, Modelski A<sup>1</sup>, Paszkowski J<sup>1</sup>, Podbrożny G<sup>1</sup>, Gnida A<sup>3</sup>, Przybyła G<sup>4</sup>

<sup>1</sup> College of studies, Silesian University of Technology

<sup>2</sup> PhD School, Silesian University of Technology, email: piotr.mendrela@polsl.pl

<sup>3</sup> Environmental Biotechnology Department, Faculty of Energy and Environmental Engineering, Silesian University of Technology, email: anna.gnida@polsl.pl

<sup>4</sup> Department of Thermal Technology, Faculty of Energy and Environmental Engineering, Silesian University of Technology, email: grzegorz.przybyla@polsl.pl

---

## Abstract

The production of bioethanol from biomass constituting post-production waste is one of the alternatives in the context of the crisis of energy raw materials. The aim of this report is to show the potential of fruit waste, especially apple waste, for the recovery of valuable ingredients and their use in the production of biofuel, such as bioethanol.

**Keywords:** biowaste, apple pomace, biofuel, bioethanol

---

## 1. Introduction

The use of apple pomace in bioethanol production is, on the one hand, a response to the need for waste management from fruit processing industry: approximately 10-35% of the initially processed raw material goes unused, and during traditional juice extraction, unused biomass accounts for 20-25% of the raw material [1]. On the other hand, these pomaces are playing an increasing role in the development of biofuel production technology, becoming a stronger alternative to fossil fuels [2]. This allows for cost-effective, efficient, and environmentally beneficial production in the context of sustainable development.

## 2. Characteristics of bioethanol as a fuel

Ethanol as a fuel exhibits a range of unique properties that set it apart from traditional fossil fuels. In comparison to industrial ethanol, it has much better availability, as we can utilize bio-waste for its production. Additionally, the costs associated with obtaining ethanol from fruit waste, such as apples, are practically negligible compared to industrial ethanol production [2]. Biofuel is characterized by a high oxygen content, which directly translates to better combustion efficiency and a reduction in hydrocarbon and carbon monoxide emissions. Bioethanol also has a high octane rating (107), which is a direct indicator of engine performance, as well as a high ignition energy (0.91 MJ/kg) [3]. The higher the octane number, the greater the compression pressure the fuel can withstand before ignition. Therefore, high-performance engines should be powered by high-octane fuel to prevent knocking. Despite the low energy content per litre of fuel (21.2 MJ/dm<sup>3</sup>), it is possible to increase the engine compression ratio, shorten the combustion time, which directly affects the unit's power. Ethanol can be made from starch-based crops by dry mill or wet-mill. In that type of production to get ethanol special crops are used that are specifically grown to be converted into ethanol. While bioethanol is using biomass, which means that there are no wasted crops. Main environmental issues related to bioethanol production are land and water resource requirements air and ground water pollution. Depending on production process or even feedstock biofuels can emit more GHGs than some fossil fuels on an energy equivalent basis.



### 3. Apple pomace as a raw material

Apple pomace is a byproduct in the apple processing industry when making juice, cider, wine, distilled spirits, or vinegar. The solid residue constitutes 20–35% of the fresh fruit's mass. This means that this residue consists of a mixture of seeds, skin, core, pulp, calyx, and stems. This mixture typically contains 9.5% to 22% carbohydrates and 3.6% sugars, with a low pH level of 3–4 [4]. To maximize its conversion into bioethanol suitable for replacing fossil fuels in internal combustion engines, it is important for this residue to contain a significant amount of organic compounds, including complex sugars like cellulose, and to have substantial moisture content [5]. The water content in this mixture is crucial for bioethanol production because fermentative microorganisms, such as yeast, require water for converting sugars into alcohol. The average dry matter content in apple pomace was 93.2% [6]. The plant fiber content in such pomace was 99.5%, with the largest amount of cellulose (43 g/100 g of dry matter). Hemicelluloses were determined at a value of 24 g/100 g dry matter. Apple pomace had a significant pectin content (12 g/100 g dry matter), which is considered rich in this ingredient to such an extent that it is recovered from them. The lignin content was determined in apple pomace, i.e. 20 g/100 g of dry matter [6].

The chemical composition can vary depending on the apple variety, processing method, and fruit ripeness. In summary, apple pomace mainly contains chemical compounds such as carbohydrates (fructose, glucose, sucrose), dietary fiber (including cellulose, hemicellulose, and pectin), polyphenols (flavonoids like quercetin and catechins, as well as phenolic acids like chlorogenic acid), lignin, proteins, lipids, as well as vitamins and minerals (vitamin C, potassium) [7]. Apple pomace of a 12.6% moisture contain 1.05% of ash and characterises with mass density of 1552 kg/m<sup>3</sup>. Its combustion value and net calorific value is 21299 kJ/kg and 19775 kJ/kg, respectively [8]. Elemental analysis of such apple pomace is presented in Figure 3.1.

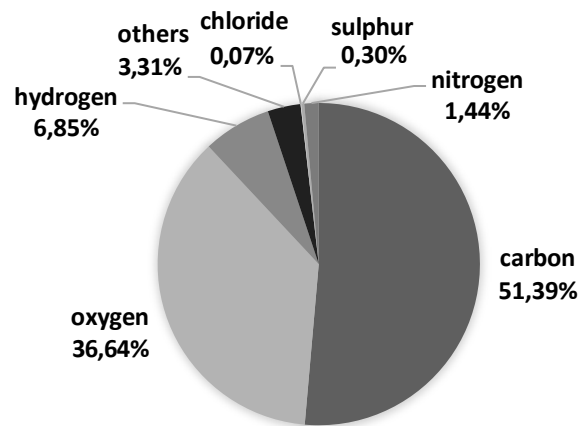


Fig. 3.1 Apple pomace elemental composition (based on [8])

In Poland, apple trees accounted for half (50.2%) of the total area occupied for growing fruit plants, and its share in the total apple harvest in the EU accounted for 24.3% [1]. According to data Central Statistical Office in Poland in the 2018/2019 season for juice production 3.15 million tons were allocated for dense tons of apples [9]. Comparing it to the harvest from apple orchards in 2023, this year is initially estimated at almost 3.9 million tons [10]. However the apple harvest has decreased compared to the previous year i.e. 2022 by 9%. A significant drop in yield is caused by the effort of the trees in the previous season and unfavourable weather conditions in present. Assuming, that pomace, which is produced during the production of juices, constitute 20% of the raw material used, as many as 780 thousand tons of pomace may be obtained.

### 4. Production of bioethanol from apple pomace

Typically the production of bioethanol rely on the processing of lignocellulosic biomass (LCB). Cellulose-hemicellulose complexes are surrounded by lignin, creating a physical barrier for biomass during hydrolysis, which aims to produce fermentable sugars. The process begins with pretreatment, which breaks down the LCB structure, making it more amenable to hydrolysis [11].

Hydrolysis is a critical step in the bioethanol production process, where fermentable sugars are derived from lignocellulosic pulp. This process can be carried out using either dilute or concentrated acid. In the dilute acid method, a 1% sulfuric acid solution is heated to 215°C to rapidly hydrolyze cellulose and hemicellulose. This method achieves a sugar recovery efficiency of around 50%, but there's a risk of glucose degradation. On the other hand, the concentrated acid method employs higher acid concentrations at lower temperatures and pressures, resulting in nearly 100% sugar recovery efficiency. However, this method is slower and is typically used in batch processes [12].

Following hydrolysis, the next phase is fermentation. This is where the fermentable sugars are converted into bioethanol. There are several methods of fermentation, including batch, fed-batch, and continuous [13]. Batch fermentation is simple but not efficient for large-scale production due to its low ethanol yield and extended fermentation time. Fed-batch fermentation combines the batch and continuous modes, increasing ethanol production through controlled substrate addition. This method offers higher yields, increased oxygen, shorter fermentation time, and low medium toxicity. Continuous fermentation involves the constant addition of nutrients, substrate, and culture to the bioreactor. This method is beneficial due to its smaller reactor size, higher ethanol yield, and cost efficiency, but it has a higher susceptibility to contamination.

The last one is purification which involves removing water and impurities from ethanol to complete the process.

Processing of fruit-based waste in the alcoholic fermentation can be carried out as fermentation in the liquid (LSF) or solid state (SSF). Due to the natural state of matter of apple pulp/pomace, the second option seems to be more natural. In this case, biomass is not only a source of substrates for ethanol-producing organisms, but also their habitat. Literature data also indicate that SSF requires less water thus smaller reactors can be used and the energy consumption from aeration is lower. There is also lower contamination probability due to low water availability. However, diffusion of nutrients can be a limiting factor and the process monitoring due to the state is also problematic and not yet solved [14].

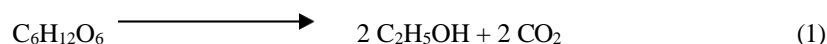
The solid-state fermentation (SSF) using apple pomace for bioethanol production may involve several main steps: pomace preparation, alcoholic fermentation, ethanol recovery and purification, as well as storage of the final product.

- Preparation of pomace

Apple pomace, which is a byproduct of apple juice pressing, is produced in a hydraulic press and then dried. If the biomass is to be used for laboratory research, it may be additionally crushed or milled to powder form. It is stored for a short time in sterile containers. The finished raw material mainly consists of fruit peel (95%), seeds (2-4%), and stem pieces (1%) [15]. These parts of the plant are rich in carbohydrates, which transform into alcohol during the fermentation process.

- Alcoholic fermentation

Alcoholic fermentation is a process in which microorganisms (such as yeast and bacteria) under anaerobic conditions convert sugar into ethanol and carbon dioxide. The reaction can be presented in a simplified form:



Yeasts are aerobic organism, so under anaerobic conditions, their metabolism undergoes changes, intensifying the glycolysis process. As a result of glycolysis, pyruvate is produced from sugar. Subsequently, in the reaction catalyzed by pyruvate decarboxylase, acetaldehyde is formed, which is then reduced to ethanol in the alcohol dehydrogenase process [16].

The method of solid-state fermentation (SSF) can be defined as a way of fermentation that occurs with a minimal amount of moisture required for microorganisms to grow and metabolize optimally on solid substrates. Noteworthy advantage of this method is high product concentration with a relatively low energy being required. This technique has been developed since ancient times and currently offers prospects for the utilization or management of solid waste (such as apple pomace) [17]. When planning an experiment, it is essential to select an appropriate amount of substrate, the type of microorganisms (usually these are yeasts like *Saccharomyces cerevisiae*, but sometimes strains of bacteria are also used) and to plan suitable reaction conditions, considering factors such as the concentration of additional enzymes (if used), temperature, pH, and time. It is also essential to protect the experiment from contamination by other microorganisms and undesirable chemical compounds, so they do not influence the research results.

- Obtaining and purifying bioethanol

After the fermentation process, bioethanol is obtained in a water mixture. Therefore, it needs to undergo a purification process. The primary method for this is to carry out distillation, which allows the separation of ethanol from water and other organic impurities. Distillation is a method of separating mixtures that utilizes differences in the volatility of mixture components. When the mixture is heated in a distillation apparatus, components with a low boiling point accumulate in the vapor phase. The vapor is then condensed to obtain the separated component in the liquid phase. To obtain pure ethanol, other methods can also be used, such as adsorption, ozonation, or stripping (during which one or more components are removed from the liquid stream using a vapor stream) [18].

- Bioethanol storage

An important consideration is the storage of obtained bioethanol. It is a highly flammable and combustible substance and must be appropriately secured [19]. It should be stored in a cool, dry place, away from direct sunlight and hot surfaces. It is best to choose containers that will not corrode due to the presence of bioethanol and may be made of stainless steel. It's advisable for them to have a quality certification. Also, it should be kept out of the reach of children and animals.

### 5. Bioethanol versus conventional fuel

Ethanol, characterized by its high octane number, oxygen content, and biodegradability, serves as an effective additive to automotive fuels or as an independent fuel. Ethanol is a clean, colorless and non-toxic liquid. It has a higher octane number than that of gasoline and therefore it can be used at higher compression ratios in spark ignition (SI) engines. Ethanol has a higher flame speed according to other liquid fuels such as diesel and gasoline due to contains hydroxyl group [20]. In terms of environmental issues such as global warming, ethanol can significantly reduce CO<sub>2</sub> emissions as fuel, because of his ecofriendly production with an use of natural ingredients. Currently, ethanol is primarily utilized in gasoline-ethanol blends to power internal combustion engines. Brazil stands as a notable example of a nation employing pure ethanol as a motor fuel. This country has an extensive history of utilizing sugarcane-derived ethanol for fuel, and a significant portion of the vehicles operating in Brazil are flex-fuel vehicles. These vehicles are capable of running on either pure ethanol or a combination of petrol and ethanol. Table 5.1 presents a comparison of selected properties relevant to internal combustion engine fueling for ethanol, gasoline, and diesel fuel.

Table. 5.1. Comparison of ethanol properties with gasoline and diesel fuel [21]–[23]

Parameter		Ethanol	Gasoline	Diesel oil
Chemical formula		C <sub>2</sub> H <sub>5</sub> OH	A mixture of lighter hydrocarbons (C <sub>4</sub> to C <sub>12</sub> )	A mixture of heavier hydrocarbons (C <sub>8</sub> to C <sub>25</sub> )
Lower heating value	MJ/kg (MJ/dm <sup>3</sup> )	26.7 (21.1)	43.4 (32)	42.6 (36)
Composition	Carbon	52.2	85 - 88	84 - 87
	Hydrogen	13.1	12 - 25	13 - 16
	Oxygen	34.7	0 - 4	0
Density	kg/dm <sup>3</sup>	0.79	0.69-0.79	0.81-0.89
Flash point	°C	13	-43	74
Autoignition temperature	°C	423	257	316
Flammability limit	Lower	4.3	1.4	1
	Higher	19	7.6	6
Octan number (Cetene number)	RON	108.6	88-100	(44 – 51)
	MON	89.7	80-90	

When comparing the properties of ethanol to those of gasoline and diesel oil, it becomes evident that ethanol can serve as a standalone fuel for spark-ignition engines. In a comparative analysis of ethanol, gasoline, and diesel oil

properties, it is observed that ethanol can function as an independent fuel for spark-ignition engines. However, due to its high auto-ignition temperature, this fuel is not suitable for direct use in compression-ignition engines [24]. Ethanol exhibits a lower calorific value compared to both gasoline and diesel. Assuming an internal combustion engine maintains equivalent energy efficiency with both ethanol and gasoline, utilizing fuel tanks of identical capacity for each fuel would result in a diminished driving range for vehicles powered by ethanol. Within the context of Europe's existing filling station infrastructure, this aspect does not present a significant challenge. However, it does require users to refuel their cars more frequently.

Despite gasoline's calorific value being approximately 38% higher than that of ethanol, combustion engines can achieve similar power levels with both fuels. This is attributed to ethanol's lower air requirement for combustion, resulting in nearly equivalent calorific values for ethanol-air and petrol-air mixtures, when temperature, pressure, and excess air ratio are held constant for both mixtures [24].

## **6. Prospects for the use of apple pomace based bioethanol**

### **6.1 Potential of bioethanol production from apple pomace**

Apple pomace (AP) is a material rich of sugars. Depending on the species, this biomass may contain from 33-69% of sugars (328 - 689 mg of sugar per gram of dry apple pomace) [25]. Taking into account the average moisture of pomace and the theoretical maximum ethanol yield of 0.51 per unit of sugar (g/g) resulting from equation (1), it can be calculated that theoretically app. 50-106 g of ethanol could be recovered from one kilogram of wet pomace. This gives app. 48-100 ml of 95% ethanol from one kilogram of fresh AP. Taking into account the annual production of apples, which is approximately 90 million tons of apples per year, which gives at least 18 ml tons of pomace [26], most of which is waste sent to landfills, the use of AP for the production of bioethanol seems to be justified. Moreover, it should be mentioned that on a global scale, Poland is the fourth country in terms of apple production. The annual production of apples is over 3 ml tons, and their processing generates approximately 0.6 - 1.1 million tons of pomace [26]. If the potential of this biomass is used entirely for the production of bioethanol, a yield of 0.2 - 0.8 million tons of ethanol can be expected.

### **6.2 Challenges of producing bioethanol from apple pomace**

The first significant issue related to processing apples into bioethanol is the waste management. Waste generated from the bioethanol production process, including apple residues, tends to decompose during prolonged storage. This necessitates proper waste storage. One of the factors accelerating this degradation is the presence of methane, which naturally occurs in apples, as well as in other food products. Methane speeds up the degradation process, posing a challenge to maintaining the quality of the raw material and negatively impacting the profitability of production [7].

Another challenge is the logistics of raw materials. The production of ethanol and other products from apple residues requires continuous access to the raw material throughout the year. Unfortunately, most apple processing facilities may struggle to ensure a consistent supply of raw materials. The lack of consistent access adversely affects the profitability of production. One solution to this problem is the drying of apple residues, which enhances their durability and allows for storage. Dried residues can also be concentrated, reducing transportation costs to the processing facility. However, it's worth noting that the drying and concentration process introduces additional production costs [7].

Other issue concerns apple seeds, which contain amygdalin, a cyanogenic glycoside. In the presence of the enzyme  $\beta$ -glucosidase, which naturally occurs in the human body, amygdalin can degrade, leading to the formation of cyanide. Cyanide is an exceptionally toxic substance to humans, and exposure to it poses a serious health risk. Therefore, it is necessary to exercise caution when handling apple seeds and ensure proper disposal practices to avoid potential cyanide-related risks [27].

A different problem pertains to fruit pomace, such as those derived from apples. They are characterized by low durability and stability. Due to their high water content, which can reach as high as 73% in the case of apple pomace, they are particularly susceptible to the rapid growth of microbiological contaminants. This means that fruit pomace can easily spoil, posing a challenge in terms of waste disposal and efficient raw material management.

Effective processing and disposal of pomace are required to prevent resource wastage and ensure hygienic and safe management of fruit waste [1].

### 6.3 Applications of bioethanol as fuel

Currently, bioethanol has a range of applications, contributing to sustainable development in various areas. This results in reduced emissions of pollutants [28]. It is used as a component in vehicle fuel blends, promoting sustainable transportation by adding it to gasoline. Beyond the transportation sector, bioethanol finds applications in the medical, cosmetic, and food industries. In terms of energy, research suggests that bioethanol can be effectively used in co-combustion with coal in existing energy facilities, especially in modern installations equipped with advanced emissions control systems [29].

In the transportation sector, ethanol is widely used. Many reports predict that the most promising solution is adding ethanol to gasoline, because of lack of changes that need to be implemented in modern internal combustion engines. Ethanol is often used as an add-on to gasoline, because of its properties. Blends with low ethanol content show a more notable synergy effect and vaporize well. The property described above combined with the high flame speed of ethanol leads to a rapid combustion and increased power. Based on ethanol/gasoline ratios we can list certain value combination where E stands for ethanol and number is equivalent of ethanol percentage in the mix – E0, E5, E10, E15, E20, E25, E30, E50, E75, E100 (border values represent pure ethanol and gasoline). In case of constructing slightly modified engines, internal combustion engines (ICE) can be more efficient and more environmental friendly while using only ethanol as a fuel [12]. For example, most gasoline in the United States and Brazil contains ethanol additives. However, litre of ethanol contains less energy than a litre of gasoline, which can lead to lower fuel economy when operating ethanol-powered vehicles, especially in the case of E85 blends, which contain 83% ethanol [3].

Bioethanol plays a significant role in various types of fuels, offering different ethanol content ratios and thus allowing its use in different types of vehicles and machinery. Below are a few examples of fuels containing bioethanol:

- E5: Standard gasoline that contains up to 5 percent bioethanol by volume.
- E10: Standard gasoline containing 10 percent bioethanol. Available in the markets of 18 European Union countries and the United Kingdom, including Hungary, Slovakia, Bulgaria, and Romania. It can be used in most car models produced after the year 2000.
- E20: Gasoline containing 20 percent bioethanol.
- E85: A blend of ethanol and gasoline containing up to 85 percent ethanol. Widely available in the USA, Brazil, Scandinavia, and France. Its use requires a flex-fuel system-equipped vehicle.
- ED95: A bioethanol-based fuel designed for semi-trucks and buses. It consists of 95 percent bioethanol, with the remaining portion being additives that support engine performance.

These various bioethanol-based fuels allow for flexible adaptation to different transportation needs while supporting sustainable development goals and the reduction of greenhouse gas emissions. Their introduction to the market represents a step towards a more environmentally friendly and sustainable future in the transportation sector [30].

## 7. Conclusions

Due to the amount of apple waste in Poland and other countries not only producing but also processing apples, their management through the recovery of valuable ingredients seems to be justified. The use of sugar resources contained in apple pomace can be used to produce bioethanol, which has been gaining popularity in recent years as a fuel in itself or as a fuel additive, providing similar energy properties.

## Acknowledgment

The necessary financial support for carrying out the research activities among the project entitled “Bioethanol from apple pomace as engine fuel” is provided by Fluor Global University Sponsorship Program (GUSP).

## References

- [1] L. Kawecka and S. Galus, Fruit pomace – characteristics and possibilities of recycling (in polish). *Technol. Prog. food Process.*, vol. 1, pp. 156–167, 2021.
- [2] M. M. Khandaker, A. U. Abdullahi, D. M. Abdulrahman, A. N. Badaluddin, and S. K. Mohd, Bio-Ethanol Production from Fruit and Vegetable Waste by Using *Saccharomyces cerevisiae*. *Bioethanol Technologies*, no. November, IntechOpen, 2020. doi: 10.5772/intechopen.94358.
- [3] L. Meng, Ethanol in Automotive Applications. *Ethanol*, Elsevier, 2019, pp. 289–303. doi: 10.1016/B978-0-12-811458-2.00011-0.
- [4] P. A. Gulhane, A. V Gomashe, and K. Kadu, Apple Pomace: A Potential Substrate for Ethanol Production. *Int. J. Res. Stud. Biosci.*, vol. 3, no. 6, pp. 110–114, 2015, [Online]. Available: [www.arcjournals.org](http://www.arcjournals.org)
- [5] S. Vaez, K. Karimi, J. F. M. Denayer, and R. Kumar, Evaluation of apple pomace biochemical transformation to biofuels and pectin through a sustainable biorefinery. *Biomass and Bioenergy*, vol. 172, p. 106757, May 2023, doi: 10.1016/j.biombioe.2023.106757.
- [6] A. Nawirska and M. Kwasniewska, Fiber fractions in fruit pomace. *Acta Sci. Pol. Technol. Aliment.*, vol. 03, no. 1, pp. 13–20, 2004.
- [7] M. Magyar, L. da Costa Sousa, M. Jin, C. Sarks, and V. Balan, Conversion of apple pomace waste to ethanol at industrial relevant conditions. *Appl. Microbiol. Biotechnol.*, vol. 100, no. 16, pp. 7349–7358, 2016, doi: 10.1007/s00253-016-7665-7.
- [8] W. Kosakowski, M. A. Bryszewska, and P. Dziugan, Biochars from Post-Production Biomass and Waste from Wood Management: Analysis of Carbonization Products. *Materials (Basel)*, vol. 13, no. 21, p. 4971, Nov. 2020, doi: 10.3390/ma13214971.
- [9] W. Plochanski, M. Mieszczakowska-Frać, K. Rutkowski, and D. Konopacka, Traditional and innovative directions for apple management in Poland (in Polish), Skierniewice, 2019.
- [10] Central Statistical Office, Preliminary estimate of the main agricultural and horticultural crops in 2023 (in polish). 2023.
- [11] E. Gołębiwska, M. Kalinowska, and G. Yildiz, Sustainable Use of Apple Pomace (AP) in Different Industrial Sectors. *Materials (Basel)*, vol. 15, no. 5, 2022, doi: 10.3390/ma15051788.
- [12] R. Ilves, A. Küüt, and J. Olt, Ethanol as Internal Combustion Engine Fuel. *Ethanol*, Elsevier, 2019, pp. 215–229. doi: 10.1016/B978-0-12-811458-2.00008-0.
- [13] S. T. Magar, Batch vs Fed-Batch vs Continuous Culture- 20 Key Differences. *Microbe Notes*, 2021. <https://microbenotes.com/batch-vs-fed-batch-vs-continuous-culture/>
- [14] C. R. Soccol, E. S. F. da Costa, L. A. J. Letti, S. G. Karp, A. L. Woiciechowski, and L. P. de S. Vandenberghe, Recent developments and innovations in solid state fermentation. *Biotechnol. Res. Innov.*, vol. 1, no. 1, pp. 52–71, 2017, doi: 10.1016/j.biori.2017.01.002.
- [15] A. Kailay, Production of ethanol from apple pomace using *saccharomyces cerevisiae*, *Trichoderma reesei* and *Myceliophthora thermophila* fungi. McGill University, Quebec, 2019.
- [16] A. Ziemińska-Buczyńska and A. Węgrzyn, *Microbiology laboratory - selected exercises in general and applied microbiology (in polish)*. Gliwice: Silesian University of Technology Publishing, 2013.
- [17] A. Pandey, Solid-state fermentation, *Biochem. Eng. J.*, vol. 13, pp. 81–84, 2003.
- [18] S. Onuki, J. A. Koziel, J. (Hans. van Leeuwen, W. S. Jenks, and D. Grewell, Ethanol production, purification, and analysis techniques: a review. *An ASABE Meet. Present.*, no. Paper Number: 085136, 2008.
- [19] Y. Ma, X. R. Wang, T. Li, J. Zhang, J. Gao, and Z. Y. Sun, Hydrogen and ethanol: Production, storage, and transportation. *Int. J. Hydrogen Energy*, vol. 46, no. 54, pp. 27330–27348, Aug. 2021, doi:

- 10.1016/j.ijhydene.2021.06.027.
- [20] L.-W. Jia, M.-Q. Shen, J. Wang, and M.-Q. Lin, Influence of ethanol–gasoline blended fuel on emission characteristics from a four-stroke motorcycle engine, *J. Hazard. Mater.*, vol. 123, no. 1–3, pp. 29–34, Aug. 2005, doi: 10.1016/j.jhazmat.2005.03.046.
- [21] S. Eran, Ed., *Handbook of Air Pollution From Internal Combustion Engines*. Elsevier, 1998. doi: 10.1016/B978-0-12-639855-7.X5038-8.
- [22] The Engineering ToolBox, Fuels - Higher and Lower Calorific Values, [https://www.engineeringtoolbox.com/fuels-higher-calorific-values-d\\_169.html](https://www.engineeringtoolbox.com/fuels-higher-calorific-values-d_169.html)
- [23] R. L. Bechtold, *Alternative Fuels Guidebook: Properties, Storage, Dispensing, and Vehicle Facility Modifications*. Society of Automotive Engineers Inc, 2014.
- [24] V. R. Roso, N. D. S. A. Santos, C. E. C. Alvarez, F. A. Rodrigues Filho, F. J. P. Pujatti, and R. M. Valle, Effects of mixture enleanment in combustion and emission parameters using a flex-fuel engine with ethanol and gasoline. *Appl. Therm. Eng.*, vol. 153, pp. 463–472, May 2019, doi: 10.1016/j.applthermaleng.2019.03.012.
- [25] K. Bindon, S. Qi, S. Kassara, L. Nicolotti, A. Jouin, and M. Beer, Apple Pomace Compositional Data Highlighting the Proportional Contribution of Polymeric Procyanidins. *Molecules*, vol. 28, no. 14, 2023, doi: 10.3390/molecules28145494.
- [26] Atlas Big, Apple’s global production by country, <https://www.atlasbig.com/pl/kraje-wedlug-produkcji-jablek>
- [27] G. A. Martău, B.-E. Teleky, F. Ranga, I. D. Pop, and D. C. Vodnar, Apple Pomace as a Sustainable Substrate in Sourdough Fermentation. *Front. Microbiol.*, vol. 12, no. December, pp. 1–16, Dec. 2021, doi: 10.3389/fmicb.2021.742020.
- [28] D. Bacovsky, D. Matschegg, R. Janssen, D. Rutz, and B. Costanzo, Unlocking the bioethanol economy. United Nations Industrial Development Organization, 2022.
- [29] B. Latkowska, H. Fitko, and S. Stelmach, Assessment of fuel properties of a by-product from bioethanol production (in polish). *J. Ecol. Eng.*, no. 25, 2011.
- [30] Polska Organizacja Przemysłu i Handlu Naftowego, Zielony transport - Stan obecny i perspektywy. Polska organizacja przemysłu i handlu naftowego, 2022.

# Prospects for the application of mycorrhizal fungi in phytoremediation techniques

Daria Sławczyk, Anna Grobelak

*1*Affiliation: Faculty of Infrastructure and Environment, Czestochowa University of Technology, e-mail: [dariaslawczyk@gmail.com](mailto:dariaslawczyk@gmail.com)

*2*Affiliation: Faculty of Infrastructure and Environment, Czestochowa University of Technology, e-mail: [anna.grobelak@pcz.pl](mailto:anna.grobelak@pcz.pl)

---

## Abstract

The development of remediation technologies is essential in view of the generation of significant amounts of pollutants ending up in soils. The basis for such development is research and optimization of processes that can be used to improve the state of the natural environment. Phytoremediation with the application of mycorrhizal fungi might be considered as one of the future techniques used in the remediation of soils contaminated with heavy metals. In the article the basics of this process and its possible applications are described. What is more, the role of arbuscular mycorrhizal fungi and their impact on plants and soil are raised. Glomalin-related soil protein is specified as a glycoprotein of particular importance for this process. Furthermore, the possibilities of using organisms assisting in remediation are discussed.

**Keywords:** phytoremediation, mycorrhiza, mycorrhizal fungi, soil remediation, phytostabilization, arbuscular mycorrhizal fungi, glomalin-related soil proteins, heavy metals

---

## 1. Introduction

The main source of soil pollution is human activity, specifically the development of various industries, mining and agriculture, which lead to decline in soil fertility. The quality of soil may be significantly reduced due to the accumulation of pollutants such as heavy metals, which pose a severe threat to the environment and human health. The presence of such elements in soils causes a decrease in the content of nutrients available to plants and negatively interferes with the structure and properties of soils [1]. However, the main threat to human health in the context of the accumulation of heavy metals in soils, is the possibility of their entering the body through the consumption of contaminated food. This may lead to poisoning, kidney and liver damage, ovulation disorders, infertility, increased risk of cancer, etc. [2].

There are many remediation techniques aimed at reducing pollutants or completely removing them from contaminated areas. Physicochemical and biological processes can be mentioned here. Physical remediation techniques include for instance vitrification, rinsing and sorting, while chemical processes comprise methods based on oxidation and reduction reactions, hydrolysis or binding of contaminants through the use of lime, silicates or polymers [3]. Unfortunately, these methods do not result in the complete removal of contaminants such as heavy metals. Physical and chemical processes usually lead to the formation of transformed forms of metals or their accumulation in a specific place in soil [4]. However, technologies that use living organisms to clean the environment are a promising alternative to physicochemical processes. This is due to the multiple advantages of biological methods related to economic and social issues and low environmental risk.

## 2. Phytoremediation techniques

Phytoremediation is one of the biological technologies for the removal of pollutants by using plants. Name of this technology itself – „phytoremediation”, where the prefix „phyto-” (plant) has been added to word „remediation” - emphasizes the key role of plants as a remedy in improving the state of environment. Phytoremediation is based on the ability of plants to absorb, transform, metabolize and reduce the toxicity of pollutants. Plants used in this technology preeminently ought to be effortless to control, able to absorb large amounts of contaminants and characterized by a high tolerance to the presence of pollutants [5]. For instance, alfalfa (*Medicago sativa* L.) and poplar (*Populus* L.) are classified as hyperaccumulators, i.e. plants capable of absorbing and accumulating



significant amounts of heavy metals [6]. The basic characteristics of hyperaccumulators are presented in Figure 1.

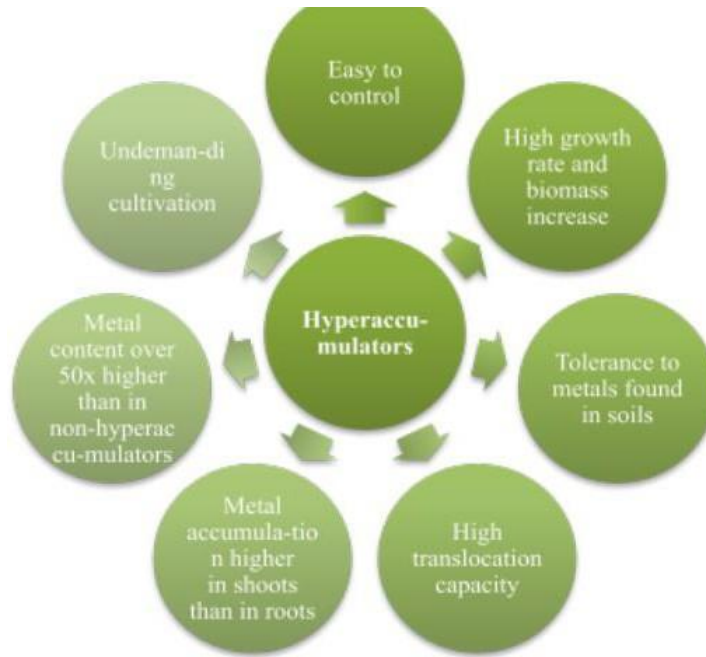


Fig. 1. Features of hyperaccumulators [5, 7]

After metals accumulation in plants, the biomass can be harvested and subjected to smelting processes aimed at metal recovery [7]. The most common phytoremediation techniques include phytoextraction, phytostabilization, phytodegradation, phytovolatilization and phytofiltration. A summary of these processes is presented in Table 1.

Table 1. Comparison of selected phytoremediation techniques [3, 5, 7-13]

Phytoremediation technique	Principle of operation	Type of contamination removed	Plant example
Phytoextraction	Uptake of compounds by roots, transport and accumulation in harvestable parts of plants;	Heavy metals;	<i>Alyssum bertolonii</i> , <i>Thlaspi caerulescens</i> , <i>Pteris vittata</i> , <i>Berkheya coddii</i> , <i>Phragmites australis</i> , <i>Miscanthus giganteus</i> , <i>Hordeum L.</i> ;
Phytostabilization	Limiting the possibility of pollutant transport in the environment through chemical substances secreted by plants. Immobilization may also take place due to the ability to accumulate pollutants through roots, precipitation reactions in the rhizosphere and mycorrhiza;	Heavy metals;	<i>Populus nigra L.</i> , <i>Nicotiana tabacum L.</i> , <i>Lemna minor L.</i> , <i>Brassica juncea L.</i> , <i>Festuca rubra L.</i> ;
Phytodegradation	Enzymatic decomposition of pollutants inside plant tissues;	Polycyclic aromatic hydrocarbons (PAHs), herbicides, pesticides;	<i>Solanum tuberosum</i> , <i>Populus sp.</i> , <i>Raphanus sativus</i> ;
Phytovolatilization	Transport of low molecular weight compounds to leaves and	Organic pollutants (e.g. volatile organic carbons),	<i>Astragalus bisulcatus</i> , <i>Oryza L.</i> , <i>Brassicca L.</i> ,

	evapotranspiration (release into the atmosphere);	Volatile inorganic compounds (e.g. arsenic, mercury);	<i>Brassica juncea</i> , <i>Medicago L.</i> ;
Phytofiltration	Purification of the water and water-soil environment with the participation of plant root system. Includes processes of absorption and precipitation;	Heavy metals, solutions with radionuclides, sewage components;	<i>Pteris vittata</i> , <i>Phragmites sp.</i> , <i>Salviniaceae</i> , <i>Helianthus annus L.</i> , <i>Carex sp.</i> ;

Due to the inability of heavy metals to biodegradation, they constitute one of the most consequential threats for soils. Therefore, more and more effective methods of removing them from the ground are constantly being sought. Phytoremediation can be mentioned here. To increase the solubility of heavy metals and, consequently, phytoavailability, soil acidification treatments or the addition of chelating agents are used. Moreover, liming the soil or adding organic substances results in a reduction in the phytotoxicity of these elements [5]. Mycorrhiza is also applied in metal phytoremediation.

### 3. Arbuscular mycorrhizal fungi (AMF)

Mycorrhiza-assisted remediation (MAR) includes ectomycorrhiza and endomycorrhiza. However, due to the limitation of ectomycorrhiza mainly to woody species [14] and wider range of tolerance of endomycorrhizal fungal species to unfavourable conditions [15], endomycorrhiza is fundamentally used in recultivation.

Arbuscular mycorrhizal fungi (AMF) are common in the environment and are capable of symbiosis with over 80% of land plant species [16]. AM fungi are classified in a phylum called *Glomeromycota* [7]. In most cases, AMF symbiosis with plants is based on the production of hyphae, spores, vesicles and arbuscules inside the plant roots and production of the same structures except arbuscules outside the roots [17]. The participation of mycorrhizal fungi in remediation increases the treatment area due to the extensive morphology of the mycelium [18]. The parameter determining the ratio of roots colonized by AMF to all examined segments is mycorrhization [15].

The role of mycorrhizal fungi in symbiosis with plants is based on the absorption of water and nutrients (mainly phosphorous) by the fungi and deliver them to the plant, while sequestering trace elements in the ground in form of unavailable chemical compounds [1]. A connection between the presence of mycorrhizae and the chlorophyll content in plants has also been noted. In the case of mycorrhizal colonization, the chlorophyll content increases. What is more, it has been proven that the plant defense system, specifically the activity of enzymes such as catalase, peroxidase and superoxide dismutase with antioxidant activity, is enhanced in the presence of mycorrhizal fungi [18]. Peroxidase protects plants against free radicals generated as a result of metal stress. It can be assumed that AMF inoculation minimizes plant stress due to the reduction of reactive oxygen species [7]. The impact of arbuscular mycorrhizal fungi on plants and soil is shown in Figure 2.

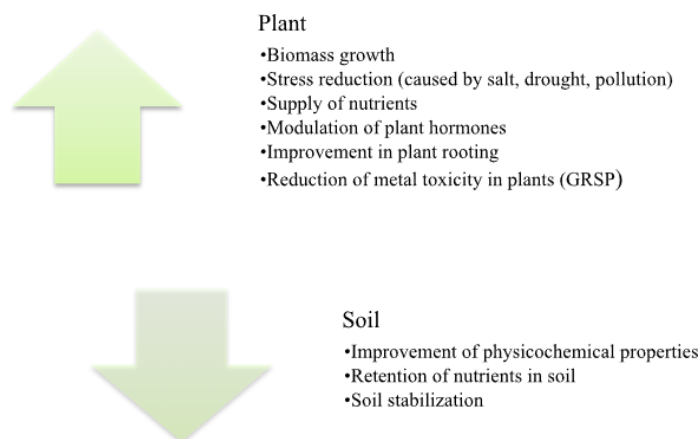


Figure 2. Impact of AMF on plants and soil [7, 14, 18]

AMF contribute to the phytostabilization of pollutants and changing the properties of the rhizosphere [16]. On the other hand, these organisms can increase the uptake of metals by plants through the phytoextraction process. This may be due to the specificity of mycorrhiza, type of contamination and soil properties. Detoxifying abilities of

AMF have also been reported. Fungal hyphae take up arsenate, detoxify it into arsenite in cytosol, and then release it back into the soil [7]. Generally, it is assumed that the use of native species gives better results than inoculating plants located in contaminated areas with commercial fungal species [1]. The use of native AMF occurring in saline environments may provide the most favourable results in improving plant tolerance to salt stress [18].

### 3.1. The role of mycorrhizal fungi in the remediation of soil contaminated with heavy metals

AMF has been reported to be involved in the uptake of elements such as zinc, cadmium and arsenic from the environment. What is more, these fungi are able to reduce the metal content in shoots and increase it in plant roots. Their presence also enhances the uptake of phosphorus, which is one of the key elements required for the growth and proper functioning of the entire plant [18]. This is due to the organic acids secreted by AMF, for example oxalic acid, which can intensify the absorption and transport of this element by plants. Additionally, available forms of phosphorus may be present in the soil as a result of the action of phosphatase derived from AM fungi [4].

Accumulation of heavy metals in the mycelium usually occurs through extraradical or intraradical mycelium. Adsorption takes place via positively charged particles such as cysteine or glutathione [15].

Research conducted by Li et al. (2023) confirmed the positive effect of AMF on the phytoremediation process. It has been proven that inoculation of rice (*Oryza sativa* L.) with the species *Glomus etunicatum* and *Glomus mosseae* results in reduction of mercury transport to plant tissues, increased rice biomass and its resistance to environmental stress [16]. Especially at higher concentrations of heavy metals in the soil, arbuscular mycorrhiza fungi promote the accumulation of these metals in roots [4]. Research may also focus on analyzing the reduction of plant stress on heavy metals. Luo et al. (2022) investigated the effects of AM fungi on *Canna indica* seedlings exposed to copper oxide nanoparticles stress. Authors observed a reduction in metal concentration in plant tissues and a reduction in the expression of genes responsible for copper transport and metallothionein. Moreover, improvement in the production of organic acids and the activity of antioxidant enzymes was noted [19].

It is worth emphasizing that in the discussed remediation process, additional factors that enhance the efficiency of the process, such as ethylenediaminetetraacetic acid (EDTA) or biochar, can also be used. Selection of the appropriate additive depends on the intended effect – limiting or enhancing the phytoextraction process. By absorbing metals, biochar limits their translocation. What is more, it increases soil pH and improves cation exchange capacity [20]. While, EDTA increases the bioavailability and phytoextraction of heavy metals [21].

In addition to the removal of heavy metals, research was also conducted on phytoremediation of soils contaminated with benzo(a)pyrene, polycyclic aromatic hydrocarbons (PAHs) or polyvinyl chloride with the application of mycorrhizal fungi [14].

### 3.2. GRSP as an indicator of remediation effectiveness

Spores and hyphae of AM fungi produce glomalin-related soil proteins (GRSP). The role of these proteins is to improve the properties of the rhizosphere, modulate the concentration of plant hormones and stimulate root development and plant growth also under stressful conditions. In a soil environment where drought is a stress factor, GRSP modulates the levels of auxins, abscisic acid and methyl jasmonate, which is reflected in the physiological state of plants [18].

GRSP, as a water-soluble glycoprotein, reduces the bioavailability of heavy metals by chelation. There is a certain connection between the presence of GRSP and the concentration of metals in plant tissues. Based on the results of numerous studies, it can be concluded that glomalin-related soil proteins limit the translocation of heavy metals such as lead, nickel, cadmium, zinc and copper from the soil to the plant. What is more, the amount of GRSP produced by arbuscular mycorrhizal fungi increases under stressful conditions [15]. Research indicates the ability of glomalin to sequester carbon and heavy metals. It was reported that 1 gram of glomalin sequesters 4.3 mg of copper, 0.08 mg of cadmium and 1.12 mg of lead [7]. Binding of metals takes place with the participation of functional groups in the GRSP molecule, such as hydroxyl and carboxyl groups [22].

The content of glomalin-related soil proteins can be increased, e.g. by species such as *R. intraradices*, *F. mosseae* and *G. versiforme*, which is also related to a decrease in the accumulation of heavy metals in plants [16]. Besides application of different species of AMF to reduce the concentration of lead and cadmium accumulating in corn proved profitable. In this instance, an increase in the GRSP content in the soil was noted [15].

Interestingly, some of the amino acid sequences of this glycoprotein are similar to those found in heat shock protein 60. This protein is produced by cells in response to environmental stress, similarly to glomalin-related soil protein [22].

#### 4. Participation of other soil organisms in phytoremediation with the application of fungi

Soil is a reservoir of numerous organisms that interact with each other, modifying its condition. Microorganisms existing in soil are involved in biogeochemical cycle due to their participation in the flow of energy or decomposition of organic remains [23].

The effectiveness of mycorrhiza-assisted remediation is influenced, among others, by bacteria and earthworms that inhabit the soil. It has been shown that the Rhizobium bacteria additionally promotes the mycorrhiza process between legumes and fungi. The nitrogen-fixing bacterium increases mycelial growth [14] and simultaneously fungi provide phosphorus, which assists in nitrogen fixation [5]. Moreover, the interaction between microorganisms indirectly enhance enzymatic activity of soil. Analyzing the results of research conducted by Ren et al. (2019), it can be concluded that the production of phytochelatin synthase and low molecular weight organic acids is increased when *Sesbania rostrata*, rhizobia and AMF are used in the remediation of uranium-contaminated soil. This is a beneficial phenomenon because phytochelatin is involved in detoxification and sequestration of a certain amount of heavy metals in plants. In turn, low molecular weight acids such as malic, succinic and citric acids, determined in the above-mentioned study, as bioactive substances, may increase the bioavailability of heavy metals [24]. In addition to the beneficial effect of bacteria, mycorrhiza is also influenced by the presence of earthworms. The role of earthworms is based on regulating the rate of plant colonization by fungi through the participation in the spread of spores. These organisms can be used adjunctively in the processes of soil purification from heavy metals [14]. Research was also conducted to determine the impact of *Trichoderma* sp. and *Fusarium* sp. as an addition to mycorrhizal-assisted remediation. An increase in remediation efficiency was noted. Tested species are able to decompose biodegradable organic compounds [5].

#### 5. Conclusions

To prevent the negative effects of soil pollution, the most efficient and least harmful recultivation technologies should be used. In this case, it is worth considering the possibilities of using phytoremediation. To comprehensively assess the profitability of the phytoremediation process using fungi, the ecological and economic aspects of this technology should be considered. The undoubted advantages of phytoremediation are environmental friendliness, abandonment of the use of high-efficiency technologies that could have a negative impact on the environment and high effectiveness of pollutant accumulation. Moreover, it is a relatively cheap technology that can be used directly in places where specific pollutants occur. However, phytoremediation has certain limitations, such as long duration of the remediation process and limited plant growth at high concentrations of pollutants in soil. Nevertheless, the efficiency of this process can be increased by appropriate selection of hyperaccumulators and symbiotic fungi. In addition, the process is influenced by other organisms inhabiting the soil, such as bacteria and earthworms. It is necessary to match the most favourable plant species for the contamination characteristics. To achieve this, it is required to conduct studies considering various variables. Phytoremediation with the application of mycorrhizal fungi may become one of the most profitable technologies used for land recultivation.

#### Acknowledgment

Research was conducted as a part of preparation for a master's thesis carried out at the Faculty of Infrastructure and Environment of the Czestochowa University of Technology. The research was financed as part of the GeneInUse Student Science Club project and the student project No. SKN / SP / 496788/2021 financed by the Minister of Education and Science from the state budget as part of the program "Student science clubs create innovation" and the internal project of PCz BS / PB-400/301 / 23.

#### References

- [1]. Madejón P., Navarro-Fernández C. M., Madejón E., López-García A., Marañón T., *Plant response to mycorrhizal inoculation and amendments on a contaminated soil*, vol. 789, Science of the Total Environment 789 (2021) 147943, 2, 5, 6, 2021.

- [2]. Mitra S., Chakraborty A. J., Tareq A. M., Emran T. B., Nainu F., Khusro A., Idris A. M., Khandaker M. U., Osman H., Alhumaydhi F. A., Simal-Gandara J., *Impact of heavy metals on the environment and human health: Novel therapeutic insights to counter the toxicity*, vol. 34, issue 3, Journal of King Saud University – Science, 2, 4-7, 2023.
- [3]. Antonkiewicz J., Gworek B., *Remediacja zanieczyszczonych gleb i ziem*, ISBN 978-83-01-22827-9, PWN publishing house, 64, 118, 119, 131-133, 135-137, 2023.
- [4]. Gong X., Tian D. Q., *Study on the effect mechanism of Arbuscular Mycorrhiza on the absorption of heavy metal elements in soil by plants*, doi: 10.1088/1755-1315/267/5/052064, IOP Conference Series: Earth and Environmental Science, 1, 3, 5, 2019.
- [5]. Kazemalilou S., Delangiz N., Lajayer B. A., Ghorbanpour M., *Insight into plant-bacteria-fungi interactions to improve plant performance via remediation of heavy metals: an overview*, doi: 10.1016/B978-0-12-818469-1.00010-9, Molecular Aspects of Plant Beneficial Microbes in Agriculture, Elsevier, 124, 126, 127, 129, 2020.
- [6]. Gómez-Sagasti M. T., Garbisu C., Urrea J., Miguez F., Artetxe U., Hernández A., Vilela J., Alkorta I., Becerril J. M., *Mycorrhizal-Assisted Phytoremediation and Intercropping Strategies Improved the Health of Contaminated Soil in a Peri-Urban Area*, vol. 12-2021, doi: 10.3389/fpls.2021.693044, Frontiers in Plant Science, 2, 2021.
- [7]. Krishnamoorthy R., Venkatramanan V., Senthilkumar M., Anandham R., Kumutha K., Sa T., *Management of Heavy Metal Polluted Soils: Perspective of Arbuscular Mycorrhizal Fungi*, doi: 10.1007/978-981-13-2772-8\_4, Sustainable Green Technologies for Environmental Management, 68, 75, 77-80, 2019.
- [8]. Zulfiqar U., Jiang W., Xiukang W., Hussian S., Ahmad M., Maqsood M. F., Ali N., Ishfaq M., Kaleem M., Haider F. U., Farooq N., Naveed M., Kucerik J., Brtnicky M., Mustafa A., *Cadmium Phytotoxicity, Tolerance, and Advanced Remediation Approaches in Agricultural Soils; A Comprehensive Review*, doi: 10.3389/fpls.2022.773815, Frontiers in Plant Science, vol. 13, 12, 2022.
- [9]. Romero-Estonillo M., Ramos-Castro J., Rfo Y. S. M., Rodríguez-Garrido B., Prieto-Fernández Á., Kidd P. S., Monterroso C., *Soil amendment and rhizobacterial inoculation improved Cu phytostabilization, plant growth and microbial activity in a bench-scale experiment*, doi: 10.3389/fmicb.2023.1184070, 3, 2023.
- [10]. Bakshe P., Jugade R., *Phytostabilization and rhizofiltration of toxic heavy metals by heavy metal accumulator plants for sustainable management of contaminated industrial sites: A comprehensive review*, doi: 10.1016/j.hazadv.2023.100293, Journal of Hazardous Materials Advances, Elsevier, 12, 2023.
- [11]. Nebeská D., Trogl J., Sevců A., Spánek R., Marková K., Davis L., Burdová H., Pidlisnyuk V., *Miscanthus x giganteus role in phytodegradation and changes in bacterial community of soil contaminated by petroleum industry*, doi: 10.1016/j.ecoenv.2021.112630, Ecotoxicology and Environmental Safety, Elsevier, 2, 2021.
- [12]. Zayed A., Pilon-Smits E., deSouza M., Lin Z., Terry N., *Remediation of Selenium-Polluted Soils and Waters by Phytovolatilization*, doi: 10.1002/047147844X.gw851, CRC Press LLC, 75, 2005.
- [13]. Marzi D., Antenzoio M. L., Vernazzaro S., Sette C., Veschetti E., Lucentini L., Daniele G., Brunetti P., Cardarelli M., *Advanced Drinking Groundwater As Phytofiltration by the Hyperaccumulating Fern Pteris vittata*, doi: 10.3390/w13162187, Water, 1, 2021.
- [14]. Sharma K., Gupta S., Thokchom S. D., Kapoor R., *The Potential Roles of Arbuscular Mycorrhizal Fungi in Soil Health and Conservation*, doi: 10.18811/ijpen.v7i01.4, International Journal of Plant and Environment, Volume 7 Issue 1, 44, 45, 2021.
- [15]. Bhandana P., Rana M. S., Sun X., Moussa M. G., Saleem M. H., Syaifudin M., Shah A., Poudel A., Pun A. B., Bhat M. A., Mandal D. L., Shah S., Zhihao D., Tan Q., Hu C., *Arbuscular mycorrhizal fungi and its major role in plant growth, zinc nutrition, phosphorus regulation and phytoremediation*, doi: 10.1007/s13199-021-00756-6, Symbiosis, 20, 30, 31, 2021.
- [16]. Li X., Zhou M., Shi F., Meng B., Liu J., Mi Y., Dong C., Su H., Liu X., Wang F., Wei Y., *Influence of arbuscular mycorrhizal fungi on mercury accumulation in rice (Oryza sativa L.): From enriched isotope tracing perspective*, 255 (2023) 114776, Ecotoxicology and Environmental Safety, 2, 9, 2023.

- [17]. Pandey D., Kehri H. K., Zoomi I., Akhtar O., Singh A. K., *Mycorrhizal Fungi: Biodiversity, Ecological Significance, and Industrial Applications*, doi: 10.1007/978-3-030-10480-1\_5, Recent Advancement in White Biotechnology Through Fungi, 184, 2019.
- [18]. Ortas I., Rafique M., Çekiç F. Ö., *Do Mycorrhizal Fungi Enable Plants to Cope with Abiotic Stresses by Overcoming the Detrimental Effects of Salinity and Improving Drought Tolerance?*, ISBN 978-3-030-51915-5, Symbiotic Soil Microorganisms Biology and Applications, Springer, 393-395, 397-399, 2021.
- [19]. Luo J., Yan Q., Yang G., Wang Y., *Impact of the Arbuscular Mycorrhizal Fungus *Funneliformis mosseae* on the Physiological and Defence Responses of *Canna indica* to Copper Oxide Nanoparticles Stress*, doi: 10.3390/jof8050513, Journal of Fungi, 2, 15, 2022.
- [20]. Ibrahim E. A., El-Sherbini M. A. A., Selim E. M., *Effects of biochar, zeolite and mycorrhiza inoculation on soil properties, heavy metal availability and cowpea growth in a multi-contaminated soil*, doi: 10.1038/s41598-023-33712-z, Nature Scientific Reports, Article number: 6621, 5, 2023.
- [21]. Kereeditse T. T., Pheko-Ofitlhile T., Ultra Jr V. U., Dinake P., *Effects of Heavy Metals on the Yield of Essential Oil From Vetiver Grass Cultivated in Mine Tailings Amended With EDTA and Arbuscular Mycorrhizal Fungi*, doi: 10.1177/1934578X231164813, Sage Journals, 2, 10, 2023.
- [22]. Ai Y., Li F., Yang J., Lu S., Gu H., *Research Progress and Potential Functions of AMF and GRSP in the Ecological Remediation of Metal Tailings*, doi: 10.3390/su14159611, Sustainability, 7, 9, 2022.
- [23]. Bi Y., Xiao L., Liu R., *Response of arbuscular mycorrhizal fungi and phosphorus solubilizing bacteria to remediation abandoned solid waste of coal mine*, doi: 10.1007/s40789-019-00270-7, International Journal of Coal Science & Technology, 604, 2019.
- [24]. Ren C., Kong C., Wang S., Xie S., *Enhanced phytoremediation of uranium-contaminated soils by arbuscular mycorrhiza and rhizobium*, doi: 10.1016/j.chemosphere.2018.11.085, Chemosphere, Elsevier, 774, 777, 778, 2019.

# Scientific analysis of the negative effect of the war in Ukraine on environment

Viktoria Pitulei<sup>1</sup>

<sup>1</sup>Department of psychiatry, narcology and medical psychology, Ivano-Frankivsk National Medical University, e-mail: pituley@ukr.net

---

## Abstract

The war in Ukraine affects not only food security and has economic consequences for all countries. Today it is also a question of environmental security and a common future. Because the truth, which the Russian Federation does not understand, but the whole world is aware of, is very simple: any military conflict does not have a local character when it comes to the environment. Ecosystems cannot be divided by conventional boundaries simply by drawing them on a map. If the natural balance is destroyed in one geolocation, it will definitely be felt by another. The article highlights the ecological danger of military operations in Ukraine. The impact of the war on all layers of the earth is characterized. Attention is focused on the flooding of mines and the exit of mine waters to the surface, the destruction of treatment facilities, chemical and radiation pollution of water resources, pollution of atmospheric air and soils, the destruction of landscapes, vegetation, and large areas of forests.

**Keywords:** military operations, pollution, destruction, protected areas

---

## 1. Introduction

Russia's war in Ukraine is the first international conflict in the last twenty years with such significant and irreparable damage to the environment. From the first days of the Russian invasion, we have been recording all the damage they are causing to the Ukrainian environment. We can already talk about 257 cases of ecocide. These are the explosions of fuel and lubricant warehouses, oil product storages with corresponding consequences for the environment. These include airstrikes on enterprises that use dangerous chemicals in production. This includes the damage and destruction of treatment facilities, and the spilling of sewage into our reservoirs, as well as damage to the soil cover, burning of forests - especially in the territories of the nature reserve fund. Today, 2.5 million hectares of Europe's nature conservation network are under threat of destruction due to the actions of the Russian Federation. These are 160 objects of the Emerald Network - territories of existence of species and habitats protected at the pan-European level. And another 17 Ramsar sites with an area of 627.3 thousand hectares - wetlands of international importance. In general, 20% of the area of all protected areas of Ukraine remains in danger from the actions of the Russian Federation. European biodiversity is dying from enemy technology.

These are thousands of plant species that are listed in the Red Book of Ukraine and protected by law. Fighting disturbs the peace of wild animals. They either die or try to escape from hot spots.

The Russian Federation conducts hostilities in protected territories of international and European importance, thereby destroying the habitats of rare and endemic species and habitats. This can change the behavior of birds, including their migration. So that everyone understands what the consequences of the invasion of the Russian Federation into Ukraine can be, I will give just one example. When in 2015 Russian troops began to use Kryvyia Kosa in Donetsk region for landing, all bird diversity disappeared there. Although before that, three thousand pairs of Caspian martins nested en masse on the coast. It was their largest colony in Europe.

Military operations are destroying the forests of Ukraine, which will also affect the food security of the world. Fighting is currently taking place in the eastern and southern regions of Ukraine. These regions are characterized by low forest coverage. But here forests perform protective functions. Their destruction and damage will affect the climate of these regions and may lead to significant erosion processes. In particular, in the south of Ukraine, the consequences may be wind erosion and desertification. This, of course, will affect agriculture.

In total, almost three million hectares of forest in Ukraine have been engulfed in war since the start of the full-scale invasion of the Rashists. For comparison, this is almost the territory of Belgium. When the Rashists, under

the pressure of Ukrainian weapons, fled in disgrace from Zhytomyr region, Kyiv region, Chernihiv region and Sumy region, 567 thousand hectares of Ukrainian forests remain under occupation.

### **2. Environmental pollution**

Russia has fired more than 2,500 missiles over Ukraine since February 24. Enemy shells that hit our critical infrastructure and residential buildings every day cause significant fires, including forests. This leads to significant pollution of atmospheric air with dangerous substances. During the detonation of rockets and projectiles, a number of chemical compounds are formed - carbon monoxide, brown gas, nitrogen dioxide, formaldehyde, etc. During the explosion, all substances are completely oxidized, and the products of the chemical reaction are released into the atmosphere.

It should be taken into account that the occupier is shelling our oil depots, industrial enterprises that use various chemical substances in their activities. And these are also tens of thousands of tons of harmful substances released into the atmosphere.

At the same time, polluted air has no borders. Emissions into the atmospheric air, which were caused by the military aggression of the Russian Federation on the territory of Ukraine, are transferred, settle and have an impact on the territories of other states, sometimes at a distance of thousands of kilometers.

A separate topic is mined territories. Mine ruptures lead to soil contamination with heavy metals - lead, strontium, titanium, cadmium, nickel. This makes the soil dangerous, and in some cases, unsuitable for further agricultural use. Explosions also cause forest fires. So we return again to the problems of emissions into the atmosphere and food security. The cyclical nature of the consequences and interconnectedness of the processes is obvious.

Water is one of the most important natural resources. Agree, without gas, coal and oil - people lived for centuries, and without water and air - only days and minutes. Clean water is needed not only by humans, but also by thousands of different species of animals and plants, water gives life and connects everything into one big system. And it is precisely because of this that war has such a devastating effect on water resources.

Pollution of rivers as a result of Russian aggression can also affect neighboring countries. After all, we share large rivers such as the Danube, Dniester, Prut, Tisza, and Western Bug with neighboring countries: Poland, Hungary, Romania, and Moldova.

Our rivers and lakes are hit by missiles, our coast is filled with sea mines, a huge amount of oil products and the bodies of dead Russian soldiers fall into the water. Pollutants that end up in even the smallest water bodies eventually get into underground waters, and through the extensive system of rivers - into the Black and Azov Seas, and then - into the World Ocean. At the same time, these war-generated pollutants undergo chemical transformations, affect aquatic flora and fauna, and some elements even accumulate in the bodies of aquatic animals.

A simple example: an abnormal increase in the mortality of dolphins near the coast of Turkey and Bulgaria due to Russian aggression in Ukraine. News about this has recently been circulating in the media. However, in reality, the consequences of war are much deeper.

Due to Russian aggression, biodiversity is decreasing, which affects the change in balance in some ecosystems. Fires, poisoning of water and air - these consequences of war do not just change and burn the environment, they kill dozens of species of animals and plants. In particular, due to military actions, 900 protected areas, 600 species of animals, and about 750 species of plants and mushrooms are now in danger. The loss of even one PZF object is a tragedy, because unique species of animals and plants die, unique reliefs, soils, ecosystems are destroyed, and it is almost impossible to restore them.

The impact of losing large numbers of animals or even entire species is initially imperceptible. However, over time, changes begin in the ecosystem where this happened, which over time can turn one ecosystem into a completely different one. For example, it is already known that 50 thousand dolphins have died in the Black Sea, and this will greatly affect the ecosystem of the sea, because the decrease in the number of dolphins will lead to an increase in the populations of those species that were the food base for dolphins, which in turn will lead to a decrease in the volume their food base. If the dolphin population does not recover due to climate change and other processes, over time their ecological niche may be occupied by other organisms. And all this will lead to a global change of the Black Sea ecosystem, and it is impossible to predict exactly how this will affect the coastal countries and their population.



According to ecoactivists, rockets cause the worst damage to the environment: their fuel poisons the soil and water, provokes chemical poisoning of the environment. Fires not only cause air emissions and atmospheric pollution, but also destroy the upper, fertile layer of our earth. In the future, such soils will not produce crops.

Three species of dolphins live in the waters of the Black Sea, and all of them are red-listed. About 20,000 dolphins die there every year, the most common causes being poaching nets and sea pollution. But this year, scientists from the Black Sea countries recorded an increased number of deaths. Dead individuals were also found in Ukraine, including in the Tuzliv estuaries in Odesa. Scientists attribute the abnormal number of dolphin deaths to the presence of Russian warships in the water area, which use sonars that emit powerful signals. These very strong and low-frequency signals hit the dolphin's inner ear, the organ of navigation and hearing. Because of this, the animal becomes "blind". Having lost their orientation, animals lose acoustic control over the environment, cannot find food and die of starvation. In stressed dolphins weakened by sonar, their immunity sharply decreases, in which case the animals die from infections. Oil spills also play their tragic role - according to the official resource of the Ministry of the Environment EcoZagroza, 11 thousand tons of oil products got into the water during the year of the war.

Ivan Rusev, a leading scientist of the Tuzlovsk estuary research center, estimates the number of dead dolphins to be 50,000. Other marine scientists treat this number with caution, because the exact number of victims will be known only after the accounting of dolphins in the water area, which will become possible only after the deoccupation of the entire Ukrainian coast.

Since the beginning of the conflict, abandoned coal mines have filled Donbas with toxic and sometimes radioactive substances. Many environmental risks arise from sudden interruptions in mine production: mine water must be continuously pumped out; if pumping is stopped, toxic water fills mine shafts and moves upward, eventually reaching and contaminating land and drinking water. Contaminated water from one mine overflows into others because many mine shafts are interconnected.

According to the Ministry of Ecology and Natural Resources of Ukraine, in just ten months as a result of the war, more than 42 million tons of carbon dioxide were released into the atmosphere, which is approximately equal to the annual volume of emissions of Bulgaria. Forest fires caused by shelling, as well as Russian attacks on Ukrainian oil depots, which ignited 680,000 tons of oil and fuel, are largely responsible for the emissions.

### **2.1 Soil pollution.**

The war poisoned large areas of Ukrainian agricultural land. Dangerous chemicals and fuel released from exploding rockets and tens of thousands of artillery shells fired daily by both sides seeped into the ground along the entire length of the front line. Such pollution can damage local ecosystems and crops decades after the guns fall silent, says Oleksiy Angurets, author of a forthcoming report on the environmental impact of war. The damage caused to agricultural lands has already cost Ukraine 18 billion dollars.

Among the factors that have the greatest impact on soil pollution, we include the following:

- **Mining territories**

According to the UN, more than 180,000 square meters of territory in Ukraine have been mined. This area is almost a third of our entire country. According to estimates, more than 10 million Ukrainians are at risk. As of today, 350,000 explosive objects have been defused, but the scale of the tragedy is shocking. Demining such an area may take decades.

- **Detonation of ammunition**

The explosion of any ammunition is the release of toxic compounds into the soil (nitrogen and carbon dioxide, water vapor, vapors of cyanic acid, nitrogen and other toxic organics). Chemicals can also enter the soil with precipitation. Fragments of munitions are also a danger - poisonous substances get into the soil, then into groundwater, and later - into the food chains of animals and people.

- **Burial of the killed**

Due to the mass burials of the killed Russian invaders, the areas of fierce fighting are turning into huge burial grounds. It is clear that it is strictly forbidden to grow agricultural crops on such land in the near future.

- **Movement of ground military equipment**

The movement of heavy military equipment leads to critical changes in the landscape. Also, as a result of movement, soils are contaminated with fuel and lubricants and other petroleum products. As a result, the water permeability of the soil decreases, oxygen is displaced, the root nutrition of plants is disturbed, and their growth and development are inhibited. A slightly smaller source of pollution is burnt military equipment and other remnants of hostilities.

- **Burnt chernozems**

The formation of chernozem in nature takes about 10 thousand years. It can be destroyed in a moment when the rocket explodes. Most of the fighting on the territory of our country takes place exactly where the unique and very fertile soil layer is spread. Sulfur that settles in the soil after the explosion reacts with dew or fog to form sulfuric acid, which burns vegetation, bacteria and worms - everything that forms the soil.

Another 3 million hectares of forests, about a third of the total area, have already been affected by hostilities. Of these, at least 23,300 hectares were completely burned. Illegal logging has been recorded in many of the 18 national parks and reserves that were illegally occupied by the Russians.

### **2.2. Consequences of blowing up the Kakhovskaya hydroelectric power plant**

The destruction of the Kakhovskaya HPP dam became a real environmental disaster. Animals and fish are already dying en masse, agricultural lands have suffered greatly, and the ecosystem of the region has essentially begun to collapse. As a result, the affected areas will change irreversibly. We can single out the main ecological consequences of the destruction of the dam.

Currently, more than 3,600 houses in 32 settlements have been flooded in the Kherson region. The water level is decreasing, but very slowly. People and animals remain in the flooded cities. On the contrary, in the territory located above the dam, shallowing of water bodies awaits. Water problems have already started in some cities. And these are only the obvious environmental consequences of the destruction of the Kakhovskaya HPP dam. Others will become known in the coming years, scientists say. The streams of water that have flooded cities, villages and fields carry with them everything in their path, such as garbage, dangerous chemicals or even mines.

The vicinity of the dam, which is controlled by the Russian military, was heavily mined. Now these mines are drifting in the water, the Red Cross and Care International warn. First of all, the left bank of the Dnieper and the agricultural land there will suffer from this, and this will make it difficult to put them into circulation in the near future, says Brian Kons. The water flow from the Kahovsky Reservoir may contain toxic industrial waste, ecologist Evgeny Simonov told the BBC. Deposits that will remain in the shallow part will dry out and be blown away by dust storms.

These forecasts are confirmed by the "Ukrainian Nature Conservation Group": its experts write about the "presence in the bottom deposits of the reservoir of heavy metals and other pollutants that have been accumulating for decades from the emissions of industrial enterprises in Zaporizhzhia, Dnipro, Kamiansk, etc."

According to the group, in general, due to the destruction of the dam, a lot of fuel and lubricant materials, which are toxic to aquatic life and can form a film on the surface of the water, got into the water.

In addition, the flooding of settlements, including cesspools, agricultural land, and gas stations means that an unusually large amount of pollutants entered the sea. This can affect various groups of living organisms - from plankton to cetaceans [in the Black Sea]," the group writes. And these predictions are already coming true. According to the Security Council of Ukraine, at least 150 tons of machine oil washed into the Dnipro by mid-afternoon on Tuesday, and another 300 tons could potentially enter the river. In addition, the fauna of the reservoir, carried with the flow of water into the floodplains formed below the Kakhovskaya HPP dam, will also die. This will happen as the level of the flood wave decreases - then these aquatic inhabitants will be on land.

Another problem will be the death of freshwater fish that will fall into the salty waters of the Black Sea. At the same time, the Black Sea fauna may die from a massive influx of fresh water, the Ministry of Agrarian Policy notes.

On Thursday, the Ukrainian side reported on the threat of flooding of the sturgeon breeding plant in the Kherson region. The only state plant of this type in Ukraine has been operating since 1984 and compensated for the reproduction of sturgeon species that lost the possibility of natural reproduction due to the construction of a cascade

of reservoirs on the Dnieper. Dead fish will be a problem in itself. On June 7, the Ministry of Health of Ukraine warned that there will be a fish plague in the Kherson region in the coming days. Collecting and eating it is deadly dangerous for health.

Experts of the "Ukrainian Nature Conservation Group" divide the numerous consequences for nature into several categories: the consequences of draining the bottom of the Kakhovsky Reservoir, the consequences of flooding the territories below the dam, and the consequences for the Black Sea. They write that even in the short term, the consequences of the destruction of the HPP dam for nature will be incomparably greater than the consequences of all military actions since the beginning of February 2022.

In the long term, experts note, it may turn out that for climatic and other reasons it will be more expedient to restore the natural flow of the Dnieper and repurpose the economy of southern Ukraine from arable farming to pasture livestock. Or, with the funds needed to restore the Kakhovskaya HPP, modern pumping stations will be built, which will allow taking water for the needs of industry and agriculture directly from the Dnipro River, and not from the reservoir.

### Conclusions

War has a negative impact on the environment. Attacks on forests, terrestrial and marine ecosystems, industrial facilities, transport infrastructure and buildings, destruction of water supply, sewage and waste management systems provoke large-scale and serious damage with long-term consequences for the environment and human health.

The global environmental community is concerned about the events in Ukraine, because the issue of ecology and climate change is not the problem of one country. Therefore, the world mass media repeatedly wrote about the war and its consequences for ecology. In addition to thousands of deaths and the destruction of critical infrastructure, another, more invisible crisis related to Russia's invasion could haunt Ukraine for years – environmental damage. From shelling of chemical plants to forests burned by rockets, the consequences will be felt not only by the ecosystems of Ukraine, but also by its people.

The environmental danger Ukraine faces as a result of the armed conflict is also exacerbated by the country's industrial background. Heavy industry is a significant part of Ukraine's economy, especially in the east of the country. The largest nuclear power plant in Europe is located in Ukraine, in the city of Zaporizhia, and Ukraine's industry accounts for almost 29% of its gross domestic product. Ukrainian officials and architects are already thinking about how to rebuild cities destroyed by the Russian invasion in a way that is also environmentally friendly and helps fight climate change. For the most part, it will be necessary to wait until the end of the war to eliminate the damage caused to the environment. But some projects are already being implemented. Last year, the State Agency of Forest Resources of Ukraine planted more than 180 million new trees as part of the reforestation program. At the end of September 2022, a new forest seed center was opened just a few kilometers from the border with Belarus, from where one of the waves of the Russian invasion came in February 2022.

### Acknowledgment

Ukraine, Ivano-Frankivsk National Medical University, the department of psychiatry, narcology and medical psychology.

### References

- [1]. "Ekodiya Center for Environmental Initiatives", 2023
- [2]. 2.Kravchenko O . Study of the impact of military operations on the environment in Eastern Ukraine. Kravchenko O, Vasylyuk A, Voytsikhovska K. Philosophy, 2015
- [3]. 3.Lisova N. Military affairs and nature use . Nature use. Study guide N. O. Lisova. Ternopil: editorial and publishing department of TNPU, 2015
- [4]. 4.Shevchuk V. Greening of energy: teaching manual . Shevchuk V. Kyiv, Higher education, 2002

# Selectively collected biowaste as an organic-rich feedstock for composting

Thi Cam Tu Le\*, Katarzyna Bernat, Dorota Kulikowska

Department of Environmental Biotechnology, Faculty of Geoengineering, University of Warmia and Mazury in Olsztyn, 10-709 Olsztyn, Poland,

e-mail: \*corresponding author - [camtule@uwm.edu.pl](mailto:camtule@uwm.edu.pl); [bernat@uwm.edu.pl](mailto:bernat@uwm.edu.pl); [dorotak@uwm.edu.pl](mailto:dorotak@uwm.edu.pl).

---

## Abstract

Because aerobic stabilization is the most commonly used process in the biological part of MBT plants in Poland, it would be easier and economically favorable to use the existing installation for the treatment of separately collected biowaste in the composting process. Moreover, composting is one of the most promising treatment methods for biowaste, as it can reduce the volume and weight of biowaste, make it stable, and produce valuable compost as a final product that can be used as a fertilizer. The aim of the present study was to monitor the two-stage composting of real separately-collected biowaste. The first stage of composting was carried out in a laboratory-scale 100 L reactor; the second stage, in a turned windrow. The temperature was monitored, as the main factor in composting. The changes in the content of organic matter (OM) during composting were also determined. Based on the changes in OM content, the kinetics were determined. Just after starting the process of composting, the temperature in the bioreactor rapidly increased up to 55°C, and then remained over 55°C for 14 days. This complies with the requirements for the temperature profile during the composting process, i.e.,  $\geq 55^\circ\text{C}$  for at least 14 days (EU, 2019). After this, the temperature started to decrease, reaching ambient temperature after 30 days. The OM content decreased rapidly while the temperature in the bioreactor was high. In the windrow phase, the OM content decreased slightly and then remained stable until the end of the process.

**Keywords:** separately collected biowaste, composting, organic matter removal, bioreactor, windrow

---

## 1. Introduction

In view of population growth and the associated increase in demand for energy, food, and chemicals, the issue of environmentally friendly treatment of municipal solid waste (MSW) is currently becoming even more important. In 2021, around 236.8 million tons of municipal waste were generated in the European Union (EU-27), compared to 233.2 million tons in 2020 (Statista, 2023). The EU's waste policy objective is not only to recycle at least 65% of municipal waste by 2030 (Waste Framework Directive (WFD), 2018/851), but also to phase out landfills (Landfill Directive 1999/31/EC) and focus instead on the goal of "zero waste" and a "circular economy" in order to fulfill the EU's plans for sustainable development (EC, 2015b).

The "waste management hierarchy" established by the EU states that the best practices are prevention and reuse, then recycling (including organic recycling), recovery (e.g., incineration of waste to generate energy), and disposal (e.g., landfilling, which is the cheapest but most environmentally and health-damaging option) (WFD, 2008/98/EC). More than 25% of biodegradable municipal waste was disposed of in landfills in 2021, which is associated with pollution of the environment by emitting greenhouse gases and creating leachate (Eurostat, 2023). This is practiced even though the landfilling of biodegradable municipal waste should be reduced or even completely eliminated (Landfill Directive 1999/31/EC; Dz.U.2017/poz.2412). To reduce landfilling of biodegradable municipal waste, mechanical-biological treatment plants (MBT) are currently being developed in many EU countries, including Poland (Dz.U.2023/poz.56). In MBT plants, secondary materials (e.g. plastics, glass, metals, and high-calorific alternative fuels) are recovered and the organic fraction of municipal solid waste (OFMSW) is mechanically separated on a screen. However, the end product of OFMSW stabilization (stabilizate) can only be landfilled and cannot be considered compost. Stabilization of OFMSW is therefore not included in calculation of recycling rates. Additionally, EU regulations (EU, 2018b) state that, by 2027, compost from MSW will no longer count towards achieving compliance with recycling targets for municipal waste. Referring to the recycling rate as defined by legal regulations in Poland, this rate has been calculated differently over the last several years. The recycling rate is the ratio of the mass of waste materials that are actually recycled divided by the whole mass of MSW generated in the country. This means that the ratio is lower than when previously calculated because the mass of waste materials actually recycled was divided by the mass of waste materials present in MSW

generated in the country (Dz.U.2021/ poz.1530). In order to increase the recycling rate of MSW, the recycling of biowaste is now one of the most important elements in achieving the relevant targets, as biowaste makes up a large proportion of municipal solid waste. In 2017, biowaste accounted for over 35% of MSW generated, amounting to 86 million tons in the EU-28 (EEA report, 2020). This includes both separately collected biowaste and biowaste that is collected together with mixed waste, but not self-composted biowaste. However, in the EU-28, around 43% of the overall amount of biowaste was separately collected in 2017, while 57% of biowaste ended up in mixed municipal waste and was therefore lost for recycling. In Poland, separately collected biowaste constituted around 30% of the overall amount of biowaste.

The new concept is that currently existing MBT plants should process separately collected waste, not mixed MSW (WFD, 2018b/EU). This aims to increase the quality and uptake of secondary raw materials. MBT plants should act as recycling centers where waste products such as glass, paper, metal, and plastic only need to be cleaned to be accepted by recyclers. After separation in the MBT plant, the waste materials can then be sold as secondary raw materials and fed back into the production cycle, thus supporting the circular economy and increasing the recycling rate. There is also a need to collect biowaste separately because only organic recycling of biowaste would allow for an increase in the recycling rate.

There are currently two potential methods for biowaste recycling these are anaerobic digestion and composting. Because aerobic stabilization is the most commonly used process in the biological part of MBT plants in Poland, it would be easier and economically favorable to use existing installations for biowaste treatment via the composting process. This means that composting of biowaste could be easily adopted. Biowaste composting accounted for 20% and 70% of the treatment capacities for biowaste in Poland and the EU, respectively. Moreover, composting is one of the most promising treatment methods for biowaste, as it can reduce the volume and weight of biowaste, make it stable, and produce valuable compost as a final product (EEA, 2020; Nidhi et al., 2021; Žitnik and Vidic, 2016; ECN, 2019).

Composting is a process of aerobic decomposition of waste, in which the concentrations of organics are reduced by the activity of microorganisms, resulting in the production of compost, water, carbon dioxide, and heat. Compost from biowaste can be a valuable product created during this process and can serve as an organic fertilizer.

## 2. Materials and Methods

### 2.1. Composting feedstock

In the present study, biowaste used for composting was collected from containers (Fig. 1) for selective collection located in a city with 200,000 inhabitants (north-eastern Poland). The biowaste was relatively wet (Fig. 2.), with a moisture content of 77.88%, and the dry matter content (DM) was around 22.12% (Table. 1.).



Fig. 1. The biowaste collected from containers

Table. 1. Characteristics of the composting feedstock

Characteristic	Unit	Value
<i>Basic analyses of biowaste</i>		
DM	%	22.12
OM	%DM	86.81
Moisture	%	77.88
<i>Water extract from real biowaste after filtration</i>		

pH	–	5.48
TA	mval/L	10.60
VFA	mg/L g/kg DM	454.29 20.54
P-PO <sub>4</sub>	mg/L g/kg DM	287.64 13.00
NO <sub>2</sub>	mg/L g/kg DM	0.77 0.03
NO <sub>3</sub>	mg/L g/kg DM	81.40 3.68
N-NH <sub>4</sub>	mg/L g/kg DM	25.20 1.14

## 2.2. Experimental Setup

The composting process was carried out for 60 days in a two-stage system. The first stage was an aerated bioreactor with an active capacity of 100 liters, and the second was a periodically turned windrow. The bioreactor was made of acid-resistant steel, surrounded by a water jacket, and equipped with a fan that blew air into the aeration box that formed the bottom platform of the bioreactor. The upper part of the bioreactor contained a lid that allowed batch feeding and sampling of the composting material. The temperature sensors in the bioreactor were located 0.3 m and 0.7 m below the top cover of the reactor (Fig. 3).



Fig. 2. A) Real biowaste after separation; b) The 100 L bioreactor used for the experiment

## 2.3 Analytical Procedures

Water extracts were prepared from feedstock and tap water at a ratio of 1:10 (w/w) and then shaken for 2 hours. The water extracts were centrifuged at 9000 rpm for 15 min and then filtered through a membrane filter. The following characteristics of the water extract from the feedstock material were determined after filtration: NO<sub>3</sub>, VFA, N-NH<sub>4</sub>, P-PO<sub>4</sub>, NO<sub>2</sub>, pH, and alkalinity (TA). These procedures were carried out in accordance with standard methods for the analysis of water and wastewater (APHA standards, Greenberg et al., 1992) and in accordance with the procedures of the Polish Committee for Standardization.

During the biowaste composting experiment, temperatures in the center and at the bottom of the reactor were measured automatically with a PC THERM REM 84 m dual-channel temperature sensor with an accuracy of  $\pm 0.1^\circ\text{C}$ . The temperatures in the reactor were recorded every day. During the 60-day composting period, samples weighing approximately 0.5 kg were taken every few days for analysis. These samples were taken from the upper, middle, and lower parts of the reactor and mixed to produce representative samples. To prepare the samples for analysis of dry matter (DM), they were dried to a constant weight (24 hours at 105°C), then ground (0.5 mm

diameter) and stored in boxes at room temperature. The organic matter (OM) content was determined by combustion at 550°C for about 4 hours.

### 2.3. Kinetic Equations

The rate constant of organic matter (OM) removal and the maximum amount of organic matter removed were determined with the following first-order kinetics equation:

$$OM_{\text{removal}} = OM \cdot e^{-k \cdot t}$$

where

OM is the maximum content of OM removed in the bioreactor or in the windrow (g/kg DM),  
k is the rate constant of OM removal in the bioreactor or in the windrow ( $\text{day}^{-1}$ ), and  
t is the composting time (days).

The initial rate of organic matter removal ( $r_{\text{OM}}$ ) was calculated using the k and OM values.

## 3. Results and Discussion

The temperature of compost is an indicator of microbial activity during the composting process, and a return to temperatures close to ambient is a good indicator of the end of the bio-oxidative phase (Teixeira et al., 2015). Composting proceeds through three phases: i) the mesophilic, or moderate-temperature phase, which lasts for a couple of days; ii) the thermophilic, or high-temperature phase, which can last from a few days to several months (i and ii were carried out in the bioreactor); and finally, iii) the several-month-long cooling and maturation phase, which was carried out in the turned windrow (Robert, 2002). According to Zhang and Sun (2014), the composting temperature should remain in the thermophilic range (50–60°C) for at least 3 days to achieve maximum sterilization. Under thermophilic conditions, the pathogenic organisms present in the waste will be destroyed and the compost will be completely hygienized. According to the EU regulation (2019) containing the updated guidelines regarding the temperature suitable for fertilizers made from secondary raw materials, the temperature of the bioreactor must comply with one of the following temperature profiles during the composting process:  $\geq 70^\circ\text{C}$  for at least 3 days,  $\geq 65^\circ\text{C}$  for at least 5 days,  $\geq 60^\circ\text{C}$  for at least 7 days or  $\geq 55^\circ\text{C}$  for at least 14 days in laboratory conditions.

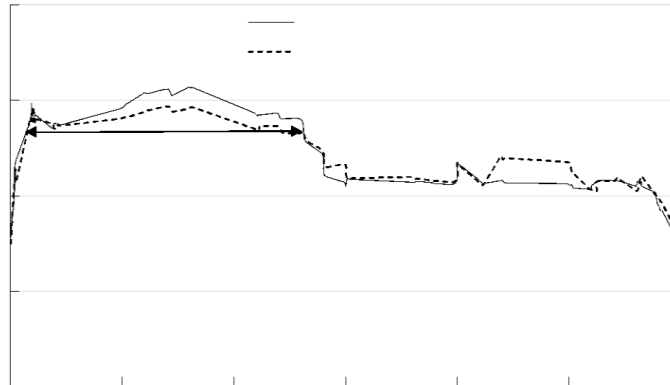


Fig. 4. Temperature profiles of compost in the bioreactor during composting (30 days)

The temperature profiles of two depths in the composting material in the bioreactor during the 30 days are shown in Fig. 4. In the bioreactor, the composting material reached thermophilic temperatures (55°C) after 1 day at both measurement depths (0.3 m, 0.7 m). The temperature then increased slightly and remained at 55°C–60°C at both depths during the next 14 days. After the 15<sup>th</sup> day, the temperature at both measurement depths was reduced to around 45°C and did not change until the 29<sup>th</sup> day. However, on the 30<sup>th</sup> day, the temperature decreased rapidly to 30°C at both measurement depths. After 4 weeks of modular composting, the material was transferred to a periodically turned windrow platform. The temperature was kept at room temperature (24–27°C) for about 30 days under natural conditions. The temperature of the composted material dropped towards ambient temperature, which indicated the beginning of the maturation process of the substrate.

12851 \* y) + (663.4011)

12851 \* y) + (663.4011)

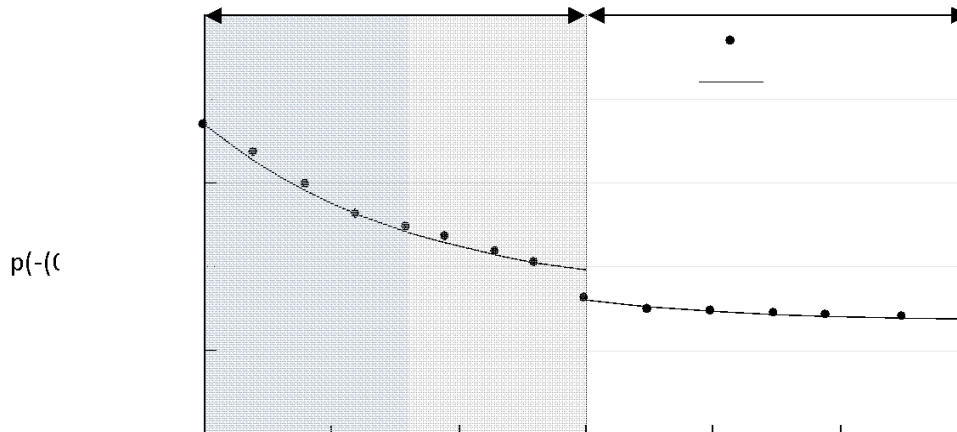


Fig. 5. The changes in OM content during 60 days of composting

During the composting of biowaste, OM removal took place. Based on the changes in OM, the kinetic parameters were determined. Changes in the OM content in biowaste during composting are presented in Fig. 5. The initial OM content in the feedstock was 868 g OM/kg DM. We can distinguish two phases of OM removal, the first one (taking place in the bioreactor), with an intensive decrease, and the second phase (in turned windrow), with a slight decrease. In the first phase, during the first 14 days, when a high temperature was noted, the OM content decreased very rapidly to ca. 750 g OM/kg DM. When the temperature had trended reduced from the 14<sup>th</sup> day to the 30<sup>th</sup> day, OM content was decreasing, but slower than initially, and reached 715 g OM/kg DM. During the second phase of the composting process, OM content slightly decreased, and it ranged from 663 to 639 g OM/kg DM. The maximum content of OM removed in the bioreactor was 205 g OM/kg DM, and the initial rate of OM removal was 12.3 g OM/(kg DM·d). While, the maximum content of OM removed in the windrow was almost 8 times lower than in the bioreactor (24 g OM/kg DM). The initial rate of OM removal in the windrow was also lower than its the bioreactor (1.9 g OM/(kg DM·d)).

#### 4. Conclusions

During composting of selectively collected biowaste in a bioreactor, a very high temperature (above 55°C) was noted during ca. 2 weeks due to mineralization of OM. This complies with the demands that time profile during the composting process:  $\geq 55^{\circ}\text{C}$  for at least 14 days (EU, 2019). The content of OM removal proceeded in two phases, the first phase in the bioreactor, was characterized by an intensive decrease in OM content, whereas in the second phase, in turned windrow, a slight decrease of OM content was noted. The effectiveness of the removal of OM content during composting of biowaste, based on the Paredes model (Paredes et al., 2000), was around 73%. The results indicated composting of biowaste is an effective method to produce compost with great potential for agricultural purposes. Overall, compost from biowaste produced can be used as a fertilizer. Producing compost conforms with the principles of a circular economy and will contribute to an increase in recycling rates.

#### Acknowledgment

We are grateful for the financial support of the Ministry of Education and Science, Poland (statutory project No. 29.610.024-110).

#### References

- [1]. Robert, J.H., *Basic principles for composting of biodegradable household wastes*, Publisher Urban Vegetable Gardening Semina, 6, 2002.
- [2]. Statista, statista.com, date of access (30/11/2023)
- [3]. Eurostat, europa.eu, date of access (30/11/2023)



- [4]. Dz.U. 2017 poz. 2412 ROZPORZĄDZENIE MINISTRA ŚRODOWISKA z dnia 15 grudnia 2017 r. w sprawie poziomów ograniczenia składowania masy odpadów komunalnych ulegających biodegradacji
- [5]. Dz.U.2023/poz.56 ROZPORZĄDZENIE MINISTRA KLIMATU I ŚRODOWISKA z dnia 28 grudnia 2022 r. w sprawie mechaniczno-biologicznego przetwarzania niesegregowanych (zmieszanych) odpadów komunalnych
- [6]. Dz.U.2021/ poz.1530 ROZPORZĄDZENIE MINISTRA KLIMATU I ŚRODOWISKA z dnia 3 sierpnia 2021 r. w sprawie sposobu obliczania poziomów przygotowania do ponownego użycia i recyklingu odpadów komunalnych
- [7]. Nidhi, K., Swayansu, S.M., Sunita, V., Ngo, H.H., Jonathan, W.C.W, Mohammad, J.T, Chang, J.C, Kim, S.H, Bui, X.T. A review on integrated approaches for municipal solid waste for environmental and economical relevance: Monitoring tools, technologies, and strategic innovations. *Bioresource Technology*. 2021, 342, 125982.
- [8]. European Union (EU) 2019/1009 of The European Parliament and of The Council of 5 June 2019 laying down rules on the making available on the market of EU fertilising products and amending Regulations (EC) No 1069/2009 and (EC) No 1107/2009 and repealing Regulation (EC) No 2003/2003.
- [9]. European Union (EU). Council Directive 1999/31/EC of 26 April 1999 on the landfill of waste. 1999. (OJ L 182, 16.07.1999, pp. 1-19).
- [10]. European Union (EU). Directive (EU) 2018/850 of the European Parliament and of the Council of 30 May 2018 amending Directive 1999/31/EC on the landfill of waste (text with EEA relevance). 2018. (OJ L 150, 14.6.2018, pp. 100-108).
- [11]. European Commission (EC). Communication from the Commission to the European Parliament, the Council, the European Economic and Social Committee and the Committee of the Regions - Closing the loop - an EU action plan for the circular economy (COM (2015) 614 final). 2015.
- [12]. EEA. Waste recycling in Europe. 2021. <https://www.eea.europa.eu/ims/waste-recycling-in-europe> (accessed on 16 December 2022).
- [13]. European Environment Agency (EEA). Biowaste in Europe turning challenges into opportunities. Report No 4/2020. ISSN 1977-8449 EEA: Copenhagen, Denmark. 2020.
- [14]. Greenberg, A.E.; Clesceri, L.S.; Eaton, A.D. Standard Methods for the Examination of Water and Wastewater, 18<sup>th</sup> ed.; Publisher American Public Health Association (APHA), Washington, DC, USA, 1992.
- [15]. ECN, 2019, ECN status report 2019 - European bio-waste management, an overview of biowaste collection, treatment and markets across Europe, European Compost Network, Bochum, Germany.
- [16]. EU, 2008, Directive 2008/98/EC of the European Parliament and of the Council of 19 November 2008 on waste and repealing certain Directives (OJ L 312, 22.11.2008, pp. 3-30).
- [17]. Žitnik, M. and Vidic, T. Food among waste, Statistical Office of the Republic of Slovenia, Ljubljana ([https://www.stat.si/StatWeb/File/DocSysFile/9206/ FOOD\\_AMONG\\_WASTE\\_internet.pdf](https://www.stat.si/StatWeb/File/DocSysFile/9206/ FOOD_AMONG_WASTE_internet.pdf)) (accessed 10 February 2020).
- [18]. Zhang, L., and X.Y. Sun. Effects of rhamnolipid and initial compost particle size on the two-stage composting of green waste. *Bioresource Technology*, 2014, 163:112–22.
- [19]. Teixeira, D.L., Matos, A.T., Melo, E.C. Resistance to forced airflow through layers of composting organic material. *Waste Management*, 2015, 36, 57-62.
- [20]. Paredes, J.C, Roig, A., Bernal, M.P., et al. Evolution of organic matter and nitrogen during co-composting of olive mill wastewater with solid organic wastes. *Biology and Fertility of Soils*, 2000, 32: 222–227.
- [21]. Polish Committee for Standardization. *Polish Standard. PN-R-04017:1992. Agrochemical Soil Analyses—Determination of Assimilated Copper Contents*; PKN: Warsaw, Poland, 1992. (In Polish)



# The application of numerical modal analysis in simulation of dynamics of HDPE fuel tank

Kamil Stencel<sup>1</sup>, Mariola Jureczko<sup>2</sup>, Sławomir Kciuk<sup>3</sup>

<sup>1</sup>Affiliation: PhD School, Silesian University of Technology, Gliwice, Poland, e-mail: [kstencel@polsl.pl](mailto:kstencel@polsl.pl)

<sup>2</sup>Affiliation: Department of Theoretical and Applied Mechanics, Faculty of Mechanical Engineering, Silesian University of Technology, Gliwice, Poland, e-mail: [mjureczko@polsl.pl](mailto:mjureczko@polsl.pl)

<sup>3</sup>Affiliation: Department of Theoretical and Applied Mechanics, Faculty of Mechanical Engineering, Silesian University of Technology, Gliwice, Poland, e-mail: [skciuk@polsl.pl](mailto:skciuk@polsl.pl)

---

## Abstract

Fuel tanks are critical components in automotive applications, ensuring the safe storage and transportation of flammable liquids. However, accurately predicting the dynamic behavior of High-Density Polyethylene (HDPE) fuel tanks under various loading conditions, including vibrations and impacts, remains challenging. This paper describes of numerical modal analysis of a fuel tank made of HDPE. Finite Element Analysis (FEA) is a powerful tool for simulating the structural response of these tanks, but it often relies on material parameters that are static and do not account for rate-dependent behavior. The study aims to evaluate the effect of the rate-dependent stiffness material model on the results of numerical modal analysis results of the HDPE fuel tank. The numerical model was developed using Finite Element Analysis (FEA) and ANSYS software. The study concludes that it is essential to consider the rate-dependent stiffness of materials in numerical models to obtain more accurate and reliable modal analysis results.

**Keywords:** fuel tanks, HDPE, numerical modal analysis

---

## 1. Introduction

The design and manufacturing of automotive fuel tanks are critical endeavors within the automotive industry. These components are responsible for storing and delivering fuel safely, and they must withstand a variety of mechanical stresses during the vehicle's operation. The patent [1] and the article [2] discuss in detail the process of constructing and manufacturing both the frame and the fuel tank of the motorcycle. The design and production of automotive fuel tanks have been discussed in many publications. When designing fuel tanks, scientists take several factors into account related to the materials used and their required strength. Metals have been used historically for the manufacture of fuel tanks. Since 1972 plastic materials began to replace metal materials. The reason for this was that they have many advantages such as less weight, no corrosion problems, decreased explosion damage during fire accidents, and sound and vibration damping [3]. Researchers around the world are conducting research to find better plastic fuel barrier materials that meet increasingly stringent requirements, both because of tighter emission regulations and the fact that fuels with very different compositions are used. In [4] the authors describe the fuel tank made of alumina steel material, which combines the strength of steel with the corrosion resistance of aluminum. One important issue is the use of composite materials such as plastic and carbon fiber, which offer advantages such as minimizing deformation and providing strength to the tank walls [5][6]. Fuel tanks in cars are made of various materials such as plastic, polyketone, aluminum alloy, and high-pressure plastic. Plastic fuel tanks can be made from PVC resin, carboxyl nitrile butadiene rubber, polyvinyl butyrate butyral, and glass fiber [7][8]. Due to the unique balance of mechanical properties and high chemical resistance, polyketones (POK) are described as high-performance and multifunctional polymer materials that can be used, among others, for the production of fuel tanks [9]. Article [10] focuses on the integration of self-healing polymers or composites with cellular fillers made of wrinkled aluminum foil for fuel tanks. The analysis of fuel tanks made of high-pressure plastic has been extensively studied in the literature. Various aspects such as thermal management, failure behavior analysis, and structural optimization have been investigated [11]. In the articles [12][13], the authors discussed the results of the numerical structural analysis of a low-pressure hydrogen canister.

Many articles describe testing of fuel tanks made of high-pressure plastic. The article [14] presents the results of static and dynamic analysis of plastic fuel tanks. In the static analysis, equivalent static loads are applied to the fuel tanks. However, in the dynamic analysis, the time-varying loading and the inertia of the fluid and fuel tanks are taken into account using modal transient analysis.

## 2. Assumptions made during the numerical modeling

For numerical modeling of the behavior of physical objects under dynamic loading using Finite Element Analysis (FEA), linear dynamics, especially modal analysis, has been a commonly used method to analyze and understand the dynamic behavior of structures. This method is primarily used to determine eigenfrequencies, mode shapes, and damping characteristics, which allows for obtaining information on the structure's response to dynamic loads. However, the numerical modal analysis has some limitations, especially when simulating complex structures and materials like High-Density Polyethylene (HDPE). One of the primary challenges when dealing with complex structures in FEA is accurately modeling contact phenomena. The majority of physical objects involve intricate contact conditions, such as components coming into contact with the ability to separate from each other, sliding against each other, or undergoing frictional interactions. These contact interfaces are not possible to model, and inaccuracies in modeling contacts can lead to discrepancies between the simulation results and the actual structural behavior. With complex structures and large assemblies, this is one of the main factors of problems with simulation accuracy.

Furthermore, when dealing with materials like HDPE, which are soft materials compared to metals like steel, there is a notable difference in behavior. Soft materials tend to exhibit higher susceptibility to high strain values, which makes them more prone to deformation and non-linear behavior under dynamic loads. This poses a significant challenge when the load characteristics involve high strain rate cases, such as rapid mechanical loads. In such situations, the assumption of linear elasticity in modal analysis may not hold, and more advanced material models, capable of capturing non-linear responses, become necessary for accurate simulations. Of course, the material models used in numerical modal construction do not support nonlinearities, which requires that the numerical model of the object be tuned and prepared in such a way as to ensure these discrepancies. Besides, relying solely on static tensile test material data may not provide a complete and realistic representation of how soft materials like HDPE respond to dynamic loading conditions. These materials often exhibit rate-dependent material properties, meaning their mechanical behavior changes with the rate at which they are loaded or deformed. To accurately reflect the mentioned rate-dependent effects, advanced material models such as the viscoelastic model should be used during FEM simulations.

### 3. Materials and Methods

HDPE is the material from which the fuel tank is made. A very important issue that should be considered during dynamic analysis of structures made of HDPE or other polymers is the behavior of these materials depending on the rate of loading. Rate dependence means that the mechanical properties of a material change with the rate at which it is loaded or deformed. In the context of FEA, where simulations are employed to predict structural responses to dynamic loads, it is essential to account for this rate-dependent behavior. Even in quasi-static simulations, where the loading conditions are relatively slow and gradual, the use of a simple elastic material model may prove inadequate when dealing with materials like HDPE. This inadequacy arises primarily from the plastic nature of the material. HDPE, like many polymers, exhibits a nonlinear stress-strain response, especially under higher stress levels. In simpler terms, even within what might be considered the elastic range, the stress-strain curve for HDPE is not a line, as it would be in a purely linear elastic material. Instead, HDPE demonstrates plastic deformation characteristics, where stress and strain exhibit a non-linear relationship, making it necessary to account for these complexities in FEA simulations. The non-linearity in the stress-strain behavior of HDPE, which often includes plastic or viscoelastic regions in the stress-strain curve, needs to be addressed in FEA. The utilization of a more sophisticated material model, such as a viscoelastic or viscoplastic model, allows engineers to accurately capture the material's complex behavior. Such models incorporate additional parameters to describe the plastic or rate-dependent aspects of the material response, enabling more precise predictions of structural deformation and stress distribution under quasi-static and dynamic loading conditions. These advanced material models are essential for ensuring that FEA simulations not only consider the linear elastic properties but also account for the non-linear and time-dependent behavior of HDPE and other similar materials, ultimately resulting in more accurate and realistic representations of their responses in real-world engineering applications. Many real-world applications involve dynamic loading scenarios, and for these cases, a linear elastic model may not suffice. In these instances, a viscoelastic material model becomes necessary. A viscoelastic model incorporates both elastic (Hookean) behavior, which represents instantaneous deformation, and viscous (dashpot) behavior, which accounts for time-dependent deformation or energy dissipation. By integrating the viscoelastic material model into FEA simulations, engineers can accurately capture the rate-dependent stiffness and response of HDPE and similar materials in the frequency domain. This modification ensures that the material's mechanical behavior under dynamic loads is realistically represented in the simulation results. Consequently, FEA simulations provide valuable insights into the performance and safety of components made from HDPE, such as fuel tanks, ensuring that they meet the stringent requirements of real-world applications. By accounting for the rate-dependent behavior in the viscoelastic material model while retaining the fundamental linearity of the material, engineers can predict structural responses more accurately.

Dynamic Mechanical Analysis (DMA) is a highly effective technique used to evaluate the viscoelastic properties of materials. DMA involves subjecting a material to a range of dynamic mechanical forces, typically in the form of controlled oscillatory stress or strain, while monitoring its response in terms of storage modulus (elastic behavior), loss modulus (viscous behavior), and damping or tan delta (a measure of energy dissipation). This method provides critical insights into a material's behavior under varying frequencies and temperatures, allowing engineers and researchers to determine its viscoelastic parameters.

The simulation was meticulously carried out within the ANSYS software platform, utilizing version 2022R2. To faithfully represent the real-world modal analysis conducted on the HDPE fuel tank mounted on a steel frame, the CAD geometry employed in the simulation closely mirrored the production drawings of the actual components. However, in the interest of computational efficiency and reasonable calculation times, certain simplifications were applied to the geometry. These simplifications aimed to reduce the node count of the mesh without compromising the overall quality of the simulation. Notably, minor details such as welding joints on the steel frame and markings on the fuel tank were excluded to streamline the model. The blow-molded fuel tank, a central component of the analysis, was set to maintain a constant nominal thickness of the wall. To further streamline the simulation, some of the bulkier components of the system, such as the fuel delivery module, were represented as point masses with appropriate connections to the underlying steel structure. The fig.3.1. shows the model of the fuel tank in the CAD software, based on which a modal analysis was performed using the FEA method. These simplifications allowed for efficient computations while preserving the essential characteristics of the system under investigation. This comprehensive approach to simulation setup, combining accurate representation of the original geometry with strategically applied simplifications, ensured that the modal analysis results could be obtained with great computational efficiency, facilitating a deeper understanding of the material behavior and system response to dynamic loads.

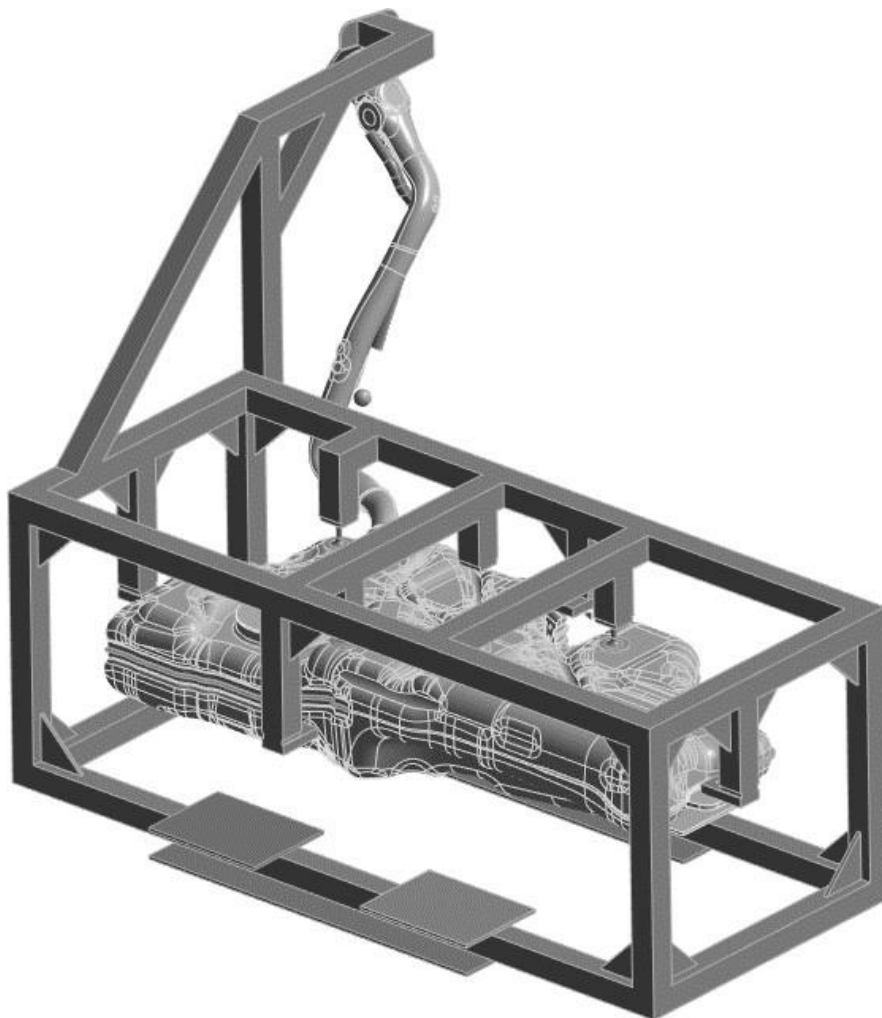


Fig. 1. The model of the fuel tank in the CAD software

In the second simulation, a key parameter was altered to examine the impact on the results. Specifically, the material model was changed from a linear elastic model to a viscoelastic model. This change allowed us to isolate the influence of the material's viscoelastic properties on the structural response. By keeping the geometry and contact conditions consistent between the two simulations, any differences in the results could be attributed solely to the use of the viscoelastic material model. This approach enabled a detailed assessment of how the rate-dependent stiffness and behavior of HDPE, represented by the viscoelastic material model, affected the modal analysis outcomes, providing valuable insights into the importance of accurately accounting for these properties in FEA simulations. Storage modulus and loss modulus were acquired as general parameters of HDPE materials.

#### 4. Results and Discussion

Fig. 2, Fig.3, and Fig.4 show the accelerometer data acquired during the sine sweep simulation, a method designed to closely mimic the real-world conditions of experimental modal analysis. Within the simulation framework, virtual measurement points were strategically placed on the geometry at precisely the same locations as the physical accelerometers used during the experimental testing. These charts illustrate the recorded accelerometer data, where the X-axis corresponds to the frequency in Hertz (Hz), and the Y-axis represents acceleration in G-forces (G). It is evident from the results that the introduction of the viscoelastic material model has notably improved the accuracy of the simulation outcomes when compared to the standard elastic model. In particular, the frequencies corresponding to the maxima in the data closely align with the experimental test results, reflecting a significant improvement in the predictive capabilities of the viscoelastic material model. Notably, in Fig.2., the G-force values and the overall shape of the curve present a substantial enhancement in the accuracy of the simulation data at that specific point in the frequency spectrum.

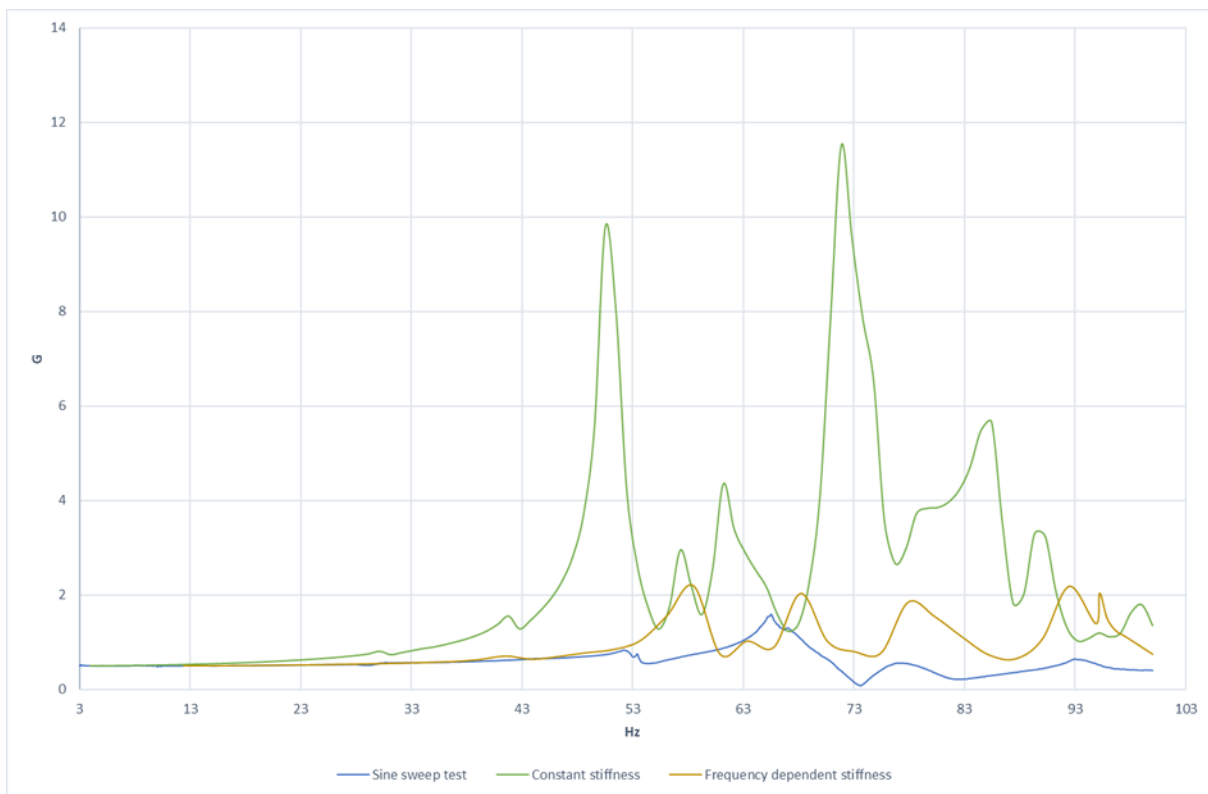


Fig. 2. Acceleration compared during sine sweep

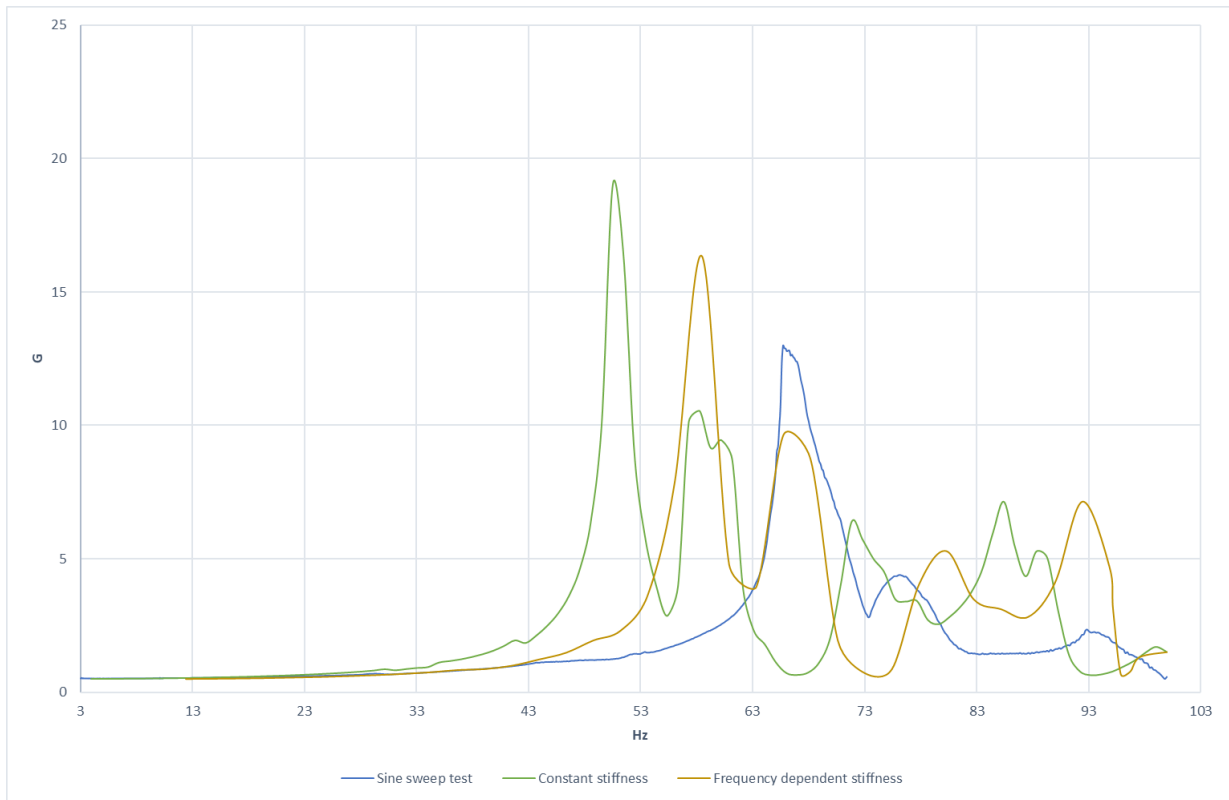


Fig. 3. Acceleration compared during sine sweep

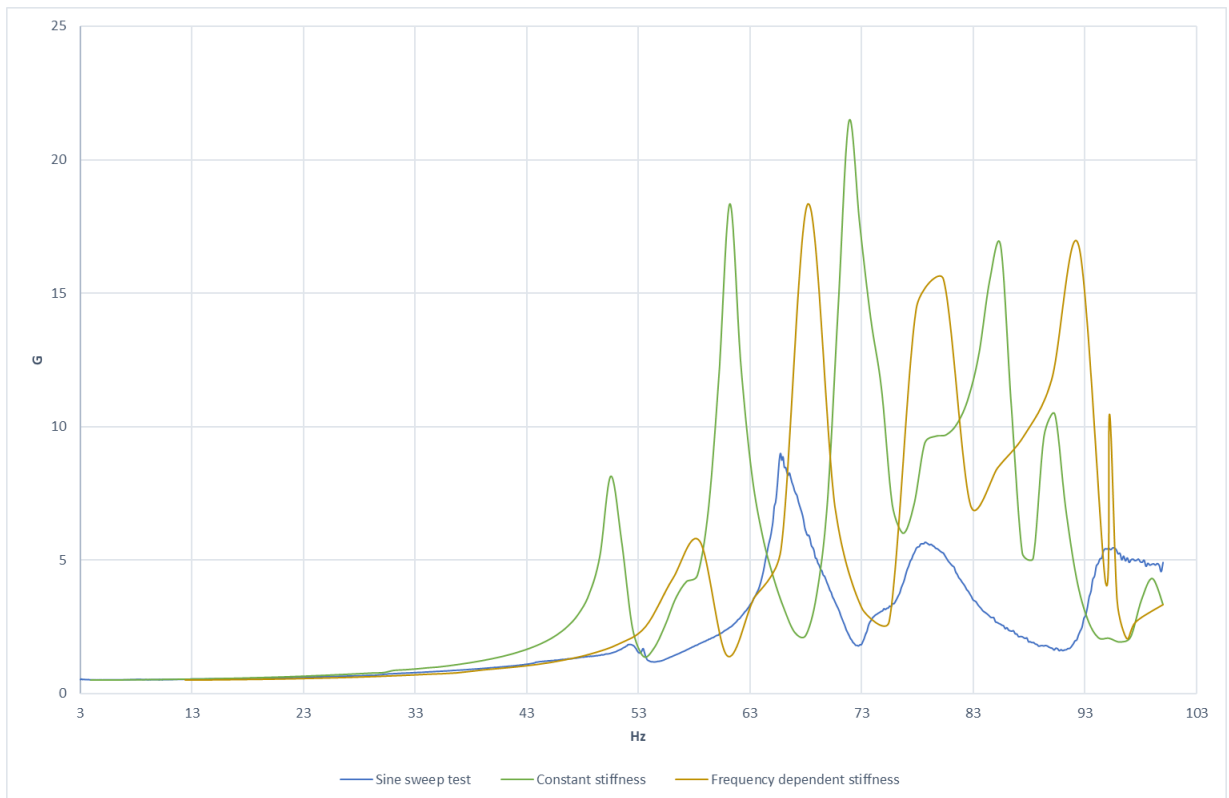


Fig. 4. Acceleration compared during sine sweep

## 5. Conclusions

In conclusion, this study has provided valuable insights into the dynamic response of High-Density Polyethylene (HDPE) fuel tanks during modal analysis. By conducting detailed simulations closely mirroring real-world experimental modal analysis, we sought to evaluate the performance of the viscoelastic material model in comparison to the standard elastic model. Our findings demonstrate the effectiveness of the viscoelastic material model in improving the accuracy of the simulation results, particularly in terms of aligning the frequencies of the maxima with the experimental data. However, despite these promising advancements, it is imperative to acknowledge that the general reliability of the simulation outcomes remains below the desired standard for dependable use in the development process. Further investigation is warranted to address the existing discrepancies and refine the model's accuracy. This scientific assessment underscores the value of incorporating viscoelastic material models during modal simulations, especially when dealing with rate-dependent materials like HDPE, and underscores the importance of ongoing research to refine the simulation methodology, ultimately contributing to more reliable and precise numerical models.

Future research in this domain should primarily direct its efforts towards enhancing the computational efficiency of geometry models capable of representing variable wall thickness of the fuel tank. Furthermore, a crucial aspect for future investigation involves exploring and characterizing damping parameters within the context of modal analysis. Damping is a critical factor in understanding how energy dissipates within a structure under dynamic loading conditions. This knowledge is invaluable for refining simulation accuracy and aligning it with real-world behavior.

## References

- [1]. D. Erhard, M. Holtdirk, *Fuel Tank for a Motor Vehicle, in particular for a Motorcycle, and Method for Producing a Fuel Tank*. Patent Grant Number 11794841, September 2020.
- [2]. K. Stencel, M. Jureczko, *Optimal Design of Electric Motorcycle Tubular Frame using Topology Optimization*, WSEAS Transactions on Applied and Theoretical Mechanics, 18, pp. 150-160, 2023, DOI:10.37394/232011.2023.18.14.
- [3]. L. Xue, R. Rohrbach, P. Unger, D. Bause, G. Jones, *Advances in Plastic Gasoline Barrier Research for Automotive Applications*. SAE Transactions, 109, pp. 513–518, 2023, <http://www.jstor.org/stable/44643869>.
- [4]. R. Ch. Kumaran., R. Adepu, et al., *Design and Development of Fuel Tank for High Mobility Military Vehicle*, 1342, SAE Technical Paper Series, 2023, DOI: 10.4271/2023-28-1342.
- [5]. Ch. Urdl, M. Erhart, F. Wimmer, R. Puchleitner. *Fuel Tank and Method for Manufacturing a Fuel Tank*. Patent no EP 3 822 062 B1, October 2021.
- [6]. J. Wu, Q. Yang, Y. Luo, Y. Duan, M. Du and Y. Pan, *Simulation Research on Electrostatic Distribution of Aircraft Composite Fuel Tank*, In: J. He et al. (Eds.): The proceedings of the 16<sup>th</sup> Annual Conference of China Electrotechnical Society. Springer 3(891), pp. 50-59, 2022, DOI: 10.1007/978-981-19-1532-1\_7
- [7]. H. B. Ustaoglu, S. Ayhün, G. Simitcioğlu, S. Süsler, E. Akay, V. Z. Doğan, Z. Mecitoğlu, H. S. Türkmen, S. Atamer, *Static and Dynamic Analysis of Plastic Fuel Tanks Used in Buses*, Elsevier Procedia Engineering, 101, pp. 509-517, 2015, <https://doi.org/10.1016/j.proeng.2015.02.061>.
- [8]. L. N. Shafigullin, A. M. Sotnikov, N. V. Romanova, E. S. Shabaeva, D. R. Sarimov, D. et al. *Development of a Polymeric Fuel Tank with High Barrier Properties*. IOP Conference Series: Materials Science and Engineering. 570(1):012088, 2019, DOI: 10.1088/1757-899X/570/1/012088
- [9]. Y. Yang, S. Y. Li, R. Y. Bao, Z. Y. Liu et al.. *Progresses of Polyketone Materials: Blends and Composites*. Polymer International. 67(111), 2018, DOI: 10.1002/pi.5624
- [10]. G. Janszen, A. M. Grande., P. Bettini., L. Di Landro, *Integrated Solutions for Safe Fuel Tanks*. International Journal of Safety and Security Engineering, 4(8), pp. 271-279, 2014, doi: 10.2495/SAFE-V4-N3
- [11]. M. Zhang, H., Lv, H. Kang, W. Zhou, C. Zhang, *A Literature Review of Failure Prediction and Analysis Methods for Composite High-Pressure Hydrogen Storage Tanks*. International Journal of Hydrogen Energy, 44(47) pp. 25777-25799, 2019, doi: 10.1016/J.IJHYDENE.2019.08.001



- [12]. Sz. Zając, M. Jureczko, *Structural Analysis of a Low-Pressure Hydrogen Storage Canister*, K. Pikoń, M. Bogacka Magdalena (eds.), Contemporary problems of power engineering and environmental protection 2022, Gliwice, Politechnika Śląska, pp. 250-259, 2023, ISBN 978-83-964116-2-4
- [13]. J. Ochmann, M. Jureczko, Sz. Zając, M. Jurczyk, *Analiza Ciepłna i Wytrzymałościowa Niskociśnieniowych Zbiorników do Magazynowania Wodoru*, Rynek Energii, 4, pp. 23-28, 2023
- [14]. H. B. Ustaoglu, S. E. Ayhün, G. Simitcioğlu, et al. *Static and Dynamic Analysis of Plastic Fuel Tanks Used in Buses*. Procedia Engineering. 101:509-517, 2015, DOI: 10.1016/j.proeng.2015.02.061

# The coffee industry and environmental protection: New trends in wastewater treatment

Angelika Skorupa

*Czestochowa University of Technology, e-mail: angelika.skorupa@pcz.pl*

---

## Abstract

Coffee plays a significant role on a global scale, emerging as one of the key agricultural and food products. Its extensive cultivation, widespread consumption, and impact on the economy contribute to its crucial position on the world stage. The influence of the coffee industry on ecosystems, especially concerning wastewater treatment, is becoming increasingly significant. Characterizing the wastewater from coffee processing underscores potential harmful effects on aquatic ecosystems and public health. Directly releasing coffee wastewater into the ecosystem can lead to serious consequences, such as surface water pollution, negative effects on aquatic flora and fauna, and even threats to human health. Implementing diverse wastewater treatment methods, including chemical and biological processes, can provide an effective response, although each method comes with its challenges. Further research into coffee production wastewater treatment is necessary to understand the effectiveness of different techniques and tailor them to the specifics of manufacturing facilities, contributing to minimizing the industry's negative impact on the natural environment.

**Keywords:** coffee, coffee processing wastewater, sustainability, pollution, technology

---

## 1. Introduction

The available data indicates that coffee production is a significant agro-industrial sector, enjoying substantial interest in the global market. This extensive undertaking involves the cultivation and export of coffee in several tons by around 80 countries worldwide [1]. The global coffee production, according to the International Coffee Organization (ICO) report from 2023, reached a value of 168.5 million 60 kg bags in the coffee year 2021/22. However, it is estimated that this value will increase to 171.3 million bags in the coffee season 2022/23. It is also estimated that global coffee consumption will rise from 175.6 million bags in the coffee year 2021/22 to 178.5 million bags in the coffee year 2022/23 [2].

To obtain a ready-to-consume coffee product, coffee cherries and their green coffee beans must undergo a series of processes. Each stage of production generates significant amounts of solid and liquid waste, contributing to the substantial global coffee-related waste estimated at around 33 million metric tons. It is essential to implement a sustainable management system that takes into account the quantity and characteristics of this waste as a potential source of energy or nutrients [3-4].

Additionally, in the process of processing coffee beans using the so-called "wet method," a significant amount of water is consumed, resulting in the generation of large quantities of wastewater, potentially harmful to the natural environment. Up to 15 liters of water can be used for every kilogram of green coffee at various stages of production post-harvest. This process generates substantial amounts of waste that pollute both the water system and the soil. It is estimated that during some coffee bean processing operations, 40 to 45 liters of wastewater can be produced for every kilogram of green coffee [3-6]. For example, to process 6250 kg of ripe coffee, as much as 125,000 liters of water are consumed, resulting in the production of 1000 kg of green coffee. However, this process also generates 25,000 liters of wastewater and 2500 tons of pulp. These waste products contaminate rivers, rendering them unsuitable for household, recreational, and commercial purposes, simultaneously leading to the degradation of sewage systems and treatment plants, thereby increasing the costs associated with their processing [4,7-8].

In addition to the large amount of water consumed and the generation of liquid waste, wastewater produced during coffee bean processing is characterized by a significant pollution load, mainly due to high levels of organic substances such as pectins, proteins, polyphenols, sugars, alkaloids (caffeine) and tannins [4]. Three key parameters for coffee production wastewater are high organic substance content (BOD up to 20,000 mg/L and COD up to 50,000 mg/L), low pH (down to 3.5) and a significant amount of phenolic compounds (up to 390 mg/L) [4]. These characteristics of coffee wastewater may indicate a negative impact on water bodies, soil, vegetation,

and consequently, the health of animals and humans unless an appropriate water and wastewater management system is implemented [4,9-12]. Effective management of coffee production wastewater should focus primarily on neutralization to increase pH (due to the acidic nature of coffee wastewater) and on efficient removal of the mentioned pollutants, including caffeine. It is crucial to develop environmentally friendly technologies that enable sustainable management of such wastewater [4].

A series of scientific reports have been published regarding potential solutions for managing wastewater from coffee processing. Among the presented methods for treating wastewater from coffee production are advanced oxidation, chemical flocculation, adsorption, Fenton oxidation, electrochemical oxidation, wetland systems, anaerobic digestion, radiation, soil nutrient enrichment, combinations of biological and chemical processes with radiation, aerobic and anaerobic processes, as well as electrochemical and anaerobic systems [6,13-21]. There is still limited literature data on specific technologies used for treating wastewater from the coffee industry. Therefore, it is suggested to conduct an additional review of existing wastewater treatment methods that can be compared and potentially applied. Additionally, attention should be paid to issues related to the limitations and priorities of technologies, considering ease of application and costs, which have not been thoroughly discussed so far [4].

This study focuses on reviewing the literature related to wastewater treatment from coffee production and examining methods that have been researched or implemented so far. It prioritizes these methods based on their suitability for developing regions engaged in coffee production, to achieve effective solutions at lower costs in these specific areas.

## 2. Methods of processing coffee beans

To maintain the high quality of coffee beans, it is necessary to subject the harvested coffee fruits to processing within a few hours. Therefore, coffee processing facilities should be located near the coffee plantation. Each applied technique of coffee bean processing carries the potential for environmental impact (Fig. 1). Furthermore, the type of processing method employed for coffee beans (dry, semi-dry, and wet) significantly influences the ultimate quality of the desired end product [22-23].

Processing coffee beans is a crucial stage in the coffee production process as it significantly influences the flavor profile of the final coffee. The oldest and simplest method of processing coffee beans "dry" usually involves placing freshly harvested coffee cherries on special tables in the sun for drying. This process takes several weeks, during which the skin and parchment layers naturally dry and crack, revealing the beans. In a more intricate method of processing coffee beans "wet," coffee cherries undergo a peeling process to remove the outer skin. Subsequently, the coffee beans undergo a fermentation process aimed at removing the mucilage layer. After the fermentation is complete, the beans are meticulously washed and then subjected to the drying process. The "semi-dry" coffee bean processing method is an intermediate technique, positioned between the dry and wet methods. After the peeling process, a certain portion of the pulp intentionally remains on the coffee beans, giving them a sticky or honey-like coating. Subsequently, the drying process is carried out [22-23].

After drying, coffee beans go through a peeling and husking stage to remove the remaining layers such as parchment and husk, revealing the green coffee beans. Subsequently, the beans undergo a sorting and classification process to ensure consistent size and quality. This step is crucial for achieving uniformity in the final product. Roasting is a separate but highly significant process in coffee bean processing. Green beans undergo roasting to develop their flavor, aroma and attain the desired color [22-23].

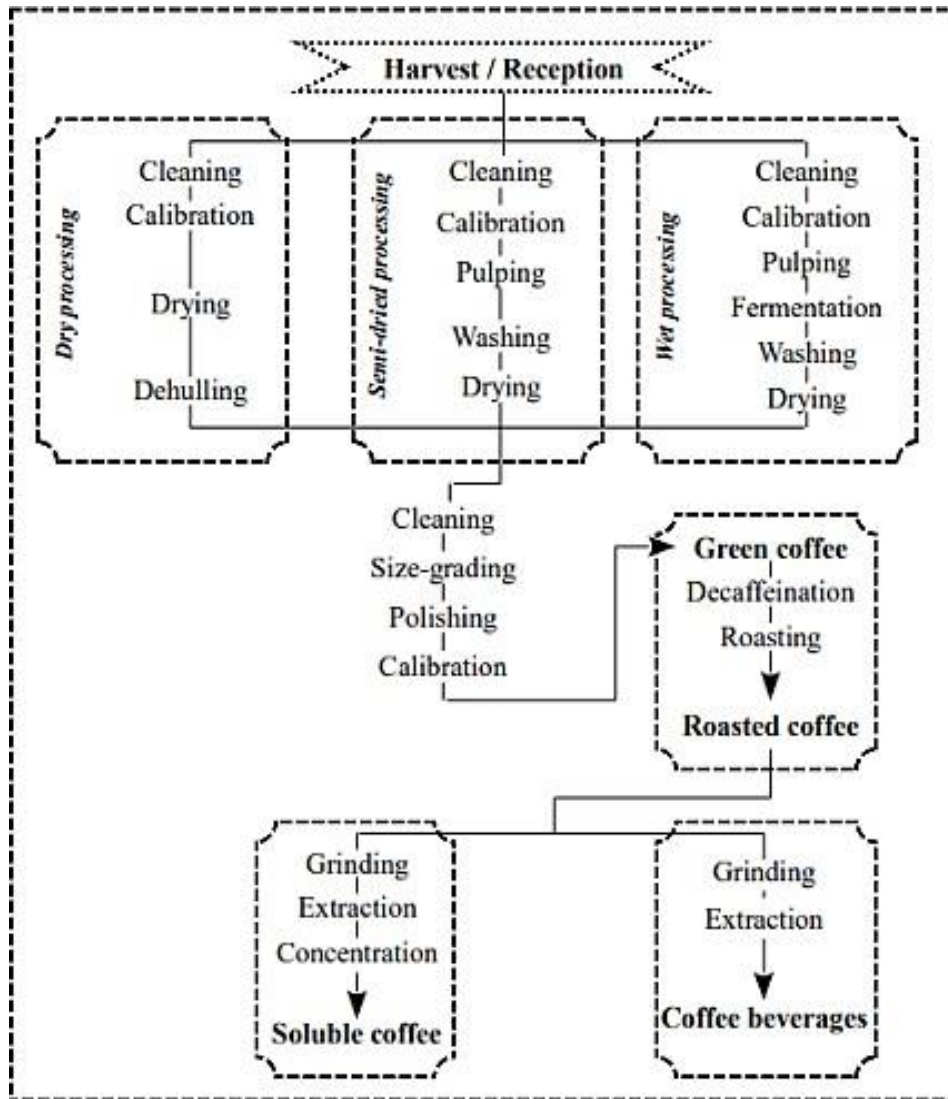


Fig. 1. Processing diagram of harvested coffee cherries and the coffee beans contained within them. Developed based on literature review [22-23].

### 3. Characteristics of wastewater from coffee processing

The wastewater from coffee bean processing has a darker hue, typically appearing dark brown, characterized by high acidity, and containing a significant amount of organic compounds and nutrients (including phenols). This makes such wastewater from coffee production environmentally burdensome and challenging for wastewater treatment plants. The organic matter present in coffee mucilage and pulp (sugars, pectins, proteins) influences the organoleptic properties of the resulting wastewater (e.g., contributing to high viscosity) [24].

The high acidity results from transformations occurring during the fermentation process, as sugars in the coffee mucilage convert into organic acids. This occurs during the dissolution of coffee mucilage in the fermentation process. Additionally, the presence of phenols, acidic substances, accounts for low pH values typically ranging from 3.5 to 4.5 (Tab. 1) [4,25]. Therefore, when neutralizing wastewater from coffee bean processing, methods to remove phenols and sugars from the wastewater must be considered. This poses a real threat to the environment, especially when untreated coffee wastewater is directly discharged into the natural environment without prior purification. Untreated coffee wastewater can contribute to lowering the natural pH value of water in natural reservoirs (usually in the range of 6.5 to 7.5) [10].

The biodegradability index of coffee wastewater is approximately 82%. This indicates the potential for subjecting coffee wastewater to biological processes, after which it may be suitable for enriching the soil environment. However, such coffee wastewater must undergo neutralization (pre-treatment) before being considered for these processes [4].

Table. 1. Physical and chemical characteristics of coffee wastewater based on literature data.

Characteristics	Value	References
pH	3.57-4.21	[20,26]
Color (Pt-Co)	17966.7	[27]
COD (mg/L)	8480-45955	[4]
BOD (mg/L)	3700-5861	[26,28]
BOD:COD	0.56-0.59	[20,26]
DO (mg/L)	2.0-2.6	[4]
Turbidity (NTU)	1481.7	[27]
TS (mg/L)	3520-4200	[20]
TSS (mg/L)	2390-2820	[4]
TVS (mg/L)	8208	[28]
TDS (mg/L)	1002-3933	[29]
TN (mg/L)	125.8-700	[26,27]
TOC (mg/L)	11.400	[27,28]
EC (Ds/m)	0.96-1.20	[20]
Total phenol (mg/L)	45-278	[30,31]
Mg (mg/L)	42.5-62.1	[20,26,29]
K (mg/L)	20.4-45.8	[20]
Cl (mg/L)	25.2-46.8	[4]
Ca (mg/L)	67.8-92.0	[29]
TSO <sub>4</sub> <sup>2-</sup> (mg/L)	10	[27,28]
Na (mg/L)	7.8-13.8	[4]
Biodegradability index	0.82	[27]

#### 4. Coffee wastewater treatment

Based on the conducted research on wastewater from coffee production and the available literature data, it can be inferred that the wastewater from coffee bean processing poses a significant threat to the natural environment. This is especially true for water reservoirs located near coffee processing factories, as well as the local aquatic flora and fauna. The greatest risk occurs when coffee wastewater is directly discharged into surface waters without prior treatment [20,32-33]. Reports indicate that coffee wastewater may harm human health. The literature suggests that these wastewater streams can cause serious issues such as nausea, stomach pain, dizziness, irritation of the skin, eyes, and ears, as well as breathing difficulties. This primarily concerns residents living in the vicinity of factories generating large quantities of coffee wastewater [11].

Due to the potential threat posed by discharging untreated wastewater from coffee production into the environment, efforts have been initiated to explore solutions aimed at finding the most beneficial and environmentally friendly methods for managing coffee wastewater. Literature data are available, demonstrating several options for treating and managing wastewater from coffee production. This article focuses on discussing the most popular methods of treating wastewater from coffee production. Several wastewater treatment technologies using anaerobic processes in coffee production have been described in the available literature [28]. Figure 4.1. presents the classification of the most commonly studied wastewater treatment processes for coffee.

Fig. 4.1. Diagram of applied wastewater treatment processes in coffee production [22,28].

The wastewater treatment techniques in coffee production come with both numerous advantages and disadvantages, which constitute a significant aspect of analyzing the effectiveness of these methods [22]. In terms of advantages, it is worth highlighting that some chemical treatment processes, such as advanced oxidation and coagulation-flocculation, can effectively reduce the content of organic substances, pollutants, and potential toxins in wastewater [4,34]. Additionally, biological treatment methods, including aerobic and anaerobic processes, can

be efficient tools for eliminating organic pollutants through the activity of microorganisms [4,22,31]. However, it is essential to consider certain drawbacks of these techniques. Chemical treatment processes often require the use of specialized chemical substances, leading to additional costs and potential negative environmental impacts [4,22]. Moreover, some biological treatment methods may be time-consuming and necessitate precise control of environmental conditions, making them less practical in certain situations [4,22,35].

Therefore, analyzing the advantages and disadvantages of various wastewater treatment techniques in coffee production is crucial for selecting the most suitable method, taking into account both the effectiveness of purification and the sustainable impact on the environment.

## 5. Environmental effects of wastewater from coffee processing

Organic acids and other chemical substances formed during the coffee fermentation process impart an acidic character to the wastewater, causing its pH to drop to 3.8. Direct discharge of such acidic wastewater into the natural environment poses a risk of negatively impacting higher plants and animals. The organic substances dissolved in coffee wastewater undergo slow microbiological degradation, leading to significant consumption of oxygen. Consequently, anaerobic conditions may arise. The Biological Oxygen Demand (BOD) values indicate the amount of oxygen required for the breakdown of organic matter in coffee wastewater. BOD can reach up to 150 g/l for coffee wastewater, while the Chemical Oxygen Demand (COD) can go as high as 40 g/l and more [36].

Due to high Chemical Oxygen Demand (COD) and Biological Oxygen Demand (BOD) levels, anaerobic conditions quickly develop, leading to unpleasant odors and accelerated death of aquatic organisms due to the rapid consumption of dissolved oxygen. Bacteria thriving in anaerobic conditions can also pose a health risk when present in water suitable for consumption. In addition to the unpleasant odor, coffee wastewater gradually takes on a dark green or black color, resulting from the chemical components of red cherry coffee, namely flavonoids. Despite the unsightly appearance of coffee wastewater, the presence of black hues itself does not harm the environment or significantly impact BOD or COD [36].

In general, the combination of high acidity from the coffee production process and increased BOD becomes problematic, leading to the removal of significant dissolved oxygen from the aquatic ecosystem. To enhance the effectiveness of treating wastewater from coffee production, it is necessary to address these challenges [36].

## 6. Wastewater from coffee production as a potential energy source

Given the increasing global demand for energy and the unequal distribution of energy resources, the efficient use of waste for energy generation has become a matter of paramount importance. In the context of coffee processing wastewater, the two most commonly employed techniques currently are hydrogen production from this wastewater and biomethane production. These innovative approaches not only enable the effective utilization of pollutants present in the wastewater but also contribute to the promotion of sustainable use of energy resources, which is crucial in the current global energy landscape. Further research and development of these technologies are essential for maximizing the ecological and energy-related benefits derived from the processing of coffee wastewater [37].

Researchers Beyene et al. (2014) have already explored the possibility of using wastewater from coffee processing as a raw material for energy production, including bio-hydrogen and methane [26]. Some studies focus on increasing the efficiency of energy extraction using coffee wastewater as a raw material, while others concentrate solely on effectively treating the generated wastewater to enable its discharge with pollutant loads well below the limit set by local regulations. Combining both approaches, where the parameters of both processes are optimized, would be a more innovative approach and could contribute to solving a larger problem related to self-sustainability [37-38].

## 7. Conclusions

- In the context of emerging trends in environmental protection, the issue of the coffee industry and its impact on the ecosystem, particularly in terms of wastewater treatment, is becoming increasingly significant. The characterization of wastewater from the coffee processing highlights its potentially harmful effects on water ecosystems and public health. Without effective treatment, the discharge of this wastewater into the natural environment can lead to serious consequences, such as surface water pollution, negative effects on aquatic fauna and flora, and even a threat to human health.
- The introduction of diverse wastewater treatment methods for coffee, such as advanced chemical processes, adsorption, or biological processes, may provide an effective response to these challenges.

However, each of these methods comes with both advantages and disadvantages. Chemical processes may be costly and generate additional chemical waste, while biological methods may require precise control of conditions.

- In conclusion, there is an urgent need for further research in the field of coffee production wastewater treatment to better understand the effectiveness of different techniques, their environmental impact, and their adaptation to the specificities of individual production facilities.
- Implementing more sustainable wastewater treatment practices can contribute to minimizing the negative impact of this industry on the natural environment.

## Acknowledgment

The scientific research was funded by the statute subvention of Czestochowa University of Technology.

## References

- [1]. Murthy P.S., Naidu M.M., *Sustainable management of coffee industry by-products and value addition — A review*. Resources, Conservation and Recycling 66, 45–58, 2012.
- [2]. Coffee Market Report October 2023. International Coffee Organization, <https://www.icocoffee.org/documents/cy2023-24/cmr-1023-e.pdf>, date of access 28.11.2023.
- [3]. Padmapriya R., Tharian J.A., Thirunalasundari T., *Treatment of coffee effluent by Moringaoleifera seed*, International Journal of Current Microbiology and Applied Sciences, Volume 4 Number 1, pp. 288-295, 2015.
- [4]. Alemayehu, Y.A., Asfaw, S.L. & Tirfie, T.A., *Management options for coffee processing wastewater. A review*. Journal of Material Cycles and Waste Management, 22, 454–469, 2020.
- [5]. Hue N.V., Bittenbender H.C., Ortiz-Escobar M.E., *Managing Coffee Processing Water in Hawaii*, 2006.
- [6]. Zayas Pérez T., Geissler G., Hernandez F., *Chemical oxygen demand reduction in coffee wastewater through chemical flocculation and advanced oxidation processes*, Journal of Environmental Sciences, Volume 19, Issue 3, 300-305, 2007.
- [7]. Moneim A., Sulieman E.A., Wahid A., Yousif M.A., Mustafa, A., *CHEMICAL, PHYSICOCHEMICAL AND PHYSICAL PROPERTIES OF WASTEWATER FROM THE SUDANESE FERMENTATION INDUSTRY (SFI)*, Fourteenth International Water Technology Conference, Egypt, 2010.
- [8]. Blinová L., Sirotiak M., *Utilization of Waste-Based Sorbents for Removal of Pharmaceuticals from Water: A Review*, Research Papers Faculty of Materials Science and Technology Slovak University of Technology, 29, 22 – 36, 2021.
- [9]. Aguiar L.L., Andrade-Vieira L.F., de Oliveira David J.A., *Evaluation of the toxic potential of coffee wastewater on seeds, roots and meristematic cells of Lactuca sativa L.* Ecotoxicology and Environmental Safety, 133:366-372, 2016.
- [10]. Fernandes A.S., Mello F.V.C., Thode Filho S., Carpes R.M., Honório J.G., Marques M.R.C., Felzenszwalb I., Ferraz E.R.A., *Impacts of discarded coffee waste on human and environmental health*, Ecotoxicology and Environmental Safety, 141:30-36, 2017.
- [11]. Haddis A., Devi R., *Effect of effluent generated from coffee processing plant on the water bodies and human health in its vicinity*, Journal of hazardous materials, 152 1, 259-62, 2008.
- [12]. Kulandaivelu V., Bhat R., *Changes in the physico-chemical and biological quality attributes of soil following amendment with untreated coffee processing wastewater*, European Journal of Soil Biology, 50, 39-43, 2012.
- [13]. Ramya P., Jayasravanthi M., Dulla B., Venkata N., *Chemical oxygen demand reduction from coffee processing wastewater – A comparative study on usage of biosorbents prepared from agricultural wastes*, Global Nest Journal 17(172):291-300, 2015.
- [14]. Kumar B.M., Ulavi S.U., Ramesh H.S., Asha G., Pallavi R.B., *Pretreatment of coffee pulping wastewater by Fenton's reagent*, Indian Journal of Chemical Technology, Vol. 19, pp. 213-217, 2012.

- [15]. Bejankiwar R.S., Lokesh K.S., Gowda T.P., *Colour and organic removal of biologically treated coffee curing wastewater by electrochemical oxidation method*, Journal of environmental sciences, 15 3, 323-7, 2003.
- [16]. Zheng C., Zhao L., Zhou X., et al., *Treatment Technologies for Organic Wastewater*, Water Treatment, InTech, 250-284, 2013.
- [17]. Asha G., Kumar B.M., *Performance Evaluation of Sequencing Batch Reactor for Treatment of Coffee Pulping Wastewater*, Journal of Scientific Research and Reports 9(5):1-9, 2016.
- [18]. Rattan S., Parande A.K., Nagaraju V.D. et al., *A comprehensive review on utilization of wastewater from coffee processing*, Environmental Science and Pollution Research, 22, 6461–6472, 2015.
- [19]. Mohana V.S., Nandini N., Pramila C.K., Manu K.J., *Effect of treated and untreated coffee wastewater on growth, yield and quality of Palmarosa grass (Cymbopogon martini L.) var. motia*, International Journal of Research in Chemistry and Environment, Vol.1 No.2 pp.111-117 ref.18, 2011.
- [20]. Selvamurugan M., Doraisamy P., Maheswari M., *An integrated treatment system for coffee processing wastewater using anaerobic and aerobic process*, Ecological Engineering, 36, 1686-1690, 2010.
- [21]. Kumar B.M., *Coffee Pulping Wastewater Treatment by Electrochemical Treatment followed Anaerobic Sequencing Batch Reactor*, International Journal of Scientific & Engineering Research, Volume 6, Issue 7, 2015.
- [22]. Ijanu E.M., Kamaruddin M.A., Norashiddin F.A. *Coffee processing wastewater treatment: a critical review on current treatment technologies with a proposed alternative*, Applied Water Science, 10, 1-11, 2020.
- [23]. Skorupa A., Worwąg M., Kowalczyk M. *Coffee Industry and Ways of Using By-Products as Bioadsorbents for Removal of Pollutants*, Water, 15(1), 112, 2022.
- [24]. Moberg E., *The water footprint of coffee production in Mirafior, Nicaragua*, Student thesis, 2016.
- [25]. Fier P.S., Maloney K.M., *Synthesis of complex phenols enabled by a rationally designed hydroxide surrogate*. Angewandte Chemie, 129(16), 4549-4553, 2017.
- [26]. Beyene A., Yemane D., Addis T., Assayie A.A., Triest, L., *Experimental evaluation of anaerobic digestion for coffee wastewater treatment and its biomethane recovery potential*, International Journal of Environmental Science and Technology, 11, 1881-1886, 2014.
- [27]. Cruz-Salomón A., Ríos-Valdovinos E., Pola-Albores F., Meza-Gordillo R., Lagunas-Rivera S., Ruíz-Valdiviezo V.M., *Anaerobic treatment of agro-industrial wastewaters for COD removal in expanded granular sludge bed bioreactor*, Biofuel Research Journal 16, 715-720, 2017.
- [28]. Cruz-Salomón A., Ríos-Valdovinos E., Pola-Albores F., Lagunas-Rivera S., Meza-Gordillo R., Ruíz-Valdiviezo V.M., *Evaluation of Hydraulic Retention Time on Treatment of Coffee Processing Wastewater (CPWW) in EGSB Bioreactor*, Sustainability, 10, 83, 2018.
- [29]. Lathem A.P., Heiden Z.M., *Quantification of Lewis acid induced Brønsted acidity of protogenic Lewis bases*, Dalton Transactions, 46(18), 5976-5985, 2017.
- [30]. Oliveira R.A.D., Bruno N., *Start-up of horizontal anaerobic reactors with sludge blanket and fixed bed for wastewater treatment from coffee processing by wet method*, Engenharia Agrícola, 33, 353-366, 2013.
- [31]. Prado M.A.C., Campos C.M.M., Silva J.F.D., *A study on the variation of methane concentration in biogas produced from coffee wastewater*, Ciencia e Agrotecnologia, 34, 475-484, 2010.
- [32]. Enden J.C., Calvert K.C., *Limit Environmental Damage by Basic Knowledge of Coffee Waste Waters*. Available online: [http://www.venden.de/pdfs/Coffee\\_Waste\\_Water\\_treatmentV4.pdf](http://www.venden.de/pdfs/Coffee_Waste_Water_treatmentV4.pdf) (accessed on 1 December 2023).
- [33]. Deepa G.B., Chanakya H.N., de Alwis A.A.P., Manjunath G.R., Devi V., *Overcoming pollution of lakes and water bodies due to coffee pulping activities with appropriate technology solutions*. In Proceedings of the Symposium on Conservation, Restoration and Management of Aquatic Ecosystems, Bangalore, India, 9–13, 2002.
- [34]. Novita E., Bagastyo A.Y., Sudarjanto G., *Chemical coagulation of coffee wastewater for smallholder coffee agro-industry*, 2012.
- [35]. Hubbe M.A., Metts J.R., Hermosilla D., Blanco M.A., Yerushalmi L., Haghghat F., et al., *Wastewater treatment and reclamation: a review of pulp and paper industry practices and opportunities*, BioResources, 11(3), 7953-8091, 2016.
- [36]. Von Enden J. C., Calvert K. C., *Limit environmental damage by basic knowledge of coffee wastewaters. GTZ–PPP Project, Improvement of coffee quality and sustainability of coffee production in Vietnam*, 2002.



- [37]. Sengupta B., Priyadarshinee R., Roy A., Banerjee A., Malaviya A., Singha S., et al., *Toward sustainable and eco-friendly production of coffee: abatement of wastewater and evaluation of its potential valorization*, Clean Technologies and Environmental Policy, 22, 995-1014, 2020.
- [38]. Etiégni L., Orori B.O., Senelwa K., Mwamburi M.M., Balozi B.K., Maghanga J. K., *Ash leachate used as supporting electrolyte during wastewater treatment by electrocoagulation*, Geophysical Research Abstracts Vol. 13, EGU2011-626, 2011.

# Water quality assessment of Vjosa river near an oil extraction area

Blerina Beqaj <sup>1</sup>, Lira Aliaj <sup>2</sup>

<sup>1</sup>Polytechnic University of Tirana, Faculty of Civil Engineering, Department of Environmental Engineering, Tirana, Albania e-mail: belabeqaj@gmail.com

<sup>2</sup>Polytechnic University of Tirana, Faculty of Civil Engineering, Department of Environmental Engineering, Tirana, Albania e-mail: lira.aliaj2001@gmail.com

---

## Abstract

This study consists in the evaluation of the water quality in the Vjosa river after the pollution caused in this river by an oil bearing area. The study was carried out in the Gorrisht-Kocul oil-bearing area. The article describes and identifies the problems of this area in relation to petroleum pollution, which is directly related to the activity of oil extraction and decantation in this petroleum source place. The analysis of pollution was done, determining exactly the sources of pollution, discharges as well as impacts on the waters of the Vjosa river. Analysis and laboratory measurements of the river's waters were made at different points. In this way, a series of water parameters were determined. Completion of the layer injection project will finally solve the pollution of the Vjose River from the Gorisht decantation. From the analysis of the whole issue of pollutant concentrations in water, we can say that the pollution from this case is significantly high. Therefore, it is recommended to take immediate measures on the part of the private company, which uses the Gorrisht-Kocul oil-bearing field. The improvement of this problem and its elimination is entirely under the responsibility of the company that uses the oil-bearing field.

**Keywords:** Vjosa river, pollution, petroleum, oil extraction area , oil extraction and processing

---

## 1. Introduction

Water, whether it is in the form of surface or underground flows, is necessary for the development of life. Surface water collects ever greater amounts of polluted and untreated water from residential areas. These areas are heavily influenced by industrial activities, by the intensive development of livestock, as well as by agricultural production [1]. Poor water quality is a particularly serious problem and one that shows great interest in solutions, especially for developing countries, where environmental management practices do not ensure adaptation to economic development [2]. The non-management of urban water discharges from residential areas, industrial discharges, the use of pesticides and herbicides in agriculture, as well as the lack of measures for proper treatment and reuse of waste, have led to a degradation of surface water quality [3]. Every pollutant or undesirable substance has a source of discharge, the knowledge of which is very important, in order to avoid or minimize the pollution coming from it. If the pollutant stays for a very long time, then it can be deposited in a tank that is a long-term storage site. The sources of water pollution are natural and human. The anthropogenic sources that cause water pollution are classified into some categories, each of which has its own subcategories and characteristics. In general, oil extraction wells cause environmental pollution during the work process. This comes as a result of not sealing the mouths of the wells well and as a result, we have leaks in more than 80% of them. A part of the oil and formation water that comes out of the wellhead spreads into the surrounding environment, while another part goes into the wellbore, which is a simple earthen pit intended, among other things, to collect the fluids that are taken during performing various repair works in the wells themselves. [4]. The number of these pits has been the same as the number of wells in operation. In the rainy season, the water level in these pits rises and the oil that is in them comes out, polluting the surrounding environment or passes into the irrigation drainage channels and from there into the hydraulic water system of the area.

The waters containing oil and surfactants, which are discharged from these facilities, are not subjected to cleaning processes, but in some cases they pass through simple separators, in order to remove part of the oil [5]. During the technological process, the processing waters, carrying oil and its products, pollute the environment where they are discharged. The technological discharge waters from the plant are divided into: - waters containing oil and its products, which are discharged from washing plants. - acidic or alkaline waters that contain sulphur, ammonia, phenols, etc. Which come out of the processes of distillation and coking or purification of gases containing SO<sub>2</sub> water containing soda, which come out of plants for cleaning petroleum products with caustic soda. The waters must pass to the cleaning block, where they must be treated with H<sub>2</sub>SO<sub>4</sub>, flotation and separation to remove oil particles, while for the removal of H<sub>2</sub>S, they must pass through a separate column, through evaporation. Normally,

these waters, after cleaning from oil, should be subjected to the microbiological cleaning process for the elimination of phenols, which was not done [6]. Vjosa catchment is an essential area for conservation due to the diversity of habitat types it offers. Upstream, the average discharge of water is about 60 m<sup>3</sup>/s in Vjosa, while the downstream has about 175 m<sup>3</sup>/s on average (200 m<sup>3</sup>/s in the delta). Most important for the formation of active channels is the regular and frequent annual flood discharge of about 900 m<sup>3</sup>/s, while extreme 100-year floods can reach 3000 m<sup>3</sup>/s in the upper part and up to 6000 m<sup>3</sup>/s in the downstream [7]. The area of Gorrishti, which is located 31 km from the city of Vlora. Gorrishti is located southeast of Vlora, half of which lies on the banks of the Vjosa River. The discharges into water from Albpetrol's operations are of the liquid type. The main sources of surface water pollution are two: petroleum discharged at the mouths of the wells (or near various technological devices) and accumulated in pits specially built for this purpose; in rainy weather, a part of this oil can be transported by water and end up in the surface water network, becoming a source of pollution; the water discharged after the decantation process [8]. This source deserves a wide treatment as by the amount that is discharged and the high pollution potential. At the current stage of exploitation of Albpetrol's resources, the extracted fluid has an average of 50% associated water.

## 2. Material and methods

The associated waters that are separated from the oil after the decantation process. These discharges are an integral part of the oil production process. In the decantation of the Gorishti Station, the amount of technological water produced per year is 105,000 m<sup>3</sup>. The bottles from which the water samples were taken were clean and before being filled, they were rinsed two or three times with river water. Sampling was carried out by means of a special plastic bottle, 1 liter, sufficient amount for carrying out water analyses. Sampling was carried out at a considerable depth. Depending on the analysis or determination to be performed, the container is filled full (when most organic compounds are determined) or a space is left for aeration, mixing, etc. (for the case of microbiological analyses). In cases where the sample must be taken in the presence of preservatives, care must be taken when filling the container to avoid water spillage. For the samples in which the determination of volatile organic compounds will be performed, an empty space of about 1% of the volume of the container was left in the container, to allow thermal expansion during transportation. In case the sample for the above analysis is taken using a preservative, it is important that the vessel has no empty space. The plastic bottle is filled completely until a flat surface is created at its mouth, ensuring in this way that we do not take in air, as it can affect the change in the values of some parameters. After this, the bottle is tightly closed and placed in a thermal bag. Water analysis was performed 1 hour after taking the water sample. Sampling was carried out under conditions of full sunlight and air temperature of 25°C. The first measurement was carried out at a distance of 337 meters from the point where the stream joins the Vjosa river. The second measurement was carried out at a smaller distance about 100 meters from the point where the river meets the stream. The third measurement was carried out at a distance of approximately 100 m from the point of confluence of the river with the stream, but unlike the first two cases, this point is located before the point of confluence of the river with the stream.

## 3. Results and discussions

The calculations show that the amount of water discharged during oil decantation at the decantation stations is on average of 105,000 m<sup>3</sup>/year. The quality of the water discharged from the Gorisht decantation station is far from the permitted rates and these cannot be discharged without being treated to reduce the amount of HS, phenols and oil. The water discharged from the petroleum decantation station ends up in Vjosa river. From this amount, about 31,500 m<sup>3</sup>/year or about 30% of the total amount is injected into the layer in the G<sub>6</sub>-30 well. The remaining amount is discharged into Vjosa River. There is also a high level of mineralization in the accompanying oil water that flows into the river. The content of pollutants causes deterioration of other water indicators such as: COD, BOD<sub>5</sub>, acidic or basic environment, etc.; example, in general, the values of water indicators are: COD from 230-450 mg/l; BOD<sub>5</sub> from 63-68 mg/l and the average content of phenols from 1.9-3.4mg/l.

All the above indicators are definitely several times higher than the allowed rates (COD 150 mg/l, BOD<sub>5</sub> 30 mg/l and phenols 0.5 mg/l). This river is not much affected by Gorisht decantation discharges due to the large flows of the latter. Completion of the layer injection project will finally solve the pollution of the Vjosa River from the Gorisht decantation. As a result of the damage at larger levels of the system in the structural components of extraction, collection, transport or decantation, there has been a flow of a significant amount of crude oil which flows into the waters of one of the streams of the Gorrisht-Kocul area. , which has its discharge directly into the river Vjosa. So regardless of the residue along the entire length of its flow, water flows into Vjosa with a significant amount of crude oil and a large load of pollutants.

According to this study carried out at the decantation stations of the Gorrisht-Kocul oil field, the following results were obtained: The table shows the values measured in the technological waters from the Gorisht decantation station.

Table. 1. Values measured in the technological waters

Analyzed parameters	Method	Unit measure	Values	Detection limit
pH	ISO 10523:2012 Water Quality, Determination of pH. WTW Multi 340i		7.02	0.01
Suspended solids	Filtration, Whatman (filter <0.45 m)	mg/l	55.2	1
Petroleum products	SSH EN 1588 Water quality Standart Method for Water and Waste Water Oil and Grease	mg/l	350	0.1
BOD <sub>5</sub>	Respiration/Blogas determination with Oxitop controle/Acording to EN 1899-1 and EN 1899-2/EPA methods	mg/l	28	1
Volatile phenols	US Standard Methods 5530, EPA 420.1/4 Amoniantupyrin analog ISO 6439/Test kits method	mg/l	0.14	0.002
Sulphides	Photometric/Test kit method/US Standart Methods 4500- 52- D, dhe ISO 10530	mg/l	0.11	0.02
Aluminum	Photometric/Test kit method/US Standart Methods 3500 -AI D and ISO 10566 E30	mg/l	0.48	0.02
Arsenic	Photometric/Test kit method/US Standard Methods 3500-As	mg/l	<0.01	0.001
Cadmium	Photometric/Test kit method/Reaction:with Cadion derivative	mg/l	<0.02	0.002
Chromium VI	Photometric/Test kit method/US Standart Methods 3500-Cr D	mg/l	0.05	0.01
Copper	Photometric/Test kit method/Reaction:with Cuprizon	mg/l	0.4	0.02
Mercury	Standard Methods for the Examination of Water and Wastewater/3500 Hg	mg/l	<0.01	0.01
Lead	Photometric/Test kit method/Reaction: with Pyridylazoresorcinol PAR	mg/l	0.02	0.01
Nickel	Photometric/Test kit method/US Standart Methods US 3500-NI E	mg/l	<0.01	0.02

Table. 2.. Summary table of the results obtained from the three measurements carried out

Mesured parameters	Measurements		
	First	Second	Third
pH	5	4	6
Cu	0.05	0.1	0.04
dissolved oxygen (O <sub>2</sub> )	10	8	10
Mg	4	11	6
SiO <sub>2</sub>	5	6	1.2
NO <sub>2</sub>	0.01	0.05	0.01
NO <sub>3</sub>	0.5	0.04	0.5
NH <sub>4</sub>	0.2	0.5	0.04
PO <sub>4</sub>	0.4	2	0.1
Fe	0.4	1	0.1

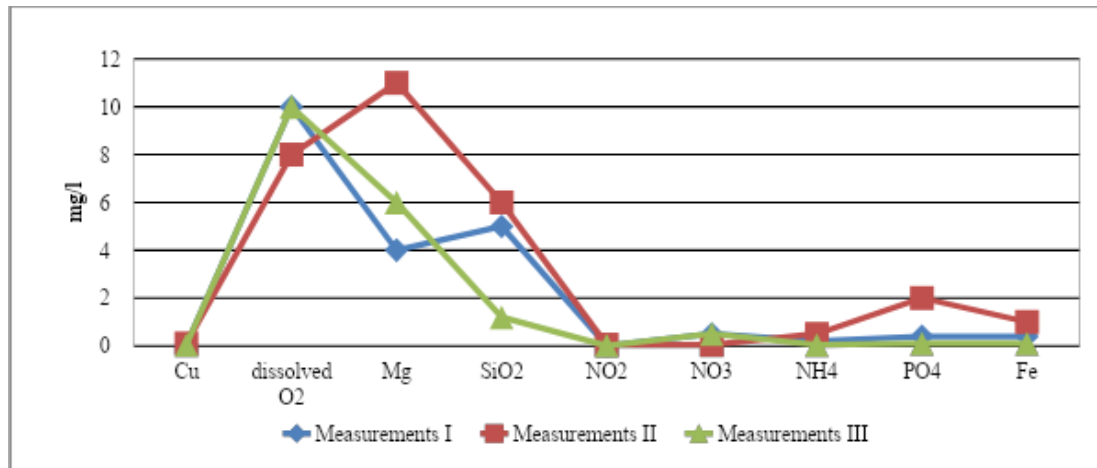


Fig. 1. Average values of the monitored parameters for three measurements

#### 4. Conclusions

The values found from the third measurement are closer to the recommended values, of the allowed rates, while the values found which are farthest from these allowed rates are those of the second measurement. Between the values found of the first measurement and the second measurement, the most positive values, i.e. closer to the allowed rates, are those of the first measurement, which is located far from the source of pollution, in contrast to the measurement of second, located near the source of pollution. This is proven by the fact that the closer we are to the source of pollution, the higher the concentrations of pollutants and the greater the pollution. The further we move away from the source of the pollution, the more the pollution is dispersed and the pollutant concentrations are reduced. The values found from the third measurement are closer to the permitted rates because at this point we do not have discharge of the polluted stream into the river. The discharge of the stream into the river is approximately 100 m from this point and considering the flow of the river, the distribution of pollutants downstream is very small, almost negligible. From the analysis of the whole issue of pollutant concentrations in water, we can say that the pollution from this case is significantly high. Therefore, it is recommended to take immediate measures on the part of the private company, which uses the Gorrish-Kocul oil-bearing field. The improvement of this problem and its elimination is entirely under the responsibility of the company that uses this field.

#### References

- [1]. Cheng, C., Zhang, F., Shi, J., Te Kung H. (2022). What is the relationship between land use and surface water quality? A review and prospects from remote sensing perspective. *Environ Sci Pollut Res* 29, 56887–56907 (2022). <https://doi.org/10.1007/s11356-022-21348-x>.
- [2]. Mishra, B.K.; Kumar, P.; Saraswat, C.; Chakraborty, S.; Gautam, A. (2021). Water Security in a Changing Environment: Concept, Challenges and Solutions. *Water*, 13, 490. <https://doi.org/10.3390/w13040490>.
- [3]. Akhtar, N.; Syakir Ishak, M.I.; Bhawani, S.A.; Umar, K. (2021). Various Natural and Anthropogenic Factors Responsible for Water Quality Degradation: A Review. *Water*, 13, 2660. <https://doi.org/10.3390/w13192660>.
- [4]. Devold H. *Oil and gas production handbook An introduction to oil and gas production, transport, refining and petrochemical industry*. Edition 3.0 Oslo, August 2013. Pp. 162. ISBN 978-82-997886-3-2.
- [5]. Tian, Y.; Zhou, J.; He, C.; He, L.; Li, X.; Sui, H. The Formation, Stabilization and Separation of Oil–Water Emulsions: A Review. *Processes* 2022, 10, 738. <https://doi.org/10.3390/pr10040738>.
- [6]. Eldos H.I., Khan M., Zouari N., Saeed S., Al-Ghouthi M.A. (2022). Characterization and assessment of process water from oil and gas production: A case study of process wastewater in Qatar. Case study in chemical and environmental engineering. Volume 6. <https://doi.org/10.1016/j.cscee.2022.100210>.
- [7]. <https://akzm.gov.al/wp-content/uploads/2020/07/International-Competition-VRNP.pdf>.
- [8]. <https://balkaninsight.com/2018/12/05/oil-pollution-threatens-europe-s-last-wild-river-11-30-2018/>.



# EPAE 2023

ENVIRONMENTAL PROTECTION & ENERGY CONFERENCE

Gliwice, 2024

**iSBN 978-83-964116-5-5**